

TALLINN UNIVERSITY OF TECHNOLOGY
DOCTORAL THESIS
28/2018

Wearable Solutions for Monitoring Cardiorespiratory Activity

MARGUS METSHEIN



TALLINN UNIVERSITY OF TECHNOLOGY
School of Information Technologies
Thomas Johann Seebeck Department of Electronics

This dissertation was accepted for the defence of the degree 20/05/2018

Supervisor: Senior Researcher Paul Annus
Thomas Johann Seebeck Department of Electronics
Tallinn University of Technology, Tallinn, Estonia

Co-supervisors: Prof Emeritus Mart Min
Thomas Johann Seebeck Department of Electronics
Tallinn University of Technology, Tallinn, Estonia

Prof Alvo Aabloo
Institute of Technology
University of Tartu, Tartu, Estonia

Opponents: Prof Gerard Cybulski
Department of Mechatronics
Institute of Metrology and Biomedical Engineering
Warsaw University of Technology

Prof Ørjan Grøttem Martinsen
Department of Physics
The Faculty of Mathematics and Natural Sciences
University of Oslo

Defence of the thesis: 14/06/2018, Tallinn

Declaration:

Hereby I declare that this doctoral thesis, my original investigation and achievement, submitted for the doctoral degree at Tallinn University of Technology has not been submitted for doctoral or equivalent academic degree.

Margus Metshein

Signature



Copyright: Margus Metshein, 2018
ISSN 2585-6898 (publication)
ISBN 978-9949-83-281-1 (publication)
ISSN 2585-6901 (PDF)
ISBN 978-9949-83-282-8 (PDF)

TALLINNA TEHNIKAÜLIKOO
DOKTORITÖÖ
28/2018

**Kehal kantavad vahendid
kardiorespiratoorse aktiivsuse jälgimiseks**

MARGUS METSHEIN



Contents

Approbation and List of Publications	8
Author's Contribution to the Publications.....	10
Introduction.....	11
Historical Perspective.....	15
Overview of the Methods and Technologies	16
Problem Statement and Objectives	21
Abbreviations.....	23
1 Background.....	25
1.1 Analyze of Electrical Properties.....	25
1.1.1 Electrical impedance	25
1.1.2 Phasor diagrams of RC circuits	26
1.1.3 Electrical bioimpedance	27
1.1.4 Effect of geometry of object in EBI measurement.....	30
1.1.5 Dielectrics.....	31
1.2 Composition and Electrical Properties of Human Body.....	32
1.2.1 Composition of human skin and its equivalent circuit.....	32
1.2.2 Respiratory and cardiovascular systems of human.....	33
1.2.3 Characterization of cellular tissue (dispersion regions)	35
1.3 Theory and Methods for Bioimpedance Analysis	37
1.3.1 Motion artifact	40
1.3.2 Origin of cardiorespiratory impedance signal.....	41
1.3.3 Approach for evaluating the measured signals of time varying volumetric changes in human body	43
1.4 Electrodes for Measuring EBI	44
1.4.1 Electrode characteristics and electrical properties.....	44
1.4.2 Basic electrode configurations for impedance measurements	46
1.4.3 Sources of error in measurement of EBI	48
1.4.4 Electrode constructions and materials	48
1.5 Chapter Summary	50
2 Wearable Solutions Based on Capacitive Coupling	51
2.1 Cardiorespiratory Activity Monitoring by Using Capacitive Coupling.....	52
2.2 State of the Art of Monitoring Cardiorespiratory Activity by Using Capacitive Coupling	53
2.3 Experimental Evaluation of Alternatives of Measurement of EBI for Monitoring Cardiorespiratory Activity.....	56
2.4 Characterization of Electrodes for Capacitive EBI Measurements	57
2.5 Design and Implementation of the Electrode Shirts.....	58
2.6 Development of Optimized Experimental Electronic EBI Measurement Device	60
2.7 Qualitative Evaluation of the Results of Monitoring Cardiorespiratory Activity by Using the Electrode Shirts in the Case of Capacitive Coupling	62
2.7.1 Qualitative evaluation of the measurement results of respiratory activity.....	62
2.7.2 Qualitative evaluation of the measurement results of cardiac activity	65

2.7.3 Qualitative evaluation of the influence of concurrent movements on the measured signal of EBI with the goal of monitoring cardiorespiratory activity ...	66
2.8 Quantitative Evaluation of the Results of Monitoring Cardiorespiratory Activity by Using the Electrode Shirts in the Case of Capacitive Coupling	67
2.8.1 Quantitative evaluation of the results of monitoring cardiorespiratory activity by using variety of EPC's in the case of ES1	68
2.8.2 Comparative evaluation of the results of monitoring respiratory activity by using the both EBI measurement devices.....	72
2.8.3 Comparative evaluation of the results of monitoring cardiac activity by using the both EBI measurement devices	75
2.9 Utilization of Coils as EBI Measuring Electrodes for Capacitive Monitoring of Cardiorespiratory Activity.....	79
2.10 Chapter Summary	81
3 Wearable Solutions Based on Inductive Coupling	83
3.1 Cardiorespiratory Activity Monitoring by Using Inductive Coupling	84
3.2 State of the Art of Monitoring Cardiorespiratory Activity by Using Inductive Coupling	86
3.3 Variations in Cardiorespiratory Waveform in the Case of Magnetic Induction Monitoring by Varying the Position of Single Coil	89
3.4 Design, Implementation and Characterization of Flexible Coils for Monitoring Cardiorespiratory Activity by Using Inductive Coupling	92
3.5 Setup and Results of Monitoring Cardiorespiratory Activity by Using the Prepared Coils in the Case of Inductive Coupling	94
3.6 Comparative Evaluation of the Results of Monitoring Cardiorespiratory Activity in Thorax by Using Capacitive, Inductive and Resistive Coupling	99
3.7 Chapter Summary	101
4 Wearable Solutions Based on Resistive Coupling	103
4.1 Cardiac Activity Monitoring by Using Resistive Coupling	104
4.1.1 Pulse wave detection in radial artery by using the measurements of EBI.....	105
4.2 State of the Art of Monitoring Pulse Wave in Radial Artery by Using Resistive Coupling	106
4.3 Determination of Most Suitable Placements of Electrodes on the Surface of Wrist for Monitoring Pulse Wave in Radial Artery	109
4.3.1 Experimental determination of the effect of distal placement of electrodes on wrist on the results of monitoring pulse wave in radial artery	110
4.3.2 Experimental determination of the effect of circular placement of electrodes around wrist on the results of monitoring pulse wave in radial artery	115
4.4 Experimental Determination of the Effect of Exact Positioning of Small Area Electrodes on the Results of Monitoring Pulse Wave.....	120
4.5 Development of Wrist Wearable Electrode for Optimal Detection of Pulse Wave and the Evaluation of Preliminary Results	122
4.6 Theoretical Considerations of the Origin of Cardiac Activity Waveform when Measuring the EBI of Wrist	123
4.7 Comparative Evaluation of the Results of Monitoring Pulse Wave in Radial Artery by Using Capacitive, Inductive and Resistive Coupling	126
4.8 Chapter Summary	128
Conclusions	129

List of Figures	131
List of Tables	135
References	137
Acknowledgements	151
Lühikokkuvõte	153
Abstract	155
Appendix	157
Publication 1	159
Publication 2	165
Publication 3	171
Publication 4	181
Publication 5	189
Curriculum Vitae.....	199
Elulookirjeldus.....	200

Approbation and List of Publications

Parts of the content of this thesis were presented and published in the subsequent publications. Copies of the publications are available in Appendix.

The list of author's publications, on the basis of which the thesis has been prepared:

1. Metshein, Margus (2015). A device for measuring the electrical bioimpedance with variety of electrode placements for monitoring the breathing and heart rate. [Proceedings of the 26th Irish Signals and Systems Conference (ISSC2015), 24–26 June, 2015, Carlow, Ireland]: IEEE, 1–4.
2. Metshein, Margus; Annus, Paul; Land, Raul; Krivošei, Andrei; Ojarand, Jaan; Aabloo, Alvo; Min, Mart (2017). Variation of cardiac and respiratory waveform on human thorax in the case of inductive coupling. [IFMBE Proceedings Vol. 65 – Joint Conference of European Medical and Biological Engineering Conference (EMBEC'17) and Nordic-Baltic Conference on Biomedical Engineering and Medical Physics (NBC'17), 11–15 June, 2017, Tampere, Finland]: Springer Nature, 671–674.
3. Metshein, Margus; Parve, Toomas; Annus, Paul; Rist, Marek; Min, Mart (2017). Realization and evaluation of the device for measuring the impedance of human body for detecting the respiratory and heart rate. [Elektronika ir Elektrotehnika 23 (3)]: 36–43.
4. Metshein, Margus; Annus, Paul; Land, Raul; Min, Mart; Aabloo, Alvo (2018). Availability and variations of cardiac activity in the case of measuring the bioimpedance of wrist. [Proceedings of the 2018 IEEE International Instrumentation & Measurement Technology Conference (I²MTC2018), 14–17 May, 2018, Houston, USA]: IEEE, 147–151.
5. Metshein, Margus; Köiv, Hip; Annus, Paul; Min, Mart (2018). Electrode optimization for bioimpedance based central aortic blood pressure estimation. [IFMBE Proceedings Vol. 68/2 – World Congress on Medical Physics & Biomedical Engineering (IUPESM2018), 3–8 June, 2018, Prague, Czech Republic]: Springer Nature.

Some of author's other publications listed below (I–V), are related to the current thesis by covering only some narrow part of research, contributing in the frames of preliminary or supportive activities. Some of author's other publications listed below (VI–VII), are indirectly related to the current thesis though, giving the overview of side research activities that are providing the insight into possible future work in the present field.

The list of author's other publications, related to the thesis:

- I Metshein, Margus (2014). Alternatives of measurement of electrical bioimpedance of the body with the aim to determine the cardiac and respiratory activity. [Proceedings of the 14th Biennial Baltic Electronics Conference (BEC2014), 6–8 October, 2014, Tallinn, Estonia]: IEEE, 197–200.
- II Metshein, Margus; Parve, Toomas (2015). Electrical bioimpedance based monitoring of cardiac and respiratory activity: positioning of capacitive electrodes for wearable human monitoring device. [International Journal of Bioelectromagnetism 17 (2)]: 64–67.
- III Metshein, Margus; Gordon, Rauno (2016). On the possibility of detecting the electrical bioimpedance of human body by using non-contact electrodes in

- capacitive connection. [Proceedings of the 15th Biennial Baltic Electronics Conference (BEC2016), 3–5 October, 2016, Tallinn, Estonia]: IEEE, 171–174.
- IV Metshein, Margus (2016). Hardware imitation of the varying bioelectrical impedance for testing the device for measurement of the impedance of human trunk by using a JFET. [Proceedings of the 21st International Conference on Applied Electronics (AE 2016), 6–8 September, 2016, Pilsen, Czech Republic]: IEEE, 173–176.
 - V Annus, Paul; Min, Mart; Land, Raul; Märtens, Olev; Priidel, Eiko; Metshein, Margus (2017). "Patentne leitlus: Meetod ja seade vastussignaali erinevuste kvantimiseks sünkroonmõõtmisel" P201700023, 9.06.2017. (Method and device for quantization of the response signal differences during synchronous measurements).
 - VI Annus, Paul; Land, Raul; Priidel, Eiko; Metshein, Margus; Min, Mart; Märtens, Olev (2017). Quantization of the response signal differences for the electrical bioimpedance measurement. [IFMBE Proceedings Vol. 65 - Joint Conference of European Medical and Biological Engineering Conference (EMBEC'17) and Nordic-Baltic Conference on Biomedical Engineering and Medical Physics (NBC'17), 11–15 June, 2017, Tampere, Finland]: Springer Nature, 290–293.
 - VII Märtens, Olev; Min, Mart; Annus, Paul; Land, Raul; Krivošei, Andrei; Metshein, Margus (2018). PLL-based extraction of the cardiac component from the bio-impedance signal. [Proceedings of the 2018 IEEE International Instrumentation & Measurement Technology Conference (I²MTC2018), 14–17 May, 2018, Houston, USA]: IEEE, 1177–1182.

The results of this thesis have been and are subject to be presented at following conferences:

- A. Irish Signals and Systems Conference (ISSC), Carlow, Ireland, 2015.
- B. Joint Conference of European Medical and Biological Engineering Conference (EMBEC) and Nordic-Baltic Conference on Biomedical Engineering and Medical Physics (NBC), Tampere, Finland, 2017.
- C. Electronics, Palanga, Lithuania, 2017.
- D. International Instrumentation & Measurement Technology Conference (I²MTC), Houston, USA, 2018.
- E. World Congress on Medical Physics & Biomedical Engineering (IUPESM), Prague, Czech Republic, 2018.

Some of the results of this thesis have been included into the report of the EU ERA-NET FLAG-ERA 2016 project "CONVERGENCE" ("Frictionless energy efficient convergent wearables for healthcare and lifestyle applications") and some of the solutions proposed in this thesis have been introduced during this project. Some part of the research, introduced in this thesis have been implemented in the frames of project VEU17072 "Wearable robots for augmentation, assistance or substitution of human motor functions". Also, some of the results of this thesis have been included into the reports of ELIKO Competence Centre program project "ELIKO Competence Centre EU30017", incorporating the feasibility study of monitoring health status of wearer in cold sea areas and harsh environments and some of the solutions proposed in this thesis have been evaluated during this project.

Author's Contribution to the Publications

Contribution to the papers in this thesis are:

1. Phrased the research problem. Designed and implemented the measurement device in the form of the first electrode shirt. Planned and prepared the experimental measurement setup, performed the experiments, processed and analyzed the results, discussed the results, made the conclusions and wrote the paper.
2. Planned and performed the experiments, processed and analyzed the results, discussed the results and wrote the paper.
3. Designed, modelled and implemented the experimental electronic electrical bioimpedance measurement device. Designed and implemented the measurement devices in the form of electrode shirts. Planned and prepared the experimental measurement setup, performed the experiments, processed and analyzed the results, discussed the results, made the conclusions and wrote the paper.
4. Phrased the research problem. Planned and prepared the experimental measurement setup, performed the experiments (including the study on several volunteers). Processed and analyzed the results and wrote the paper.
5. Planned and prepared the experimental measurement setup, performed the experiments, processed and analyzed the results. Contributed to the discussion of the results and writing of the paper.

Introduction

Heart and respiratory rate are named among two others in the classical list of vital signs that are denoting the status of the body's life-sustaining functions. The measure of vital signs indicate the physical health of a man, though, the normal ranges vary related to the age, weight, gender etc. Also, they give indication of the diseases and disorders, proposing valuable access into the overall status of organism. It is clear that the monitoring of these signs is of the interest of individuals, medical personnel and, at the very top, of government bodies to achieve the preliminary data for predicting and improving public health.

Traditionally the monitoring of cardiorespiratory activity is done in a quiet room in the case of sitting patient. Nevertheless, together with the development of technology, the decrease in dimensions and increase in complexity of the devices for monitoring cardiorespiratory activity has happen. This has resulted in wearability of the devices, capable of monitoring the vital signs during everyday activities.

The main and tightly related obstacles related to the development of wearable devices are the motions of human body and the reliable (and comfortable) attachment of the devices for proposing wearability. The motions include the movements of limbs, head, thorax etc.; and also the inner movements, including the deformation of organs and contractions of muscles. Thereby, the processes of heart beating and breathing can also be considered as a movement: the changes in volumes of matter in organism.

Cardiac and respiratory activities are diverging in many aspects: the locations of the circulatory and respiratory systems in human body are different; the matter of the varying volume is different (air vs. blood) etc. The rhythmically pulsating amount of volume of blood in heart and arteries and the varying amount of volume of air in lungs that is caused by in- and exhalation may be of tenfold difference. In the sense of monitoring the desired volume changes, cardiac activity is present in majority of areas of the body, while respiratory activity is largely not. Accordingly, the placement of sensors for determining the volume changes, caused by these volume changes may differ.

In current thesis, couplings to the object of interest with the goal of monitoring cardiorespiratory activity are divided into three main groups: resistive (Figure 0.1a), capacitive (Figure 0.1b) and inductive (Figure 0.1c).

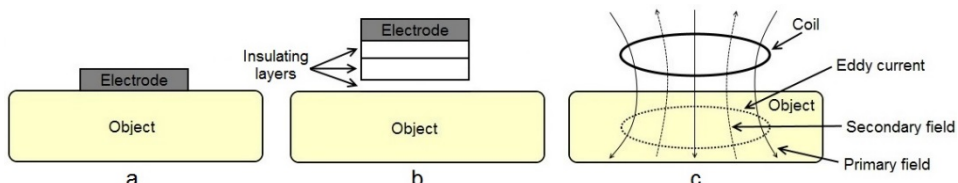


Figure 0.1 Illustration of the principles of coupling types on which the focus of current thesis is turned to: resistive (a), capacitive (b) and inductive (c)

In the sense of measuring the electrical bioimpedance (EBI), the classical coupling type is resistive. This classical approach is based on the use of direct contact electrodes that are constituting the galvanic contact with tissue electrolyte. Though, for measuring the EBI, the presence of galvanic contact is not obligatory—object may be excited by producing displacement currents as a product of time varying electric and magnetic fields. Similarly, the response can be measured by registering the displacement currents that are the products of secondary electric and magnetic fields, caused by the excited

object. These two types of non-galvanic contact are called capacitive and inductive couplings, capable of reflecting the volumetric changes in objects.

The focus of the research that is described in this thesis is balancing on the borderline of medical care and personal health monitoring. The implementation of the wearable devices, experimentations and relevant analyze, done in the cases of capacitive and inductive coupling to thoracic surface is incline on providing input to the development of personal wearable health monitoring devices. However, the focusing on local volume of wrist with the aim of establishing the means for improving the setup of resistively coupled electrodes for estimating the CAP in radial artery appertains in the shell of medical care. Even more, the experiments are performed as part of the project of EBI measurements and direct invasive aortic pressure recordings from number of voluntary patients, admitted to the Heart Centre of the East-Tallinn Central Hospital.

There are classical placements of electrodes for monitoring the impedance cardiography (ICG) and pneumography (IP) non-invasively by using the contact electrodes, declared to propose most linear response and superior access to cardiorespiratory activity. Despite this, the positioning of electrodes in the classical locations is not always possible and practical when looking through the prism of everyday or special clothing. Moreover, plain monitoring of pulse and respiratory rate does not require the output of the measurement device to be linear.

The utilization of direct contact electrodes have become an obstacle in the sense of continuous monitoring of cardiorespiratory activity because of the desire for unnoticeable and maximally comfortable solutions. Though, the alternatives in the form of capacitive and inductive coupling emerge the familiar group of problems, related to variety of movements of human body relative to the placement of electrode(s) that appear as changing distance between body surface and the sensor, effect of friction etc.

These problems have been tried to solve and have been conditionally solved. The sophisticated algorithms have been developed for separating cardiorespiratory activity from motion artifact; complicated filtering and modulation/demodulation schemes have been presented for detecting pulse and respiratory rate from high level background noise (Hoog Antink, Schulz, Leonhardt, & Walter, 2017); model based approaches have been introduced for decomposition of thoracic impedance variations into cardiac and respiratory components (Krivošei, 2009) etc. The modifications to construction of electrodes has been applied in vast scale to reduce the impact of movements and friction by adding a soft conductive layer in skin-electrode contact interface (Gruetzmann, Hansen, & Müller, 2007). The complex solutions by utilizing several measurement techniques to support the measurement of volume changes have been introduced, though transforming the devices bulky and overcomplicated (D. Teichmann, Foussier, Jia, Leonhardt, & Walter, 2013). To the best of my knowledge, there is no commercial wearable device that utilize capacitive measurement of impedance of human body for monitoring cardiorespiratory activity.

The following hypothesis can be set up: the dimensions, area and material of the electrodes influence the results of monitoring cardiorespiratory activity when measuring the EBI on thorax. Moreover, one can relate the measurability and the shape of the waveform of cardiac and respiratory activity to the placement of the electrodes on skin surface. The effect of varying frequency and amplitude of the excitation signal is presumed to affect the quality of the response of measured signal of cardiorespiratory activity. The utilization of capacitive coupling for mapping thoracic surface with the goal of determining the best combinations of large area electrodes, placed on outer surface

of ordinary cotton shirt is constituting a pioneering approach. The approach provided an option of evaluating the effect of concurrent movements of the body on the monitored signal of cardiorespiratory activity, when no special close-fitting garments have been used. The prior assumptions constitute the first major part of the thesis.

The prior hypothesis apply principally likewise on the utilization of inductive coupling. The exact configuration of coils, including the number of windings, diameter and shape is expected to have influence on the shape and degree of deepness of modulation in measured signal, caused by cardiorespiratory activity. The location of single coil on thoracic surface is assumed to have effect on the shape of measured cardiorespiratory waveform. Moreover, specifically to magnetic induction monitoring, the choice of resonant frequency and the deformation of the coils can be seen as possible variables for adjusting the access to the interesting signals. The novelty of performed research lies in the evaluation of Fo8 coils for determining cardiorespiratory, being typically used for transcranial magnetic stimulation. The description of practical experimentation and the outcomes of analyze of the results by using different coils in variety of positions on thoracic surface constitute the second main part of the thesis.

The third main part of this thesis focuses on monitoring pulse wave in radial artery by measuring the EBI of wrist during the utilization of resistive coupling. The study is somewhat different from the research done in the frames of two first major parts of this thesis, mainly because of the presence of single volume change in local volume. However, the appearing questions overlap, requiring the solutions to the problems of positioning of the electrodes relative to radial artery, the most suitable measurement setup and the characterization of the influence of anatomical differences of different individuals. By concentrating on radial artery, the current distributions in local volume of wrist can be explored by simplified models and the sensitivities predicted in order to find the most suitable positions of electrodes. As an outcome, a glow is thrown to researches where the current distribution is depicted to apply mainly on the electrically well conductive blood in radial artery and excluding the effect of surrounding tissues. On top of that the contribution appears, lying in the proposal of most suitable electrode placements of wrist surface for monitoring pulse wave by measuring the EBI. The outcome suggest supplementary data to already gained knowledge and proposes solution for specific task of determining the central aortic pressure (CAP) by measuring the time-varying EBI of radial artery.

I propose the possibility of using large area electrodes in capacitive connection for measuring the EBI with the goal of monitoring cardiorespiratory activity. Three electrode shirts, containing large area electrodes were designed and implemented which I verify to give access to pulse and respiratory rate. Based on the performed experiments, I ascertain the placements and configurations for large area electrodes that are most suitable for monitoring cardiorespiratory activity by measuring the EBI. I claim that the influence of motions is applying on the measured value of EBI with unequal power when detected from different positions on the body.

As a possible parallel application to EBI, I propose the placements for single coil on thoracic surface for monitoring cardiorespiratory activity in the case of inductive coupling. I claim the presence of variability in the case of influence of motions and the dependence of cardiorespiratory waveform when measuring the varying equivalent parallel resonance impedance of a single coil on top of body surface.

In order of granting access exclusively to cardiac activity and providing input to the improvement of electrode contact in the frames of CAP estimation, I propose solutions

of monitoring pulse wave in radial artery by using the measurements of EBI. Based on practical experimentation I propose the most suitable placements and configuration of electrodes on the surface of wrist for monitoring the interesting physiological process. I claim that there is an optimal point of externally applied pressure on the resistively coupled EBI measuring electrodes that result on average as the highest modulation on measured signal, caused by pulse wave. I demonstrate the vast effect of displacement of small area electrodes relative to the location of radial artery.

The scientific contributions of this thesis are phrased in the following listing:

- A. The determination of placements and configurations of large area electrodes on thoracic surface that propose the best outcome in the case of monitoring cardiorespiratory activity by using capacitive coupling.
- B. The verification of the electrode placements and configurations that propose less influence of concurrent movements of the body in the case of measuring the EBI for monitoring cardiorespiratory activity by using capacitive coupling.
- C. The confirmation of the variations in the shape of the monitored cardiorespiratory waveform, depending on the placement of a single coil on thoracic surface in the case of inductive coupling to thorax.
- D. The experimental proof of the differences in the effect of O shaped and figure-of-eight (Fo8) shaped coils on the results of determination of cardiorespiratory activity in the case of inductive coupling to thorax.
- E. The determination of the positions and configurations of resistively coupled EBI measuring electrodes on wrist that propose the best access to the data of highest time varying change of blood volume, representing pulse wave in order to gain the signal of best possible quality.
- F. The characterization of the effect of externally applied pressure on resistively coupled EBI measuring electrodes that are positioned on top of the location of radial artery in the case of several subjects on the monitored signal of pulse wave and the determination of the optimal pressure point.
- G. The demonstration of destructive effect of displacement of small area in-line placed resistively coupled EBI measuring electrodes relative to the location of radial artery in both lateral directions in the case of distal placement more than 5 mm on the monitored signal of pulse wave.

Table 0.1 Contribution matrix of this PhD work

Contributions	Paper I	Paper II	Paper III	Paper IV	Paper V	Thesis
A	✓		✓			
B	✓		✓			
C		✓				
D						✓
E					✓	
F				✓	✓	
G				✓		

Historical Perspective

The documented roots of monitoring cardiorespiratory activity reach to the ancient times. This is suggested already in ancient Egyptian medicine that there is a relationship between the heart beat and peripheral circulation. Also, the respiratory activity is named in the oldest medical textbooks that is known—Ebers Papyrus (c. 1500 BC) (Gandevia, 1970).

The importance of the arterial pulse was discern in ancient China, where the theory of pulse was based upon the various stages of interaction between Yin and Yang. The ancient Chinese physicians were capable of judging the state of disease by the four main varieties of pulse beats: superficial, deep, slow and quick (Curran, 2008). Moreover, the ratio between the beating pulse and breathing was used evaluated to assess the state of health – the normal ratio was considered to be four beats to one breathing.

The same importance was attached to pulse in ancient India, examined also as a part of Ayurvedic medicine (Lad, 2006). An ancient Indian physician Sage Kanada (600 BCE) described in his book “Science of Sphygmica” the variety of pulses during different physiological and pathological states (Ghasemzadeh & Zafari, 2011).

In Hindu culture and medicine, the respiration has huge importance—largely related to the philosophy and practice of Yoga. This included the training of the regulation of respiration by breathing exercises based on the following knowledge that emotions influence breathing (Gandevia, 1970).

Development continued during the Hellenistic period, Roman Empire and Medieval Age, where the knowledge concerning the mechanics of cardiovascular and respiratory systems was improved.

Nevertheless, the first device with the capability of monitoring the action of the vessel and visualizing pulse wave in numerical scale was invented by Jules Herisson, called the sphygmometer (Herisson, 1834). The semiglobular end of the device was placed over an artery and pulse wave was visualized on the scale on the glass tube filled with mercury. The author described the correlation between the sphygmometric findings related to observations related to different valvular heart diseases. This was the first time, when the cardiac mechanics have been associated to objective findings of a device (Ghasemzadeh & Zafari, 2011).

The first documented wearable device for monitoring cardiac activity in the form of arterial pulse was constructed by French physiologist Étienne-Jules Marey (1830-1904) in 1860, called the sphygmometer with the capability of graphic recording (Ghasemzadeh & Zafari, 2011). The principle of the device included the application of a needle onto artery and recording the ballistographic movement.

The first scientific experiments on respiration were performed by Strato of Lampsacus (c. 335–269 BC) where he demonstrated that the air could be forced through a large rigid container that is filled with water, by blowing the air in or sucking it out (Farrington, 1981).

Overview of the Methods and Technologies

The progress is inherent in all of the occupancies of a man, exhibiting the desire for unending development through new discoveries and inventions. The solutions for monitoring cardiorespiratory activity is no exception, revealing in development of increasingly complex algorithms for signal processing and in growing capability of the devices for measuring the interesting signals. Though, the pioneering discoveries in the field of monitoring the volume changes that are reflecting cardiorespiratory activity have been reported already in the first half of 19th century, the first experimental devices were clumsy. Since that time, in correlation with the developments in technology and science, the methods have been sophisticated and devices have become smaller. Moreover, the elaborate structure and functions of human body has been researched extensively in the frames of monitoring cardiorespiratory activity.

The property of wearability sets limitations to the technologies and methods that can be utilized in wearable solutions of monitoring cardiorespiratory activity. As, ideally, the wearable solutions are defined to be unnoticeable and not to disturb daily activities (depending on the application), the size and weight play crucial role. Still, several technologies and methods propose opportunities in the form of measurement principles and techniques to be included into wearable devices. The methods can be categorized in number of ways—for example: physical contact requiring methods and no physical contact requiring methods; near and remote monitoring methods. Alternatively, this can be done based on the utilized method:

- electrical,
- electromagnetic,
- acoustic,
- light-based (optical),
- volumetric-based,
- image-based,
- composition-based.

Electrical-based methods.

A well-known solution for monitoring the cardiac activity is the detection of the electrical activity of heart i.e. electrocardiography (ECG)—falling into the category of electrical methods. ECG is measured by using the standard 12-lead configuration or, as typical for wearable devices, by following the Einthoven's triangle (Gorgels, 2007). This basic method presumes the attachment of the electrodes on the skin, either directly or in capacitive contact (A. Ueno et al., 2007). Respiratory activity can be extracted from ECG, requiring signal processing—a thorough work on this field is available in (Charlton et al., 2017). The extraction of respiratory activity from ECG is still an emerging field, possessing the concerns related to the real and extracted respiration waveform and errors that are originated from motion artifacts (Zhao, Li, & Tsien, 2015). The disadvantage of direct contact ECG is the possible skin irritation and unsuitability for long-term monitoring. In the case of non-contact monitoring of ECG, the high skin-electrode contact impedance makes the setup sensitive to motion artifacts (Zhao et al., 2015).

ECG has shown to be available by using capacitive electrodes according to Einthoven's triangle in number of publications (Arcelus, Sardar, & Mihailidis, 2013; Chi & Cauwenberghs, 2010; L. F. Wang et al., 2013). Though, the problems arise due to the

lateral and transversal movements between the electrode and skin surface (Arcelus et al., 2013). The problem hereby is somewhat simpler because of the difference between the one-sided monitoring of bioelectric signals (endogenic signal source) and the signals that respond to externally applied electrical stimulus (exogenic signal source). In first case, only the measuring has to be performed, but in another case, two tasks have to be solved correspondingly: excitation and measuring. The impedance measurements in the case of capacitive monitoring of ECG have been reported in literature (Eilebrecht, Willkomm, Pohl, Wartzek, & Leonhardt, 2013), though with the goal of determining and collecting the information of movements in between skin and electrode through the varying value of measured impedance.

IPG, including ICG and IP fall into the same category, reflecting the volume changes in human body, caused by cardiorespiratory activity. These methods are based on the measurement of EBI i.e. by applying the electric current (or voltage) in chosen frequency range onto the volume conductor and measuring the response—thoroughly described in Section 1.2. The disadvantage of EBI measurement is the changing properties of biological objects in time. The changes in the humidity of surrounding air causes the impedance of the skin to change with sweating and temperature (Zhao et al., 2015).

There are several attempts and, even more, successful implementations of devices that exploit the technique of measuring the EBI for following cardiorespiratory activity with the goal of gathering, analyzing and representing the interesting data. Though, the measured variable may be presented sometimes in related units like the measurement of capacitance between large electrode plates when chest that is located in between for monitoring the respiratory rate (Kundu, Kumagai, & Sasaki, 2013). Moreover, the measured variable may be the changing frequency of a simple oscillatory circuit, caused by the change of the value of one of the circuit elements like capacitance (Oum, Lee, Kim, & Hong, 2008). These simple designs are typically used just for monitoring pulse and respiratory rate and are based on some commercially available capacitance-to-digital IC's. In order to monitor cardiorespiratory activity with the goal of gaining access into the physiological signals that would contain further data, related to the condition of circulatory and respiratory systems and possible diseases, the measurement of total impedance can be performed.

The utilization of EBI measurements for monitoring the status and vital signs of human body has been and still is a popular field of research. The reasons can be found from the capability of gaining access into a number of cardiodynamic and respiratory-related parameters which contain information about health. Another reason is the potential of the technology that reveals in unsolved concerns like the decomposition of the variations of EBI into cardiac and respiratory components; suppression of motion artifacts; uncertainties that arise from the connection to the skin surface in the case of contact measurements etc. Because of the enumerated problems, the implementation in the composition of commercial devices is complicated and typically requires direct electrical (Cañadas, Dell'Aquila, & Laciár, 2016; Młyńczak, Niewiadomski, Żyliński, & Cybulski, 2014). Direct electrical contact is achieved, in turn, typically by using the standard ECG electrodes which is suitable in the case of minimally moving patient under hospitalized treatment or in special short-term activities like diving or parachute jump. The development in the field of electrodes has disclosed other materials like foils, conductive rubber (Muhlsteff & Such, 2004), conductive fabrics (Merritt, Nagle, & Grant, 2009), textiles (Stoppa & Chiolerio, 2014) and different conductive polymeric materials

(Cunico, Marquez, Hilke, Skrifvars, & Seoane, 2013), though, utilized in direct contact to the object for EBI measurements.

The electrical-based methods gather also the approaches of using variety of oscillatory circuits like Colpitts oscillator (D. Teichmann et al., 2013), applied in a way that a change in electrical properties of body changes a component in oscillatory circuit (capacitor or inductor). Another solution is to detect the phase shift that is caused by the changes in the volume of lungs during respiration (Watzek, Weyer, & Leonhardt, 2011).

Electromagnetic-based methods.

The electromagnetic based methods embrace the magnetic induction monitoring of biological events by inducing the eddy current in an object and measuring the emerging secondary magnetic field(s)—introduced in 1967 by Vas et al (Vas, 1967). Inductive coupling is prone to several physical movements: change in the distance between the coil and body surface, deformation of the coil etc. Additionally, the solutions for monitoring cardiorespiratory activity based on radars fall also into this category, consisting of two main subcategories: continuous wave and ultra-wideband radar (Zito et al., 2008). The main idea of both is the same: emitting the stream of electromagnetic radiation and detecting, filtering and analyzing the reflecting energy (Scalise, 2012). The development of the radars for monitoring cardiorespiratory activity has lead already to the development of specialized integrated circuits, capable of sensing the heart beating in the composition of a portable device (Kao, Chen, Yan, Shen, & Lin, 2012). Radars are very sensitive to movements and the extraction of the interesting data from the gathered waveform of cardiac activity presumes the knowledge of the presence and the thickness of biological layers in the object.

Acoustic-based methods.

However, the phonocardiography, which principle is to listen (record) the heart originated sounds, has reached to smart phone related acoustic applications. Classically, there are defined two fundamental and easily recognizable heart sounds: S1, which occurs at the beginning of ventricular contraction; and S2, which is shorter and arises and is caused by the closure of the aortic and pulmonary valves. In a simple solution, the acoustic sounds are converted into electrical signals, for example, by using a microphone, processed by using the desired tools and plotted as phonocardiogram (Thoms, Colicchia, & Girwidz, 2017). Wearable body sensor networks, containing phonocardiography, have been reported – for example, a flexible tag that is capable of detecting the pulse (Mandal, Turicchia, & Sarpeshkar, 2010). The disadvantages of this method are the need for direct contact and the unsuitability for long term measurements (Zhao et al., 2015).

Light-based methods.

Light based methods can be divided into two categories: the direct use if light emitting and sensing devices to light the object or using optical fibers which parameters vary, caused by deformations. From optical methods, the photoplethysmography (PPG) is the most widely known and used technique. This simple technique uses the illumination of the body tissue (including skin) and measures the changes in light intensity, caused by the changes in perfusion in the catchment volume. A PPG device requires only few optoelectronic components: a light source, typically in the form of light-emitting diode and photodetector, which, in very simple case is just a photodiode (Allen, 2007). As a result, cardiac activity can be detected by obeying the following phenomenon: the greater the blood volume, the more the light is attenuated. In addition, a latest work proposes an approach of extracting also the breathing rate from PPG (Charlton et al., 2017). The usage

of lasers has gained popularity since the first experiments with bulky laser interferometers to today's solutions of laser Doppler (optical) vibrometry—which, although, have not reached to become as wearable solutions yet. The usage of optical fibers on the other hand propose a solution, where the deformation of coils (change of radius), made of optical fibers, caused by the movement of body surface, present a loss effect that has influence on transmitted optical power (Augousti, Maletras, & Mason, 2005). The variations in the selected parameter reflect the bending radius of the fiber-optic coil, caused e.g. by the thoracic movements (Krehel et al., 2014).

Volumetric-based methods.

Another approach for detecting cardiorespiratory activity is the monitoring of the volumetric changes of the body of human. Very generally, during the employment of this approach, the acceleration that is caused by the occurrence of the volumetric change, the pressure that is caused by this change of volume is transformed into an electric signal by changing some physical property of sensor. In literature, there are described variety of sensors that have been used to play this role. Piezo-resistive sensors have been reported to be utilized for monitoring cardiorespiratory activity, measuring the pressure that is applied to the sensor. In more detail, the expansion of thorax during the respiratory activity and the ballistic forces, that are caused by the repetitive motions of the body, arising from the ejection of blood into aorta and pulmonary artery during each heart cycle, are transformed to modulation of measured resistance of the sensor (Hamdani & Fernando, 2015). There are number of piezoelectric materials that have been used to monitor cardiorespiratory activity: multilayered polypropylene films like ElectroMechanical film (EMFi) (Karki, Kaariainen, & Lekkala, 2007), polymer films like polyvinylidene fluoride (PVDF) (Zuckerwar, Pretlow, Stoughton, & Baker, 1993) etc. Or a capacitor-like structure that is connected to a belt which is attached around thorax and which plates overlap varies together with the capacitance in correlation with in- and exhalation (Grlica, Martinović, & Džapo, 2015). Another possibility is to use the accelerometers and gyroscopes to detect the periodical movements of thorax for the access to the respiratory activity (Hung, Bonnet, Guillemaud, Castelli, & Yen, 2008); by placing the named sensors on wrist (Hernandez, McDuff, & Picard, 2015) or by placing the accelerometer directly above the carotid artery (Muehlsteff et al., 2015). As a classical device for monitoring the respiratory activity, the spirometer has to be noted. The principle of this device includes a turbine, which direction of rotation alternates depending on the cycle of breathing: inhalation or exhalation.

The clinical pressure detecting methods are realized typically in the form of on-desk medical devices, capable of monitoring the central arterial pressure waveform. A much used non-invasive method today is the applanation tonometry—a method, during which the strain gauge pressure sensor is placed over the radial artery and the modulation of pressure is detected. Within the procedure, gentle pressure is applied over the radial artery during which a slight flattening of artery takes place (Nelson et al., 2010). The pressure in artery (i.e. the peripheral blood pressure) is transmitted to the sensor and, by using special algorithms, the CAP is estimated (US20100016736 A1, 2010; Krivošei et al., 2013). However, the monitoring of blood pressure in radial artery by using a hand-held tonometer requires trained medical personnel to achieve repeatable results and, even in this case, may take time depending on the thickness of superficial layers of wrist that influences the visibility of radial artery (Min et al., 2017).

Image-based methods.

Image recording and processing constitutes a separate method for detecting cardiac and respiratory activity, basing on collection of images or video stream and the real time of subsequent analyze. The approach may contain recording of video stream of visually recognizable markers on abdomen of subject that are rhythmically moving because of the respiratory activity and the following processing of the gathered data (Wiesner & Yaniv, 2007). Or a more sophisticated real-time human chest movement video processing with the goal of following the respiratory parameters of human (Tan, Saatchi, Elphick, & Burke, 2010). For daily monitoring of pulse rate by using a web camera has been proposed in (Poh, McDuff, & Picard, 2010). Typically, the devices for image-based methods in the form of video cameras are bulky and not suitable for incorporation into wearable monitoring devices.

Composition-based methods.

An option in the monitoring of respiratory activity is the detection of the composition and temperature of the air in the upper respiratory tract. The exhaled air is warmer, with higher humidity and contains more CO₂ than the inhaled air. The proposed solutions contain the attachment of nasal thermistor (Storck, Karlsson, Ask, & Loyd, 1996) and measuring the concentration of CO₂ (J. Yang, Chen, Zhou, & Lv, 2015). The measuring of the levels of CO₂ in expired gas is called capnography (Care, 2003).

Complex solutions of different methods.

Complex solutions are gaining more and more attention nowadays, proposing the possibility of monitoring the vital signs and other interesting events simultaneously by using several methods: ECG, IP, PPG, temperature monitoring, acceleration, piezoelectric sensors etc. (Mundt et al., 2005; Vuorela, Seppä, Vanhala, & Hyttinen, 2010). The incorporation of selection of sensors into garment has been investigated and implemented during the development of health monitoring systems named WEALTHY (Paradiso, Loriga, Taccini, Gemignani, & Ghelarducci, 2005), MyHeart (Luprano, Sola, Dasen, Koller, & Chetelat, 2006) and HeartCycle (Luprano et al., 2013). In the case of WEALTHY, the fabric electrodes of relatively small area in direct contact to skin surface have been used to monitor the IP—incorporated into skin-tight suit. Larger investigation of fabric electrodes has been reported to be implemented during the development of HeartCycle and IMPACT shirt projects, where the monitoring of ICG was performed, though, the direct contact was presumed. Or, the complex monitoring through layers of textile by using the magnetic induction and PPG, being, though, sensitive to motions (D. Teichmann, Matteis, Bartelt, Walter, & Leonhardt, 2015). Complex solutions hold its positions in the field of wearable devices, proposing an option of following greater number of parameters. However, this comes with the price of increasing complexity in signal processing and decision making in the level of microcomputer—depending on the desired output.

Problem Statement and Objectives

The volumetric changes in organism, caused by cardiorespiratory activity are accessible by applying stimulation on object and measuring the response. The variety of techniques, containing the described approach proposes number of choices that include the questions of selection of sensor placement, structure, dimensions etc. – influencing expectedly the accessibility and content of the interesting signal. Moreover, the locations of corresponding organs, the amounts of natural volume changes and the matter of changing volume are different. The effect of motions of object onto the sensors, and thereby, simultaneously on the measured signal is expected. Even more, the choice of connection type may be prescribed by predefined requirements: either to utilize the resistive, capacitive or inductive coupling. Each coupling type causes additional concerns related to undesirable current density distribution, non-linear response etc.

To address the described challenges, the experimental measurements by utilizing resistive, capacitive and inductive sensors of different physical parameters and dimensions are required to perform. This, in turn, implies the design and development of wearable experimental instrumentation to verify the most suitable configurations for monitoring cardiorespiratory activity by utilizing resistive, capacitive and inductive coupling.

The overall goal is to design, implement and evaluate components of wearable systems for monitoring cardiorespiratory activity.

The principle objective is to provide the best possible signal, containing the information of cardiorespiratory activity.

The main tasks of this thesis are rephrased as follows:

- A. To investigate the potentiality of monitoring cardiorespiratory activity by using the capacitive, resistive and inductive coupling.
- B. To develop and implement wearable experimental measurement devices with the goal of determining the most suitable placements and configurations of electrodes for monitoring cardiorespiratory activity in the case of capacitive coupling.
- C. To design and implement flexible coils of different shapes with the goal of experimentally determining the most suitable positions on thoracic surface for monitoring cardiorespiratory activity in the case of inductive coupling.
- D. To experimentally determine the most suitable placements and configurations of electrodes for monitoring pulse wave in radial artery in the case of resistive coupling.

This thesis focuses on answering the following research questions:

1. Which are the most suitable placements and configurations of large area electrodes for monitoring cardiorespiratory in the case of using capacitive coupling?
2. Which are the placements and configurations of large area electrodes that experience less influence from the motions of the body in the case of using capacitive coupling?

3. Can cardiorespiratory activity be monitored by using capacitive coupling in the case of concurrent movements of human body?
4. Does the exact position of single coil on thoracic surface influence the shape of cardiorespiratory waveform in the case of inductive coupling?
5. Which are the most suitable positions of single coil on thoracic surface for monitoring cardiorespiratory activity by using inductive coupling?
6. Which are the positions of single coil that experience less influence from the motions of the body in the case of using inductive coupling?
7. Can cardiorespiratory activity be monitored by using inductive coupling in the case of concurrent movements of human body?
8. Are the different shapes of coils influencing the selection of position that is most suitable for monitoring cardiorespiratory activity in the case of inductive coupling?
9. Which are the most suitable placements and configurations of electrodes on the surface of wrist for monitoring pulse wave by using resistive coupling?
10. What influence does the positioning of small surface area circular electrodes which diameter is comparable to the diameter of radial artery relative to the location of radial artery have on the measurability and shape of pulse wave?
11. What effect does the individual anatomical differences have on the detectability of pulse wave in radial artery in the case of measurements of EBI by using resistive coupling?
12. Does the exploitation of externally applied pressure on the electrodes on top of the location of radial artery have effect on the measured signal of pulse wave in the case of measuring the EBI by using resistive coupling?

Abbreviations

AC	Alternating Current
BIA	Bioimpedance Analysys
CAP	Central Aortic Pressure
CPE	Constant Phase Element
CS	Current Source
DC	Direct Current
DRT	Distribution of Relaxation Times
ECG	Electrocardiography
EBI	Electrical Bioimpedance
EPC	Electrode Placement Configuration
ES1	Electrode Shirt no. 1
ES2	Electrode Shirt no. 2
ES3	Electrode Shirt no. 3
FEM	Finite Element Method
FIM	Focused Impedance Measurement
Fo8	Figure-of-Eight
HF	High Frequency
ICA	Invasive Coronary Arteriography
ICG	Impedance Cardiography
IHP	Inner Helmholtz Plane
IP	Impedance Pneumography
IPG	Impedance Plethysmography
LVET	Left-Ventricular Ejection Time
OHP	Outer Helmholtz Plane
PAT	Pulse Arrival Time
PCB	Printed Circuit Board
PEP	Pre-Ejection Period
PPG	Photoplethysmography
PT	Propagation Time
PTT	Pulse Transit Time
PWV	Pulse Wave Velocity
SMAR	Signal-to-(motion) Artifact Ratio
SCMIS	Single Coil Magnetic Induction Sensor
SV	Stroke Volume
TF	Transfer Function
TMS	Transcranial Magnetic Stimulation
VHF	Very High Frequency

1 Background

Monitoring of cardiorespiratory activity necessitates the prior knowledge of the composition and the behavior of human body in the case of externally applied stimulus. As the response of biological structures to externally applied electrical stimulus depends on number of factors, the understanding of basic physical concepts of electricity is supported. The principles of measuring the EBI together with the theory of electrodes that constitutes the environment of shift from electronic to ionic conduction and vice versa gains great attention. This chapter targets to provide the overview of the interesting physiological events in living organisms together with the technological concepts that are crucial for understanding the research that is described in this thesis.

The Section 1.1 introduces the essential in characterization of biological tissues in the frames of measuring the EBI.

The Section 1.2 presents the composition and structure of human body with the aim of enlighten the source of cardiorespiratory impedance signal.

The Section 1.3 deals with the basic techniques for gathering cardiorespiratory impedance signals, illustrated with the explanations of the interesting cardiopulmonary data that can be acquired from the waveforms.

The Section 1.4 gives overview of EBI measurement electrodes types and constructions with the focus on the connection to the skin surface.

In the Section 1.5 the related basics of monitoring cardiorespiratory activity in human body is summarized.

1.1 Analyze of Electrical Properties

All (biological) objects can be described according to their passive electrical properties, releasing the information of their content and structure. The measurement of opposition of the material to an externally applied electrical stimulus is called the electrical impedance, expressing the data of magnitude and phase. For the visual representation of impedance, the phasor diagrams can be utilized, constituting the model based approach of representation of biological objects.

1.1.1 Electrical impedance

Electrical impedance shows the ratio between voltage and current, applied in both cases: DC and AC. If DC is exploited, the current flow is inhibited by purely resistive component—caused by the collisions of charged particles and the structure of the matter. In the case of AC, the current flow is inhibited by accompanying reactive component—caused by voltages that are induced in the matter by self-induced magnetic fields and electrostatic phenomenon of storage of charge by capacitive elements in the matter during the flow of AC. The influence of reactance on current flow is analogous to resistance, nevertheless, the frequency dependency is introduced:

$$X = -\frac{1}{2\pi f C} \quad (1)$$

where X is the reactance and f is the frequency. AC voltage that applies across the ideal capacitive element as a result to current flowing through it, is 90° out of phase—in opposite to ideal resistive element that exhibits in-phase properties. The voltage lags

the applied current, caused by the repeated charging and discharging of plates of capacitor. In a circuit, where there are both elements present, the phase difference is somewhere in between 0° and 90° , depending on the actual values. The electrical impedance is deduced from Ohm's law and can be expressed by

$$Z = R + jX = Re Z + jIm Z \quad (2)$$

where Z is the impedance and j is the imaginary unit ($j = \sqrt{-1}$). As it can be seen, it is possible to divide impedance Z into real ($Re Z$) and imaginary part ($Im Z$). The length of vector $|Z|$ can be represented by

$$|Z| = \sqrt{Re Z^2 + Im Z^2} \quad (3)$$

and phase angle can be given by

$$\phi = \arctan(Im \dot{Z} / Re \dot{Z}). \quad (4)$$

The resulting vector in Cartesian coordinate system can be seen in Figure 1.1.

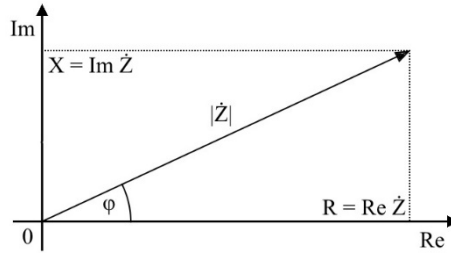


Figure 1.1 The impedance vector with its real and imaginary parts

1.1.2 Phasor diagrams of RC circuits

For mathematical representation of the terms “in-phase” and “out-of-phase” and visualization of angular or phasor differences between two or more sinusoidal waveforms, it is common to use phasor diagram (also called Wessel diagram). In phasor diagram, a rotating vector, representing a scaled line, which length denotes the AC quantity with defined magnitude and direction at some point of time, is presented.

The impedance of simplest series RC circuit can be expressed by

$$Z = R - \frac{1}{j\omega C}. \quad (5)$$

If the $Re Z$ and the $Im Z$ are known, impedance Z can be calculated at any frequency—this is because the impedance values on a complex plane overlap a straight line that is parallel to the imaginary axis. This line is at a distance of the value of R of imaginary axis, starting from $-\infty$ (when $\omega = 0$) and ending at real axis at R when $\omega = \infty$. This means that the voltage, being the dependent variable, is lagging current (since $i = C(du/dt)$). The reactance of the capacitance C in a circuit is expressed as $Im \dot{Z} = -1/j\omega C$, i.e. the phase angle ϕ is negative. The $-$ sign can be shown in phasor diagrams in front of the axis

name near the imaginary axis, denoting the fact that the phasor diagram is mirror to x-axis in the first quadrant of Cartesian coordinate system (Figure 1.2).

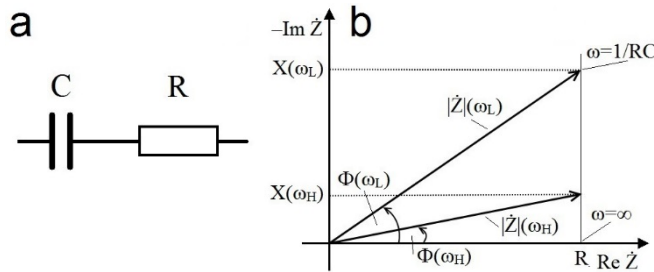


Figure 1.2 Serial RC circuit (a) and its phasor diagram (b)

In the case of a circuit, where the third element is included, the behavior of the phasor diagram becomes more complicated. For example, by adding a resistor in parallel with serial connection of RC. For characterizing such a circuit, it is not enough to carry out single measurement at single frequency. The vector diagram constitutes a semi-circular line, denoting the frequency for rotating vector (Figure 1.3).

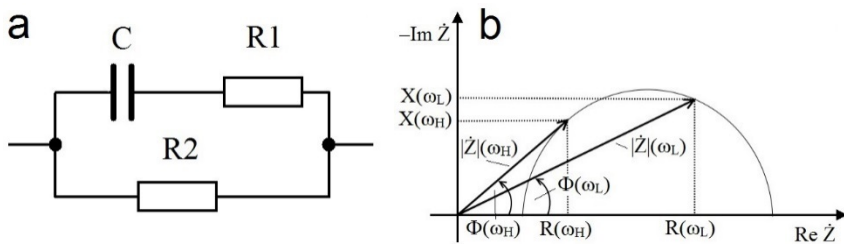


Figure 1.3 Serial 2R-1C circuit (a) and its phasor diagram (b)

This presentation of frequency dependence is called as Cole plot, showing the real versus imaginary parts of the circuit impedance. Biological objects consists principally more than three components, altering the characterization of the measured data even more complicated. The complicated models of biological objects can be simplified to serial and parallel RC circuits that contain two or three elements. The inverse variable to impedance is admittance that can be expressed in its complex form by

$$Y = \frac{1}{Z} = \text{Re } Y + j\text{Im } Y = G + jB \quad (6)$$

where G is the conductance and B is the susceptance. Both described interpretations of the electrical properties of objects are used in scientific literature and the choice is made according to the measurement setup and the ease of calculations.

1.1.3 Electrical bioimpedance

The EBI is used to describe the response of the living organism or its parts to an externally applied electrical current or voltage (Grimnes & Martinsen, 2008). It shows the ratio between voltage and current, representing the opposition of the biological matter (tissue) to flow of electrical current. The employment of measurement of EBI is utilized

with the goal of following the biological processes and determining the composition of living organisms. Biological objects are complicated in the sense of its structure—this causes the complicity also to the equivalent circuits that are used in modelling.

Cell membrane separates the extra- and intracellular fluid and because of its building stones—bilayer lipid—can be considered to be dielectric. Besides presenting this passive role, membrane contains ionic channels and pumps that allow some ions to flow from one cell to another one—constituting resistive gateways to current carriers (Grimnes & Martinsen, 2008). For the above stated reason, the cell membrane can be depicted as two plated capacitor C_m that is connected together with a parallel resistor R_m (Figure 1.4). By knowing that at the same time the extra- and intracellular fluid act as resistors R_e and R_i , the cell can be described in electrical point of view by using an equivalent circuit.

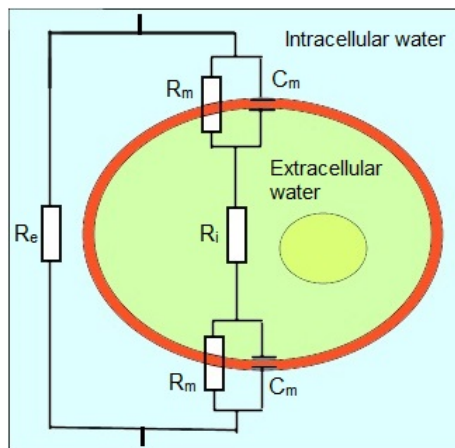


Figure 1.4 Drawing of a single cell and its expected equivalent circuit

Simplification can be done for the model in Figure 1.4 by merging the resistors in series and capacitors in parallel (Figure 1.5a). Moreover, as the membrane of the cell behaves mostly as dielectric, further simplifications can be done by discarding the parallel resistance R_m —called as the Fricke-Morse model (Figure 1.5b).

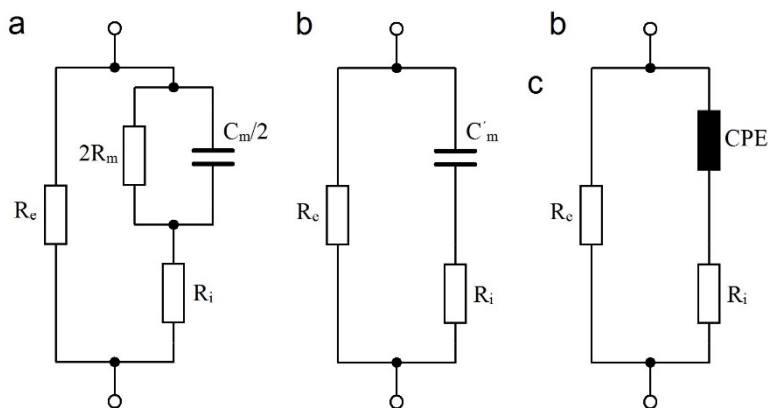


Figure 1.5 Equivalent circuit for single cell: simplified model (a), Fricke-Morse model (b) and Cole model (c)

The relationship between the impedance $Z(j\omega)$ and the values of elements in the simplified equivalent circuit at arbitrary frequency can be calculated by

$$Z(j\omega) = \frac{R_e(R_i + 1/j\omega C_m)}{R_e + (R_i + 1/j\omega C_m)}. \quad (7)$$

However, in the case of tissues, the circumstance of the presence of several cells has to be taken into account. Cells in tissue are of wide variety of dimensions and are located randomly—this property can be described by heterogeneity anisotropy. The above described frequency dependence of current flow in this medium is depicted in Figure 1.6.

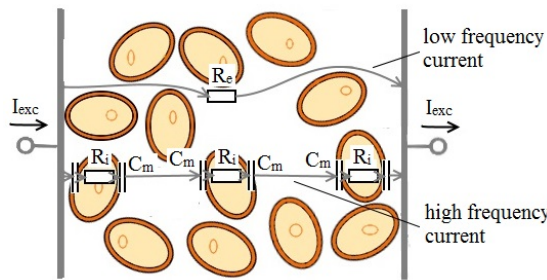


Figure 1.6 Current paths in tissue in the cases of low and high frequency

At low frequencies ($\omega \rightarrow 0$), the current flows in its majority in extracellular space because of the capacitive properties of cell membranes, meaning that $Z = R_e$. At high frequencies ($\omega \rightarrow \infty$), the capacitive effect is reduced and current can flow through the whole tissue, revealing as

$$Z = \frac{R_e R_i}{R_e + R_i}. \quad (8)$$

Nevertheless, the developments in the field of characterization of electrical properties of living organism showed that the correct derivation of complex permittivity cannot be obtained by using Debye's concept of relaxation of polarized molecules. Debye's concept anticipates that a group of cells (e.g. tissue) is composed of many single-time relaxations (Kuang & Nelson, 1998) (described in Paragraph 1.2.1). This is possessing a rare case—in most of the cases, however, they are exhibiting a certain non-symmetrical distribution of relaxation times (DRT), supported by the dispersion concept (Grimnes & Martinsen, 2008) (see the Paragraph 1.2.3).

Solution was proposed in (Cole & Cole, 1941) by Kenneth S. Cole and Robert H. Cole, where they added an additional parameter α into Debye's concept, revealing in

$$\varepsilon(\omega) = \varepsilon_\infty + \frac{\varepsilon_0 - \varepsilon_\infty}{(1 + j\omega\tau_0)^{1-\alpha}}. \quad (9)$$

Parameter α obtains the values in the range of $0 \leq \alpha \leq 1$, denoting the displacement of center of the circular line below the real axis in impedance phasor diagram, resulting in flatter line of semicircular arc. The addition of parameter α supposed the description of so-called constant phase element (CPE) to depict the effective non-ideal capacitor instead of ideal capacitor (in the case of $\alpha = 1$) in Debye's model. The Cole-

Cole equation is expected to correspond to certain DRT, which is reported not to be the only one—there are other DRT's that match the measured tissue values as well (Grimnes & Martinsen, 2008).

The dependence of impedance to frequency (due to the capacitive effects of cell membranes) was later rewritten in Cole-Cole equation

$$Z = R_\infty + \frac{R_0 - R_\infty}{1 + (j\omega\tau_0)^\alpha}. \quad (10)$$

The impedance of CPE reveals as

$$Z_{CPE} = \frac{1}{(j\omega C)^\alpha} \quad (11)$$

in the case where in Fricke-Morse model (Figure 1.5b) the capacitance C_m' is replaced by CPE, constituting the Cole model (Figure 1.5c). The Cole model is not fully accurate, though popular because of its simple mathematical representation.

1.1.4 Effect of geometry of object in EBI measurement

In the sense of volume conductors, the geometrical aspect together with the inhomogeneities of biological tissues has to be taken into account. In human body, there are bones and organs like liver, stomach, heart, lungs etc., which can't be model by simple parallel RC equivalent circuit. Instead, one can look the flow of electric current in volume conductor as a distribution of charged particles, constituting a lead field (which is vector field). In an inhomogeneous object, the flow of charged particles prefers to finds its way through the layers of lower impedance. The same is corresponding also to the voltage lead field \mathbf{J}_{LE} , being interchangeable to current lead field \mathbf{J}_L and together they constitute the sensitivity field \mathbf{S} (Geselowitz, 1971) (which is scalar field), revealing in

$$\mathbf{S} = \mathbf{J}_L \cdot \mathbf{J}_{LE} \quad (12)$$

The impedance of volume conductor is defined as follows (Lehr, 1972)

$$Z = \int_V \rho \mathbf{S} dV \quad (13)$$

where V is the volume, ρ is the resistivity of volume conductor. This theoretical description gives rise to the discussion concerning the formulation of sensitivity field in volume conductor. In the case of two-electrode system (Paragraph 1.4.2) where the excitation and measurement is done by using the same pair of electrodes, the \mathbf{J}_{LE} and \mathbf{J}_L are uniform and \mathbf{S} is positive. In the case of four-electrode system (Paragraph 1.4.2), where the excitation and measurement is done by using separate pair of electrode, the sensitivity fields may form, besides positive, the areas of zero and negative sensitivity.

The zero conductivity in volume conductor appears if the fields are perpendicular (90°) or only a single field if present. The negative sensitivity in volume conductor appears if the fields are overlapping with the degree of more than 90° . In the case of the presence of the areas of negative sensitivity the impedance denotes the decrease in total measured Z (Seppä, 2014).

1.1.5 Dielectrics

Dielectric is a material that can be placed in the range of electric field with zero or almost zero power losses. In this condition, the dielectric polarization of material takes place, causing the shift of the electric charges in the material according to the direction of the electric field and, thereby, introducing the loss of electrical energy in the form of heat. If a dielectric is solution of weakly bounded molecules, they displace physically. When AC is applied two parallel conductive plates, that have dielectric material between the plates, the charge is stored. Different dielectrics have different properties concerning the ability to store energy, which can be expressed by

$$\varepsilon_r = \frac{C_x}{C_0} \quad (14)$$

where ε_r is the relative dielectric permittivity of the material, C_0 is the capacity in vacuum and C_x is the capacity in arbitrary material. The properties of a capacitive element—capacitor—are determined by dielectric, dimensions and the distance between the plates. This is expressed by

$$C = \varepsilon_r \varepsilon_0 \frac{A}{d} \quad (15)$$

where A is the area overlap of the two plates, ε_0 is the electric permittivity of free space ($\varepsilon_0 = 8.854 \times 10^{-12} F \cdot m^{-1}$) and d is distance between the plates. This equation applies in the case of ideal dielectric material, but in practice, as noted above, there is also an imaginary component included, bounded to dielectric loss. This is related to the poor conductivity of the material and is the reason to call ε_r as relative complex permittivity. To describe the total interaction of dielectric materials with the electric field, the following applies

$$\varepsilon_r = \varepsilon'_r - j\varepsilon''_r. \quad (16)$$

Component ε'_r in above equation is the real part of relative complex permittivity, describing the storage of electric charge and ε''_r is the imaginary part of relative complex permittivity, describing the loss of electric charge. The latter can be depicted in vector diagram, proposing insight to the emergence of loss tangent (Figure 1.7).

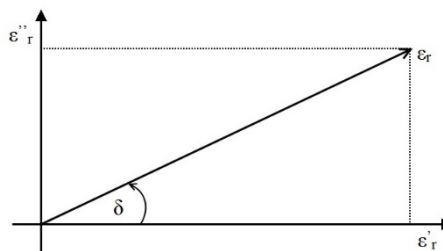


Figure 1.7 Vector diagram of relative complex dielectric permittivity

In the phase difference between the real component ε'_r and imaginary component ε''_r , which is 90° , the vector can be modeled for an arbitrary material for actual relative

complex dielectric permittivity ε_r . The angle δ , which forms with real axis, describes the tangent loss that is an important indicator in characterizing the dielectric materials. As the charges and losses in capacitive element are proportional, the degrees of relaxation of dielectrics can be found from the ratio of emitted and stored energy in certain amount of time. This can be shown by

$$\tan \delta = \frac{\varepsilon''_r}{\varepsilon'_r}. \quad (17)$$

The relaxation of dielectric material in time domain is frequency dependent—the fact that can be associated with the different properties of polarization in different frequencies. If the frequency is low and all charges are able to displace, polarization is maximal (Grimnes & Martinsen, 2008). With increasing frequency the polarization will decrease. This dependence is referred as a concept of relaxation, adapted by Dutch-American physicist Peter Joseph William Debye (1884–1966) in his equation, derived in frequency domain for single dispersion (Debye, 1929)

$$\varepsilon(\omega) = \varepsilon'_{\infty} + \frac{\varepsilon'_0 - \varepsilon'_{\infty}}{1 + j\omega\tau_0} \quad (18)$$

where $\varepsilon(\omega)$ is the complex permittivity of medium, ε_{∞} is the permittivity at very high frequency, ε_0 is the permittivity at very low frequency and τ is time constant of the relaxation process.

1.2 Composition and Electrical Properties of Human Body

Human body is a complex structure that is composed of different types of cells that jointly constitute tissues which are the building blocks of organs. The largest organ in human body is skin, forming the outer surface of the body that gains the property of eternal process of renewing. The ex vivo measurements of impedance of human body, that constitute the successive topic of current thesis, presume the placement of electrodes on the surface of the body.

1.2.1 Composition of human skin and its equivalent circuit

Human skin can be considered to consist of three main layers (plus stratum corneum) (Figure 1.8):

- Epidermis is the outer layer of the skin that is composed mainly of stratified layers of flattened cells. This layer is dictating the placement of the electrode on body surface.
- Dermis is irregular connective tissue that is located between epidermis and fat, containing sweat glands and hair follicles. This layer provides elasticity to the skin through the embodiment of proteins, cellulose and elastic fibers.
- Hypodermis constitute the layer right underneath the skin, containing mainly of body fat. This layer contains larger blood vessels and nerves.

The outermost layer of epidermis is stratum corneum that contains dead cells and has a property of renewing constantly. The impedance of stratum corneum is greatly variable and may be, depending for example on sweating of the skin and the level of moisture in the air, very high in dry condition. In dry condition, stratum corneum can be considered as dielectric, capable of holding charge. Nevertheless, stratum corneum has interesting

property of filling up the dead cells with water (sweat) when covered with dry metal plate. Sweat consists of salts (e.g. sodium chloride NaCl), behaving as effective conducting electrolyte. The process is time dependent—the water from the bottom layers slowly fulfills the dry content and accumulate underneath the metal. Thereby the impedance of the skin diminishes (Grimnes & Martinsen, 2008).

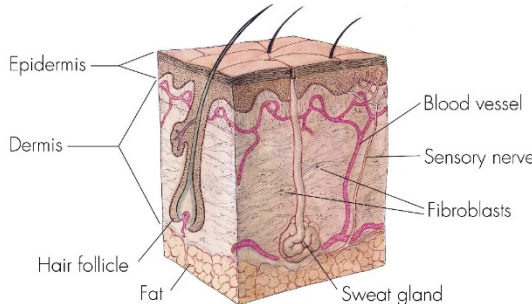


Figure 1.8 Cross section of skin anatomy (picture provided by the National Institute of general Medical Sciences, source: <https://images.nigms.nih.gov/Pages/Home.aspx>)

The impedance of the skin in low frequencies (<100 Hz) is dominated by stratum corneum (Grimnes & Martinsen, 2008). Sweat ducts together with nail and hair constitute DC current pathways in the skin (Martinsen, Grimnes, & Nilsen, 2008). The equivalent circuit of electrode-skin contact interface can be seen in Figure 1.9, demonstrating the possible pathways for electric current.

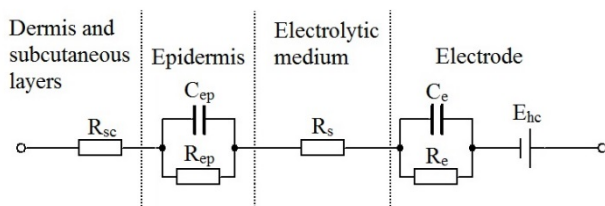


Figure 1.9 Equivalent circuit of skin-electrode contact interface

The dermis and subcutaneous layers can be considered to have resistive nature, depicted by R_{sc} . The skin, including dermis and epidermis together with stratum corneum exhibits resistive and capacitive properties, denoted by C_{ep} and R_{ep} . The electrolytic medium represents the sweat or conductive gel, located between the skin and electrode, indicated by R_s . Electrodes can, depending of its type, exhibit frequency dependent properties, shown by C_e and R_e . E_{hc} denotes the half-cell potential. The dominating element in the equivalent circuit is the impedance of skin (McAdams, 2006).

1.2.2 Respiratory and cardiovascular systems of human

The respiratory system of human is divided into upper and lower respiratory tract and its task is the process of exchanging gases i.e. breathing. The upper part includes nose, nasal cavities, pharynx and upper portion of larynx. The lower part is mainly formed by the largest organ in respiratory tract—lungs, nevertheless, is considered to start from the lower part of larynx (Figure 1.10).

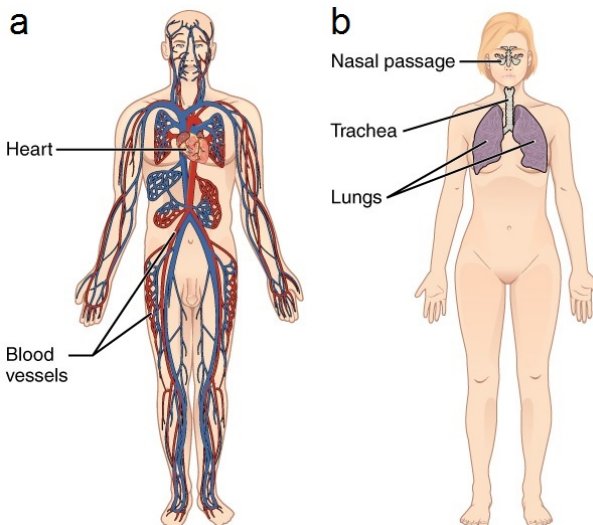


Figure 1.10 Cardiovascular (a) and pulmonary (b) systems of human (picture provided by OpenStax, Anatomy & Physiology. OpenStax CNX. May 18, 2016, source: <http://cnx.org/contents/14fb4ad7-39a1-4eee-ab6e-3ef2482e3e22@8.25.>)

Lungs are located in chest within rib cage. The tops of both of lungs extend slightly above the level of first rib and the bottoms reach down to diaphragm. The right lung is larger of volume and heavier but is a bit shorter than the left lung. The left lung is smaller of volume, mainly because of the cardiac notch where heart is located but is a bit longer than right lung. Typically, an adult takes 15–20 breaths a minute, which makes 0.25–0.34 Hz in frequency scale.

The cardiovascular system contains heart and circulatory system which task is to circulate blood with the goal of delivering oxygen and nutrients to every single cell in the body and remove the carbon dioxide. Heart is located behind and slightly left of breastbone (Figure 1.10). Heart pumps blood rhythmically into the circulatory system.

The cardiac cycle can be divided into two principle phases: diastole and systole. Diastole represents the period of time when ventricles are relaxed and during which blood is flowing into ventricles: the venous oxygen-poor blood flows into the right ventricle and the oxygen rich blood from lungs flows into the left ventricle. At the end of diastole, both atria contract, pushing an additional amount of blood into ventricles. Systole represents the period of time when ventricles are contracting, ejecting blood into aorta and pulmonary artery. During systole, the atrioventricular valves are closed, denoting the state when no blood is entering ventricles; though, blood continues to collect into the atria through vena cavae and pulmonary veins. In the circulatory system, blood is carried to the body by the network of arteries, arterioles and capillaries and returned to heart through venules and veins.

Blood in arteries carry oxygen-rich pulsating blood and veins carry oxygen-poor non-pulsating blood back to heart. The typical heart rate of healthy adult stays in between 60–100 beats per minute, which makes 1–1.67 Hz in frequency scale.

Heart has electrical conduction system, transmitting the signals that are generated by the pacemaker cells in sinoatrial node to induce the contraction of heart muscle and, thereby, contracting firstly atriums and secondly ventricles. The first known recording of bioelectric signals was implemented by English physiologist Augustus Desiré Waller

(1856–1922) in 1887. The electrical activity of heart can be depicted by electrocardiogram by using standard 12-lead electrode placement configuration.

In ECG, the standard leads, denoting the stretch between two limbs (arm or leg) are named by Dutch doctor Willem Einthoven (1860–1927) the Einthoven's triangle. The standard leads I, II and III are referring electrodes on both arms and left leg and heart is constituting the null point. By recording the electrocardiogram, the trace of the electrical activity of heart can be gained gathering the overall magnitude and the direction of the heart's electrical depolarization (point Q in electrocardiogram in Figure 1.13).

1.2.3 Characterization of cellular tissue (dispersion regions)

The conductivity and permittivity ϵ'_r of biological objects are frequency dependent, meaning that they can be considered in both ways: either to be of conductors or dielectrics. To describe this phenomenon, German-American biophysicist Herman Paul Schwan (1915–2005) established the concept of dispersion (Schwan, 1999), meaning the frequency dependence according to relaxation theory. Biological objects rarely exhibit a single time constant Debye response as described in the Section 1.2 but exhibit a certain asymmetrical distribution of relaxation times.

The dispersion characteristics of biomaterials are detected by electrical experimentation at different frequencies—called dielectric spectroscopy (Grimnes & Martinsen, 2008). Dispersion has been categorized by Schwan into three regions: α -, β - and γ -dispersions. Later, an additional dispersions of small magnitude were determined in the higher frequencies of β -dispersion. These were named to δ -dispersion, assumed to be caused by proteins and cell organelles in living object. In the latest publications, this phenomenon has been profoundly research and concluded that the δ -dispersion is not only connected to the single-particle dynamics of water shells around the proteins but more to the relaxation processes, unique to the collective nature of the dielectric experiment. This collective nature is due to the relaxation processes that take place in δ -dispersion region like protein-water cross-correlation and protein-water self-correlations (Braun, Schmolngruber, & Steinhauser, 2017).

All of these groups of relaxation mechanisms are related to some specific phenomenon that has effect in biological objects. The dispersion regions are typically shown in classical graph, defined for frequency ranges (Figure 1.11).

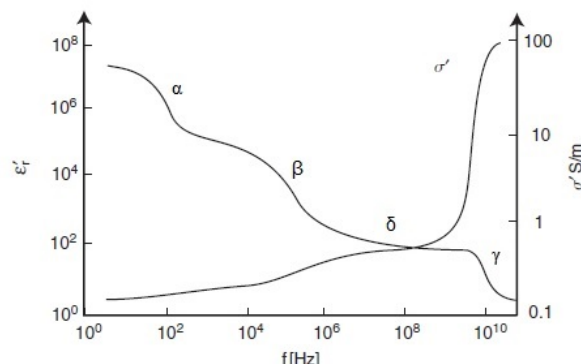


Figure 1.11 Idealized dispersion regions of the biological matter (modified from (Schwan, 1988))

It is evident from Figure 1.11 that the ε'_r of biological material decreases with increasing frequency—constituting clearly distinguishable dispersions because of the inability of charges (dipoles) to follow the speed of changes in the electric field. Such a clearly distinguishable response can be found with cell suspensions, however, in the case of tissues (and even more—in complex biological matter), the dispersion regions may not even be recognized in evenly falling graph (Grimnes & Martinsen, 2008, p. 90).

The mechanism behind the α -dispersion (frequency range of 1 mHz–1 kHz) is believed to be the polarization of the channel systems of the cells together with the counter ion polarization at the cell surface (Foster & Schwan, 1989). It is associated with counter ion layer (electrical double layer) which can take the shape of the object that is interacting with this layer. The emergence of counter ion layer in the case of biological tissue is explained by the ion passages—formed by intermembrane and intracellular space, membrane pores etc. (Kuang & Nelson, 1998).

According to (Schwan, 1988), the ε'_r can reach values of higher than a million at very low frequencies. However, as described in (Grimnes & Martinsen, 2008), this designated high value of ε'_r does not mean the domination of capacitive properties of living tissues at low frequencies. The impedance of living tissue is claimed to be dominated by the conductive properties of liquids (Grimnes & Martinsen, 2008) as the major component of tissues is water (constituting up to 65–70 % of the mass) (Kuang & Nelson, 1998). However, here the difficulties start, related to the complexity of the tissue structure and electrode polarization which deteriorates the true measurements.

The description of the emergence of double layer (see Paragraph 1.3.1) is discovered to be more complex as it was described originally, where the excess charge is depicted to lie on the surface of a metal plate and the counter ions in the electrolyte solution as rigid parallel layer very close to the metal plate. The ions are actually expected to be continuously distributed throughout the electrolyte, being regulated by the ion concentration gradient and the potential that is applied in the metal plate (Kuang & Nelson, 1998). Additionally, the interfacial polarization is appearing—emerging during the accumulation of charge at the interface of two materials of different permittivity or between two regions in a material because of an external field.

β -dispersion (frequency range of 1 kHz–100 MHz) is induced mainly by cell and organelle membranes, which charging depends on the different dielectric constants and electrical conductivities of different regions. This is called the membrane charging effect, arising principally from interfacial polarization of biological membrane systems (Kuang & Nelson, 1998). The membrane resistance is short-circuited during the increasing frequency by the membrane capacitance. If the interesting volume does not contain membranes, like blood, the β -dispersion is small. This can be modelled in the case of single cell but for the complicated structures of tissues of different conductivities, the model becomes complex. Also, the rotational relaxations of biomacromolecules (proteins, nucleic acids etc.) have been assumed to contribute to β -dispersion.

In the case of measuring the EBI by using the resistively coupled electrodes on the surface of skin (as described in the Chapter 4), the complexity of the tissues result in the sense of membrane abundance. The charging effect of membranes appears, being highly dependent on the water content—the water content in human tissues is high and the effect of β -dispersion is expected to apply in high magnitude (ε'_r reaching 10^5). The interfacial polarization in heterogeneous volume of tissue takes place at the interfaces of tissues of different conductivities, being dependent on geometry of these volumes, conductivity and permittivity. However, with the increasing frequency,

more and more resistive components are cancelled by the parallel capacitances and the structure is expected to become progressively homogenous (Pethig & Kell, 1987).

In the highest frequency range, 0.1–100 GHz, the dispersion γ is caused by the dipolar mechanism in total electrolyte content. In more detail, it is arising from polarization due to reorientation of water molecules (Gabriel, Gabriel, & Corthout, 1996) e.g. the dielectric characteristics of tissue can be expected to incorporate the data of intra- and extracellular water. In VHF band, the dielectric properties of tissue become independent of the charging effect of membranes (Pethig & Kell, 1987). In the case of γ -dispersion, the properties of tissues are influenced by their water content: described in (Pethig & Kell, 1987) as relatively lower ϵ'_r and σ in the case of individuals with higher fat percentage (as the water content of fat is much smaller than of muscular tissue).

The dispersion concept is phenomenological i.e. depending on certain process or property of biological material which appears at different frequencies.

1.3 Theory and Methods for Bioimpedance Analysis

In a very simple approximation the determination and analyze of the compartments of human body can be done by representing it with a homogenous cylinder—this is constituting the base for bioimpedance analysis (BIA). The BIA is a tool that uses the EBI to assess the composition of human body (more specifically: hydration status) (Grimnes & Martinsen, 2008). The BIA can roughly be divided to fall into two categories: time and frequency domain. In time domain, the access to time varying changes in the body can be accessed while in frequency domain, the changes in response of the body to externally applied electrical stimulus at chosen range of frequencies can be obtain.

As the biological processes in human body that are of interest of current thesis, are variable, the reach of techniques for following the changes in volumes are of higher interest. In the case of volume detection, the assessment is falling into the time domain and done typically at single frequency at a time. Nevertheless, the combination of time and frequency domain is possible to be implemented at the same time (Gracia, Seppä, Viik, & Hyttinen, 2012; Min et al., 2012).

There are techniques available for monitoring the changes in volumes in the object (or parts of the objects)—commonly called IPG. In (Grenvik et al., 1972), there are listed the purposes of monitoring the IPG of human body:

- respiratory rate;
- changes in lung gas volume;
- changes in lung water;
- heart rate and stroke volume (SV).

IPG can be used to follow two main vital signs of human that have changing nature: breathing and heart beating. The known techniques of IPG are ICG and IP. ICG is a technique that can estimate the changes in blood volume in transthoracic region over time, expressed in the changes of transthoracic impedance (Bera, 2014). The circulation of blood in human body, caused by the heart rhythms, is causing the impedance of the body to vary. When considering a single blood vessel, depicted as a cylinder with cross section A (Figure 1.12), the flow of pulsating blood periodically expands the walls of the vessel, increasing the area of the cross section by ΔA .

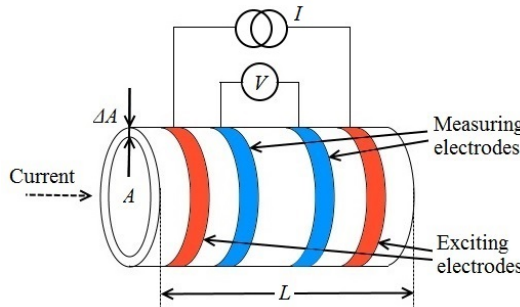


Figure 1.12 Impedance measurement of cylinder like body with four-electrode system

The conductivity of blood is better than of the tissue around the blood vessel and the impedance (ΔZ) of ΔA is calculated (Nyboer, Kreider, & Hannapel, 1950) according to

$$\Delta Z = \left(\frac{Z_b Z}{Z_b + Z} \right) - Z = -\frac{Z^2}{Z + Z_b} \quad (19)$$

where Z_b is the impedance of the blood, ΔZ is the additional impedance that arises from the expansion of the blood vessel and Z is the impedance of original volume A . Accordingly, the volume of expanded area can be rewritten as (Nyboer et al., 1950)

$$\Delta V = -\frac{\rho_b L^2}{Z^2} \Delta Z \quad (20)$$

where ρ_b is the resistivity of blood and L is the length of the distance between the measuring electrodes. As a result, by analyzing the transthoracic impedance, number of hemodynamic parameters can be evaluated together with cardiac output and SV.

ICG is mostly recognized as non-invasive technique for monitoring the cardiac output, nevertheless, the same definition applies to other regions of human body as well. In heart and large arteries, the interval of the change of volume is larger and in arterioles, the interval of the change of volume is smaller. The opening of ventricles, i.e. the start of the flow of blood into arteries which is induced by the R wave in electrocardiogram has time delay when compared to the point of an arterial pulse waveform.

In the case of ICG, the pulse arrival time (PAT) depends on the placement of the electrodes—the farther away from heart, the longer the PAT (Geddes, Voelz, Babbs, Bourland, & Tacker, 1981). To denote the time delay between two arterial pulse waveforms that are simultaneously measured at different distances from heart, the term pulse transit time (PTT) is used. The difference between PAT and PTT is that PTT involves the time delay only due to the propagation of the pulse along arteries, while PAT contains also the pre-ejection period (PEP) (Figure 1.13). PEP is defined as the delay between the onset of electrical activity of heart (R wave) and the beginning of mechanical ventricular ejection of blood (Payne, Symeonides, Webb, & Maxwell, 2006).

Related to the previous ones, another important term can be emphasized: pulse wave velocity (PWV). Conventionally, PWV is measured on the ground of the time delay between the opening of the aortic valve (point B in impedance cardiogram in Figure 1.13) in the proximity and in the distance from heart (wrist, neck etc.). This period of time, called the propagation time (PT) can be estimated by measuring the time delay between

the R wave in electrocardiogram and relevant point in arterial waveform of distal monitoring of ICG (D. Xu et al., 2010).

PT is an important parameter, reflecting the condition of arteries—it decreases with the increasing stiffness of arteries. The another important period of time is left-ventricular ejection time (LVET)—indicating the period during which blood flows across aortic valve (Kolev & Zimpfer, 1995). An illustration of the timing of relevant points on electrocardiogram, impedance cardiogram and pulse wave together with the defined time intervals can be seen in Figure 1.13.

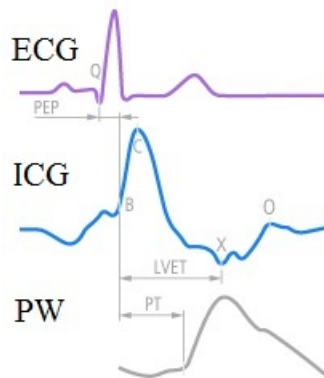


Figure 1.13 Example signals of ECG, ICG and PW together with illustrations of defined time intervals (redrawing from <https://medis.company/cms/index.php?page=icg-impedance-cardiography>)

The points B, X, C and O in impedance cardiogram denote the opening and closing of the aortic valve, the maximum systolic flow and opening of atrioventricular valve respectively. The point Q in electrocardiogram represents the depolarization of interventricular septum.

In addition to previously defined parameters, correlation between the monitored pulse wave from wrist, gained by measuring the EBI and the CAP is reported (Min et al., 2017). Specifically, the work towards the estimation of TF that relate the invasively measured systolic blood pressure with the measured pulse wave from peripheral circulation has shown promising results. As indicated, blood can't reach immediately the peripherals of arterial tree because of the resistance of the wall of aorta and is temporarily accumulating in the proximal aorta, increasing the pressure onto the wall. In the beginning of diastole, the supply of blood from ventricles stops and the pressure on the wall of aorta decreases. During this process, the systolic pressure waves are spreading through the arterial tree, forming pulse wave, which exact shape is dependent on the condition of circulatory system, age of the individual and the position of sensor relative to arterial tree.

The typical shapes of pulse wave, measured as modulation of measured systolic pressure in peripheral arteries in the case of aorta, carotid artery, brachial artery and radial artery can be seen in Figure 1.14.

Point A is base point, denoting the moment where pulse wave has not arrived to the position of sensor and in the sense of volumes is proportional to local volume. Point P denotes the maximum blood volume in radial artery i.e. the arrival of pulse wave (percussion wave). Point V indicates the dicrotic notch, which marks the moment of

closure of aortic valve. Point D or the dicrotic wave is the consequence of reflected waves from the lower peripherals of circulatory system and aorta. The same points can be indicated in the waveform of measured EBI of radial artery.

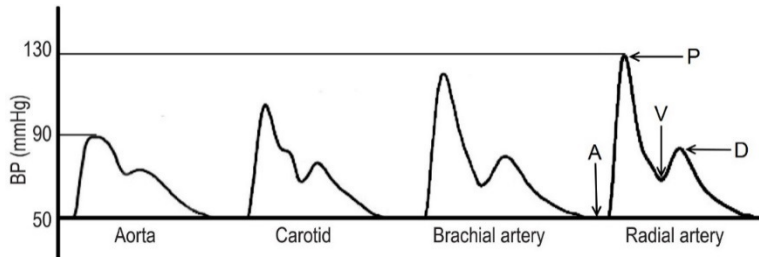


Figure 1.14 Systolic pressure waveforms from central to peripheral arteries (modified from (Brandão et al., 2017))

The technique of IP is used to measure the respiration-induced changes in impedance in thorax by using surface electrodes (Seppä, 2014). During inhalation the conductivity of thorax decreases and lengths of the conductivity paths increase because of the expansion of the volume of lungs (Grenvik et al., 1972). Figure 1.15 represents the outcome of waveform of IP, measured by using the spot electrodes according to Figure 1.16c together with reference signal of breathing by using a spirometer.

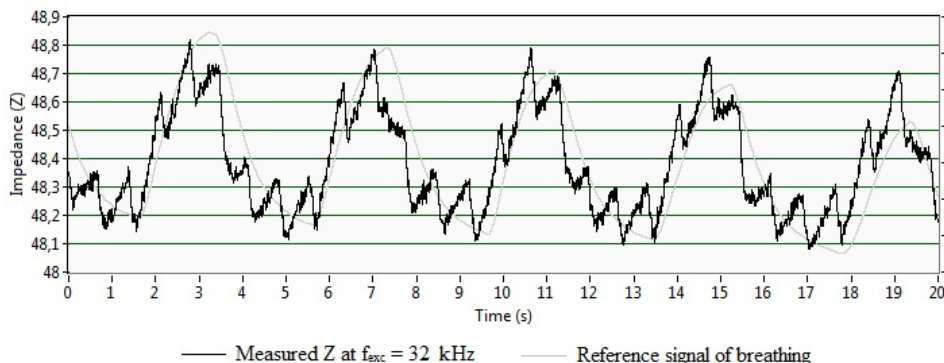


Figure 1.15 Example signal of IP in the case of spot electrodes according to Figure 1.16c (authors' previously unpublished illustration)

However, human body should be characterized as a complex system, i.e. the heart beating physically influences lungs and vice versa, the in- and exhalation applies pressure to heart (Krivošei, 2009).

1.3.1 Motion artifact

The crucial topic to cover, when discussing the monitoring of EBI of biological objects is the motion (movement) artifacts. Motion artifacts originate from variety of movements in electrode-skin contact interface and in biological object. It, likewise other artifacts, can be considered as noise that is interfering the measured signal of EBI or any other biopotential that appears as additional voltage potential to the interesting signal. The movements in electrode-skin contact interface results from the movement of electrodes respect to the surface of the object as well as the movement between layers of the skin of human. Motion artifacts influence the measurements in the case of

capacitive electrodes but appears also during low-resistance measurements by using standard (wet) direct contact electrodes.

The motion of electrode can be generally divided into two categories (Chi, Jung, & Cauwenberghs, 2010): transversal (1) and lateral (2).

Transversal motion causes changes in skin-electrode contact impedance, i.e. the distance between the electrode and skin to vary, resulting as polarization of the contact interface resulting as additional voltage potentials. The lateral motion can cause friction in the case of direct contact setup, resulting as triboelectric charge to be added to the measured potential (Chi et al., 2010). To reduce the effect of motion artifact, conductive gels are used in skin-electrode contact surface for reducing the polarization impedance. Besides this, other solutions, like signal processing in the form of adaptive filtering (Thakor & Zhu, 1991) and movement of electrode by using 3-D accelerometer has been used (Tong, Bartels, & Honeyager, 2002).

The relative movements of different layers in biological objects (for example between dermis and epidermis) are causing skin potential artifacts to arise. These potentials reach the order of several millivolts (Searle & Kirkup, 2000), depending on the stretching and pressure that is applied to the skin. To some extent, this can be reduced by removing the stratum corneum. Other than that, improvements concerning the structure of the electrodes have been implemented to reduce the skin potential artifacts—for example by adding a conductive foam layer between the contact surfaces. The foam layer possess elastic properties that maintains contact with the skin in the case of movements and does not cause friction (Gruetzmann et al., 2007).

1.3.2 Origin of cardiorespiratory impedance signal

In the sense of mechanical principle of volume changes (caused by the processes of cardiac and respiratory activity), the resulting time varying change in measured signal of EBI is comparable in to the cases. However, the processes of cardiac and respiratory activity are different in essence (described in the Paragraph 1.2.2.) and the question can be divided into two parts:

1. the origin of the cardiac impedance signal,
2. the origin of the respiratory impedance signal.

Concerning the respiratory activity, the exhaustive overview is done in (Seppä, 2014), where the impedance signal is defined to originate from the change of the impedance of the lung tissue. When lungs are filled with air, the sponge-like lung tissue stretch and its impedance increases. When air is breathe out, the lung tissue is contracting to the normal state and its impedance decreases. Next to that, the linearity of the relationship of volume and impedance is depending on the placement of electrodes (Seppä, 2014).

The effective placement of electrodes for IP is reported to be in lateral on sides of thorax (Seppä, Viik, & Hyttinen, 2010)—low and high bilateral midaxillary placement (Figure 1.16a). Nevertheless, the lower positioned electrodes (below the lower border of lungs) result in the impedance that may include the volume changes in other organs and lose in linearity between lung volume change and impedance change (Seppä, 2014).

In the case of ICG, the diversity of possible placement of electrodes is apparent as the blood vessels are carrying blood from heart to all body parts. Not to mention here the debate concerning the details of the contribution of other cardiovascular related aspects, the changes in time varying signal of impedance are caused by blood (good overviews in the topic are available e.g. in (Mughal, Annus, Min, & Gordon, 2014; Patterson, 1989)).

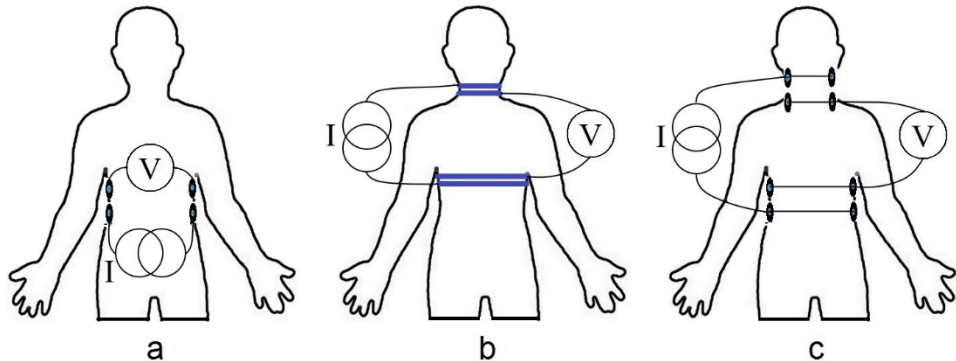


Figure 1.16 An effective placement of electrodes for monitoring IP (a) and the traditional placements of electrodes for monitoring ICG by using the band (b) and spot (c) electrodes

Blood is electrical conductor because of the inclusion of iron-containing protein called hemoglobin. Related to this, the increase in blood volume in thorax (and other body parts) following the heart beating, produces changes in thoracic resistance. The first actual model of determining the SV in the case of cylindrical regions of body by finding the change of volume (ΔV) from the corresponding change of electrical impedance (ΔZ) was proposed by Nyboer et al in 1950 (Nyboer et al., 1950). After that, extensive work has been published and the formula for determining the SV derived (Kubicek, Karnegis, Patterson, Witsoe, & Mattson, 1966)

$$SV = \rho_b \left(\frac{L}{Z_0} \right)^2 \cdot LVET \cdot \frac{dZ}{dt_{(max)}} \quad (21)$$

where Z_0 is the baseline impedance between the measuring electrodes and $dZ/dt_{(max)}$ (Ω/sec) is the absolute value of maximum rate of change in the impedance signal, caused by the pulsating flow of blood. Nevertheless, there are limiting factors of above stated Kubicek equation like the constancy of ρ_b throughout the whole cardiac cycle because it is declared to vary, caused by the changing orientation of red blood cells (erythrocytes) (Sherwood et al., 1990). Concerning the result of changing orientation of erythrocytes, the so called Sigman effect have to be mentioned, specifically, the flow-dependence of the resistivity of blood (Sigman, Kolin, Katz, & Jochim, 1937). Sigman effect appears as decrease in resistivity of blood with the increasing velocity of blood from 0.1 to 0.4 m/s.

Like in the case of IP, the placement of electrodes play crucial role in the case of ICG. The historical type and placement of electrodes for determining the SV, used by Kubicek (Kubicek et al., 1966), were the band electrodes, placed around thorax and neck—claimed to provide the reproducibility (Figure 1.16b) (Patterson, 1989). Later, the discovered disadvantage of band electrodes—the non-uniform distribution of contact impedance between the band and the body—suggested the use of spot electrodes, placed on sides of thorax and neck (Figure 1.16c) (Vedru, 1994).

1.3.3 Approach for evaluating the measured signals of time varying volumetric changes in human body

The measured response Y of an object at every moment of time can be depicted to consist of the basal i.e. the invariable value of measured response Y_0 and $\Delta Y(t)$ that is caused by volumetric change. Y can be declared by

$$Y = Y_0 + \Delta Y(t). \quad (22)$$

The modulation on the measured response signal $\Delta Y(t)_{card}$, caused by cardiac activity is appearing on top of the modulation $\Delta Y(t)_{resp}$ that is caused by respiratory activity which can be called as the carrier signal. $\Delta Y(t)_{resp}$ is larger than $\Delta Y(t)_{card}$ and conditionally the following is true:

$$\Delta Y(t) = \Delta Y(t)_{resp} + \Delta Y(t)_{card}. \quad (23)$$

Nevertheless, the (23) is true only when there is no any other volume change present. Even more, in the case of electrical methods, the volume changes are not the only changes that modulate the measured response. It is known, that electrochemical processes in body tissues have effect on current distribution, thus altering the measured response signal—establishing the means for example for detecting skin cancer (Åberg, 2004). The orientation of red blood cells is reported to have effect on the measured value of EBI, observed to increase with the increase of hematocrit of blood (Gaw, 2010). However, the motion artifact (see the Paragraph 1.4.1) i.e. the changes in response signal that are caused by the shift of sensor relative to the object is expected to have vast effect. Even more, the additional uncertainties are provided by the changes in distance between the electric sensor and the object—influencing the resulting current distribution and equilibrium conditions that ultimately effect on the measured response. So, when finding $\Delta Y(t)$, some number of time varying changes apply de facto onto the response signal together with the $\Delta Y(t)_{resp}$ and $\Delta Y(t)_{card}$, denoted as $\Delta Y(t)_x$.

Besides cardiorespiratory activity, the interest of current thesis is set on the variation in the response signal $\Delta Y(t)_{move}$ that are created by the concurrent movements and the affection of other changes $\Delta Y(t)_x$ is not considered. The relationship can be explained by the

$$\Delta Y(t) = \Delta Y(t)_{resp} + \Delta Y(t)_{card} + \Delta Y(t)_{move} + (\Delta Y(t)_x). \quad (24)$$

In current thesis, the focus is set on the volumetric changes $\Delta Y(t)_{resp}$ and $\Delta Y(t)_{card}$ and on the affection of concurrent movements $\Delta Y(t)_{move}$ —the other effects in the form of $\Delta Y(t)_x$ on the measured signal of EBI is discussed but not characterized.

The $\Delta Y(t)$ is a parameter that describes the actual measured interval of the interesting change in volume in response signal. However, often it is useful to find the ratio of $\Delta Y(t)$ to Y , denoting the sensitivity

$$S = \frac{\Delta Y(t) \times 100}{Y}. \quad (25)$$

The S characterizes the ability of the device, measurement setup, method or approach to provide certain magnitude level of output signal. However, in this thesis, no magnitude

level is specified instead, the S is compared with the goal of selecting the solutions that provide highest S . Typically, in this thesis, the S is calculated for $\Delta Y(t)_{resp}$, $\Delta Y(t)_{card}$ and $\Delta Y(t)_{move}$ separately, denoted by S_{resp} , S_{card} and S_{move} respectively or by finding the ratios of $\Delta Y(t)_{resp}$ and $\Delta Y(t)_{card}$ to $\Delta Y(t)_{move}$. The benefit of evaluating the S lies on the possibility of describing thereby number of properties, like the ability of a selected solution to withstand the externally applying interferences. Moreover, the possibility to unify the resulting response signal in the cases of different methods enhances the value of S .

A way of comparing the results is to determine the arithmetic mean (\bar{x}), expressed by

$$\bar{x} = \frac{1}{n} \left(\sum_{i=1}^n x_i \right) = \frac{x_1 + x_2 + \dots + x_n}{n}. \quad (26)$$

The (\bar{x}) proposes a way of statistically comparing the data, gained for example by using different measurement setups by using the same excitation frequency or by using different excitation frequencies at single measurement setup.

1.4 Electrodes for Measuring EBI

In solid matter (electrodes, connecting leads etc.), the current is carried by the electrons, yet in electrolytes (biological objects), the current is carried by ions. In the sense of the measurements that are directed to characterize biological objects, the following definition applies: electrode is the site of shift from electronic to ionic conduction and vice versa (Grimnes & Martinsen, 2008). Electrode may be connected to the object by using galvanic contact or without using galvanic contact (including the induction of current carriers by using electric and magnetic fields).

Moreover, the measurement of EBI can be performed by utilizing different electrode configurations, ensuing from the chosen approach of excitation and measurement: two-, three- and four-electrode system. The problems arises from the chosen configuration, emerging for example in the form of contact impedance mismatch. For selecting the electrodes, the knowledge of different types, materials and common constructions is essential. As the current thesis is focused on the ex vivo measurement of EBI of human body either on the skin or remote, the current chapter is limited to surface attachable types of contact and non-contact electrodes.

According to (McAdams, 2006), a desirable wearable electrode is defined to require:

1. no preparations;
2. be formed in a location in clothing that instantly reaches the desired position;
3. achieve good electrical contact with the skin;
4. not increase the effect of motion artifact;
5. not give rise to discomfort and skin irritation;
6. be reusable.

This idealized list characterizes well the difficulties that appear during the design of electrodes for wearable applications.

1.4.1 Electrode characteristics and electrical properties

When electrode is placed in galvanic contact with an electrolytic solution, the electrochemical processes of oxidation and reduction start. During this, half-cell potential (also known as Nernst potential) is established between the electrode and the

electrolyte. It is known that different materials have different characteristic potentials, having influence in low frequency and DC measurements (Table 1.1).

Table 1.1 Half-cell potentials for chosen materials and reactions (Neuman, 2000)

Metal and reaction	Half-cell potential (V)
$\text{Al} \rightarrow \text{Al}^{3+} + 3\text{e}^-$	-1.706
$\text{Ni} \rightarrow \text{Ni}^{2+} + 2\text{e}^-$	-0.230
$\text{H}_2 \rightarrow 2\text{H}^+ + 2\text{e}^-$	0.000
$\text{Ag} + \text{Cl}^- \rightarrow \text{AgCl} + \text{e}^-$	+0.223
$\text{Ag} \rightarrow \text{Ag}^+ + \text{e}^-$	+0.799
$\text{Au} \rightarrow \text{Au}^+ + \text{e}^-$	+1.680

When no current is applied to the measurement setup (two electrodes are required to either pick up or apply a current), the observed potential is the sum of the equilibrium potentials of electrodes and electrolyte. If desired current is applied to such measurement setup, the measured potentials can be altered. Such difference of potentials between the cases of zero current and current, has influence on charge distribution in electrolyte that is in galvanic contact with electrodes.

Under equilibrium conditions, electrode potential E equals its reversible potential E_{rev} . For real electrode-electrolyte interface, the potential E can be expressed by

$$E = E_{rev} + i_{DC}R_{shunt}, \quad (27)$$

where i_{DC} is the faradic current that is applied to the electrode-electrolyte interface and R_{shunt} is the shunting resistance of the interface, locating in parallel with capacitance C_{dl} . R_{shunt} can be imagined as a resistance that applies on charge transfer through electrode-electrolyte interface, shunting the C_{dl} (McAdams, 2006).

The described effect is called polarization and it has remarkable influence on the operation of electrodes, entailing the relevance of the choice of electrode materials in respect to the nature of the measurement setup. The electrode polarization impedance is always frequency-, concentration-, voltage-, and electrode dependent—this is the reason for the difficulty of low-frequency dielectric studies.

The degree of polarization can be adjusted by the material of electrode—noble metals (e.g. platinum, silver, gold etc.) do not tend to react with the body liquids and in majority no current distribution follows, revealing in polarizable property. The known non-polarizable electrode is silver-silver chloride (Ag/AgCl) electrode, allowing current to pass the electrode-electrolyte interface and offering minimal hindrance (Neuman, 2000).

The polarization is explained by the effect of double layer that emerges during the electrode-ion charge carrier transfer in electrode-electrolyte interface. To complete the task of transferring the charge across the interface, the ions (or electrodes) must diffuse to it, disposed by the electrostatic attraction (McAdams, 2006). As a result, layer of positive charges will be formed at the surface of electrode and layer of negative charge in the opposite side of interface in the electrolyte (called as Helmholtz plane (named after German physicist Hermann von Helmholtz (1821–1894)) (or vice versa)—called electric double layer (Figure 1.17).

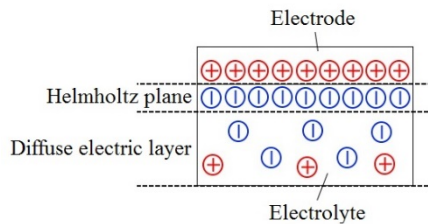


Figure 1.17 Electrical model of electrode-electrolyte interface—formation of electric double layer

The Helmholtz theory is representing the simplest explanation of the emergence of double layer, presuming reorientation of water dipoles relative to the charged surface and specifically absorbed.

Nevertheless, this model is valid for high concentration electrolytes. In the case of more dilute solutions, the thickness of double layer will increase because of the possibility for the ions to escape and generate more like an atmosphere of counter ions around an individual ion—called diffuse electric layer (also known as Gouy-Chapman layer (named after French physicist Louis Georges Gouy (1854–1926) and English physicist David Leonard Chapman (1869–1958)). This explanation is based on the Maxwell-Boltzmann distribution theory: the change in concentration of the counter ions near a charged surface follows the Maxwell-Boltzmann distribution, causing the thickness of double layer to decrease with increasing valence and concentration.

The modification of Gouy-Chapman theory was proposed by German-American physicist Otto Stern (1888–1969) in 1924 (Stern, 1924). He described the Stern layer as the layer of ions that are specifically absorbed by the charged surface. The modified theory presumes that ions can be considered as point charges with finite size and the property of not approaching the charged surface than the radius of the ion itself. By increasing the charged surface, the potential drops quite linearly in the Stern layer and exponentially through Gouy-Chapman layer. The Stern theory is used to divide the Helmholtz plane into two sections: the inner Helmholtz plane (IHP) and the outer Helmholtz plane (OHP). The notional borderline between the IHP and OHP is the centerline of specifically absorbed ions.

If an electrode is placed in contact with solution, the electric double layer is formed immediately and it can be represented as parallel plated capacitor (McAdams, 2006). The distance between the plates is argued to be in the order of 0.1–10 nm, denoting vast capacitance values (Grimnes & Martinsen, 2008).

The connection can also be capacitive—meaning that the electrode and the object do not have galvanic contact, instead, the object is influenced by electric field. For penetrating human skin and causing current flow together with secondary electric fields in tissues, the electric field is obligated to be alternative. The higher the frequency, the more efficient the connection and at the frequencies below 1 Hz the non-galvanic connection is not possible to utilize (Grimnes & Martinsen, 2008).

1.4.2 Basic electrode configurations for impedance measurements

The impedance can be measured by using two-, three- or four-electrode systems. In two-electrode configuration, the voltage is measured not only across the interesting impedance of the object (\dot{Z}), but also across the two electrode impedances Z_{e1} and Z_{e2} , locating in series with \dot{Z} (Figure 1.18a). The following can be expressed by

$$Z_{measured} = \frac{V}{I} = Z_{e1} + Z_{e2} + \dot{Z} \quad (28)$$

revealing that electrode polarization impedances cause errors in the measurement in the precise monitoring of impedance. In relative measurements of variable biological processes, two-electrode system is suitable because of its robustness. Though, the presumption for achieving the real value of impedance in the case of two-electrode system is the significantly lower value of Z_{e1} and Z_{e2} , than the value of \dot{Z} .

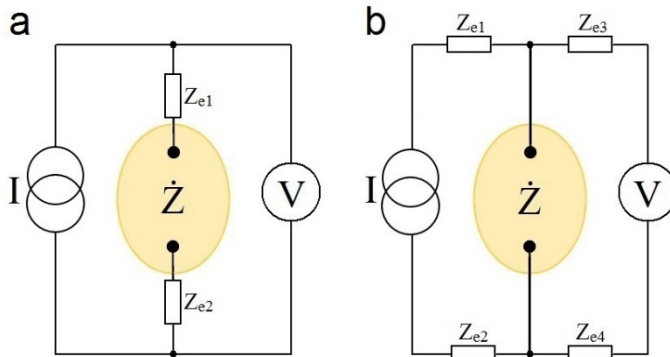


Figure 1.18 Common impedance measurement systems: two- (a) and four-electrode (b)

The solution of using separate electrodes for current application and voltage monitoring—called four-electrode system—is used to cancel the above described problem of inclusion of the electrode polarization impedances (Figure 1.18b). In this configuration, the current flows through the current carrying (excitation) electrodes and does not affect the impedance if measuring electrodes. Only voltage drop across the object can be measured and the following is truth

$$Z_{measured} = \frac{V}{I} = \dot{Z} \quad (29)$$

with the clause that the input impedance of the measurement circuit is large.

Impedance measurements by using four-electrode system is influenced by the electrode-skin contact interface. It is stated that the electrode-skin contact interface possess important capacitive component in the frequency range 10–100 kHz (Pallas-Areny & Webster, 1993).

In the case of four-electrode system it is more precise to talk about trans-impedance than to use the term impedance. The reason is the inclusion of two independent two-electrode systems—one for excitation and one for measurement—and actually the transfer parameter is computed (Grimnes & Martinsen, 2007). Also, four-electrode system does not withdraw the impedance of the leads, measuring electrodes and artifacts that are originated from the inherent complexity of the biological objects.

The optimization of four-electrode system by increasing sufficiently the area of negative excitation electrode has guided to the three-electrode measurement configuration. By increasing its area, Z_{e2} (Figure 1.18b) is reduced and the corresponding measuring electrode can be removed, denoting the common usage of negative excitation electrode for both: excitation and measuring. The benefit of three-terminal configuration

lies in the opportunity of using the third electrode to control the measured zone of the object by setting the formation of sensitivity field (Grimnes & Martinsen, 2008).

1.4.3 Sources of error in measurement of EBI

When considering a setup for EBI measurements, one can realize that there are several sources of error that can apply even when using four-electrode system—equivalent circuits proposed in several publications (Al-Hatib, 1998; Bogómez-Franco, Nescolarde, Bragós, Rosell-Ferrer, & Yandiola, 2009). An author's opinion of applying sources of errors are depicted in Figure 1.19.

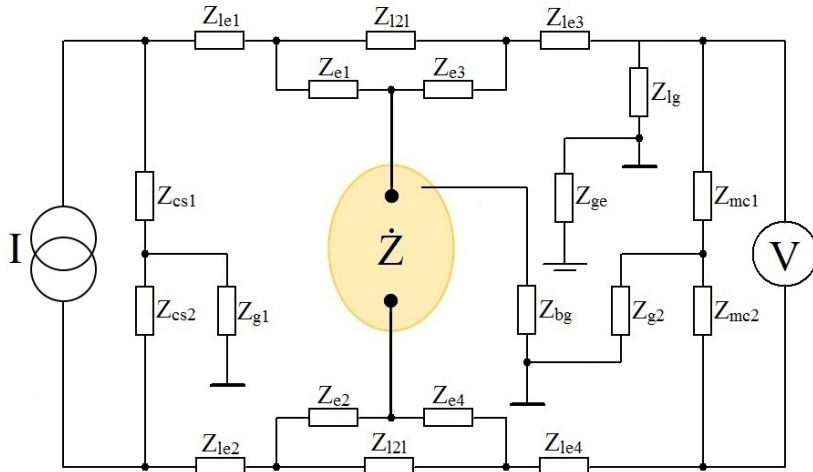


Figure 1.19 EBI measurement setup scenario together with sources of error (author's previously unpublished illustration)

The real circuitry contains always stray capacitances that present different electrical pathways for current that is meant to pervade the object (Ruiz, 2013). In real life, current source has some internal impedance (Z_{cs1} and Z_{cs2}) and measuring circuitry does not have infinite input impedance (Z_{mc1} and Z_{mc2}), resulting in measurement errors. The electrode impedances (Z_{e1} , Z_{e2} , Z_{e3} and Z_{e4}) together with the impedances of the measuring leads (Z_{le1} , Z_{le2} , Z_{le3} and Z_{le4}) together with the impedance that is caused by the parasitic capacitance between the neighboring leads (Z_{121}). The ground connections induce the common mode voltages to appear, caused by asymmetries and noise from surrounding environment. Ground errors can be depicted as the impedances, caused by the stray capacitance between the leads and ground (Z_{lg}), between the body and ground (Z_{bg}), between the current source and ground (Z_{g1}), between the measuring circuitry and ground (Z_{g2}) and between the ground and earth (Z_{ge}). Besides the enumerated errors, the biological object itself introduces multiple sources of error.

1.4.4 Electrode constructions and materials

The most common contact electrode in clinical applications today is wet Ag/AgCl electrode that has well defined DC potential and is not very dependent on DC current flow. These electrodes are easy to use and create rather firm electrical contact the skin. The structure of this electrode exhibits some kind of solid contact gel that is attached in direct contact to skin. The modern wet gel disposable types of electrodes are also in use

in clinical applications, possessing the properties of decreased effect of motion artifact and faster settling times of stable connection.

Nevertheless, wet electrodes tend to dry out after some time, causing the impedance of the contact to arise (McAdams, 2006). Furthermore, the unnoticeable monitoring of human body excludes the attachment of wet electrodes as cumbersome process. The electrode should be possibly unnoticeable, lightweight and possess electrical properties that grant the access to the interesting signal. The relevant property hereby is biocompatibility—activity and non-toxicity relative to skin and sweat.

With the developments in the manufacturing PCB's, the usage of metallic fields, designed on one side of the board often together with electronic circuit of preamplifier on other side of the board has gained popularity in construction of electrodes (G. D. Gargiulo et al., 2012; Sullivan, Deiss, & Cauwenberghs, 2007; Weyer, Weber, Kleeberg, Leonhardt, & Wartzek, 2015). However, the drawbacks of such design are the higher rigidness of even flexible PCB's than regular cloth and the property of being potentially prone to motion artifact because of the connecting leads.

The flexible conductive polymeric materials, like polydimethylsiloxane in (Hu, Cheng, Xie, & Lam, 2015) and conductive rubber in (G. Gargiulo et al., 2008; Luo, Afonso, Webster, & Tompkins, 1992; Muhlsteff & Such, 2004) have been reported to be used as contact electrodes. Their conductivity is evoked by adding metal compounds or graphite in the mold—this makes it possible to regulate the electrical properties.

The advances in the technologies of producing fibers of various ingredients for manufacturing the fabrics of desired features has created ground for development of textile electrodes. In its simplest form, textile electrode is a piece of conductive fabric that is placed on the surface of an object and connected to a measurement system. There are two ways of constructing the fabrics: weaving or knitting. Woven fabrics are built of interlacing yarn strands at right angles, are typically not stretchable and with flat surface (Figure 1.20a). Knitted fabrics are composed of loops of yarns that are interlocked, can be made of single continuous yarn and are typically stretchable (Figure 1.20b).

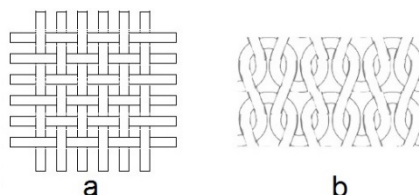


Figure 1.20 Construction techniques of textiles: woven fabric (a) and knitted fabric (b)

The conductivity of fabrics can be raised mainly in two ways: by adding fibers that are made of metallic material (ferrous alloys, nickel and nickel alloys, stainless steel, titanium, aluminum, silver or copper) (T. H. Kang, Merritt, Grant, Pourdeyhimi, & Nagle, 2008) or by coating (or plating) conductive layer on the surface of non-conductive fibers (conductive polymers, conductive ink etc.) (Rattfält, 2013).

The fabrics have some problems and technical limitations that are not present in the case of metal electrodes: the most important of them is the influence of inductance that increases because of the inherent fibrous structure of the fabric. And secondly, the appearing non-linear response, caused by the applied strain that may vary of direction and timing (T.-H. Kang, 2006). Typically fabric electrodes are used in direct

contact with the skin by adding these in the composition of tight shirt (or other garment elements) for monitoring biopotentials (Hanic et al., 2014; Paradiso et al., 2005). Textile electrodes can be used also as capacitive electrodes, added on top of some regular clothing (H. Li et al., 2017; Ng & Reaz, 2017) or covered by some insulating varnish like silicone (EP2671506 A1, 2013) or conductive ink (Kazani et al., 2012).

The electrical properties of different electrode structures depend on variety of aspects like the resistivity and the dimensions of contact area. This consideration is somewhat simpler in the case of solid materials and more complicated when interwoven structure of conductive textile is used as electrode.

1.5 Chapter Summary

From this chapter the complexity of monitoring the physiological activity in the form of cardiac and respiratory processes of human by the means of EBI can be realized. The principle of measuring and processing the data of EBI was presented together with the potentiality of the BIA to access the interesting physiological processes. The sophisticated structure of biological material in the form of different tissues, organs and bones influences the current density distribution and has relevant influence on the measurability of cardiorespiratory activity in the case of measuring the EBI.

The largest organ of the body, the skin, has major influence on the ex vivo measurements of EBI by using irrespectively either contact or non-contact electrodes because of its unique properties of endless renewal, self-healing and hydrating. The dissimilar placement of the circulatory and respiratory systems in human body require the careful design and planning of the measurement setup, including the placement of sensors in the case of ex vivo measurements. The appearing frequency dependence and changing degree of conductivity of body tissues, tissue structures and skin has to be consider when designing measurement experiments and devices.

The potential of monitoring cardiorespiratory activity by using the EBI measurements appears in the accessibility of information that is obtainable during the performance of BIA, related to the physiological processes of human. It was shown that the opening and closing of the aortic valve, the maximum systolic flow and opening of atrioventricular valve are available in impedance cardiogram. Moreover, in collaboration with other methods of monitoring the physiological parameters, like the ECG, additional parameters like the PEP can be obtained. Similarly, the volumetric changes that are related to the respiratory activity can be achieved by implementing the IP.

2 Wearable Solutions Based on Capacitive Coupling

In this chapter the analyze and detectability of cardiorespiratory activity is presented, leading to the design and implementation of experimental wearable measurement devices, actual experimentation and the proposal of most suitable placements and configurations of the non-contact electrodes. Guided by the knowledge of the dissimilar placement of circulatory and respiratory systems in human body the preparation of electrode shirts is described. At the same time, the hypothesis, related to the influence of the size, placement and material of the electrodes on the measurability of cardiorespiratory activity in the case of measurements of EBI is proposed—this will constitute the base for further implementations in practice.

The goal of the prepared electrode shirts is to experimentally find out the most suitable placements and configurations of non-contact electrodes for monitoring the cardiac and respiratory activity by measuring the EBI. The measurement experiments are described and the results presented to compare the data in the light of concurrent movements. An approach for sorting the electrode configurations, related to the proposed classification of dispositions of body in between the electrodes, was developed. Secondly, the approach was developed and employed to sort out the best placements for non-contact electrodes. The electrode shirts described here bear also the weight of serving the further activities of monitoring the interesting physiological processes in experiments, described in next main chapters.

This chapter is based on the author's 1st and 3rd main publication.

The specific tasks of this chapter are listed subsequently:

- A. To experimentally evaluate the ability of capacitively coupled large area electrodes for monitoring cardiorespiratory activity in comparison resistively coupled electrodes in the case of measuring the EBI.
- B. To characterize the chosen electrode materials with the aim of ascertain their behavior if utilized as capacitively coupled electrodes.
- C. To design and implement wearable experimental measurement devices that contain large area electrodes in different positions and possess the ability of setting different electrode configurations.
- D. To experimentally determine the most suitable positions and configurations of electrodes for monitoring cardiorespiratory activity in the case of measuring EBI by using capacitive coupling.
- E. To perform the evaluation of measured data of EBI of single volunteer with the goal of assessing the ability of different electrode placements and configurations to deliver cardiorespiratory activity.
- F. To experimentally determine the positions and configurations of electrodes which are less affected by the concurrent movements.
- G. To compare the results of measurements of prepared electrode shirts by using the implemented and commercial EBI measurement device in order to evaluate the difference between a custom made portable and commercial on-desk device.
- H. To experimentally determine the possibility of using coils as capacitive electrodes for monitoring cardiorespiratory activity.

This chapter is organized as follows.

In the Section 2.1 the principle of capacitive coupling is explained through the prism of monitoring the cardiorespiratory related changes in human body.

The Section 2.2 describes the state of the art of utilizing capacitive coupling for monitoring physiological processes in human body and introduces some important achievements in the field.

In the Section 2.3 the verification of the measurability of cardiorespiratory activity by using the measurements of EBI is shown.

In the Section 2.4 the results of characterization of chosen electrodes are presented and the assumptions rendered concerning their behavior in non-contact EBI measurement setups for monitoring cardiorespiratory activity.

The Section 2.5 introduces the prepared electrode shirts together with the proposed principles of design and placement of electrodes. The developed experimental methodology for measuring the EBI by using the prepared electrode shirts with the goal of determining the most suitable electrode placement configurations (EPC) is introduced.

In the Section 2.6 the development, implementation and characterization of an optimized electronic EBI measurement device is presented.

In the Sections 2.7-2.8 an approach for sorting out the most suitable electrode placements and configurations of non-contact electrodes is described.

The Section 2.9 introduces the possibility of utilizing coils as EBI measuring electrodes by using capacitive coupling with the goal of describing the eventuality of employing a single sensor in the cases of both types of couplings.

In the Section 2.10 the conclusions related to the preparation of electrode shirts and results of performed experimentation by using capacitive coupling are presented together with emphasized important contributions.

2.1 Cardiorespiratory Activity Monitoring by Using Capacitive Coupling

Capacitive electrode can be defined as electrodes that do not have galvanic contact with the object and the transfer of energy from one medium to another is induced by displacement currents, caused by the electric field. Capacitive electrodes may have no physical contact to the object at all or have an insulating layer on electrode contact surface (insulated electrode), providing the intentional or non-intentional capacitive approach. This enables to setup measurements even in the case of explicit gap and without any predetermined dielectric between the body surface and electrode (Chi et al., 2010). The advantages of capacitive coupling are the lack of need of conductive gel and the deficiency of electrode-skin resistance that could cause voltage drifts. The inherent problem of capacitive coupling is motion artifact (Paragraph 1.3.1).

Capacitive coupling with an object form a capacitor-like element in equivalent circuit, depending mainly on the thickness and the dielectric constant of the material between the electrode and skin (described by the (15)). To depict capacitive coupling by equivalent circuit in Figure 1.9, one can replace R_s by single capacitor. Nevertheless, the interface for capacitive electrode is more complex than in the case of resistive coupling—exhibiting the influence of the medium between the skin and electrode on the emerging capacitive element and on the movement of the charged particles, caused by the electric field in the object (Chi et al., 2010). The value of impedance is very high in the case of capacitive electrodes, causing the decrease in the sensitivity of EBI measurements.

If the electrodes are placed in capacitive contact with the object with unfilled gap, the insulation can be considered to be air that behaves almost as ideal dielectric ($\epsilon_r \approx 1$). Though, in the applications for monitoring the impedance of human body by using

wearable devices, the electrode contact surface is typically covered some insulating material, for example silicon nitrate (Si_3N_4) ($\epsilon_r \approx 7.5$) (Alizadeh-Taheri, Smith, & Knight, 1995) or polypropylene (CH_3) ($\epsilon_r \approx 2.2 - 2.36$) (Weyer et al., 2015) etc. The utilization of such layer of dielectric assures some amount of capacitance that is present even in the case of floating distance between the skin and electrode.

The presence of layers of clothing means the addition of an impedance in series with the electrode in the equivalent circuit as different fabrics have different properties. The experiments have shown that cotton possess the properties of parallel RC circuit, from which the resistive part tends to dominate (A. Ueno et al., 2007). For example, a piece of cotton with thickness of 395 μm has $R_p = 209 \text{ M}\Omega$ and $C_p = 59 \text{ pF}$ ($\epsilon_r \approx 2.3$) and a piece of cotton with thickness of 1020 μm has $R_p = 121 \text{ M}\Omega$ and $C_p = 39 \text{ pF}$ ($\epsilon_r \approx 4.0$)—acting as poorly conductive electrode. As major amount of daily clothing has some portion of polyester ($\epsilon_r \approx 2.8 - 4.5$) added to give the durability, the impedance can vary. Thorough overview of methods of characterization and parameters of chosen fabrics (cotton, linen, nylon, polyester etc.) can be found from (Ng & Reaz, 2017).

2.2 State of the Art of Monitoring Cardiorespiratory Activity by Using Capacitive Coupling

The attempts to find out the optimum placements for sensors on the surface of human body to monitor cardiorespiratory activity through following the volume changes has been described in literature. Herein, simulation environments serve the tools for setting up the models and carrying out the experiments to represent current distributions at various excitation frequencies and sensor configurations. The relevance of the choice of electrode configurations in the case of EBI measurements has been shown in number of papers, using the finite element method (FEM) to simulate the sensitivity distributions related to respiratory activity (Lewandowska, Wtorek, & Mierzejewski, 2010; Mayer, Brunner, Merwa, & Scharfetter, 2005; F. Yang & Patterson, 2008) and cardiac activity (Kauppinen, Hyttinen, & Malmivuo, 1998; Y. Wang, Haynor, & Kim, 2001).

In simulations, typically small area electrodes in resistive coupling have been modelled to determine the sensitivity distribution in the volume of trunk. However, the sensitivity distribution can be expected to emerge similarly in the case of capacitive coupling. For example, in (Lewandowska et al., 2010) the two-electrode system is used by attaching pairs of electrodes craniocaudally on frontal plane of trunk relative to thorax in FEM simulation. More precisely, electrodes are located along craniocaudally running lines in the case where several such lines with electrodes has been modelled and simulated to find the placements where the sensitivity is the highest—i.e. formed in areas of heart and aorta. The results advise the importance of the exact placement when using small area electrodes. The contribution of right ventricle to sensitivity distribution is found to be the highest when placing the electrodes craniocaudally on the surface of trunk on top of the approximate location of pulmonary artery and bottom of right ventricle. While the placement on the same craniocaudally running line where the upper electrode is placed in upper sternal region and lower in xiphisternal joint is reported to be most suitable to focus the sensitivity region on aorta.

Another interesting FEM simulation study is presented in (F. Yang & Patterson, 2008), where the four-electrode system by using small area electrodes has been used to map the emerging sensitivities in thorax. The observation concerning the appearance of negative sensitivities has been made, appearing in the cases where the angle between the two lead fields is greater than 90° (discussed in the Section 1.1.4). The highest

sensitivity is resulting mainly directly under the electrode and forming in the outer contours of the model of thorax.

Moreover, the important aspect of the effect of boundaries between tissues with different conductivities on sensitivity distribution has been studied in (F. Yang & Patterson, 2008). The results show the considerable local perturbing effects, caused by the thoracic inhomogeneities and boundaries between the volumes of different conductivities. In this study, the placement of electrodes that proposes the highest modulation in measured signal, caused by breathing, is shown to be the following: electrodes placed in horizontal line around chest about the height of 6th rib, where:

- the exciting electrodes are placed on sternum, about the height of left nipple;
- the measuring electrodes are placed in left armpit and about the height of right nipple.

The optimal electrode positions in four-electrode system for detection of lung water have been proposed in (Beckmann, Riesen, & Leonhardt, 2007)—the results suggest that the positions on axillary lines at the height of xiphisternal joint offer the highest sensitivity. Similar study for detecting lung edema has been reported in (Mayer et al., 2005), emphasizing the advantage of wide electrode spacing over the placement where the electrodes are closely concentrated on a certain region. This indicates that the larger the volume of lungs between the electrodes, the more the value of measured impedance is affected by the conductivity of lungs i.e. the presence of water which amount is influencing the sensitivity distribution.

The contribution of the respiratory activity to total impedance measurement has been researched in (J. Yang et al., 2015), showing the importance of the choice of electrode combinations that can result in the difference in contributions around 5 %. The effect of the placement of spot electrodes for monitoring the ventricular contraction has been studied in (Y. Wang et al., 2001), where the location on anterior chest wall on top of the location of heart has been demonstrated to gain the largest change of impedance from total measured impedance. The most effective placement of electrodes in four-electrode system on thoracic surface for monitoring breathing and blood flow, has been research in (Pfützner & Futschik, 2000). The position that proposes the most suitable option for monitoring cardiac activity is in the height of the 5th intercostal space where the location of heart lies approximately between the pairs of excitation-measuring electrodes, emphasizing the importance of focusing of electrodes for monitoring mechanical movements of heart.

As a conclusion, the following important findings in published results of simulation studies are listed below:

- The importance of electrode positioning relative to the location of interesting volume change in the object—the smaller the area of electrode the more important the exact positioning.
- The highest distribution of sensitivity directly under the electrodes and in the outer contours of the model (F. Yang & Patterson, 2008).
- The noticeable effect of boundaries between the volumes of different conductivities, causing the current distribution to deviate when compared to homogenous volume of matter (F. Yang & Patterson, 2008).
- The suggestion of wide distance between the pairs of excitation-measuring electrodes, placed craniocaudally on thoracic surface in the case of lung edema monitoring—the effect of water in lungs in measured signal of impedance is expected to be larger (Mayer et al., 2005).

Next to the simulations, the practical experimentation contains the relevance of determining the effective electrode positions for monitoring cardiorespiratory activity and related problems through monitoring the volume changes. The confirmation of simulation data in practical experimentation proposes valuable information and establishes base for the possibility of further utilization of a method or configuration in clinical applications.

In majority of experiments, contact electrodes in the case of resistive coupling are used for practical determination of the positions and configurations of electrodes for monitoring the volume changes that are caused by cardiorespiratory activity (Brown, Barber, Morice, & Leathard, 1994; Ikarashi, Nogawa, Yamakoshi, Tanaka, & Yamakoshi, 2006; Raaijmakers et al., 1998; H. Wang et al., 2014).

Optimal placement of small area (225 mm^2) electrodes in four-electrode system for monitoring respiratory activity have been determined experimentally in (Seppä et al., 2010) and the lateral configurations were found to exhibit the better performance. The lateral configuration denotes the positions where the pairs of excitation-measuring electrode pairs are placed on sides of chest. In principle, this denotes the effectivity of larger volume of air on measured impedance, proposed by the presence of both lungs in between the electrodes than in the case of focusing on single lung.

Importantly, signal-to-(motion) artifact ratio (SMAR) in the case of impedance based respiratory activity monitoring has been experimentally evaluated in (Luo et al., 1992) to find the optimal positions of electrodes on thoracic surface. It has been determined earlier, that the SMAR increases with the increase in electrode area when using the two-electrode system (Sahakian, Tompkins, & Webster, 1985). This is explained by the presumption that the large area electrode exhibits a physical property of averaging the random motions and, throughout, reduce the SMAR (Luo et al., 1992).

There are some interesting conclusions, based on measuring experimentation, presented in (Luo et al., 1992), related to the size of the area of electrode and the positioning of electrodes on thoracic surface, though by using resistive coupling. The highest SMAR is obtained by using several closely placed group of small contact area electrodes rather than large area single contact electrode. Moreover, it is advised to carve holes and slots in the surface of resistively coupled large area electrode to achieve higher SMAR. Secondly, the observations related to the positions of electrodes have been presented with the substantial statement, that there is no universal positions for electrodes in two-electrode system that would propose the highest SMAR in the case of all volunteers. Thirdly, the relation between SMAR and the presence of fat tissue has been found—the smaller the layer of fat tissue the higher the SMAR (Luo et al., 1992). SMAR is the highest when the small area (1400 mm^2) contact electrodes in two-electrode system are placed on the left and right second intercostal space on sternum and on the opposite position on back (Luo et al., 1992).

Another example is (Wartzek et al., 2011), where capacitive electrodes in two-electrode system have been used to monitor the phase shift that occurs between the excitation signal, applied frontally on back side of thorax, and measured signal. The degree of phase shift is expected to be time dependent on the amount of air in lungs, varying because of breathing—this, in turn, is causing varying capacitive element. The variation is expected to be available also in the case of impedance measurements, giving rise to supposed comparability in the sense of electrode placement and positioning on thoracic surface. The electrode dimensions, used in simulation model, are not specified though, expected to be of relatively small area.

A conclusion from this paper concerning the distance between electrodes for monitoring respiratory activity can be rephrased: the choice of distance is essential, effecting on the depth of penetration on current – the shorter the distance between electrodes, the lower the depth. Second interesting observation concerning the monitoring of respiratory activity has been made of the positioning of electrodes in two-electrode system on thoracic surface: if the electrodes are placed on both frontal sides of chest, the location on the central craniocaudally running imaginary line is not recommended (on top of the location of backbone and xiphisternal joint). In this case the current is distributed in conductive tissues in mediastinum and heart, presumably gaining access to cardiac activity. The suggested position by using the two-electrode configuration is shifting the electrodes on top of the location of either right or left lung.

The corresponding experiments by using the non-contact electrodes for monitoring cardiorespiratory activity has rarely been mentioned in literature and no comprehensive experimental study for determining the optimal placements cannot be referred hereby.

As a conclusion, the following findings can be listed based on the literature review of publications where the positions and configurations of electrodes have been handled:

- The insufficient presence of experimentation data where different electrode placements and configurations would have been used by utilizing capacitive coupling.
- The conformity of findings of experiments of capacitive electrodes to the result of experiments where resistive coupling has been used.
- The larger the volume of lungs between the electrodes, the deeper the modulation in the measured signal of EBI, caused by the changing volume of air—i.e. the placement of electrodes in sagittal plane in sides of thorax result better than the placement on frontal plane of thorax, responding to the conclusion of simulations.
- The SMAR is declared to increase during the increase of electrode area by using the two-electrode system (Sahakian et al., 1985).
- The highest SMAR is obtained by using several closely placed group of small contact area electrodes rather than large area single contact electrode (Luo et al., 1992).

2.3 Experimental Evaluation of Alternatives of Measurement of EBI for Monitoring Cardiorespiratory Activity

The evaluation of materials to be used as electrodes for measuring the EBI of human body presumes the number of evidences of the availability of the interesting signal. This includes the determination of the presence of cardiorespiratory activity when measuring the EBI in different body areas by using the chosen types of electrodes and devices. The commercial EBI measuring device, used in all of the experiments, is the HF2IS impedance spectrometer together with the HF2TA transimpedance amplifier.

For measuring the signal of cardiorespiratory activity in the case of measuring the EBI of human body, experiments were carried out by using direct contact and capacitive electrodes on a single volunteer. The usage of direct electrical contact reduces the effects of movement of the body and minimizes friction. On the contrary, the electrodes in capacitive contact boost the problem of motion artifact and presume the usage of higher excitation frequencies. The measurements were performed by using three different electrode placement configurations (EPC) in two-electrode system:

- wrists of both hands;
- both sides of trunk (about the height of xiphisternal joint);
- both sides of neck (about the height of laryngeal incisure).

For the experiment with contact electrodes on hands and neck, electrodes were cut in the size of 1/3 of the original.

The thorough overview of the methods, experiments and results can be found in the authors 1st other publication (M. Metshein, 2014). However, for the primary conclusions relative to the results of the experiments of the verification of the measured signal of cardiorespiratory activity, the following statements can be presented:

- The respiratory and cardiac activity are available in the cases of direct and capacitive contact when the object is not moving.
- Motion artifacts has vast influence on the results in both attachment of electrodes—contact and capacitive.
- The choice of the EPC is crucial for granting the access to the interesting parameter revealing in the amplitude of ΔReZ .
- The current excitation provides larger S_{resp} and visually better assertion against motion artifact.
- The results concerning cardiac activity are comparable in the sense of S_{card} in the cases of voltage and current excitation.

The presence of signal interferences that are caused by the movement of electrodes relative to the body surface presumes the employment of special algorithms.

2.4 Characterization of Electrodes for Capacitive EBI Measurements

The choice of the material of the electrodes play important role in designing wearable monitoring devices. The question arise more deeply in the case of direct contact electrodes, where the aspects of biocompatibility and the stability of the impedance of skin-electrode contact surface needs to be consider. Nevertheless, the electrode material has its impact also in the case of capacitive measurements, emerging from stiffness and structure to electric properties of the material. And not only the electrode itself, but also the placement and length of the connecting wires that constitute part of the measurement system and have its impact:

1. Large wet plate surface electrodes (22 4773 Electrosurgical Grounding Plates, Niko Medical Products) with original dimensions (80 × 170 mm).
2. Conductive metallized nylon fabric (rip-stop) textile (1500101130, Statex Productions & Vertriebs GmbH) with the dimensions of 80×150 mm and thickness of 0.1 mm.
3. Single side copper plated PCB (thickness of copper: 35 µm) with the dimensions 100×150 mm.

Firstly, the experiments were carried out to evaluate the electrical properties of the chosen materials in the cases of varying distance between the electrodes and in the case of different length of connecting probe wires. Secondly, the experiment by using the electrodes no. 1 and 2 in capacitive contact to thorax of a volunteer were carried out by using the electrode shirt no. 1 (ES1) (Figure 2.1) and electrode shirt no. 3 (ES3) (Figure 2.3) to evaluate their affection on the measured Z.

The thorough analyze of the results of experiments is available in the authors 3rd other publication (M. Metshein & Gordon, 2016), however, four main conclusions are presented subsequently:

- The material of the electrode has effect on the measurement result, appearing in the level of Z that is higher for conductive textile and lower for plain metal materials. Proportionally to the increase of distance between the electrodes, this variance disappears (M. Metshein & Gordon, 2016).
- The larger the distance between the electrodes and lower the excitation frequency, the greater the value of Z (M. Metshein & Gordon, 2016).
- The shorter the connecting probe wires the higher the frequency of appearance of self-resonant frequency.
- When placed on uneven surface of biological object, the inherent capacitive and inductive properties influence the results of the measurements of EBI, causing the faster recession in the value of Z in frequency scale than foil electrodes.

2.5 Design and Implementation of the Electrode Shirts

The positioning of electrodes on the surface of human body can be essentially different for monitoring the respiratory and cardiac activity. This is based on the fact that the organs that are involved in respiratory and circulatory system lie in different locations and differently in the body (Paragraph 1.2.2). Moreover, the matter of variable volume, caused by the respiratory and cardiac activity, is different in the sense of ϵ :

- Air gains almost ideal properties of dielectric.
- Blood conductive properties depend on the temperature (Schwan, 1957), frequency of the excitation signal etc. and to gain, for example, the value of ϵ_r of 3026.3 at the frequency of 1 MHz and 280.3 at the frequency of 10 MHz, being of relatively good electric conductor.

Nevertheless, as shown in the Section 2.3, both interesting changes in volumes are available in the cases when the motion artifact is not interfering the result. The influence of motion artifact, in turn, can have fatal effect that is caused by the movement of the electrodes relative to the surface of an object; the change of the shape of contracting muscles that is generating skin deformation etc.

A hypothesis was set up: by varying with the size, placement and material of the electrodes, best configurations of large area electrodes can be determined for capacitive monitoring of cardiorespiratory activity. For providing tools to control this hypothesis, wearable measurement devices with variety of electrode placements and configuration options—electrode shirts—were prepared.

Altogether three electrode shirts were composed by using two different electrode materials: aluminum foil and conductive textile (1st and 2nd material in the Section 2.4). The electrodes were attached onto a cotton shirt (with the thickness of the fabric of 0.5 mm) so that the shirt forms an insulating layer between the electrode and skin. Firstly, ES1 (Figure 2.1) was prepared with a goal of covering trunk of human—excluding the abdomen and breasts. A cotton shirt was covered with aluminum foil electrodes in a way that different EPC's could be set. The electrodes were stick on the outer surface of the shirt. Total of 18 indexed electrodes were included and attached on the shirt by covering the whole back, sides and shoulders (author's 2nd other publication) (Margus Metshein & Parve, 2015).



Figure 2.1 Positions of electrodes in the ES1 (modified from the author's 2nd other publication) (Margus Metshein & Parve, 2015)

The foil electrodes in electrode shirt no. 2 (ES2) (Figure 2.2) were positioned onto chest, shoulders and upper arms (author's 3rd main publication).



Figure 2.2 Positions of electrodes in the ES2 (modified from the author's 3rd main publication)

The placement was chosen to grant the access to pulsating blood in subclavian and axillary arteries but also to the mechanical movement of heart by placing the electrodes on the surface of chest (author's 3rd main publication). In the case of ES2, the electrodes were cut smaller because of the smaller area of targeting body parts and the desire of achieving higher electrode density:

- Electrodes J and K were cut to the dimensions of 60×80 mm (about 35 % of the original dimensions).
- Electrodes D and E were cut to the dimensions of 80×120 mm (about 70 % of the original dimensions).

In the preparation of ES3 (Figure 2.3), conductive textile electrodes with the dimensions of 80×150 mm were used (author's 3rd main publication).



Figure 2.3 Positions of electrodes in the ES3 (modified from the author's 3rd main publication)

In the case on conductive textile, the electrodes were sewed onto the outer surface of a cotton shirt by using cotton yarn. The electrodes A, B, C, D and E, F, G, H were electrically connected by using conductive thread of type Electro-Fashion Conductive Thread (Kitronik Ltd.). During the design and implementation of ES1–3, the following observations were made related to the physical behavior of the used electrode materials:

- In the case of placement on the curvilinear surface of thorax (especially on sides and shoulders), the foil electrodes tend not to follow the same shape—instead, either its edges or central area is in the vicinity to the surface of the skin. This is caused by the property of the chosen foil electrode, being not very flexible. In fact, this was one of the expectations during the choice of aluminum foil, that some surface area of electrode is always in the vicinity of skin surface and no wrinkling is expected.
- The conductive textile, in opposite, behaves similarly to the cotton shirt underneath—in the case of tight shirt, the electrode leaps against the skin surface, following the shape of the body. In the case of wrinkling of the shirt, the conductive textile wrinkles as well.

2.6 Development of Optimized Experimental Electronic EBI Measurement Device

Next to the placement and configuration of electrodes, the utilized electronic excitation and measurement circuitry plays crucial role in measuring the EBI for monitoring physiological processes. Especially in the case of capacitive coupling because of large possible interval of input impedance, caused for example by the changing gap between the electrode and skin surface that the device is required to cope with. The advantage of on-desk commercial laboratory EBI measurement devices lies in their sophisticated design, their ability to suppress noise and their signal processing options. Though, the bulkiness often becomes an obstacle in the case of experimental measurements, requiring long connecting leads that cause additional uncertainties because of the movement of the object.

To perform experiments in the case of predetermined program of movements, the body of a living object causes shifts in the position of connecting leads relative to ground and to each other resulting possibly as additional amount of impedance that is added to the value of measured Z. To reduce this effect, a wearable experimental

measurement device is desired. The idea, design and implementation of wearable experimental EBI measurement device is presented in this chapter.

Only the analogue parts of the device were designed, i.e. the excitation and measuring circuitry. The output of the designed circuitry is DC voltage, which value is expected to increase or decrease, caused by the in- and exhalation and changing amount of blood in object. The task of calculation of the impedance was not set up and the time-varying volumetric changes in object is presented in voltages (author's 3rd main publication). The proposed idea in the form of block diagram of the device can be seen in Figure 2.4.

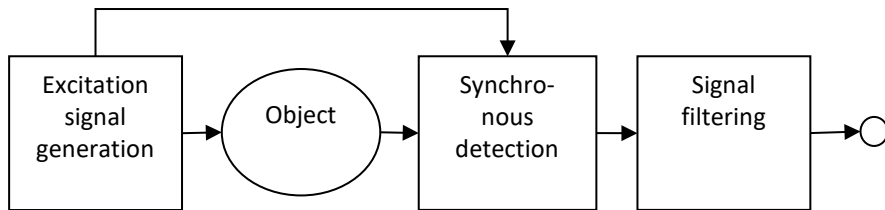


Figure 2.4 Block diagram of the proposed idea of EBI measurement device (modified from the author's 2nd other publication) (Margus Metshein & Parve, 2015)

The choice of the synchronous detection is justified by the expectation that the variations in the impedance of the object, caused by the cardiac activity, are relatively small. This technique constitutes a tool for extracting low level signals (or changes in dynamic value of these signals) from noisy environment and is often used in biomedical applications (Casanella, Casas, & Pallàs-Areny, 2005; Min, Parve, Annus, & Paavle, 2006).

The PCB was assembled and supplied with necessary connecting leads. The power was supplied by on-desk power supply that was connected by flexible cable. The thorough description of design and implementation of the device can be perceived from the author's 2nd other (Margus Metshein & Parve, 2015) and 3rd main publication.

During the measurement experiments, the assembled PCB was attached onto the electrode shirt in order to shorten the connecting leads as much as possible with the goal of minimizing the possible interferences (Figure 2.5).



Figure 2.5 Attachment of the implemented prototype of EBI measurement device on ES1 (author's previously unpublished illustration)

2.7 Qualitative Evaluation of the Results of Monitoring Cardiorespiratory Activity by Using the Electrode Shirts in the Case of Capacitive Coupling

The qualitative evaluation of the waveforms is expected to give the preliminary information of the detectability of cardiorespiratory waveform in the case of capacitive measurements of the EBI. The measurements by using the implemented and commercial EBI measurement devices are performed by using identical measurement setup in the sense of EPC's, electrode materials and dimensions. The primary results of the implemented EBI measurement device are published in the author's 3rd main publication.

The primary task of this chapter is to give notation concerning the possibility of visually recognizing the cardiorespiratory waveform in measured signal of EBI by using capacitive coupling. Secondly, the chosen EPC's of different electrode shirts were characterized in order to gain the preliminary data of the opportunity of gaining access to the interesting time-varying volumetric changes of human body.

2.7.1 Qualitative evaluation of the measurement results of respiratory activity

In order to evaluate the chosen EPC's in the case of capacitive connection to human thoracic surface the experiments were performed by utilizing the electrode shirts ES1-3, described in the Section 2.5. As the thorough overview concerning the result of the implemented EBI measurement device is presented in the author's 3rd main publication, only the conclusions and comparison with the results of reference device are presented.

2.7.1.1 The results of monitoring respiratory activity by using the ES1

In the case of ES1, the following EPC's were used in two-electrode system (author's 3rd main publication):

- EFGHIJKL / OP (craniocaudally placed electrodes relative to body);
- NPRMOQ / AEIDHL (laterally placed electrodes relative to body).

The waveforms, measured by the reference measurement device are shown in Figure 2.6 and Figure 2.7.

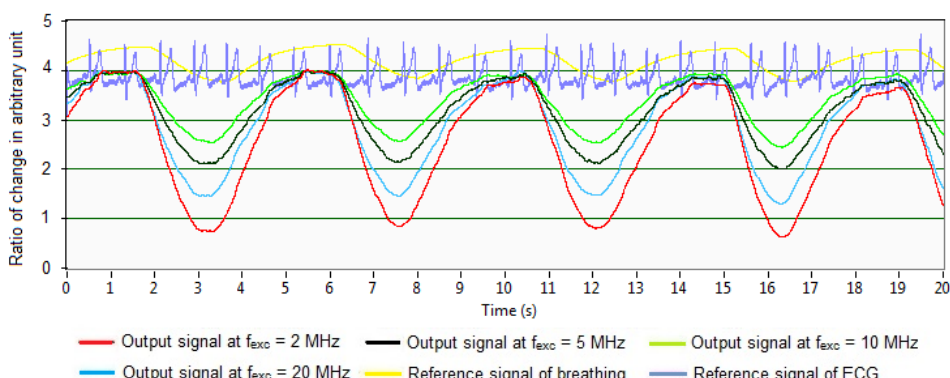


Figure 2.6 Gathered waveforms of the impedance of the body of volunteer according to the EPC EFGHIJKL / OP (ES1) that are measured by using the commercial EBI measurement device in capacitive coupling

The volume change is higher in the case of EPC NPRMOQ / AEIDHL (ES1). One can realize the trend in the cases of both EPC's that the amplitude of change, caused by the

respiratory activity is decreasing during the increase of the excitation frequency until the frequency of 20 MHz. This is differing, when comparing with the results of the implemented EBI measurement device where the result at $f_{exc} = 5$ MHz gains the highest amplitude (together with the result at $f_{exc} = 20$ MHz). Cardiac activity can be assumed to be carried by the signal of breathing.

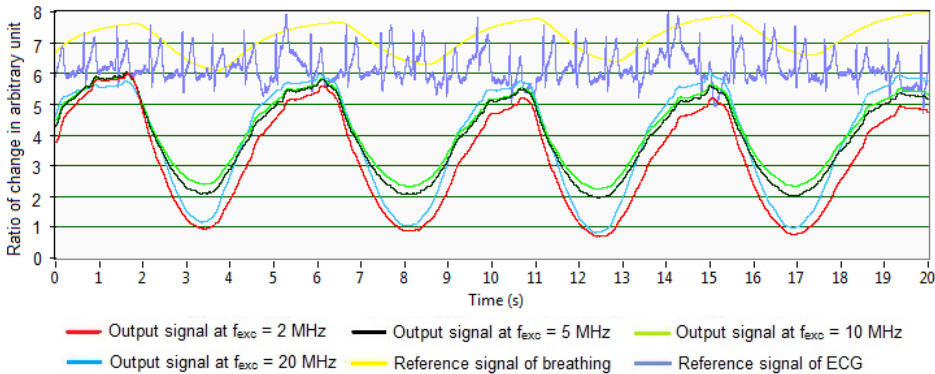


Figure 2.7 Gathered waveforms of the impedance of the body of volunteer according to the EPC NPRMOQ / AEIDHL (ES1) that are measured by using the commercial EBI measurement device in capacitive coupling

2.7.1.2 The results of monitoring respiratory activity by using the ES2

With the goal of finding access exclusively to cardiac activity, the following EPC's of ES2 were used (author's 3rd main publication):

- K / J (electrodes placed on chest);
- E / D (electrodes placed on both upper arms).

As the chosen EPC's were not intended to grant access into respiratory activity and the excitation current can be assumed in its majority not to pass the lung tissue, the amplitudes of changes in measured signal of EBI, caused by in- and exhalation are expected to be lower than in the case of ES1. The waveforms, gathered by the commercial EBI measurement device, are shown in Figure 2.8 and Figure 2.9.

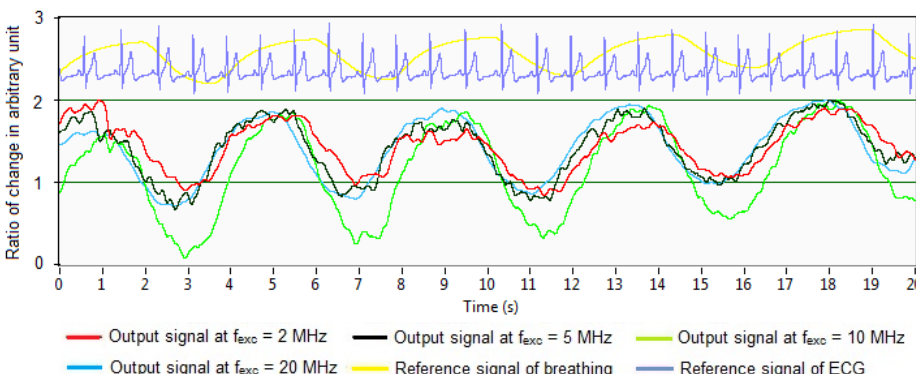


Figure 2.8 Gathered waveforms of the impedance of the body of volunteer according to the EPC K / J (ES2) that are measured by using the commercial EBI measurement device in capacitive coupling

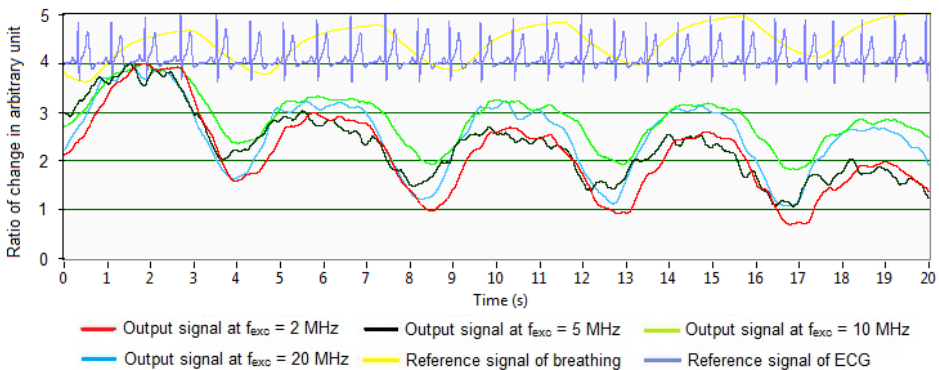


Figure 2.9 Gathered waveforms of the impedance of the body of volunteer according to the EPC E / D (ES2) that are measured by using the commercial EBI measurement device in capacitive coupling

Respiratory activity is visually clearly available in the cases of both EPC's. The ratio of change of volume, though, is larger for EPC K / J (ES2). This was expected as the electrodes in this EPC are placed on chest (on top of the location of lungs). The best excitation frequency for accessing respiratory activity can be considered to be 20 MHz.

The conclusion concerning the experimented EPC's of ES2 can be made: the cardiac activity seems to be recognizable more clearly when focused onto brachial artery (EPC E / D (ES2)). The measurements by using the commercial device, confirm this outcome. The implemented EBI measurement device exhibits the capability of monitoring cardiorespiratory activity by using the ES2.

2.7.1.3 The results of monitoring respiratory activity by using the ES3

To evaluate the implemented EBI measurement device in the case of greatly different type of electrode material, ES3 with conductive textile electrodes was used in the experiment of monitoring cardiorespiratory activity of a volunteer. Single EPC was used, where the laterally placed electrodes relative to body were applied: ABCDIJ / EFGHKLMN (ES1) (author's 3rd main publication).

The waveforms, measured by the reference device are shown in Figure 2.10.

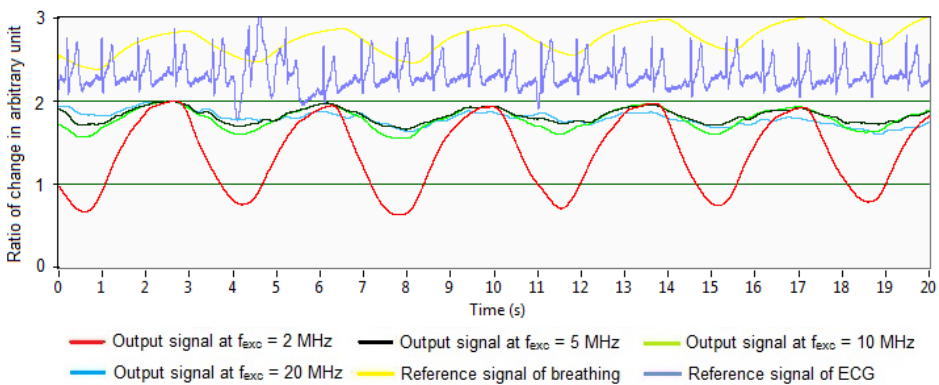


Figure 2.10 Gathered waveforms of the impedance of the body of volunteer according to the EPC ABCDIJ / EFGHKLMN (ES3) that are measured by using the commercial EBI measuring device in capacitive coupling

The visual analyze of the waveforms, gathered by the commercial EBI measurement device reveal the significantly deeper modulation in the signal of EBI caused by respiratory activity at $f_{exc} = 2$ MHz. However, the differences in the amplitudes of peaks, caused by the respiratory activity at different f_{exc} are not of the same magnitude. The deepest modulation of respiratory activity at $f_{exc} = 2$ MHz is assumed to be caused by the parasitic properties of textile electrode in the case of increasing frequency, caused by its woven structure (proposed in the Section 2.3). Cardiac activity can be assumed to be available in the cases of the other three excitation signals of higher frequency being most clear in the case of $f_{exc} = 20$ MHz.

Based on the qualitative evaluation of the results of the capacitive monitoring of cardiorespiratory activity by using the implemented EBI measurement device, the following outline can be drawn concerning the usability of the device:

- Respiratory activity is visually available at all of the chosen excitation frequencies and by using the chosen EPC's of the prepared electrode shirts.
- Cardiac activity is visually available typically at the highest excitation frequency in the cases of EPC's that cover the whole thorax and is fully visually available at all chosen excitation frequencies in the cases of EPC's that are focused on axillary arteries.

The possibility of detecting cardiorespiratory activity in measured signal of EBI was verified. The usability of large area electrodes in capacitive contact in the case of implemented EBI measurement device is confirmed in the case of minimal movements of the subject.

2.7.2 Qualitative evaluation of the measurement results of cardiac activity

In order to explicitly evaluate the possibility of determining cardiac activity by using the commercial and implemented EBI measurement device, the deeper analyze of the gathered waveforms is required. Concerning cardiac activity, visually the best result is achieved at the same f_{exc} in the case of EPC ABCDIJ / EFGHKLMN (ES3) (Figure 2.11) (author's 3rd main publication).

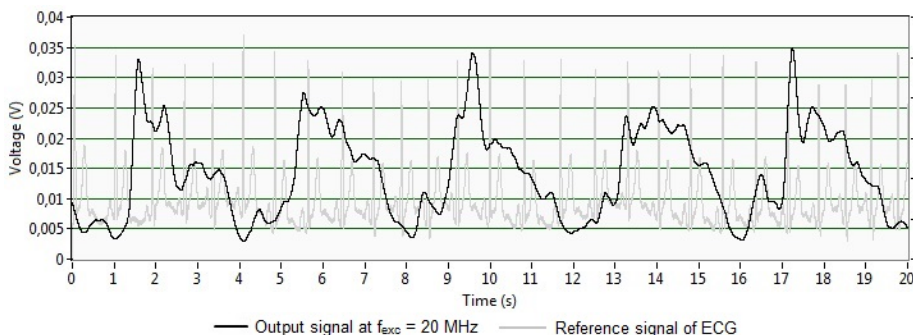


Figure 2.11 Gathered waveform of the impedance of the body of volunteer according to the EPC ABCDIJ / EFGHKLMN (ES3) at $f_{exc} = 20$ MHz that is measured by using the implemented EBI measurement device in capacitive coupling (modified from the author's 3rd main publication)

The waveform in Figure 2.11 is filtered digitally by using Savitzky-Golay filter at 400 side points to remove the high frequency noise. The frequency of the appearance of the peaks in the waveform, measured by using implemented EBI measurement device

and the rate of R wave in the ECG are matching visually. For finding the presumed signal of certain frequency from noisy background, the distribution of energy was determined.

The spectrum of the measured signal in the case of EPC ABCDIJ / EFGHKLMN (ES3) at $f_{exc} = 20$ MHz shows that the fundamental frequency of respiratory activity is clearly available however, the cardiac activity is not identifiable due to the noise – presented in the authors 3rd main publication. The presumption remains that in the case of longer data sets, the spectral power density would indicate the cardiac activity.

A similar result appears in the case of spectral density of EPC E / D (ES2) – the placement that is focused onto axillary and brachial arteries (Figure 2.12). The spectrum shows that the respiratory activity is available, but the heart beating can't be recognized due to the appearance frequency components of near frequencies. This characterizes the relative uncertainty, emerging during the use of the implemented EBI measurement device for monitoring cardiac activity.

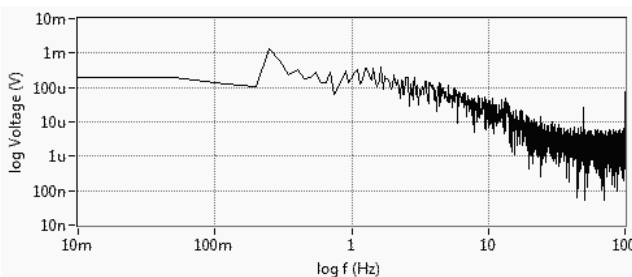


Figure 2.12 Spectrum of the cardiorespiratory signal in the case of capacitive coupling to thorax of volunteer according to the EPC E / D (ES2) at $f_{exc} = 20$ MHz (author's previously unpublished illustration)

As a conclusion, the significantly lower depth of modulation that is caused by cardiac activity in measured signal of EBI has to be emphasized. This is constituting an obstacle in the case of the implemented EBI measurement device, resulting as uncertainty concerning the detectability of the interesting waveform. This is also the reason, why in the quantitative analyze section of cardiac activity, only the results of the commercial measurement device are evaluated (Paragraph 2.8.3).

2.7.3 Qualitative evaluation of the influence of concurrent movements on the measured signal of EBI with the goal of monitoring cardiorespiratory activity

For studying the influence of motion artifacts, the experiment was made in the case of ES3 at $f_{exc} = 20$ MHz while the volunteer was sitting still on the chair and imitating the swimming of crawl just by moving hands while breathing freely. The result can be seen in Figure 2.13 together with the reference signals of breathing and ECG.

The graph reflects the visually recognized signal of respiratory activity in the case of concurrent rhythmical movements. Cardiac activity can't be recognized visually because of significantly lower intervals of change of amplitude. In the case of movements of lower frequency that is close to 0.25 Hz, one can expect a new problem to arise—the separation of the respiratory component and the component of the signal that is caused by the rhythmical movements.

The spectrum of the signal is visible in Figure 2.14, showing clearly the frequency of respiration (~ 0.25 Hz) but concerning the cardiac activity, the presence can't be argued with certainty.

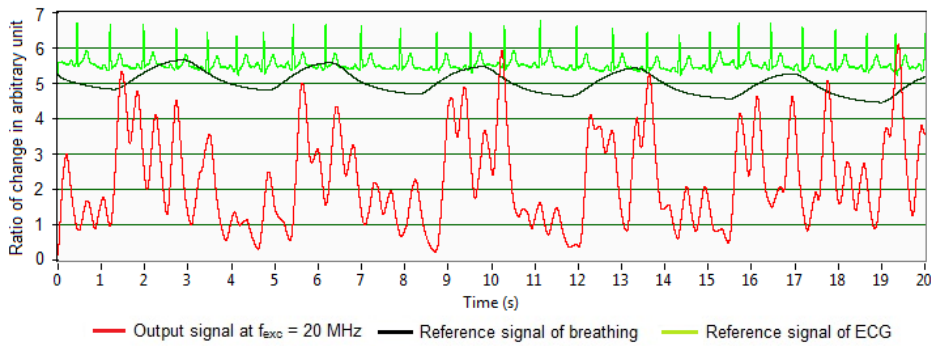


Figure 2.13 Gathered waveform of impedance of the body of volunteer who is imitating swimming of crawl while breathing freely according to the EPC ABCDIJ / EFGHKLMN (ES3) at $f_{exc} = 20$ MHz (author's previously unpublished illustration)

The significant observation of the recognizable respiratory waveform in the measured signal of EBI can be submitted. This notification creates base for future work of ascertaining the placements of electrodes on thoracic surface that are less influenced by movements. Moreover, the different movements are expected to contribute differently to motion artifact and the different electrode placements can be assumed to be less effected by the concurrent movements. This assumption is evaluated in the next chapter.

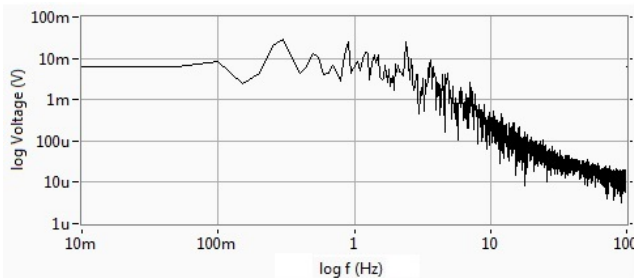


Figure 2.14 Spectrum of the signal of the impedance of the body of volunteer who is imitating swimming of crawl while breathing freely according to the EPC ABCDIJ / EFGHKLMN (ES3) at $f_{exc} = 20$ MHz (author's previously unpublished illustration)

2.8 Quantitative Evaluation of the Results of Monitoring Cardiorespiratory Activity by Using the Electrode Shirts in the Case of Capacitive Coupling

The quantitative evaluation of the results of measurements of EBI is expected to deliver additional information regarding the possibility of monitoring cardiac and respiratory activity in capacitive coupling. The goal is to control the hypothesis—by varying with the size, and placement and material of the electrodes, best configurations of large area electrodes can be determined for capacitive monitoring of cardiorespiratory activity. In addition, the measurements by using the standard ECG monitoring electrodes in resistive coupling were performed according to the placement in Figure 1.16c.

This section represents the extended version of the author's 3rd main publication.

The performed experiments were divided into two groups. First, with the goal of exhaustively evaluating the effect of electrode area, number of electrodes in EPC and

placement of electrodes, the ES1 was chosen for experimentation with the commercial EBI measurement device. Fifteen different EPC's were chosen and in this case the four-electrode system was applied for measuring the EBI of single volunteer.

Secondly, in order to compare the effect of different electrode types and materials on the monitored cardiorespiratory activity, all the implemented electrode shirts were used in the experiments.

2.8.1 Quantitative evaluation of the results of monitoring cardiorespiratory activity by using variety of EPC's in the case of ES1

In order of studying the effect of different EPC's on monitoring of cardiorespiratory activity, the ES1 was chosen because of the largest number of electrodes in this device. Fifteen different configurations were combined in the case of ES1, chosen to cover trunk craniocaudally and laterally in various combinations of electrodes. The EPC's can be represented as the positions of electrodes, connected either craniocaudally or laterally relative to body of volunteer in standing position:

- A. excitation and measuring electrodes placed craniocaudally relative to body (EPC's no. 2, 4, 5, 7–11, 15);
- B. excitation and measuring electrodes placed laterally relative to body (EPC no. 1, 3, 6, 13, 14);
- C. excitation electrodes placed craniocaudally and measuring electrodes placed laterally (EPC no. 12).

The measurements were done by using four-electrode system at the excitation frequency of 10 MHz (the range of HF) and excitation voltage 500 mV. The exact quantity together markings of the electrodes in each EPC and the placement relative to the position of body between the electrodes can be seen in Table 2.1.

Table 2.1 The chosen EPC's in the case of using the ES1 (modified from the author's 1st main publication)

EPC no.	EPC of excitation electrodes (quantity)	EPC of measuring electrodes (quantity)	Placement relative to body
1	IJKL / MN (6)	ABCD / EFGH (8)	B
2	AEIN / DHL M (8)	BFJ / CGK (6)	A
3	MN / OP (4)	ABCD / EFGH (8)	B
4	O / P (2)	ABEFIJN / CDGHKLM (14)	A
5	MO / NP (4)	ABEFIJ / CDGHKL (12)	A
6	AB / KL (4)	CD / IJ (4)	B
7	MD / NA (4)	B / C (2)	A
8	MOQ / NPR (6)	EFIJ / GHKL (8)	A
9	EFIJ / GHKL (8)	O / P (2)	A
10	MOQ / NPR (6)	ABEFIJ / CDGHKL (12)	A
11	MOQ / NPR (3)	FJ / GK (4)	A
12	OQ / PR (4)	ABCD / IJKL (8)	C
13	MN / OPQR (6)	ABCD / IJKL (8)	B
14	MN / OPQR (6)	EFGH / IJKL (8)	B
15	BFJ / CGK (6)	MOQ / NPR (6)	A

Number of experimental measurements were performed in the case of each EPC while ReZ was measured and waveforms were saved for post-processing. The ΔReZ_{resp} , ΔReZ_{card} and ΔReZ_{move} were found based on the (24). The sensitivity was calculated according to the (25) for respiratory (S_{resp}) and cardiac (S_{card}) activity to the effect of concurrent movements, marked as the following parameters (author's 1st main publication):

1. the ratio of ΔReZ_{resp} to ReZ (S_{resp});
2. the ratio of ΔReZ_{card} to ReZ (S_{card});
3. the ratio of ΔReZ_{resp} to ΔReZ_{move} ($S_{resp:move}$);
4. the ratio of ΔReZ_{card} to ΔReZ_{move} ($S_{card:move}$).

The graphical representation of the results can be seen in Figure 2.15.

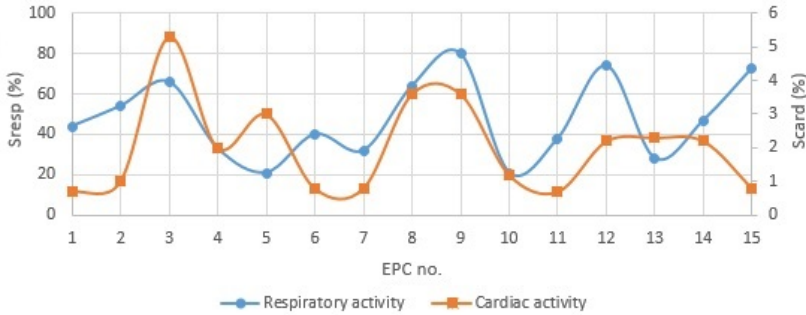


Figure 2.15 Influence of the choice of EPC on the measured S_{resp} (parameter no. 1) and S_{card} (parameter no. 2)

In order of characterizing the influence of concurrent movements, the result is presented as the intervals of ΔReZ_{resp} and ΔReZ_{card} from the ΔReZ_{move} , denoted as $S_{resp:move}$ and $S_{card:move}$ respectively. The graphical representation of the results by using the data of author's 1st main publication, can be seen in Figure 2.16.

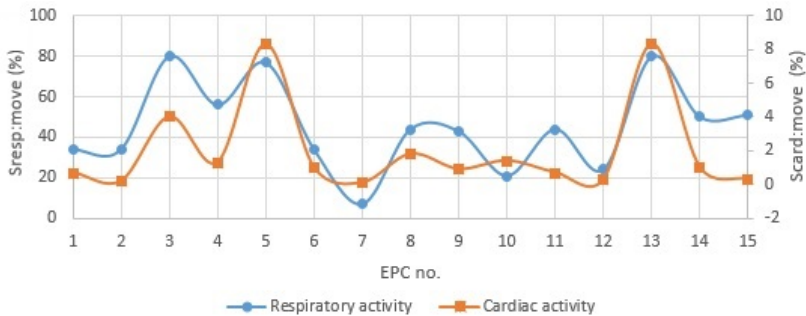


Figure 2.16 Influence of the choice of EPC on the measured $S_{resp:move}$ (parameter no. 3) and $S_{card:move}$ (parameter no. 4)

The fact that the EPC's does not provide equally good S in the cases of both interesting processes is evident. The S_{resp} is more than 10x higher than S_{card} . In comparison with the measured ΔReZ_{move} , generally the $S_{resp:move}$ and $S_{card:move}$ follow the same trace—i.e. mirroring the high impact of concurrent movements.

The following outline can be drawn concerning the best EPC's of the ES1 for monitoring cardiorespiratory activity (author's 1st main publication):

- The best result for respiratory activity concerning the parameter no. 1 was achieved in the case of using EPC no. 9 (exciting on back with the craniocaudally placed combinations of four electrodes and measuring on axillae with single craniocaudally placed electrodes) (Figure 2.17a).
- The best result for cardiac activity concerning the parameter no. 2 was achieved in the case of using EPC no. 3 (exciting on shoulders and axillae with the laterally placed combinations of two electrodes and measuring on back with the laterally placed combinations of four electrodes) (Figure 2.18a).
- The best results for respiratory activity concerning the parameter no. 3 were achieved quite equally in the cases of using EPC's no. 3 and 13 (exciting on frontal side of thorax with the laterally placed combinations of three electrodes and measuring on back with the laterally placed combinations of four electrodes) (Figure 2.17b).
- The best results for respiratory activity concerning the parameter no. 4 were achieved quite equally in the cases of using EPC's no. 5 (exciting on shoulders and chest with the craniocaudally placed combinations of two electrodes and measuring on back with the craniocaudally placed combinations of six electrodes) (Figure 2.18b) and 13.

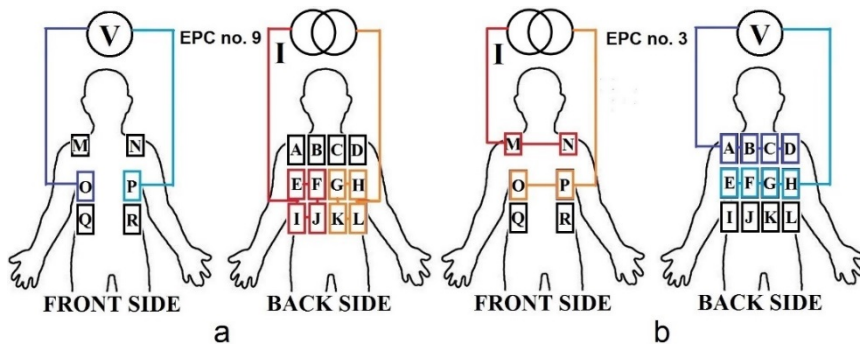


Figure 2.17 The best EPC's of electrodes for monitoring respiratory activity by using capacitive coupling in the case of the 1st and 3rd parameter (author's previously unpublished illustration)

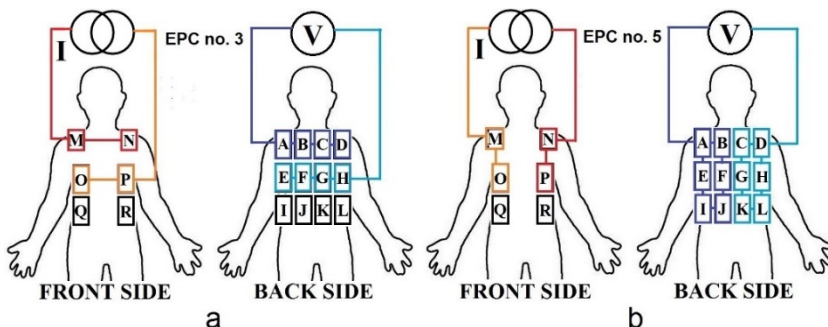


Figure 2.18 The best EPC's of electrodes for monitoring respiratory activity by using capacitive coupling in the case of the 2nd and 4th parameter (author's previously unpublished illustration)

In addition, EPC no. 5 gains only slightly worse result for cardiac activity concerning parameter no. 2. This is showing the possibility of utilizing equally the approaches A and B for monitoring cardiac activity in the case of movements of the body.

Concerning the worst EPC's for monitoring cardiorespiratory activity, the following outline was drawn (author's 1st main publication):

- The worst results for respiratory activity concerning the parameter no. 1 were achieved in the cases of using EPC's no. 5 and 10 (exciting on shoulders and axillae with the craniocaudally placed combination of three electrodes and measuring on back with craniocaudally placed combination of six electrodes).
- The worst result for cardiac activity concerning the parameter no. 2 was achieved in the case of using EPC no. 1 (exciting on shoulders and lower back with the laterally placed combinations of two and four electrodes and measuring on back with laterally placed combinations of four electrodes) and 11 (exciting on front side of thorax with the craniocaudally placed combinations of three electrodes and measuring on back with laterally placed combinations of two electrodes) (author's 1st main publication).
- The worst result for respiratory activity concerning the parameter no. 3 was achieved in the case of using EPC no. 7 (exciting on shoulders with the craniocaudally placed combinations of two electrodes and measuring on scruff with laterally placed single electrodes).
- The worst result for respiratory activity concerning the parameter no. 4 was achieved in the case of using EPC no. 7 (author's 1st main publication).

On the basis of the above listed statements concerning the best and worst EPC's, the following observations can be made:

- In majority of the cases, the craniocaudally placed EPC's relative to body (both: measuring and exciting) result in larger ΔReZ_{resp} .
- The EPC's that contain the larger volume of body in between the electrodes deliver larger interval of ΔReZ , caused by the respiratory activity.
- In the case of monitoring cardiac activity, the placement of electrodes play crucial role related to the location of heart—if heart is not located in the volume between the electrodes, the result deteriorates sharply (EPC no. 7).
- The three best results for cardiac and respiratory activity concerning parameter no. 2 are the same, i.e. the placement and configuration of electrodes in the case of reducing the effect of motion artifact is valid for monitoring cardiorespiratory activity.

When choosing a single EPC that would suit the best for monitoring the cardiac and respiratory activity, the choice could be EPC no. 3 (author's 1st main publication).

Large influence of motion artifact is confirmed, burying the signal of pulse completely in the case of concurrent movements. The respiratory activity can be imitated by moving hands back and forth, illustrated in the author's 1st main publication. Respiratory activity can be reported to be available in the case of concurrent movement (squatting) depicted in the author's 1st main publication. When choosing a single EPC that would suit the best for monitoring cardiac and respiratory activity, the choice could be EPC no. 3 (author's 1st main publication).

2.8.2 Comparative evaluation of the results of monitoring respiratory activity by using the both EBI measurement devices

The results of the commercial and implemented EBI measurement device are compared in this paragraph. The results propose an option of evaluating the capability of different electrode materials in implemented electrode shirts to monitor cardiac activity by using the EBI measurements. The results are expected to differ mainly because of the location of the utilized device: on the desk vs. on the object. The corresponding study for cardiac activity is available in the Paragraph 2.8.3.

2.8.2.1 The comparison of the sensitivity of both used EBI measurement devices

Measurements were performed by using the commercial EBI measurement device. The ΔZ was determined according to the (22). The ΔZ_{resp} and ΔZ_{card} were found based on the (23) and the sensitivity was calculated according to the (25). In this case the result is shown as ratio to the maximum value of measured impedance Z in chosen length of signal waveform—this means that the deeper the modulation and lower the maximum value of measured impedance, the better the result (Table 2.2).

Table 2.2 Results of the S_{resp} by using the commercial EBI measurement device

Device (EPC)	S_{resp} at 2 MHz (%)	S_{resp} at 5 MHz (%)	S_{resp} at 10 MHz (%)	S_{resp} at 20 MHz (%)
Contact electrodes	0.713	1.805	1.472	1.052
ES1 (EFGHIJKL / OP)	15.13	9.358	7.180	12.54
ES1 (NPRMOQ / AEIDHL)	23.85	19.76	17.58	23.91
ES2 (K / J)	2.132	2.661	3.871	2.597
ES2 (E / D)	1.969	1.666	1.373	2.184
ES3 (ABCDIJ / EFGHKLMN)	6.213	1.498	2.033	1.195

According to the gathered data, the S_{resp} shows the highest value by using the EPC NPRMOQ / AEIDHL (ES1) at $f_{exc} = 20$ MHz. The lowest S_{resp} , by using the contact electrodes at $f_{exc} = 2$ MHz. If including only the results of using the capacitive electrodes, the lowest $Interval_{\Delta Z_{resp}}$ is achieved by using the EPC ABCDIJ / EFGHKLMN (ES3) at $f_{exc} = 20$ MHz.

The calculation of \bar{x} of the results (26) at chosen excitation frequencies and utilized EPC's is expected to output the data concerning the best configuration for monitoring the respiratory activity. Moreover, the capability of the implemented device to gain access to the respiratory activity can be evaluated. The calculated values of \bar{x} of the S_{resp} at all of the chosen excitation frequencies for the implemented EBI measurement device and reference measuring device can be seen in Table 2.3 respectively.

The largest \bar{x} of S_{resp} is gained in the cases of both used EPC's of ES1. Among other explanations, this is illustrating the effectiveness of larger surface area of electrodes. Namely, the total area of electrodes in the case of EPC EFGHIJKL / OP (ES1) is 1360 cm^2 . The same area of EPC K / J (ES2) is only 96 cm^2 .

However, the material of the electrode has influence on the result, as the total area of the electrodes in ES3 is comparable to the same parameter of the used EPC's of ES1. The approximate 5x and 10x difference in the value of \bar{x} in the cases of EPC's

EFGHIJKL / OP and NPRMOQ / AEIDHL can be explained by the representation of the measured variable.

Table 2.3 \bar{x} of the results of the S_{resp} by using the implemented and commercial EBI measurement devices at all chosen excitation frequencies

Device (EPC)	\bar{x} of the S_{resp} at all chosen f_{exc} (the implemented EBI measurement device) (%)	\bar{x} of the S_{resp} at all chosen f_{exc} (the commercial EBI measurement device) (%)
Contact electrodes	0.750	1.261
ES1 (EFGHIJKL / OP)	2.070	11.05
ES1 (NPRMOQ / AEIDHL)	2.125	21.03
ES2 (K / J)	0.741	2.815
ES2 (E / D)	0.684	1.798
ES3 (ABCDIJ / EFGHKLMN)	1.559	2.735

Alternatively, the \bar{x} can be calculated for the chosen frequencies in the cases of all chosen EPC's for indicating the most suitable excitation frequencies for monitoring the respiratory activity. The results can be seen in Table 2.4.

Table 2.4 \bar{x} of the results of the S_{resp} by using the implemented and commercial EBI measurement devices at the chosen excitation frequencies in the cases of all chosen EPC's

f_{exc} (MHz)	\bar{x} of the S_{resp} in the cases of all chosen EPC's (the implemented EBI measurement device) (%)	\bar{x} of the S_{resp} in the cases of all chosen EPC's (the commercial EBI measurement device) (%)
2	1.245	8.336
5	1.472	5.959
10	0.944	5.585
20	1.626	7.247

The \bar{x} of the S_{resp} in the case of the implemented EBI measurement device shows the lowest value at $f_{exc} = 10$ MHz, which is assumed to be caused by parasitic capacitances close to the appearing self-resonant frequency (author's 3rd other publication) (M. Metshein & Gordon, 2016). Nevertheless, the above does not seem to apply similarly in the case of the reference measuring device, where the value of \bar{x} of the S_{resp} gains the lowest value equally at the excitation frequencies of 5 and 10 MHz.

The recommended excitation frequency in the case of monitoring the respiratory activity by using the implemented EBI measurement is 20 MHz, though 2 and 5 MHz are the alternatives in presented order. According to the results, the combination of electrode type and f_{exc} to be used for implemented EBI measurement device for monitoring respiratory activity would be EPC NPRMOQ / AEIDHL (ES1) at $f_{exc} = 20$ MHz.

2.8.2.2 The comparison of the depth of modulation in the measured signal of EBI that is caused by respiratory activity

Subsequently, the results of comparative measurements by using contact electrodes and ES1–3 in order to evaluate the monitored data of cardiorespiratory activity are presented. The ΔZ_{resp} , was gained during post-processing of the gathered waveforms of

EBI according to the (22)–(23). The graphical representation of the measured ΔZ_{resp} and S_{resp} can be seen in Figure 2.19a and Figure 2.19b respectively.

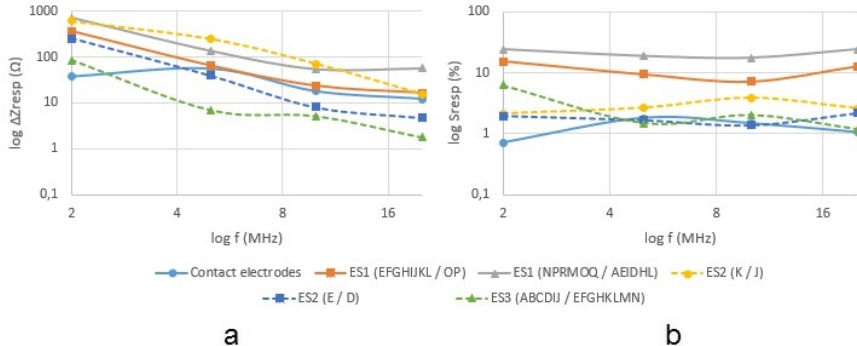


Figure 2.19 Frequency response of ΔZ_{resp} (a) and calculated S_{resp} (b) when monitoring respiratory activity by using the commercial EBI measurement device

The highest ΔZ_{resp} is gained by using the EPC NPRMOQ / AEIDHL (ES1) at the excitation frequency of 2 MHz. Surprisingly the second best result is achieved by using the EPC K / J (ES2) at the same f_{exc} . This result may be explained by the location of the electrodes—placed exactly on top of the upper portions of lungs.

What is interesting, ES3 is showing the lowest value of ΔZ_{resp} in the cases of excitation frequencies at the range of 5–20 MHz—even the contact electrodes exhibit the larger ΔZ_{resp} . Generally for all of the electrode shirts, the largest ΔZ_{resp} is achieved at lowest f_{exc} (2 MHz) and the highest f_{exc} (20 MHz)—the decreasing trend of ΔZ_{resp} is evident with increasing frequency of excitation signal. This trend can be seen if calculating the values of \bar{x} of the ΔZ_{resp} at all of the chosen excitation frequencies (Table 2.5).

Table 2.5 \bar{x} of the ΔZ_{resp} by using the commercial EBI measurement device at the chosen excitation frequencies in the cases of all chosen EPC's

f_{exc} (MHz)	\bar{x} of the ΔZ_{resp} in the cases of all chosen EPC's (Ω)
2	342.3
5	91.52
10	30.06
20	18.00

This can be explained by the alteration in the paths of current flow during the increasing excitation frequency. Specifically, in the case of higher frequencies, the current is expected to travel through outer layers of body surface (epidermis, dermis etc.) as the wavelength decreases. In the case of lower frequencies, the wavelength is higher and current finds more conductive paths in the body where breathing causes deeper modulation on the measured signal of EBI.

If finding the \bar{x} of detected values (according to the (26)) of ΔZ_{resp} when using the chosen EPC's, statistically the most suitable configurations can be determined. The values of \bar{x} can be seen in Table 2.6.

Table 2.6 \bar{x} of the ΔZ_{resp} by using the commercial EBI measurement device in the case of single volunteer at all chosen excitation frequencies

Device (EPC)	\bar{x} of the ΔZ_{resp} at all chosen f_{exc} (Ω)
Contact electrodes	30.59
ES1 (EFGHIJKL / OP)	118.6
ES1 (NPRMOQ / AEIDHL)	238.5
ES2 (K / J)	234.1
ES2 (E / D)	76.49
ES3 (ABCDIJ / EFGHKLMN)	24.56

One can realize that in the cases of experimented electrode shirts, statistically the largest ΔZ_{resp} is provided by the EPC NPRMOQ / AEIDHL (ES1). As indicated already earlier, the slightly lower value of ΔZ_{resp} is provided by the EPC K / J (ES2).

As a conclusion related to the quantitative evaluation of the gathered numerical data of respiratory activity, the following important notifications can be made:

- The depth of modulation in the measured signal of EBI, caused by respiratory activity, at different excitation frequencies may vary about 3x in the case of the same EPC of an electrode shirt, denoting the importance of the choice of the excitation frequency.
- The larger the total area of the electrodes in an EPC in the case of capacitive coupling, the larger the S_{resp} and the better the expected SNR.
- The focusing of electrodes on lungs (EPC K / J (ES2)) proposes equal depth of modulation in measured signal of EBI, caused by respiratory activity as the EPC of largest quantity of foil electrodes (NPRMOQ / AEIDHL (ES1)).
- The choice of the material of the capacitive electrode has importance in the case of monitoring cardiorespiratory activity by using the implemented EBI measurement device—the results of the ES3 are noticeably worse than the result of electrode shirts where the foil plates are used.
- Generally, the value of ΔZ_{resp} is decreasing with increasing excitation frequency while in the case of S_{resp} , the interesting value at $f_{exc} = 20$ MHz sometimes increases to similar level than it is at $f_{exc} = 2$ MHz.

2.8.3 Comparative evaluation of the results of monitoring cardiac activity by using the both EBI measurement devices

The results are expected to indicate the capability of different coupling types in the cases of different electrode materials and EPC's to monitor cardiac activity when measuring the EBI. Moreover, the effect of different excitation frequencies on the ΔZ_{card} and S_{card} is expected to reveal. The ΔZ_{card} was determined according to the (23) and the S_{card} gained by using the (25).

2.8.3.1 The comparison of the sensitivity of both used EBI measurement devices

The results of the S_{card} are available in Table 2.7 and the \bar{x} of detected values of S_{card} (by using the (26) are available in Table 2.8.

One can realize the difference in frequency response in the cases of chosen EPC's of electrode shirts. Generally, the trend of S_{card} is increasing in the cases of all setups when measuring the impedance of a single volunteer.

Table 2.7 Results of the S_{card} by using the commercial EBI measurement device

Device (EPC)	S_{card} at 2 MHz (%)	S_{card} at 5 MHz (%)	S_{card} at 10 MHz (%)	S_{card} at 20 MHz (%)
Contact electrodes	0.056	0.098	0.130	0.100
ES1 (EFGHIJKL / OP)	0.397	0.344	0.339	0.405
ES1 (NPRMOQ / AEIDHL)	1.180	1.370	1.306	1.749
ES2 (K / J)	0.328	0.354	0.358	0.239
ES2 (E / D)	0.168	0.257	0.174	0.300
ES3 (ABCDIJ / EFGHKLMN)	0.058	0.213	0.077	0.206

Table 2.8 \bar{x} of the results of the S_{card} by using the commercial EBI measurement device in the cases of all chosen EPC's at all experimented excitation frequencies

Device (EPC)	\bar{x} of the S_{card} at all chosen f_{exc} (%)
Contact electrodes	0.099
ES1 (EFGHIJKL / OP)	0.371
ES1 (NPRMOQ / AEIDHL)	1.401
ES2 (K / J)	0.320
ES2 (E / D)	0.225
ES3 (ABCDIJ / EFGHKLMN)	0.138

Evidently, the most suitable EPC for monitoring cardiac activity by measuring the EBI through capacitive connection in the sense of S_{card} is NPRMOQ / AEIDHL (ES1)—being approximately 4x better than the second best result. One can see that the EPC E / D (ES2) proposes lower value of S_{card} than the other experimented EPC of ES2, confirming the fact that the focusing on pulsating blood in subclavian arteries does not result in superior access to cardiac activity. Though, the second experimented EPC of ES2 (K / J) proposes the value of S_{card} that is comparable to EPC EFGHIJKL / OP (ES1) where the quantity of electrodes is 5x larger, denoting the potentiality of this EPC for monitoring cardiac activity. The contact electrodes propose the lowest value of S_{card} , characterizing the effect of electrode area on the measured result.

Table 2.9 \bar{x} of the S_{card} by using the commercial EBI measurement device at the chosen excitation frequencies in the cases of all experimented EPC's

f_{exc} (MHz)	\bar{x} of the S_{card} at the chosen f_{exc} (%)
2	0.453
5	0.531
10	0.528
20	0.556

The results of finding the most suitable excitation frequency by utilizing the \bar{x} can be seen in Table 2.9. The table shows that slight increase in the value of S_{card} during the

increase of excitation frequency is evident in the case of calculated \bar{x} . Generally, though, the differences are not significant, revealing in the relative non-effect of excitation frequencies in the chosen range on the calculated \bar{x} of the S_{card} .

2.8.3.2 The comparison of the depth of modulation in the measured signal of EBI that is caused by cardiac activity

Subsequently, the results of comparative measurements by using contact electrodes and ES1–3 in order to evaluate the monitored data of cardiorespiratory activity by measuring the EBI in the case of both EBI measurement device are presented. The ΔZ_{resp} was gained during post-processing of the gathered waveforms of EBI.

The graphical representation of the measured ΔZ_{card} and S_{card} can be seen in Figure 2.20a and Figure 2.20b respectively.

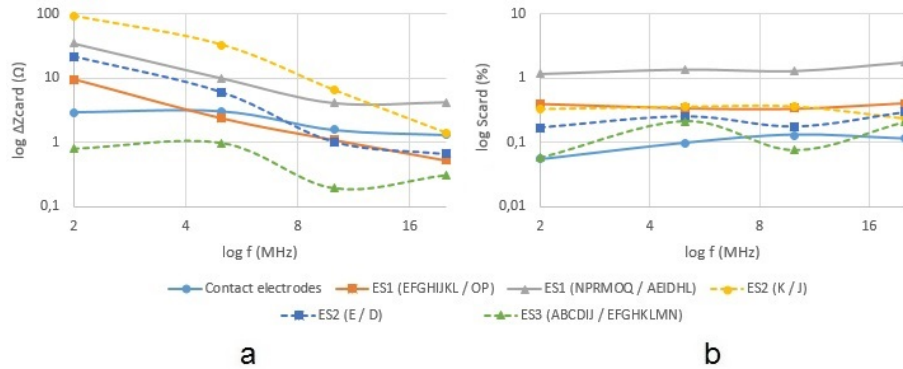


Figure 2.20 Frequency response of ΔZ_{card} (a) and calculated S_{card} (b) when monitoring cardiac activity by using the commercial EBI measurement device

One can see that the ΔZ_{card} is decreasing faster in the case of EPC K / J (ES2) in the case of increasing frequency. This can be explained by the expectation, that with the increasing f_{exc} , the current is not pervading the tissues any more, instead, travelling on the surface layer and not mirroring the volumetric changes. However, when moving into sensitivity domain, the EPC of largest number of foil electrodes is providing better result. This can be explained by the decrease of measured Z while the depth of modulation in the measured signal of EBI, caused by cardiac activity stays relatively the same. Generally, the value of ΔZ_{card} is decreasing with the increasing excitation frequency in all of the experimented EPC's. The lowest value of ΔZ_{card} is obtained by using the EPC ABCDIJ / EFGHKLMN (ES3) at $f_{exc} = 10$ MHz.

The results of determining the most suitable excitation frequency through finding the \bar{x} of can be seen in Table 2.10. Similarly, the most suitable electrode material and configuration is determined by finding the \bar{x} of the values ΔZ_{card} , through the chosen range of excitation signal frequency (Table 2.11).

Statistically the rapid decrease in the value of measured ΔZ_{card} during the increase of excitation frequency is evident, gaining significantly higher value at $f_{exc} = 2$ MHz. The opposite trend was achieved in the case of S_{card} (Table 2.8), showing the trend of increasing value of Z during the increase of excitation frequency.

Table 2.10 \bar{x} of the ΔZ_{card} by using the commercial EBI measurement device at the chosen excitation frequencies in the cases of all experimented EPC's

f_{exc} (MHz)	\bar{x} of the ΔZ_{card} in the cases of all chosen EPC's (Ω)
2	27.27
5	9.376
10	2.526
20	1.576

Table 2.11 \bar{x} of the ΔZ_{card} by using the commercial EBI measurement device at all chosen excitation frequencies

Device (EPC)	\bar{x} of the ΔZ_{card} at all chosen f_{exc} (Ω)
Contact electrodes	2.195
ES1 (EFGHIJKL / OP)	3.415
ES1 (NPRMOQ / AEIDHL)	13.281
ES2 (K / J)	33.29
ES2 (E / D)	7.326
ES3 (ABCDIJ / EFGHKLMN)	0.566

Indeed, as concluded already from Table 2.9, the best result of EPC K / J (ES2) through the chosen frequency range of excitation signals is confirmed by \bar{x} of the values ΔZ_{card} . The placement of reduced number of electrodes directly on chest in a position that the approximate location of heart stays somewhere in between, results as the largest ΔZ_{card} . The second best result is gained by using the laterally positioned electrodes (EPC NPRMOQ / AEIDHL (ES1)) relative to body.

As a conclusion related to the quantitative evaluation of the gathered numerical data of cardiac activity, the following important notifications can be made:

- The choice of frequency of excitation signal has effect on the depth of modulation in the measured signal of EBI—the lowest experimented f_{exc} proposes the highest ΔZ_{card} .
- Concerning the S_{card} that reveal the influence of noise, the difference in the results at different frequencies are not significant—though, proposing the best result at the highest chosen excitation frequency.
- The deepest modulation, caused by cardiac activity in the signal of EBI is gained by using the EPC, where two electrodes are placed on the surface of chest in a way that the approximate location of heart lies in between—suggesting a robust approach of monitoring the volume changes in heart.
- The best result concerning the S_{card} is gained by using the EPC of ES1 where the largest number of foil electrodes is in use (NPRMOQ / AEIDHL).
- In the case of monitoring cardiac activity as measured depth of modulation, the exact positioning of electrodes plays more important role than the total area of electrodes.

2.9 Utilization of Coils as EBI Measuring Electrodes for Capacitive Monitoring of Cardiorespiratory Activity

The focus in today's design of smart wearables is more and more moving to complex solutions, proposing the addition of sensors of different principles: PPG, EBI measurement, inductance measurement, ECG, pressure sensing etc. In comparison, in current work, PPG and ECG together with spirometer for monitoring respiratory activity have been used as reference measurement devices.

The utilization of different sensors open possibility for monitoring a number of variables and properties of human body at the same time. Even more, a complex approach that includes several types of sensors may propose backup in the case of applications where the interesting variable may not be available all the time by using a single approach. What if one sensor is capable of operating by using different methods?

During the experiments a hypothesis was set up: if considering coils to operate as EBI measuring electrodes, cardiorespiratory activity could be monitored. In order to verify the operability of coils as EBI measuring electrodes, coils of two different configurations were used: coil no. 4 (O coil) and 7 (figure-of-eight (Fo8 coil)) (Table 3.1). Experiments were carried out by placing the coils in positions no. 1 and 7 (Figure 3.2)—the positions that were declared to show the best result concerning the effect of concurrent movements and exhibited the average outcome related to cardiorespiratory activity.

The Z was measured by using two-electrode system with the excitation signal amplitude of 500 mV and at the frequency range of 0.256–12 MHz. The measured value of Z at the chosen frequency range of excitation signal can be seen in Figure 2.21.

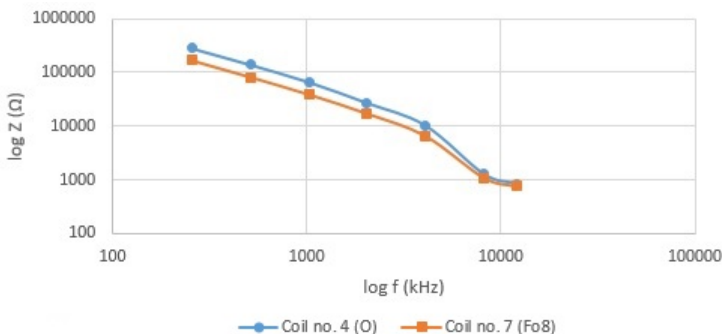


Figure 2.21 Frequency response of measured Z in the cases of using coils no. 4 and 7 as capacitively coupled EBI measuring electrodes in positions no. 1 and 7

The Z is slightly higher in the case of using Fo8 coils as EBI measuring electrodes in two-electrode system. Though, the trend is decreasing in both cases and the shape of the line is following the similar trend.

The depth of ΔZ is indicating which coil type is more suitable for monitoring cardiorespiratory activity by measuring the EBI. The result can be seen separately for respiratory (Figure 2.22a) and cardiac activity (Figure 2.22b).

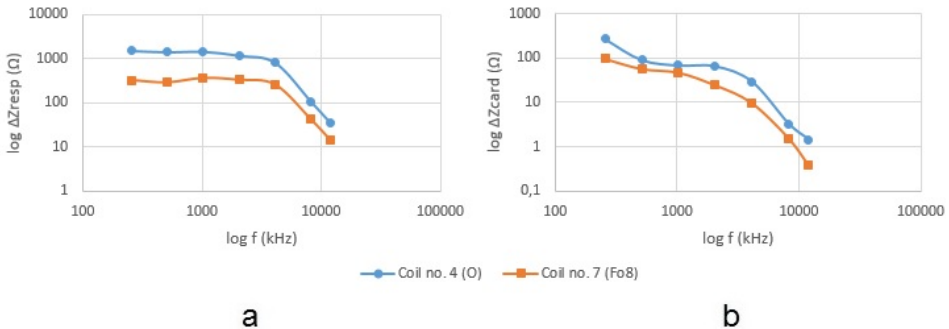


Figure 2.22 Frequency responses of ΔZ_{resp} (a) and ΔZ_{card} (b) in the cases of using coils no. 4 and 7 as capacitively coupled EBI measuring electrodes in positions no. 1 and 7

ΔZ_{resp} is noticeably higher in the case of using Fo8 coils than in the case of O coils as EBI measuring electrodes. The ΔZ_{resp} is rapidly decreasing starting from the frequency of 4 MHz in both cases of coils—until then this frequency, the ΔZ_{resp} maintains similar value. ΔZ_{card} is decreasing uniformly in the cases of both shapes of coils though, being higher for O coils.

The comparison of sensitivities of the ΔZ_{resp} (S_{resp}) and ΔZ_{card} (S_{card}) in both cases of coil shapes would give more comprehensive base for evaluating the gathered data. The results are shown in Figure 2.23a and Figure 2.23b respectively.

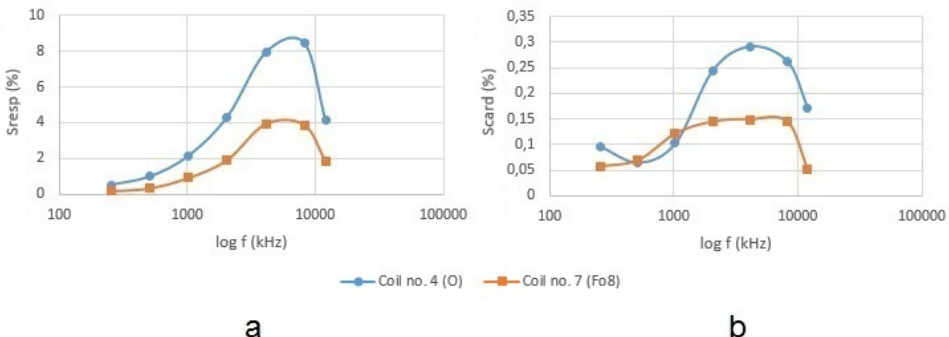


Figure 2.23 Frequency response of the S_{resp} (a) and the S_{card} (b) in the cases of using coils no. 4 and 7 as capacitively coupled EBI measuring electrodes in positions no. 1 and 7

The graphs indicate that both, S_{resp} and S_{card} are generally larger in the case of utilizing the O coils as EBI measuring electrodes through the whole chosen frequency range. One can see that the S_{resp} is achieving its top value at the frequencies of 4 and 8 MHz. The same applies generally on the S_{card} as well, but in addition, the result at the frequency of 2 MHz is also comparable with the best ones. Starting from the frequency of 8 MHz, the S_{resp} and S_{card} are decreasing rapidly.

The waveforms, gathered in the cases of using the excitation frequency which proposes the largest S_{resp} and S_{card} (4 MHz) can be seen in Figure 2.24 and Figure 2.25.

One can realize, that the modulation that is caused by cardiac activity is visually difficult to recognize because of its low depth when compared to respiratory activity.

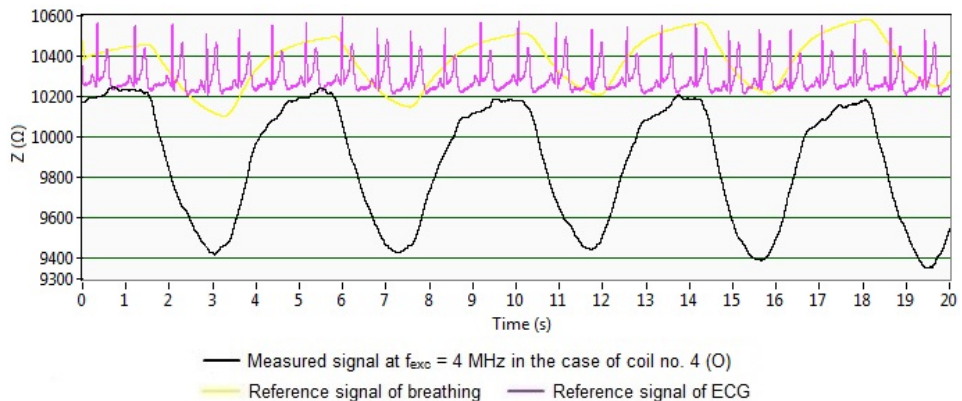


Figure 2.24 Measured signal of Z by using the coil no. 4 (O) as capacitively coupled EBI measuring electrode in positions no. 1 and 7

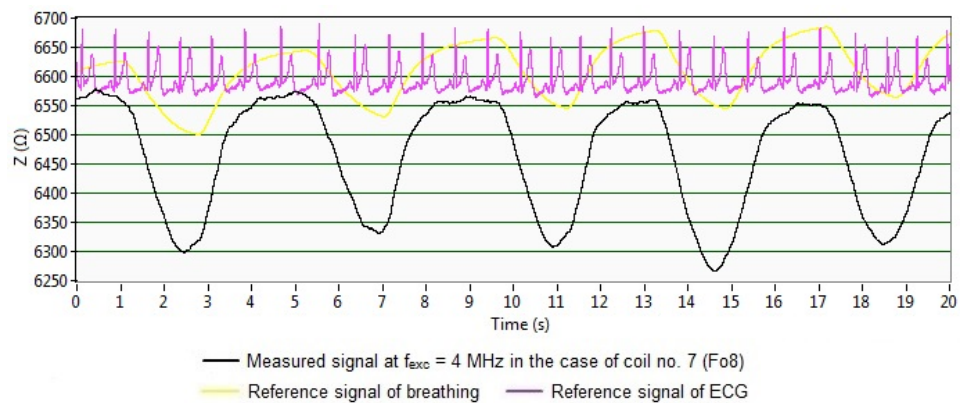


Figure 2.25 Measured signal of Z by using the coil no. 7 (Fo8) as capacitively coupled EBI measuring electrode in positions no. 1 and 7

As a conclusion, the following statements can be rephrased:

- Respiratory activity is clearly available by using the coils as EBI measuring electrodes.
- Cardiac activity is causing of significantly lower modulation on the measured signal of EBI.

However, other placements of coils are expected to propose dissimilar result concerning the depth of modulation, caused by cardiac and respiratory activity. As the goal of this chapter was to prove the usability of coils as EBI measuring electrodes, the results by utilization of coils in other positions are not shown herein.

2.10 Chapter Summary

In this chapter I have described the experimental determination of the best placements and configurations of capacitively coupled electrodes for monitoring cardiorespiratory activity of human by measuring the EBI. Although, in the literature the mapping of human thorax by utilizing the contact electrodes with the goal of determining the most suitable

electrode placements for monitoring heart beating have been reported (Ikarashi et al., 2006), the approach of fulfilling the same task by using the capacitive coupling is forming a fresh approach. There is a lack of published results of such research.

By designing and implementing the electrode shirts, the knowledge, gained during the groundwork was employed. The choice of electrodes to be used in capacitive setup was made according to the availability and ease of attachment onto textile material of everyday clothing. The aluminum foil is flexible enough to follow the changes of the shape of human body, yet rigid enough not to wrinkle. The conductive textile exhibits the properties of underlying layer of cotton fabric, being susceptible to wrinkling. The design of the electrode shirts is robust, though, proposing solid tool for mapping trunk to find the best placements. The practical design and implementation of wearable experimental measurement devices in the form of electrode shirts is described.

I introduced the experimental methodology, based on the utilization of prepared electrode shirts for determining and evaluating cardiorespiratory waveform. I have verified the usability of conductive fabrics as non-contact electrodes for measuring the EBI to detect cardiorespiratory activity. I have proposed the most suitable EPC's of aluminum foil electrodes in non-contact setup on thoracic surface that propose the best outcome relative to cardiorespiratory activity when measuring the EBI. The benefits of continuous non-contact monitoring opposite the vast influence of motion artifact, emerging in the change of distance between electrodes and body surface together with lateral movements. I showed that certain EPC's in non-contact setup propose less influence to measured cardiorespiratory waveform related to the concurrent movements of the body. On top of that, I demonstrated the possibility to visually determine respiratory activity from the signal of EBI in the case of rhythmical movements of the body in certain EPC's.

3 Wearable Solutions Based on Inductive Coupling

In previous chapter I showed the variations in the determination and quality of cardiorespiratory waveforms when measuring the EBI by applying different placements of non-contact electrodes on thoracic surface. The same dependence is assumed to appear when single coil magnetic induction monitoring is applied on thoracic surface. The first task of current chapter is to ascertain the most suitable positions for single coil at the height of 10 mm below xiphisternal joint 360° around thorax for monitoring cardiorespiratory activity in the case of inductive coupling. The above includes the purpose of confirming the variations in the shape of cardiorespiratory waveform, depending on the placement of the coil. The primary goal is supported by design and implementation of flexible coils and incorporates the task of experimentally proving the impact of variety of shapes of coils on the measured signal of cardiorespiratory activity.

The development of coils and evaluation of positions for inductive monitoring of cardiorespiratory activity was implemented with the reason of involving an alternative method to the measurements of EBI. The proposed concept incorporates the possible usage of both methods simultaneously in a wearable measurement device. The detectability of cardiorespiratory activity in the case of inductive coupling is expected to suggest the best placements for coils on the surface of thorax and propose information relative to the same data of EBI measuring electrodes.

This chapter is based on the author's 2nd main publication. The development of flexible coils and the relevant results are previously unpublished.

The specific tasks of this chapter, set up in order to answer the main research questions are listed subsequently:

- A. To experimentally determine the effect of varying position of single coil on thoracic surface on the monitored cardiorespiratory waveform in the case of magnetic induction monitoring by using inductive coupling.
- B. To experimentally determine the most suitable positions of single coil on thoracic surface for monitoring cardiorespiratory activity in the case of magnetic induction monitoring by using inductive coupling.
- C. To experimentally determine the positions of single coil that propose the signal which is less affected by the concurrent movements.
- D. To design and prepare flexible coils of different shapes and configurations, capable of following the curvilinear surface of thorax, in order to perform measurement experiments on single volunteer by using inductive coupling.
- E. To experimentally evaluate the measured cardiorespiratory waveform that is gained by using the O and Fo8 shapes of coils in number of configurations in three chosen positions on front side of thorax.
- F. To perform the qualitative and quantitative evaluation of measured data of single volunteer with the goal of assessing the ability of different coils to deliver the deepest modulation in measured signal, caused by cardiac and respiratory activity, and the less influence of concurrent movements.
- G. To find the method for comparison and to compare the results of monitoring cardiorespiratory activity by using the capacitive and inductive coupling.

This chapter is organized as follows.

In the Section 3.1 the principle of magnetic induction monitoring by using inductive coupling is explained through the prism of monitoring the cardiorespiratory related changes in human body.

The Section 3.2 describes the state of the art of utilizing inductive coupling for monitoring physiological processes in human body and introduces some important achievements in the field through the simulation models.

In the Section 3.3 the results of evaluation of positions of single coil on thoracic surface for magnetic induction monitoring with the goal of detecting cardiorespiratory activity, are shown. More specifically I demonstrate how the choice of positions about the height of 10 mm below xiphisternal joint 360° around thorax influence the delivery of cardiorespiratory activity through the difference in impedance distribution, and throughout, the difference in impact of volume changes, in different regions of thorax.

The Section 3.4 introduces the design and preparation of flexible coils of different shape, diameter and number of windings together with the proposed assumptions related to the effect of bending the coils into two different shapes.

In the Section 3.5 the results of the experimental evaluation of prepared coils at three predetermined positions on front side of thorax, determined beforehand, are presented and analyzed. Importantly, I will show how the signal of cardiorespiratory activity diverges in the case of inductive coupling to thorax by using two main shapes of coils: O and Fo8. The suggestions related to the most suitable configurations of a single coil for magnetic induction monitoring of cardiorespiratory activity are submit.

The Section 3.6 efforts to compare the results of monitoring cardiorespiratory activity by using the capacitive, inductive and resistive coupling in order to suggest the most suitable one.

In the Section 3.7 the conclusions related to the preparation of coils and the results of performed experimentation by using inductive coupling are presented.

3.1 Cardiorespiratory Activity Monitoring by Using Inductive Coupling

The monitoring of biological events—including the interest of current thesis that is cardiorespiratory activity—can be done by using the electromagnetic coupling between a coil and the object. The method, so called magnetic eddy current induction, was first introduced by Vas et al in (Vas, 1967). The principle of this method includes the driving of an AC in a single coil that excites a primary alternating magnetic field (B_1 in Figure 3.1a).

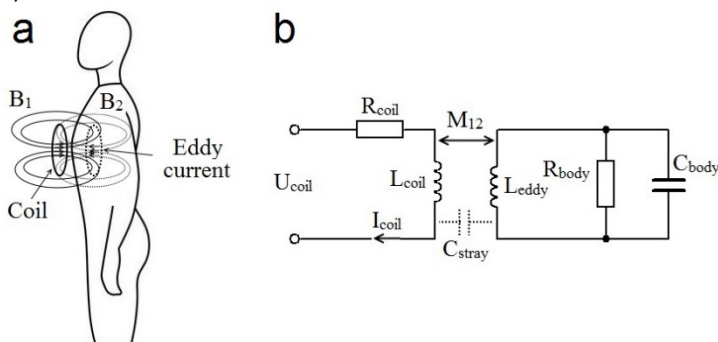


Figure 3.1 Principle of magnetic eddy current monitoring of biological events by using single coil: the emergence of magnetic fields (a) and the equivalent circuit (b) (author's previously unpublished illustration)

If there is biological tissue in the vicinity in this field, the alternating voltage is caused and eddy currents are driven in it—depending on the impedance distributions in object. The higher the conductivity of the medium, the higher the induced density of eddy currents. Related to that, the low frequency currents prefer the paths of high conductivity, which in human body are formed by blood vessels and avoid paths of low conductivity (Grimnes & Martinsen, 2008).

These eddy currents excite another alternating magnetic field (B_2 in Figure 3.1a), which contains the data of impedance distributions in the object. As the re-induced magnetic field affects the primary magnetic field, causing the impedance of the primary coil to change (so called reflected impedance), the single coil method can be used to monitor the changes of impedance in nearby objects. The principle of the described method is to consider the coil as primary coil and eddy currents in the object as the secondary coil of a traditional transformer model with mutual inductance M_{12} (Kwok & Pepper, 1991). The varying impedance of trunk, caused by cardiorespiratory activity can be gained by monitoring the changes of impedance $Z_{coil,r}$ of primary coil and can be expressed as complex reflected coil impedance (D. Teichmann et al., 2013).

$$Z_{coil,r} = \frac{U_{coil}}{I_{coil}} = R_{coil} + j\omega L_{coil} - \frac{\omega^3 C_{body} M_{12}^2}{j\omega C_{body} (R_{body} + j\omega L_{eddy}) + 1} \quad (30)$$

The stray capacitance C_{stray} in Figure 3.1b can be omitted if the distance between the coil surface and thoracic wall is constant. Nevertheless, one can imagine that in practical applications, this is a hard engineering task. Therefore, the ways in which the physiological activity can change the reflected impedance of the primary coil can be listed as follows (Daniel Teichmann, Kuhn, Leonhardt, & Walter, 2014):

- variations in thoracic impedance (volume change, boundary displacement);
- variation in distance between the sensor surface and thoracic wall;
- change of the form and shape of the coil and biological matter in the object.

An important aspect to consider hereby is the depth of penetration of generated magnetic field i.e. the skin depth. The magnetic field is attenuated as function of depth (skin effect), caused by the B_2 that opposites the B_1 . The skin depth δ can be shown as

$$\delta = \frac{1}{\sqrt{\pi f \sigma \mu}} \quad (31)$$

where μ is the magnetic permeability and σ is the conductivity. The represented equation is adaptive in the case of uniform and plane electromagnetic wave (Grimnes & Martinsen, 2008).

In engineering point of view, the monitoring of the changes, caused by the above named mechanisms can be detected by measuring different parameters of resonant circuit. One possibility is to determine the change in the value of resonant frequency of the coil, caused by the changes in the volume of thorax, caused by cardiorespiratory activity (Steffen, Aleksandrowicz, & Leonhardt, 2007). The another possibility is to monitor the change in the value of impedance (D. Teichmann et al., 2013) or inductance of the coil. There are inductance-to-digital chips available in the product list of Texas Instruments that are able to monitor the equivalent parallel resonance impedance, inductance and the resonant frequency of a LC resonator.

3.2 State of the Art of Monitoring Cardiorespiratory Activity by Using Inductive Coupling

Similarly to predicting the current distribution in an object in the case of resistive and capacitive coupling, the simulations of sensitivity distributions for predicting the influence of positioning of coil(s) in the case of inductive coupling for monitoring cardiac (Cordes, Heimann, & Leonhardt, 2012; D. Teichmann et al., 2015) and respiratory activity (Cordes et al., 2012; Gursoy & Scharfetter, 2010) has been reported to be implemented in number of papers. Namely, the induction of displacement currents in an object, induced by a coil or an electrode can be considered to base on the same mechanisms—as a result, the simulations of sensitivity distributions that are caused by different coils can give information concerning the best locations for capacitive monitoring of cardiorespiratory activity as well. Nevertheless, when focusing in simulations on the specific properties of coils, for example on the effect of different shapes and configurations or deformation of the coils, the interesting results can be expected. Especially because of the inhomogeneity of human body, caused by volumes of different conductivities and time varying changes of volumes.

The Fo8 coil is a known shape of coil in transcranial magnetic stimulation (TMS) (Klomjai, Katz, & Lackmy-Vallée, 2015), providing the property of focusing the resulting magnetic field around the intersection of the shape of 8 (Hallett, 2007). The original mathematical modelling is provided in (Cohen et al., 1990) by comparing the magnitude of resulting electric field 10 mm below the magnetic coils of O and Fo8 shapes. The results indicate the vast difference of the two chosen shapes of different coils and also the diameter of coil on the magnitude of the induced magnetic field. In the case of O shaped coil, the electric field is reported to be maximal under the winding of the coil and minimal in the center (Cohen et al., 1990). For Fo8 coil, the forming of electric field gains exactly the opposite situation being minimal under the middle of each wing. By using the today's options of modelling, the similar study has been reported to be performed in (Lu & Ueno, 2015) and indeed, the sensitivity region in the case of O shaped coil comprises around the coil. I.e. the maximum contribution on the induced magnetic field is appearing under the coil wire and not in the center of the coil. In the case of Fo8 coils, the increased depth of penetration was perceived under the intersection of the shape of 8.

The FEM simulations have been performed on models of different parts of human body—for example (Isop, 2017), where the focusing on radial artery to evaluate the distribution of current density and emergence of eddy currents in local volume of wrist has been implemented. The results show that at the lower resonant frequencies (<1 MHz), the eddy currents are forming in pulsating blood in radial artery while in the cases of higher resonant frequencies (>10 MHz), the eddy current are forming in volumes of lower conductivity as well. This suggests, that by placing an O shaped coil of relatively small diameter on approximate location of radial artery and using lower resonant frequency, the contribution of pulsating blood in radial artery is higher than in the case of higher resonant frequencies. The current density distribution is reported to be the highest, in proposed FEM simulation, in highly conductive blood but also in muscular tissue which is only slightly worse electric conductor (Table 4.2). In addition, the conclusion related to the sensitivity region of O shaped coil supports the prior presented acknowledgment: the higher distribution of eddy currents in the nearby volume to the coil wire and relatively less distribution near the center of coil (Isop, 2017).

Yet another report of simulating the induction of eddy currents in human body is reported in (Gi et al., 2015). In this paper, the focusing of O shaped coil onto heart by placing it on front side of thoracic surface is reported. The conclusion, worth of noting from this paper is the notification of the effect of increase in the size of heart on the appearance of eddy currents. The relation between the mechanical movement of living tissues, related to the varying size of heart during cardiac cycles and the varying distribution of eddy currents is proposed (Gi et al., 2015).

However, the deformation of O shaped coil is reported to have influence on the distribution of current density in nearby object (D. Teichmann et al., 2015)—illustrated by the results of FEM simulation. More precisely, two types of deformations have been analyzed from which in the case of convex curvature, the current density distribution is reported to result as two centers of current densities. While in the case of concave curvature, the current density distribution is shown to maintain the similar concentric characteristics as in the case of non-deformed coil (D. Teichmann et al., 2015). In summary, these results suggest that the coils deformed into concave curvature relative to the surface of thorax can be used equally to the non-deformed coils, resulting expectedly as similar result in the case of volume changes underneath.

As a conclusion, the following important findings in published results of simulation studies are listed below:

- The prediction of evidential difference in magnetic field distribution in the cases of O and Fo8 shaped coils that possibly results as the difference in most suitable positions on thorax for monitoring the cardiorespiratory activity induced volumetric changes in thoracic surface (Cohen et al., 1990).
- The prediction of largest contribution of mechanical movements of living tissue, caused by the cardiac cycle induced time varying increase and decrease in the size of heart on the measured inductance of single coil (Gi et al., 2015).
- The dissimilar effect of coil deformation, where the current density distribution of concave curvature is reported to maintain its relative form when compared to the current distribution in nearby object in the case of non-deformed coil (D. Teichmann et al., 2015).

The experimental positioning of single coil for monitoring cardiorespiratory activity has been covered in number of papers, proposing the alike mechanisms to evoke similarly to measurements of EBI. The latter is experimented in (D. Teichmann et al., 2013) where the examination of possible positions on backside of thorax of rigid printed circuit board (PCB) implemented coils and non-contact electrodes for monitoring exclusively cardiac activity has been experimented. The results reveal dissimilar outcome in the sense of the signal of cardiac activity by using the capacitive and inductive coupling. Specifically, for a single coil, the best position was derived to be on left sagittal plane on lower side of back—explained in (D. Teichmann et al., 2013) by the closeness of cardiac apex that introduces considerable degree of motion during the cardiac cycle.

The most suitable positions for capacitive electrodes in two-electrode system were determined to be on upper side of back—explained by the larger contribution of the motion between thoracic wall and sensor surface. The capacitive electrodes were constituted of square shaped layers on rigid PCB with diameter of 30 mm. The coils were also etched on a PCB, containing only a single winding with the diameter of 90 mm. The presented conclusion related to the presence of respiratory activity is declaring the

availability of interesting data by using the both coupling types at all of the experimented position on back side of thorax.

The utilization of an unlike coil material has been reported in (Koo et al., 2014)—a conductive textile implemented coil, which have been experimented in several positions in front side of chest derived from the positions of standard 12-lead ECG leads. The utilized coil itself has 10 windings and the diameter of 66 mm. The position for monitoring cardiac activity has been reported to be: “located 30 mm away from the left side from the center of front line on the chest circumference line” (Koo et al., 2014). By the chest circumference line, a horizontal circular line around thorax at the height of nipples has been noted. Among others, two significant conclusions have been provided in (Koo et al., 2014): the position of electrode has noticeable effect on the quality of measured signal of cardiac activity (1) and the positions of O shaped coils that are placed on flatter area below the location of pectoral muscle exhibit the cardiac signal of better quality than in the case of placing the coil on pectoral muscle (2).

A thorough study on variations in cardiac activity in the case of induction monitoring has been presented in (Vedru & Solntseva, 2007), showing the variety in the shape of the induction cardiography signal that is measured at different positions on front side of trunk. A coil of single winding and diameter of 125 mm has been used in several positions on frontal thoracic surface in the following principle: the central position was chosen to be the point V2 of standard 12-lead ECG placement. From this position, straight lines in different angles were drawn on frontal thoracic surface and single coil placed in predetermined positions during experimental measurement cycle to monitor cardiac activity. The important notification from (Vedru & Solntseva, 2007) is the attenuation of cardiac signal with the increasing distance from heart, denoting the decrease of contribution of heart into signal in peripheral regions. Moreover, the different locations of coil exhibit the property of providing the differences in the shape and the timing when compared to R peak in electrocardiogram.

The utilization of inductive coupling in wearable monitoring devices for monitoring cardiorespiratory activity has also been reported. An example is the MAIN Shirt—an array of several coils, made of flexible wire, that are attached on a shirt (Daniel Teichmann et al., 2014). Or a prototype of a wearable electronic device with PCB implemented coil that is freely lying on the surface of backside of thorax, visualizing cardiorespiratory activity in the case of motionless individual (D. Yang, Xu, Qiao, & Wang, 2017). Nevertheless, the direction of the devices for magnetic induction monitoring seems to be the implemented as planar arrays of sensors for magnetic induction tomography to achieve higher precision in surface mapping (Mooney et al., 2016).

As a conclusion, the following findings can be listed based on the literature review of publications where the positions and configurations of coils have been handled:

- The difference in the most suitable positions for capacitive electrodes and single coil for monitoring cardiorespiratory activity on thoracic surface (D. Teichmann et al., 2013).
- The variation in the most suitable positions for single coil on thoracic surface for monitoring cardiorespiratory activity (D. Teichmann et al., 2013).
- The presence of most suitable positions for O shaped coils on flatter area blow the location of pectoral muscle exhibit on top of the approximate placement of heart because of the vast disturbing effect contracting pectoral muscle (Koo et al., 2014).

- The presence of difference in measured cardiac waveform when monitored on different positions of coil, appearing as attenuation of the signal with increasing distance from heart by using different positions of coils on thoracic surface—representing presumably the cardiac-synchronous energy absorption processes in human body (Vedru & Solntseva, 2007).

3.3 Variations in Cardiorespiratory Waveform in the Case of Magnetic Induction Monitoring by Varying the Position of Single Coil

The possibility of measuring the magnetic induction for monitoring cardiorespiratory activity of human has been emphasized years ago (Tarjan & McFee, 1968). Moreover, the technology has been reported to be implemented into prototypes of wearable devices, capable of detecting the rate of breathing and heart beating (Guardo, Trudelle, Adler, Boulay, & Savard, 1995; D. Teichmann et al., 2015; Daniel Teichmann et al., 2014). As the possibility of monitoring cardiorespiratory activity in the case of inductive coupling has been shown in previous works (Vedru & Solntseva, 2007), the interest of current chapter is to verify the variations in the interesting signal when monitoring from various positions on human trunk—published in the author's 2nd main publication.

For determining these interesting variations, the custom made telemonitoring system of single coil magnetic induction sensor (SCMIS) was used, described in (Ojarand, Pille, Min, Land, & Oleitšuk, 2015). The sensor module of this device is based on LDC1000 (Texas Instruments)—this integrated circuit utilizes the principle of measuring the equivalent parallel resonance impedance R_p and the resonant frequency f_{res} of a LC resonator. R_p can be shown by

$$R_p = \frac{L_{coil} + L_o}{(R_s + R_o)C_p} \quad (32)$$

where L_{coil} is the inductance of the coil, R_s is the series resistance of the coil, C_p is the parallel capacitance, R_o is the reflected resistance of the object and L_o the reflected inductance of the object. The device is configurable and proposes option to gather the measured data by using a corresponding LabVIEW program.

A single square shaped coil of diameter of 75 mm was employed in the experiments, containing eight windings of wire with cross-section area of 0.75 mm²—indicating the coil no. 6 in (Ojarand et al., 2015). In the used setup, $f_{res} = 4.2144$ MHz, while the maximum LC frequency range for this IC is 5 kHz–5 MHz. The coil is attached into a plain rigid plastic form and its backside is shielded with a flexible ferrite sheet, making the application unwieldy and inflexible. This must be consider when placed on uneven surfaces of human body, nevertheless, making the interpretation of the results more straightforward concerning the shape of the coil.

The experiments were carried out to gather the comparable data of simultaneous measurements of cardiorespiratory activity of single volunteer by using the magnetic induction sensor synchronously with reference monitoring of ECG and respiratory activity. Twelve predetermined positions 360° around thorax were experimented, lying on a horizontal line on thoracic surface approximately 10 mm below xiphisternal joint, denoting the center of the coil (Figure 3.2). The spacing between the positions was about 80 mm and the central positions were designated according to xiphisternum and backbone. The volunteer was dressed into cotton shirt with thickness of 0.5 mm,

where the horizontal line and positions were marked—the illustration is available in the author's 2nd main publication.

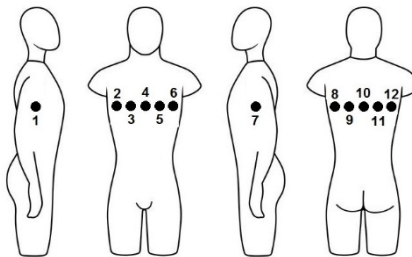


Figure 3.2 The chosen positions on thoracic surface for monitoring cardiorespiratory activity in the experiments of using single coil inductive coupling (modified from the author's 2nd main publication)

The coil was placed at the chosen position by fixing it with a belt and was shifted during the measurement cycle along the horizontal line according to the chosen order of positions. The error of positioning the coil can be estimated to remain in the range of 10 mm in both, horizontal and vertical direction. The reference signals were gathered by using standard ECG solid gel electrodes according to the Eindhoven's lead I of and spirometer. The volunteer was asked to fulfill certain program of movements while a single measurement was carried out in each position (author's 2nd main publication):

1. standing still while breathing freely for 10 sec (1);
2. standing still while holding the breath for 10 sec (2);
3. imitating walking while breathing freely for 10 sec (3).

The changing portion of R_p (ΔR_p) is assumed to be caused by pulsating blood in blood vessels and heart (ΔR_{p_card}), changing volume of lungs that is caused by breathing (ΔR_{p_resp}) and concurrent movements (ΔR_{p_move}) described by the (24). According to the (25), the sensitivity was calculated in three cases: S_{card} , S_{resp} and S_{move} .

The evaluation of the results can be found from the author's 2nd main publication, though, the main observations are referred subsequently together with graphical representation. The visual evaluation confirms that the respiratory activity is available in all of the chosen positions of the coil—though, of varying amplitude (Figure 3.3).

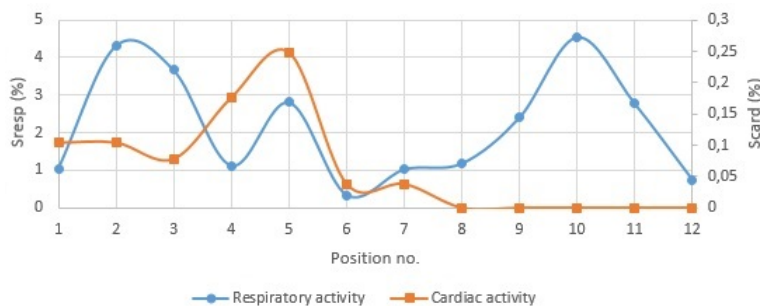


Figure 3.3 Influence of the choice of coil position on thoracic surface on the S_{resp} and S_{card} (author's previously unpublished illustration)

The largest S_{resp} is achieved in the case of position no. 10 (center on the backside of thorax), constituting 4.55 % of the median value of R_p . This was expected as in this position, the created magnetic field is affected by both lungs. Numerically, the lowest S_{resp} is achieved in the case of position no. 6 (outermost positions on backside of thorax); but also in position no. 1 and 7 (sides of thorax); and position no. 8 and 12 (outermost positions on backside of thorax). It can be assumed that in the outermost positions, some portion of lungs is not at the outreach of the magnetic field, having less influence. Moreover, the rigid placement of the coil in a plain plastic form does not allow it to follow the curvilinear shape of thorax, especially on the outermost positions—this is supposed to further decrease the affection of volume changes to the magnetic field through the ineffective current density distribution.

The largest S_{card} is achieved unconventionally in the case of position no. 5 (but also in the case of position no. 4). These positions lie on top of the location of heart and are reported to be the best ones also in (Daniel Teichmann et al., 2014). In the cases of the positions on backside of thorax, the cardiac activity can't be recognized. This can be related to the shape of the formed magnetic field, which does not pervade the volume of thorax that lies between heart and the coil. In another words, the induced current density distribution is assumed not to be focused onto heart but scatters in interim medium. Still, if it does, the change of the value of R_p that is caused by cardiac activity is incomparably smaller when compared to the remaining volume of thorax.

The S_{move} shows the lowest (i.e. the best) value in the cases of placement of the coils on sides of thorax (positions no. 1 and 7) (Figure 3.4). This shows the feature of the position in sides of thorax of having less influence on the coil that is placed in loose connection to the body concerning the movements. The same conclusion was made also in the case of measurements of EBI concerning the placement of electrodes in axillae (Section 2.7). The S_{move} shows the highest (i.e. the worst) value in the case of placement of the coil on the position of left lung (position no. 3).

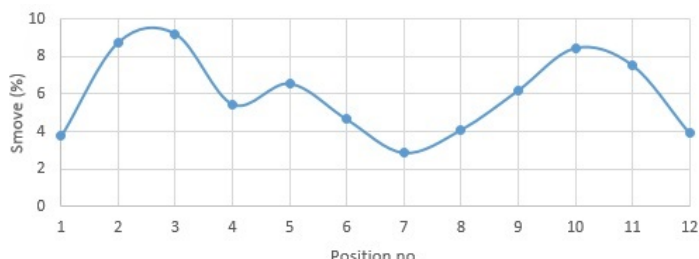


Figure 3.4 Influence of the choice of coil position on thoracic surface on the S_{move} (author's previously unpublished illustration)

The shape of the signal waveform, caused by the pulsating blood in measured graph of R_p , are of varying shape and amplitude. This can be explained by the variability of cardiac-synchronous energy absorption in the body, caused by the changing shape, volume and liquid content of organs in thorax (Vedru & Solntseva, 2007)—revealing in the placement of the coil (author's 2nd main publication).

If one should choose a single position of a coil for monitoring cardiorespiratory activity, the choice would be position no. 5, which proposes the largest S_{card} and average results concerning the respiratory activity and the influence of movements.

The diameter of the coil and the number of windings have the influence on the direction and the shape of the magnetic field. Even more, the shape of the coil could be modified to focus the magnetic field directly onto the interesting area of the object. In addition, the increase in resonant frequency of the LC resonator could have effect to the result—nevertheless, this presumes to usage of new generation of LDC chips of Texas Instruments. According to the evaluation of the data, the following general conclusions can be made:

- The respiratory activity is available in the cases of all experimented positions.
- The cardiac activity is available in the cases of positions that lie on front side and sides of thorax.

The best positions for single coil for monitoring cardiorespiratory activity and the influence of motions can be considered to be listed subsequently:

- The best position for single coil for monitoring the respiratory activity is position no. 10 (center on the backside of thorax).
- The best position for single coil for monitoring the cardiac activity is position no. 5 (left-center on the front side of thorax on top of the location of heart).
- The best positions for single coil concerning the influence of motions are positions no. 1 and 7 (sides of thorax).

According to the results of using a single coil for monitoring cardiorespiratory activity in the case of inductive coupling, the hypothesis could be set up as follows:

- The modifications in the shape, diameter and number of windings of the coil are expected to have positive effect to the availability of the interesting data.
- The increase in resonant frequency of the coil effects the presence of the interesting signal.
- The usage of flexible coil that follow the curvilinear surface of thorax instead of rigid one is focusing the magnetic field and increasing the current density when attached in concave setup.

3.4 Design, Implementation and Characterization of Flexible Coils for Monitoring Cardiorespiratory Activity by Using Inductive Coupling

Similarly to the difference in the placement of electrodes in the case of measuring the EBI for monitoring cardiorespiratory activity (Section 2.7), the same effect appears in the case of magnetic induction monitoring—shown in the Section 3.3. Nevertheless, in the case of coils, there are more properties that can be alter: shape of the coil (1); diameter of the coil (2), number of windings (3). Moreover, the resonant frequency (f_{res}) could be set for LC resonator circuit, defined by

$$f_{res} = \frac{1}{2\pi\sqrt{LC}} \quad (33)$$

where L is the inductance of the circuit and C is the capacitance of the circuit. By changing the value of C , the f_{res} could be tuned for coils of varying shape, diameter and number of windings. For establishing the means for examining the hypothesis, set up in previous chapter, coils of different physical properties were designed. Two different shapes for designing the coils were chosen: O and Fo8.

The Fo8 coil has shown to possess the property of focusing the magnetic field around the intersection of the shape of 8, utilized especially in the field of TMS (Lu & Ueno, 2015; S. Ueno, Tashiro, & Harada, 1988). The coils were implemented by using the silicone wire of type SILI-1V 0,15 (Stäubli Electrical Connectors AG) with cross-section area of 0.15 mm² and outer diameter of 1.4 mm. Silicone wire was chosen because of its highly flexible properties, proposing the opportunity of preparing flexible coils. Variety of diameters and number of winding were chosen and coils prepared on pieces of cotton fabric (with thickness of 0.5 mm). The pattern for understanding the dimensions of the prepared coils can be seen in Figure 3.5 and the physical data is available in Table 3.1.

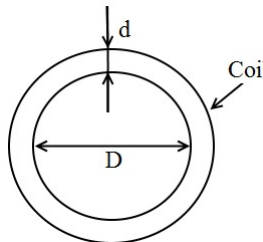


Figure 3.5 Pattern for understanding the dimensions of the designed coils (author's previously unpublished illustration)

The value of the d for coils with different number of windings can be found by multiplying it with the outer diameter of the wire (1.4 mm). The wire was fixed in desired shape on pieces of cotton fabric (thickness of 1 mm) by using common silicone sealant.

Table 3.1 The shapes, diameters and the number of windings of the prepared flexible coils together with the results of measured inductance (author's previously unpublished results)

Coil no.	Shape of the coil	Diameter D of the coil (mm)	Number of windings	Inductance L_{coil} (μ H)
1	O	50	2	0.67
2	O	50	4	2.30
3	O	100	2	1.25
4	O	100	4	4.53
5	Fo8	50	2	1.14
6	Fo8	50	4	3.69
7	Fo8	100	2	2.70
8	Fo8	100	4	9.20

To verify the ability of prepared coils to resonate, the sweep in frequency range of 0.5–50 MHz was implemented by using HF2IS impedance spectrometer. Series inductance of the coil was measured at excitation signal frequency of 10 kHz in the case of 150 mm long measuring leads with crocodile clips (Table 3.1). Examples of the prepared coils can be seen in Figure 3.6.

The influence of deformation of a flexible coil on the current density distribution has been published in (D. Teichmann et al., 2015), proposing the simulations of two opposite curvatures of the coil: convex and concave. Their results show that in the case of concave curvature, the current density distribution maintains the concentric characteristic of

non-deformed coil. The convex curvature causes the rise of two centers of high current density in the opposite edges of the center line of bending area.

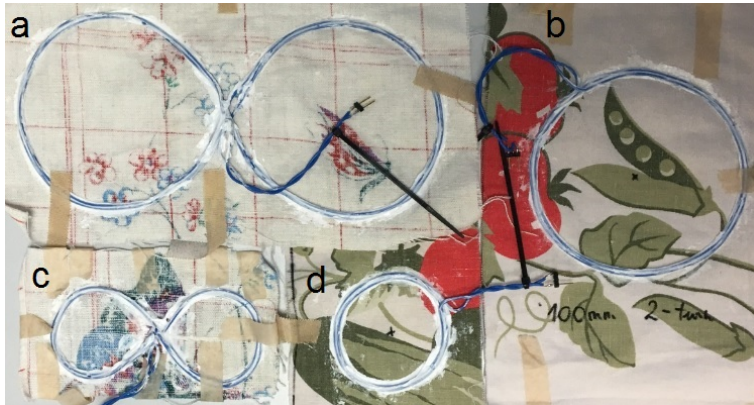


Figure 3.6 Examples of the prepared flexible O (b and d) and Fo8 coils (a and c) (author's previously unpublished illustration)

During the design and implementation of the flexible O and Fo8 coils, the following observations were made concerning the physical behavior of the chosen shapes:

- Both shapes of implemented coils follow the curvilinear surface of thorax when attached onto the clothing—gaining the concave curvature.
- According to (D. Teichmann et al., 2015), the concave curvature of coil relative to thorax maintains the similar current density distribution and is therefore more reasonable to utilize if other considerations are not present.

3.5 Setup and Results of Monitoring Cardiorespiratory Activity by Using the Prepared Coils in the Case of Inductive Coupling

For evaluating the hypotheses, set up in the Section 3.1, the measurements were carried out on a single volunteer. Nevertheless, as one of the hypotheses was the positive effect of the increase in resonant frequency of the coil, the LDC1000 based telemonitoring system of SCMS was wave aside. Instead, the evaluation module LDC1101EVM (Texas Instruments) of newer generation inductance-to-digital IC LDC1101 was used. This chip has the LC frequency range of 0.5–10 MHz. The evaluation board is equipped with onboard preprogrammed microcontroller, connected to PC through USB connection; and can be accessed, configured and data gathered by using LabVIEW program.

For setting the resonant frequency of the coil, the value of sensor capacitor C_{sen} of LC resonator circuit was calculated according to the (33). The value of f_{res} was chosen to be 9 MHz, nevertheless, as the standard capacitor tag might not exactly match the result of the calculation, the actual f_{res} may vary in the order of ± 0.5 MHz. The volunteer was dressed into the cotton shirt where the horizontal circular line and positions were marked (the same shirt as it was used in experiments described in the Section 3.2) and instructed to fulfill the following program:

1. standing still while breathing deeply for 15 sec,
2. standing still while holding the breathe for 15 sec,
3. imitated walking while breathing freely for 15 sec,
4. imitated swimming of crawl while breathing freely for 15 sec.

The resulting waveforms of R_p were gathered by using different coils, digitally filtered by using Savitzky-Golay filter at 50 side points in LabVIEW. Only positions no. 3–5 were chosen to experiment with flexible O and Fo8 coils (Figure 3.2). This choice is explained by the fact that the best placements for monitoring the cardiac activity is shown in the Section 3.3 to fall into the same range of positions (no. 4–5) and respiratory activity to be available in all of the positions. The reason for choosing position no. 3, is explained by the desire to experiment on top of the right lung which is of slightly different shape and volume than the left lung; and proposed the worst result in the Section 3.3 in the case of the influence of motions. The coil was placed by using pieces of adhesive tape to fix it onto the cotton shirt.

Single measurement was carried out in each position. The changing portions of R_p (ΔR_p), caused by cardiac activity (ΔR_{p_resp}), respiratory activity (ΔR_{p_card}) and movements (ΔR_{p_move}) were found according to the (24). The respective sensitivities were calculated according to the (25). For quantitative evaluation of the experimented positions of coils concerning the capability of granting access to the interesting data on the same basis, the results are shown in percentages for repeated measurements (Table 3.2). This choice is explained by high dependability of the measured results to the movements of the body, resulting in varying values of R_p in each repeated measurement.

Table 3.2 Results of the measurements of R_p of O and Fo8 coils in inductive coupling to predetermined positions on thorax by using the LDC1101EVM (author's previously unpublished results)

Coil no.	S_{resp} (%)			S_{card} (%)			S_{move} (%)		
	Pos. no. 3	Pos. no. 4	Pos. no. 5	Pos. no. 3	Pos. no. 4	Pos. no. 5	Pos. no. 3	Pos. no. 4	Pos. no. 5
1	1.138	0.576	0.844	0.027	0.023	0.054	7.699	2.789	5.258
2	1.597	1.115	1.489	0.067	0.086	0.083	43.87	38.27	41.36
3	1.863	1.211	3.222	0.039	0.100	0.050	17.65	13.66	12.79
4	8.134	4.250	6.061	0.268	0.132	0.266	40.25	44.45	48.33
5	9.764	2.832	7.110	0.122	0.110	0.284	57.64	25.13	64.55
6	2.935	2.038	2.460	0.033	0.106	0.101	29.74	23.82	32.97
7	7.157	5.534	8.519	0.178	0.126	0.303	56.18	40.82	56.52
8	4.465	7.961	7.775	0.126	0.105	0.197	50.13	38.03	52.12

The results show that the best position concerning the S_{resp} is achieved in the case of coil no. 5 in position no. 3—on top of right lung. The best position concerning the S_{card} is achieved in the case of coil no. 7 in position no. 5—on top of the approximate location of heart. Both coils, no. 5 and 7 are Fo-8 coils, emphasizing the promising properties of these coils to focus the magnetic field into the area of the object that is located close to the intersection of the shape of 8. When comparing the results of O coils, the best position concerning the S_{resp} is achieved in the case of coil no. 4 in position no. 3 which is not much worse from the best result of Fo8 coil.

The best position concerning the S_{card} is achieved in the cases of coil no. 4 in positions no. 3 and 5. Concerning the O coils, conclusion can be made that the coil of larger diameter and larger number of windings results in larger S_{card} and S_{resp} . Moreover, the comparison with the results of Fo8 coils, an interesting trend is revealing: the best result by using the O coils are gained in position no. 4 while the Fo8 coils propose the best

results for cardiac and respiratory activity in position no. 5 and 3 respectively. The experimental results match with the results of simulations (Lu & Ueno, 2015), proposing the differences of distributions of current densities in nearby objects in the cases of O and Fo8 coils. In the case of O coil, the magnetic field is emerging circularly around the coil wire(s), proposing the presumption that if the coil wire is on top of the location of heart or lungs, the affection of the emerging secondary field is larger. This explains the best result of O coils in the case of position no. 4.

Concerning the affection of concurrent movements, the best S_{resp} is achieved in the case of coil no. 1 in position no. 4—the O coil. When comparing the results of Fo8 coils, the less affection from concurrent movements is achieved in the case of coil no. 6 in position no. 4. Here, the drawback of shape of Fo8 coil can be realized: generally, the affection of movements is larger than in the case of O coils. Another general conclusion according to Table 3.2 can be rephrased: the less affection of the movements to the measured value of R_p , the lower the ΔR_p , caused by cardiorespiratory activity.

When finding the arithmetic means (\bar{x}) of the results according to the (26) for different coils in the cases of different positions, generalization concerning the suitability of the positions and coils for monitoring cardiorespiratory activity can be made.

The calculated values of \bar{x} of S_{resp} , S_{card} and S_{move} for two different coil shapes can be seen in Table 3.3 and Table 3.4.

Table 3.3 \bar{x} of the R_p of different configurations of O coils in inductive coupling to thorax of volunteer in predetermined positions by using the LDC1101EVM (author's previously unpublished results)

\bar{x} of S_{resp} (%)			\bar{x} of S_{card} (%)			\bar{x} of S_{move} (%)		
Pos. no. 3	Pos. no. 4	Pos. no. 5	Pos. no. 3	Pos. no. 4	Pos. no. 5	Pos. no. 3	Pos. no. 4	Pos. no. 5
3.183	1.788	2.904	0.100	0.085	0.113	27.37	24.79	26.93

Table 3.4 \bar{x} of the R_p of different configurations of Fo8 coils in inductive coupling to thorax of volunteer in predetermined positions by using the LDC1101EVM (author's previously unpublished results)

\bar{x} of S_{resp} (%)			\bar{x} of S_{card} (%)			\bar{x} of S_{move} (%)		
Pos. no. 3	Pos. no. 4	Pos. no. 5	Pos. no. 3	Pos. no. 4	Pos. no. 5	Pos. no. 3	Pos. no. 4	Pos. no. 5
6.080	4.591	6.466	0.115	0.112	0.221	48.42	31.95	51.54

The statistics confirms the above stated assumptions concerning the difference in the deepness of modulation of cardiac activity in measured signal in the cases of different coil shapes. The S_{card} gains clearly the better result in the case of position no. 5 when Fo8 coil is used. In the case of O coil, the differences between the results from the chosen positions are noticeably smaller. Concerning the respiratory activity, statistics reveals the similar division of the results, which is clearly better for both coil shapes in positions no. 3 and 5. This can be explained by the volume of lungs, constituting large volume of thorax and influencing the induced magnetic fields in the cases of all chosen positions of coils.

Though, in the sense of S_{resp} , the results gain numerically approximately twice as large the value in the case of Fo8 coils than in the case of O coils. The statistics confirm the

conclusion related to the sensitivity of Fo8 coil to concurrent movements, gaining of nearly twice as high S_{move} in positions no. 3 and 5. At the same time, the result for Fo8 coil from the position no. 4 proposes about 35 % lower value. In the case of O coil, the S_{move} gains relatively equal value. One of the explanations to this outcome can also be hidden in the differences in the shapes of the O and Fo8 coils and therefore, in the differences in the current density distributions near the coils, discussed above.

The highest current density distribution in an object in the case of Fo8 coil is induced close to the intersection of the shape of 8 and equally close to the whole coil wire in the case of O coil. According to this, the influence of movements on the coil is the highest for the section of coil that causes the highest current density i.e. the intersection of the shape of 8 in the case of Fo8 coil and the whole coil in the case of O coil. In the case of placement of the Fo8 coil in position no. 4, the intersection of the shape of 8 is not in close vicinity to the surface of thorax because of the hollow above xiphisternal joint. The explanation is that the movements of hands influence less the movements of the intersection of the shape of 8 relative to body surface because of the location of top of the hollow above xiphisternal joint.

For general evaluation of the capability of different shapes of the coils for monitoring cardiorespiratory activity, \bar{x} was calculated by using the (26) (Table 3.5).

Table 3.5 \bar{x} of the R_p of O and Fo8 coils in inductive coupling to thorax of volunteer in all predetermined positions by using the LDC1101EVM (author's previously unpublished results)

Coil no.	\bar{x} of S_{resp} (%)	\bar{x} of S_{card} (%)	\bar{x} of S_{move} (%)
1	0.853	0.035	5.249
2	1.400	0.079	41.17
3	2.099	0.063	14.70
4	6.148	0.222	44.34
5	6.569	0.172	49.11
6	2.478	0.080	28.84
7	7.070	0.202	51.17
8	6.734	0.143	46.76

Table 3.5 \bar{x} of the R_p of O and Fo8 coils in inductive coupling to thorax of volunteer in all predetermined positions by using the LDC1101EVM indicates the fact that generally the Fo8 coil possess better results concerning the monitoring of respiratory activity in positions 3-5. Only the O coil no. 4 shows the comparable results. What is interesting and emerging from the Table 3.5 is the influence of the number of windings at the same diameter of the coil in the cases of O and Fo8 coils to S_{card} and S_{resp} . Namely, S_{card} and S_{resp} increase in the case of O coils and decreasing in the case of Fo8 coils when the number of windings is increasing, confirming the essential difference of the two coil shapes.

Concerning the influence of concurrent movements, the similar pattern emerges from Table 3.5. In the sense of cardiac activity, the calculated \bar{x} gains the best result in the case of coil no. 4. This is in opposite to the results of \bar{x} of the dataset of different O and Fo8 coils, though generally indicating the existing alternative of O coil to grant access to cardiac activity.

Based on the gained results of using the flexible O and Fo8 coils for monitoring cardiorespiratory activity, observations and discussion, the following outline can be drawn:

- There are large differences in distributions of current densities in nearby objects in the cases of O and Fo8 coils that prescribe the positions of coils relative to the interesting organs in thorax: the highest current density distribution in the case of Fo8 coil is induced close to the intersection of the shape of 8 and equally close to the whole coil wire in the case of O coil.
- The above stated observation is related to the difference in the positions of the O and Fo8 coils on the front side of thorax, the best results are gained if the approximate locations of heart and lungs locate close to the section of coil where the highest current density distribution is induced.
- The above stated observation is assumed to be related also to the influence of movements of the coil that is the highest for the section of coil that causes the highest current density i.e. the intersection of the shape of 8 in the case of Fo8 coil and the whole coil in the case of O coil.
- The observation of opposite impact of the number of windings at the same diameter of the coil in the cases of O and Fo8 coils: S_{card} , S_{resp} and S_{move} increase in the case of O coils and decreasing in the case of Fo8 coils when the number of windings is increasing.

The best positions for O coils for monitoring cardiorespiratory activity and the influence of motions can be considered to be listed subsequently:

- The best position for O coil for monitoring the respiratory activity is position no. 3 (10 mm below xiphisternal joint) by using coil no 4.
- The best positions for O coil for monitoring the cardiac activity are positions no. 3 and 5 (10 mm below xiphisternal joint, placed 80 mm from both sides of xiphisternum) by using coil no. 4.
- The best position for O coil concerning the influence of motions is position no. 4 (10 mm below xiphisternal joint) by using coil no. 1.

The best positions for Fo8 coils for monitoring cardiorespiratory activity and the influence of motions can be considered to be listed subsequently:

- The best position for Fo8 coil for monitoring the respiratory activity is position no. 3 (10 mm below xiphisternal joint placed 80 mm to the right of xiphisternum—on top of the location of right lung) by using coil no. 5.
- The best position for Fo8 coil for monitoring the cardiac activity is position no. 5 (10 mm below xiphisternal joint placed 80 mm to the left of xiphisternum—on top of the location of heart) by using coil no. 7.
- The best position for Fo8 coil concerning the influence of motions is position no. 4 (10 mm below xiphisternal joint) by using coil no. 6.

If one should choose a single position for a single coil for monitoring cardiorespiratory activity, the choice would be Fo8 coil no. 7 in position no. 5, which proposes the largest interval of change of R_p in the case of cardiac activity and the second best result concerning the respiratory activity. Nevertheless, this comes with the price of large affection of concurrent movements. When considering the immunity to the affection of movements as a key factor, the choice would be O coil no. 4 in position no. 3. By attaching

two coils, these could be used simultaneously for measuring the EBI for monitoring cardiorespiratory activity—in this case, the choice would be O coils no. 4 in positions no. 3 and 5. This configuration covers the two positions that propose the results among the best ones in the cases of both: cardiac and respiratory activity and about 70 % smaller affection of concurrent movements.

3.6 Comparative Evaluation of the Results of Monitoring Cardiorespiratory Activity in Thorax by Using Capacitive, Inductive and Resistive Coupling

In order to compare the results, gained by using the inductive and capacitive coupling, the proposed way of finding the interval of depth of modulation that is caused by cardiorespiratory activity from the total measured value of signal can be used. More precisely, the comparison can be performed on the basis of relative amount of volume change that is caused by the corresponding physiological process. The respective values in percentages are shown in the chapters of quantitative evaluation, establishing preconditions for comparing the results of two different coupling types.

In order of representing the values, presented in different chapters above in suitable manner for comparison with the goal of judging the best coupling type for monitoring cardiorespiratory activity, the values are gathered into single table. The results are presented as range of values of S that is induced by the interesting volumetric changes, caused by cardiac and respiratory activity (Table 3.6).

Table 3.6 The results of monitoring cardiorespiratory activity on thoracic surface by using the inductive, capacitive and resistive coupling for comparative evaluation

Coupling type	S_{resp} (%)	S_{card} (%)
Inductive	0.576–9.764	0.023–0.303
Capacitive	1.798–21.03	0.138–1.401
Resistive	0.837–3.896	0.023–0.251

For inductive coupling, the range of S is gained by determining the lowest and highest value for breathing and heart beating from the results of the three best experimented positions that were achieved by using the O and Fo8 coils (Table 3.2). For capacitive coupling, the range of S is gained in the same manner from the results of all the experimented EPC's of electrode shirts ES1–3 (Table 2.2 and Table 2.7). The results are available in Table 3.6, shown in percentages as a ranges of intervals that are caused by cardiac and respiratory activity. For resistive coupling, the additional experiments were performed by using the EPC's (electrode shirts) that generally proposed the best outcome concerning the magnitude of measured impedance value and sensitivity: K / J (ES2) (1) and NPRMOQ / AEIDHL (ES1) (2). In the case of K / J (ES2) the large area electrodes of the same size were used. In the case of NPRMOQ / AEIDHL (ES1), the standard ECG monitoring electrodes with foam tape were used in the same positions where large area electrodes were placed in original setup. In Table 3.6, the lowest and highest value of S_{resp} and S_{card} from the gained results are shown.

According to the table above, the efficiency of capacitive coupling in comparison to inductive coupling in current setup is evident. The modulation, caused by respiratory activity in the measured signal is slightly more than 2x larger in the case of capacitive

coupling. In the case of cardiac activity, the difference is more noticeable, demonstrating about $4.5\times$ deeper modulation in the measured signal in the case of capacitive coupling. Though, as visible, the lowest value at capacitive coupling for monitoring cardiac activity is lower than the largest value in the case of inductive coupling, indicating the importance of sensor placement.

The measurements by using resistive coupling give initial notion that the determined sensitivity is the lowest. This can be explained by the fact that the large area electrodes in original dimensions were not used in reference measurements and the results can be expected to be comparable of the measurements by using capacitive coupling if that would have been the case. However, hereby the question of the origin of the signal rise—up to what degree the variation in measured variable is caused by the interesting volume change in organism and up to what degree because of:

- the change of the distance between the body surface and electrodes;
- the deformation of the capacitively coupled electrode or inductively coupled coil on curvature body surface;
- the shift of the sensor relative to body surface etc.

Hereby is expected that some amount of the change in measured value of chosen variable, presumably denoting the volumetric change in human body is actually denoting the complex value that is resulting from the above listed reasons. This is expected to be the reason, why the performed reference measurements of EBI by using resistive coupling are resulting as the lowest calculated S when comparing the top ranges provided by the other coupling types. However, the lower end of ranges is comparable to (and even higher than) the inductive monitoring, presumably reflecting the less effect of above listed reasons because of the utilization of coil as single sensor.

Some configurations in the case of EBI measurement electrodes and some positions in the case of single coil induction monitoring are proposing larger depth of modulation on carrier signal, caused by the interesting physiological process. Also, the frequency of excitation signal in the case of EBI measurements and the resonant frequency of coil in the case of magnetic induction monitoring have influence on the result.

As a summary, one can emphasize the following conclusion:

- In general, capacitive coupling is proposing the better suited option for monitoring cardiorespiratory activity, revealing in the depth of modulation that is evoked in measured signal.
- In the case of respiratory activity, inductive coupling is proposing about $2\times$ lower S_{resp} while it is almost $5\times$ lower in the case of cardiac activity when compared to the results of capacitive coupling.
- Resistive coupling is proposing more than $5\times$ lower S for respiratory activity and about $2.5\times$ lower S for cardiac activity than capacitive coupling.
- Resistive coupling is exhibiting the narrowest range of sensitivity that is proposed to be caused most directly by the volumetric changes in organism—in the contrast to the other two types of couplings which are expected to be influenced by the loose attachment of the sensors.

3.7 Chapter Summary

In this chapter I demonstrated the dependence of the shape of the signal and variations in cardiorespiratory waveform on the choice of position of a single coil on thoracic surface. This describes the experimental work towards the acquisition of essential data that serves as input to the primary tasks. The results are confirming the data that is indicated in literature—the most suitable position of single coil for monitoring cardiac activity is on the approximate location of heart on frontal thoracic surface. Nevertheless the respiratory activity is available on the positions 360° around the thoracic surface about the height of 10 mm below xiphisternal joint. I showed that the similar dependence appears for concurrent motions, rendering as an additional variable in the selection process of position of a single coil.

The groundwork for fulfilling the primary task, consisting of the design and implementation of flexible coils of different shapes, is described with the development of technique of preparation of such coils. The characterization of O and Fo8 coils of varying diameter and number of windings predicted that the induced magnetic field will be vastly different, resulting presumably in the differences in current densities and ultimately in the measurability of volume changes in thorax. The difference between O and Fo8 shapes is predicted by tint of simulations in number of publication (Lu & Ueno, 2015). The experimentation proved convincingly the trueness of the assumptions, revealing in differences in positions on single coil that suit the best for monitoring cardiorespiratory activity in the case of inductive coupling.

The collected waveforms are important relative to the similar study concerning the large area capacitively coupled electrodes. As the coils are usable as EBI measuring electrodes, the information about the most suitable positions of coils give valuable input when planning the design of complex measurement device. Moreover, as flexible coils exhibit similar concerns like bendable electrodes that are related to flexion relative to the curvilinear surface of human body, the similar problems arise: motion artifact, partial leaning of the sensor near the body surface etc. The best configurations of coils, inductively coupled at three prechosen positions on front side of thorax for monitoring cardiorespiratory activity were determined. The impact of concurrent movements was evaluated and issued oddly as having less influence on the secondary magnetic field in the positions where the change of volume that is caused by respiratory activity is the smallest. This result indicates the requisition for agreements when desired to reasonably decrease the motion artifacts.

4 Wearable Solutions Based on Resistive Coupling

In this chapter the experimentation towards the selection of electrode placements and configurations for monitoring cardiac activity is continued. The attention is paid to localized volume of body in order to monitor the time varying volume of blood in vessels, originated by the activity of heart. The main frame of the study is established by the need of proposing the most suitable placements and configurations of electrodes for monitoring pulse wave with the goal of estimating the CAP by measuring the EBI of wrist. More precisely, our research group in cooperation with East-Tallinn Central Hospital has found correlation between the resulting pressure waveform that is acquired by using the invasive coronary arteriography (ICA) and the waveform of EBI that is measured on radial artery (Min et al., 2017).

The common method for gaining the non-invasive access for estimating the CAP is the applanation tonometry, which, though, requires the stable supine position of patient and trained medical personnel. At the moment, the development of TF between these signals that are gained by the listed methods is ongoing with the aim of proposing the technique of EBI measurements of wrist for estimating the CAP (Min et al., 2017).

Wrist was chosen because of the accessibility of radial artery—reaching the outer layers of hand when approaching to scaphoid bone i.e. it is possible to detect its approximate location easily by palpation. Wrist is the least impeding location of a wearable device of sensor especially when considering the clinical procedures.

Number of experimental measurements were performed by using variety of prechosen electrode placements and configurations with the goal of selecting the ones that output the best possible time varying impedance, caused by pulse wave. Standard ECG monitoring electrodes with foam tape were used as main sensors, resistively coupled to skin surface in order to gain the lowest skin-electrode contact impedance. Besides, some custom made electrodes were utilized as well in the experiments, where small surface area and rigidness of electrodes were required in special experiments.

This chapter is based on the author's 4th and 5th main publication.

The specific tasks of this chapter, set up in order to answer the main research questions are listed subsequently:

- A. To experimentally verify the difference of the effect of distally and circularly placed electrodes on monitoring cardiac activity by measuring the EBI of wrist in the case of resistive coupling.
- B. To experimentally evaluate the effect of positioning of small area electrodes, which diameter is comparable to the median diameter of radial artery of adult male relative to radial artery on monitoring cardiac activity by measuring the EBI of wrist.
- C. To experimentally verify the effect of externally applied pressure on the electrodes in four-electrode system that is placed on top of the approximate location of radial artery on the measured impedance and time varying impedance that is caused by pulsating blood.
- D. To evaluate the influence of anatomical variations of wrists if different individuals on the value of measured impedance and time varying impedance that is caused by pulsating blood.
- E. To experimentally evaluate the effect of different placements and configurations of electrodes on the shape of the measured signal of EBI that carries the information of pulse wave.

- F. To experimentally determine the most suitable placements and configurations of electrodes for monitoring pulse wave in radial artery.

This chapter is organized as follows.

In the Section 4.1 the principle of monitoring pulse wave in radial artery by measuring the EBI in the case of resistive coupling to wrist is introduced.

The Section 4.2 describes the state of the art and conceptions of monitoring pulse wave in radial artery by the means of EBI and introduces some important achievements in the field through the simulation models and published results of experimentation.

In the Section 4.3 the evaluation of the effect of electrode placement and configuration on the availability of monitored signal of pulse wave is presented. The application of two principal positioning principles of electrodes is introduced and the most suitable one proposed.

The Section 4.4 examines the problems of positioning small area electrodes which diameter is comparable to the diameter of radial artery of a male in average. The answer will be given to a question: how does the positioning of such electrodes influence the monitored signal of pulse wave.

In the Section 4.5 the preliminary results of custom made wrist wearable electrode for measuring the EBI of wrist for determining pulse wave in radial artery are presented, giving insight also into further work in presented topic.

In the Section 4.6 the theoretical aspects concerning the impedance distribution in local volume of wrist is discussed.

In the Section 4.7 the comparison of monitoring pulse wave in radial artery by using the capacitive, inductive and resistive couplings is presented.

In the Section 4.8 the conclusions related to the performing and results experimental determination of most suitable placements and configurations of resistively coupled EBI measuring electrodes are shown together with emphasized important contributions.

4.1 Cardiac Activity Monitoring by Using Resistive Coupling

The decision of monitoring pulse wave from radial artery was made because of the relation to ongoing project of estimating the CAP by measuring the EBI of wrist (Min et al., 2017). Moreover, when compared to other non-invasive options to measure the EBI of an artery, wrist is the most comfortable, less influenced by motion artifact and most convenient for attaching the electrodes.

Contact electrode has direct electric contact with object, achieved in the cases of either using conductive gel (wet electrode) or dry contact (that may alter to wet contact as soon as stratum corneum gets moistened by body sweat). Alternatively, stratum corneum can be abraded to achieve better settling times concerning hydrating and less affection of motion artifacts (Paragraph 1.3.1). In the case of resistive coupling, the current transfer process is happening through reversible oxidation-reduction reaction (in the case of galvanic contact with some body liquid like sweat), providing low-ohmic contact between the electrodes and object. Resistive coupling can be well characterized by known mechanisms of half-cell potential, double layer capacitance and parallel and series resistances (Paragraph 1.4.1). In the case of contact electrodes, the goal is to achieve the best electric contact with the object and in medical applications typically conductive gels are used between the skin and electrodes. However, conductive gels are not discussed in current thesis in detail.

The utilization of resistive coupling enables to use lower excitation frequencies, allowing current to flow through the skin-electrode contact interface. At the same time, this claim is conditional as the properties of stratum corneum are varying over time, being dependent on number of parameters like room temperature, psychophysiological stimuli etc. Stratum corneum may be dominated by capacitive properties in dry conditions and resistive properties in moist environment (McAdams, 2006).

Hereby, the individual physiological differences in the form of the condition of skin starts to affect the measurements more than in the cases of capacitive and inductive coupling. For example, the higher density of body hair may require approaches of removing the hair or by using conductive foam electrodes to increase the effective resistive contact with body surface (Gruetzmann et al., 2007). The natural dryness of skin has effect on the measurement of EBI: in the first case the moistening may be required to perform the experiments by using resistive coupling.

4.1.1 Pulse wave detection in radial artery by using the measurements of EBI

In simple wording, pulse wave is the moment of time, when the maximum amount of blood is flowing through aorta. Pulse wave is originated by the contract of ventricles, started by the opening of aortic valve which induces the flow of oxygen rich blood into the aorta. However, because of the resistance of wall of arteries, blood is not instantly flowing into artery—in its majority it is temporarily remaining in proximal aorta and the pressure continues to increase. The situation remains until the end of systole, after which the injection of blood into aorta stops and the pressure on the wall of arteries decreases. This decrease starts at the proximal end of aorta and pressure waves spread to arteries and peripherals of arterial tree (J. Q. Li et al., 2018). In the sense of measurements of the EBI, this means the detection of time varying change of impedance $\Delta Z(t)$, caused by the described phenomenon of changing amount of blood that flows through the blood vessel. A simplified illustration can be seen in Figure 4.1.

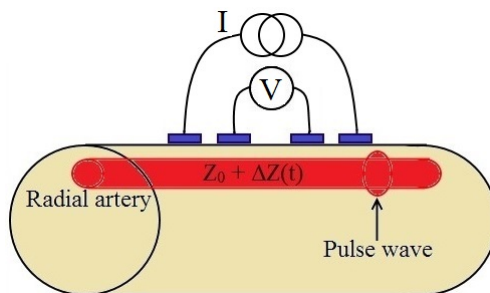


Figure 4.1 Illustration of four-electrode system for monitoring pulse wave in radial artery by measuring the $\Delta Z(t)$ (modified from the author's 4th main publication)

The impedance of wrist can be depicted to consist of the invariable impedance Z_0 and $\Delta Z(t)$ that is caused by pulse wave. The Z is decreasing during the presence of pulse wave and increasing when pulse wave has faded away. For example, by using an approach of exciting the local volume of wrist by alternative current and measuring the voltage, $\Delta Z(t)$ is appearing in EBI waveform as amplitude modulation on top of the carrier signal (Lee & Cho, 2015). An example of waveform of EBI of radial artery (measured by the author), depicting pulse wave together with concurrently monitored PPG, can be seen in Figure 4.2.

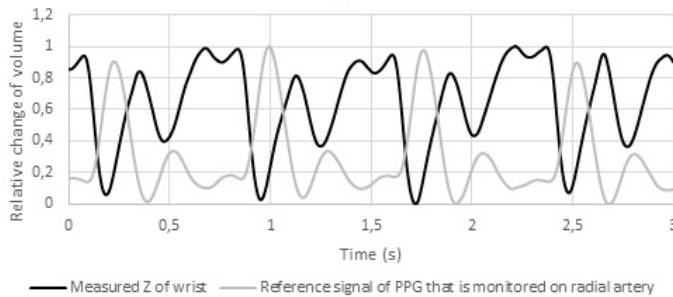


Figure 4.2 Illustration of pulse wave in the case of measured Z of wrist with the reference signal of PPG (author's previously unpublished illustration)

In order of facilitating the comparison of pulse wave in measured signal of blood pressure (Figure 1.14) and also with the signal of PPG with pulse wave in impedance signal of EBI, the last one is typically inverted. The reason is that the Z is decreasing, when pulse wave arrives i.e. at the moment when the maximum volume of blood is present, the measured Z is the lowest. In this way the events of cardiac cycle (Figure 4.2) in measured waveform of EBI follow the same route as in the case of PPG.

4.2 State of the Art of Monitoring Pulse Wave in Radial Artery by Using Resistive Coupling

The approach of measuring the EBI of radial artery for determining cardiac activity in the form of pulse wave is gaining popularity in number of reasons. Firstly, forearm is of the smallest circumference when compared to other limbs and body parts where arteries are located. Secondly, radial artery is reaching the layer of body fat (and skin) when approaching to wrist and pulse rate can be determined by palpating i.e. pressing artery against radius bone by using three fingers. The vicinity of radial artery to skin surface creates preconditions for placing electrodes of small dimensions exactly on top of the location of radial artery and measuring the EBI with the goal of monitoring cardiac activity. Thirdly, wrist is traditionally the place for wearing a wristwatch, therefore, the incorporation of EBI measuring electrodes into some wrist wearable device is feasible (as it is done e.g. in the case of wrist wearable Fitness Tracker UP3™ by Jawbone™ (Jawbone, 2018)). The Fitness Tracker UP3™ measures the EBI of wrist and among other derived parameters and the pulse rate is detected by monitoring the $\Delta Z(t)$. In UP3™ the electrodes in four-electrode system that are lying in-line, are placed circularly around wrist. More precisely, first pair of excitation-measuring electrode is placing on top of the location of radial artery and second one on top of the location of ulnar artery.

The circular placement represents a popular approach for attaching electrodes on wrist with the goal of detecting cardiac activity by measuring the EBI. It is used in experimental measurements (Liu, Cheng, & Su, 2017; J. Xu et al., 2016), but as described above, also in commercial devices.

There are different electrode placements and configurations presented for measuring the EBI of radial (and ulnar) artery. For example, by placing the corresponding excitation and measuring electrodes distally side by side onto wrist as it is done in (Moderhak, Madej, Wtorek, & Truyen, 2011). An option is to split all electrodes in four-electrode system into two parts so that the excitation and measurement is done in reduced areas of skin-electrode interfaces (Moderhak et al., 2011). Though, it is not clear, were there

any advantages over the traditional four-electrode system. The distal placement of electrodes on top of the location of radial or ulnar artery seems self-explanatory as the blood vessel in its length in local volume will lie between the electrodes.

The distal placement of non-invasive electrodes of different dimensions and with varying distance between the excitation and measuring electrodes on top of the location of radial artery has extensively been reported to be utilized (Cho, Kim, & Cho, 2009; Huang, Huang, & See, 2017).

The experimental mapping of the surface of skin with the goal of determining the most suitable placements has been also reported in literature. For example (Cho et al., 2009), where the usage of relatively small area electrodes (length of 15 mm and width of 10 mm) with the distance of 10 mm between the measuring electrodes placed distally on top of the locations of radial and ulnar artery. Surprisingly, the best $\Delta Z(t)$ was achieved when the electrodes were placed on top of the location of ulnar artery in closest position to wrist. The second best result appeared when the electrodes were located on top of radial artery in the same position. Generally, the value of $\Delta Z(t)$ has shown decreasing trend with increasing distance of electrodes in four-electrode system from wrist towards elbow when the length of gap between the measuring electrodes is not changing.

Even though there are proposed and implemented more sophisticated electrode placements strategies like focused impedance measurements (FIM) with variety of number of electrodes (Rabbani, Sarker, Akond, & Akter, 1999), the utilization of these has not been implemented to measure pulse wave in radial artery. The reason may lie in the fact that the circular placement of electrodes in four-electrode system, where one electrode pair is placed on radial artery and second electrode pair on ulnar artery, results relatively satisfactorily. Nevertheless, the usage of 4-electrode, 6-electrode and different configurations of 8-electrode FIM may propose competitive outcome—suggested by the simulation models (Pettersen, Ferdous, Kalvøy, Martinsen, & Høgetveit, 2014).

As a conclusion, the following findings can be listed based on the literature review of publications where the positions and configurations of electrodes have been handled:

- Basically there are two main approaches of electrode placements that have been used to measure the EBI of wrist for detecting cardiac activity in radial artery: distal and circular placement relative to wrist.
- The assured placement of electrodes for monitoring pulse wave in radial artery seems to be: four-electrode system of electrodes that are placed circularly around wrist and located as follows where one pair of excitation-measuring electrode placed on top of approximate location of radial artery and second pair on top of approximate location of ulnar artery.
- Pulse wave in arteries in wrist has been reported to be detected by variety of electrode placement—the solution is designed depending on the necessity.

Not many publications are available, where the implementation of virtual model of wrist is implemented and analysis performed to evaluate the sensitivity distribution in order to compare different electrode placements and configurations. One example is (Krotov, 2017), where a simplified model of wrist is created and electrode position proposed where the positive sensitivity is covering the volume of blood vessel, proposing presumably the highest $\Delta Z(t)$. The most suitable position of electrodes has been selected with the criteria that no negative sensitivity is covering the volume on blood in radial artery has been applied. As the model is simplified, then the proposed most suitable solution is a non-symmetrical placement of electrodes. More precisely, the gap between

the excitation-measuring electrode pair which is placed on volume of wrist where the distance to radial artery is shorter, is decreased by 1 mm if compared to the second excitation-measuring electrode pair.

A similar study on a virtual model of wrist has been performed in (Anand, Lowe, & Al-Jumaily, 2016), containing the layers of outer surface, fat, muscle (listed from outside to inside) and volume of blood. The simulations have been performed in order to evaluate the dielectric behavior of total volume of simplified model of wrist in the case of changing diameter of the volume of blood. The results showed the significant effect of increase in diameter of volume of blood in both: resistance and reactance. The highest values were gained in the case of smallest diameter of the volume of blood. Interesting is the reported lower current density until certain depth between the measuring electrodes in the case of in-line placed electrodes in four-electrode system.

Another example is (Jivet, 2014), where the cross-section of wrist has been modelled as circular 2-dimensional plane, consisting of a matter that has approximate resistivity of muscle. This muscle is modelled to include two sections that represent bones and single section that has the resistivity of blood. The excitation current has been applied by non-invasive electrodes and the simulation carried out in two conditions: relatively circular shape of "hand" and ellipse shape of "hand". The result show the change in sensitivity distribution when "hand" is deformed i.e. gains the ellipse shape, possibly resulting as different values of measured Z and $\Delta Z(t)$.

The studies of sensitivity distribution in simplified models that contain different conductivities in the cases of different electrode configurations have been reported more often (Ahmed, Kadir, Quaderi, Rahman, & Rabbani, 2017; Brown, Wilson, & Bertemes-Filho, 2000; Islam, Rabbani, & Wilson, 2010; Shuvo & Islam, 2016). The results of simulations in the case of four-electrode system (in-line placed electrodes) on the surface of homogenous medium have shown the presence of zero sensitivity at surface layer. The forming depth of positive and negative sensitivity have been found to be dependent on the distance between the excitation electrodes: maximum sensitivity up to one-third and negative sensitivity up to half of electrode spacing. The difference in depth of maximum sensitivity in inhomogeneous medium has been declared to reach the length of half of the gap between the electrodes (Shuvo & Islam, 2016).

In the case of two-electrode system, the mean sensitivity is declared to be positive throughout the volume conductor and the absolute values to be greater than in the case of four-electrode system. But what is important, the mean sensitivity in surface layer has been found to be maximum in the case of four-electrode system while it is the opposite for four-electrode system (Brown et al., 2000).

In some cases the advantages of FIM have been emphasized, proposing deeper sensitivity and reduced negative sensitivity areas in the case of using eight symmetrically placed electrodes (consisting of two circularly located four-electrode systems, placed in-line) (Ahmed et al., 2017). The idea of FIM was proposed by Rabbani et al (Rabbani et al., 1999), establishing an approach for focusing the maximum sensitivity on interesting region in total volume.

A comprehensive study has been presented in (Pettersen et al., 2014) by using a number of different configurations. As the focus is set on four-electrode system, the corresponding result is the object of interest of current section. In the case of placement of electrodes to form a square by exciting and measuring in crosswise directions, the areas of negative sensitivity appear between the excitation and measuring electrodes that forms a circle around the positive sensitivity area in the middle.

In the case of in-line placement where the excitation is performed by outer electrodes, the negative sensitivity areas form between the excitation and measuring electrodes and positive sensitivity in greater depth over the first one (Krotov, 2017).

As a conclusion, the following important findings in published results of simulation studies are listed below:

- The position of hand influences the shape and location of different volumes in forearm, resulting most likely in the values of the measured Z and $\Delta Z(t)$ because of the variations in sensitivity distribution (Jivet, 2014).
- The maximum sensitivity in the case of two-electrode system is appearing in close proximity to the surface and the sensitivity is positive throughout the whole volume (Brown et al., 2000).
- The maximum sensitivity in the case of four-electrode system is appearing in depth approximately equal to one-third of the gap between the excitation electrodes (Brown et al., 2000).
- Regions of positive and negative sensitivity between the excitation and measuring electrodes.
- The depth of forming the positive and negative sensitivity distribution depends on the distance between the excitation and measuring electrodes (Brown et al., 2000; Shuvo & Islam, 2016).
- The presence of small number of publications where the prediction of sensitivity distributions on virtual model of hand have been reported with the focus on detecting cardiac activity.

4.3 Determination of Most Suitable Placements of Electrodes on the Surface of Wrist for Monitoring Pulse Wave in Radial Artery

Current distribution in layered biological matter of different conductivities is dependent on the number and placement of electrodes. Wrist can be considered to be of finite volume of layers of different conductivities that are located at certain fractions of total volume. One can differentiate between two the principal placements of electrodes that are lying in-line relative to wrist: distal (Figure 4.3a) and circular (Figure 4.3b).



Figure 4.3 The two principal approaches of placing the electrodes relative to wrist: distal (a) and circular (b) (the bold red line denotes the location of radial artery)

At finite length of sample, in the first case, the volumes of certain conductivity (bone, muscle, blood in arteries etc.) can be expected to form volumes that pervade the chosen length of sample. In the second case, the volumes of certain conductivity are forming sections in two-dimensional plane that can be expected to be surrounded by muscular tissue. In order of studying the sensitivity distributions in the cases of different configurations and placements of electrodes, the experimental evaluation was performed on single volunteer by using standard ECG monitoring electrodes.

4.3.1 Experimental determination of the effect of distal placement of electrodes on wrist on the results of monitoring pulse wave in radial artery

We all are different in the sense of physique – some are slim, some are stout etc. These differences reveal as differences in the volumes of body tissues and compartments. When focusing on the non-invasive measurements of EBI of radial artery, which gains the primary interest of current chapter, the presence of tissue layers of different conductivities are expected to play important role. With the justified placement of electrodes, the measured outcome is expected to acquire the maximum quality. The following experiments are described, results presented and analyzed with the goal of ascertaining the most suitable placements and configurations of electrodes for monitoring cardiac activity in radial artery.

It is justified to believe, that the placement of EBI measurement electrodes on top of the location of radial artery grants access to the information of pulsating blood in radial artery. The belief bases on the fact that the lead fields are formulating somewhere in the volume under the electrodes and at least in some amount, the time varying volume of blood will modulate the measured Z. In order to achieve the best possible electric contact to wrist, standard ECG monitoring electrodes with foam tape of part number 2228 (3M Health Care) were used (Figure 4.4). Electrodes were cut into reduced dimensions (as shown in the Figure 4.17) and 10 electrodes were placed on wrist. The distance of the center of electrode A from the edge of scaphoid bone was about 20 mm.

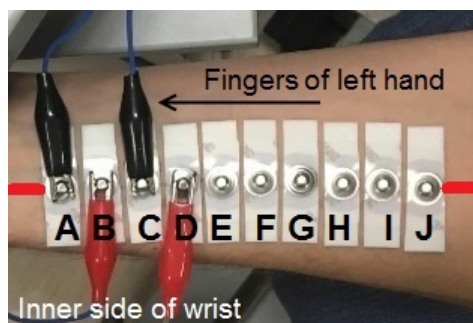


Figure 4.4 Distally placed electrodes on the wrist of left hand where the bold red line denotes the location of radial artery (author's previously unpublished illustration)

First of all, the effect of electrode placement on top of the location of radial artery in different lengths of wrist on the measured Z and $\Delta Z(t)$ was determined. The electrodes were marked (Figure 4.4) in order to compose seven EPC's, which all hold the equal distances between the measuring and excitation electrodes. During the experiment, the electrodes in four-electrode system were shifted along the row of placed ECG electrodes with the steps of 10 mm towards the elbow starting from the electrode placement no. 1 until the electrode placement no. 10 (Table 4.1).

The magnitude and phase were measured by using four-electrode system with the excitation signal amplitude of 500 mV and at the frequencies of 32 kHz, 128 kHz and 256 kHz. The excitation was performed by the outer electrodes and signal measured by using the inner electrodes as depicted in Figure 4.17. The results can be seen as graphical representations of magnitude (Figure 4.5a) and phase (Figure 4.5b).

Table 4.1 The numbers of electrode placements and the markings of corresponding distally placed electrodes on wrist that were used for excitation and measuring

Electrode placement no.	The marking of electrode	
	Excitation electrodes	Measuring electrodes
1	A and D	B and C
2	B and E	C and D
3	C and F	D and E
4	D and G	E and F
5	E and H	F and G
6	F and I	G and H
7	G and J	H and I

The magnitude in the case of shifting the electrodes in four-electrode system towards elbow exhibits a slightly rising trend. This can be explained by the enlargement of the volume of muscular tissue with the decrease in distance to elbow (also the diameter of arteries slightly decrease). The value of magnitude is the highest at the excitation frequency of 32 kHz and the lowest at the excitation frequency of 256 kHz. This is expected as in the case of higher frequencies of excitation signal, more current passes through the capacitive elements and the impedance decreases.

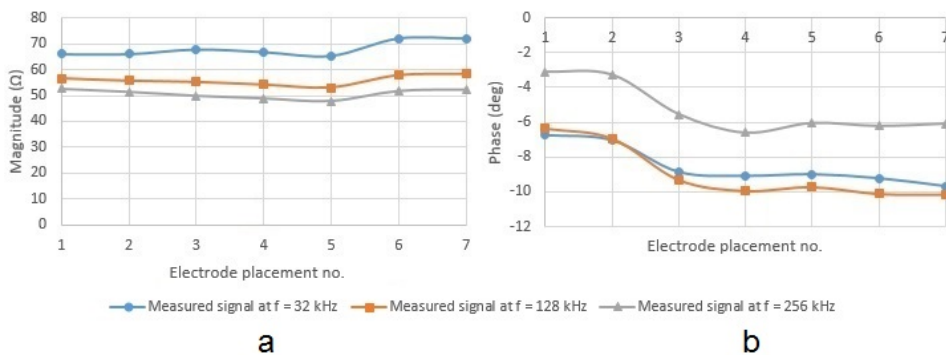


Figure 4.5 Influence of the increasing distance of electrodes in fixed four-electrode system from scaphoid bone towards elbow by the steps of 10 mm on magnitude (a) and phase (b) of the EBI of wrist

The same knowledge reflects from the graph of phase, where the lowest phase shift is gained in the case of the highest excitation frequency. In the cases of 32 kHz and 128 kHz, the difference in phase shift is not so significant, presumably showing the dielectric properties of tissue layers in wrist, which result as frequency dependence—the phase shift tends to be similar up to 128 kHz. The result shows the increase in phase shift in starting about the electrode placement no 3. This can be explained by the increase in the thickness of the tissue layer starting from the distance that is close to electrode placement no. 3 and the relocation of artery away from skin surface.

The value of $\Delta Z(t)$ is expected to exhibit the information of the suitability of certain electrode placement for monitoring the cardiac activity. The resulting graphs of $\Delta Z(t)$, measured by using all of the prepared electrode placements at previously determined excitation frequencies can be seen in Figure 4.6.

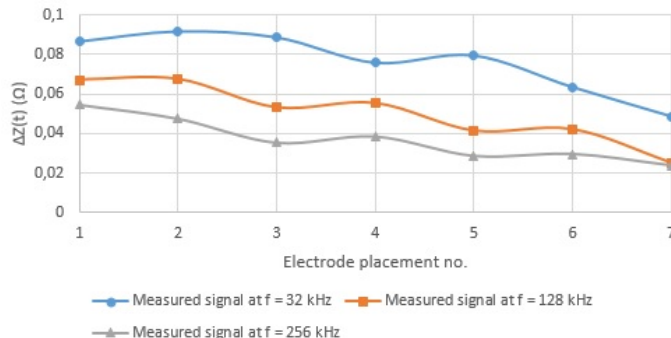


Figure 4.6 Influence of increasing distance between electrodes in fixed four-electrode system from scaphoid bone towards elbow by the steps of 10 mm on $\Delta Z(t)$

The trend of $\Delta Z(t)$ is falling with the decrease in distance to elbow at all of the excitation frequencies. One can realize, that the $\Delta Z(t)$ proposes the best result in the case of the lowest experimented excitation frequencies and the worst result in the case of the highest experimented excitation frequencies. However, the sensitivity exhibits the same outcome, deteriorating with the decreasing excitation frequency. This means that the signal at 32 kHz is interfered and its shape relatively deformed (which is magnified by filtering). In the following experiments, typically the excitation frequency of 128 kHz is used. When excluding the result of 32 kHz, one can conclude that the electrode placements no. 1 and 2 are justified to be used for measuring the EBI of wrist with the goal of monitoring pulse wave.

What if the distance between the electrodes is increased or what if the positions of excitation and measuring electrodes are swapped? The argumentation related to the difference in sensitivity distributions provided the motivation for performing experiments on wrist with the goal of determining the effect of variations in electrode configurations on the measured Z and $\Delta Z(t)$. The Z was measured to experimentally assess the sensitivity distributions in local volume of wrist. $\Delta Z(t)$ was determined with the goal of providing an additional parameter to evaluate different electrodes, placements and configurations.

The magnitude and phase were measured with the excitation signal amplitude of 500 mV and at the frequency of 128 kHz by using four-electrode system. The excitation was performed by the outer electrodes and signal measured by using the inner electrodes. Six different measurement configurations were used by placing the electrodes on the location of radial artery in the setup that is shown in Figure 4.4:

1. Distance between the electrodes was increased in 10 mm steps by moving one pair of excitation and measuring electrodes by one step further.
2. Distance between the electrodes was increased in 10 mm steps by moving one pair of excitation and measuring electrodes by one step further while removing the unused electrodes from in between the measuring electrodes.
3. Distance between the electrodes was increased in 10 mm steps by moving one measuring electrode by one step further while the excitation electrodes were permanently set on outermost positions.

In order to gain comparable result from other areas of wrist, the electrodes were placed approximately on the location of FCU muscle:

- Distance between the electrodes was increased in 10 mm steps by moving one pair of excitation and measuring electrodes by one step further when placed on the location of FCU muscle.

In order to gain comparable results by using different approach of electrode placement, the placements of excitation and measuring electrodes were inverted:

- Distance between the electrodes was increased in 10 mm steps by moving one pair of measuring and excitation electrodes by one step further in the case of excitation by inner electrodes and measuring by outer electrodes.

The results can be seen as graphical representation of magnitude (Figure 4.7a) and phase (Figure 4.7b).

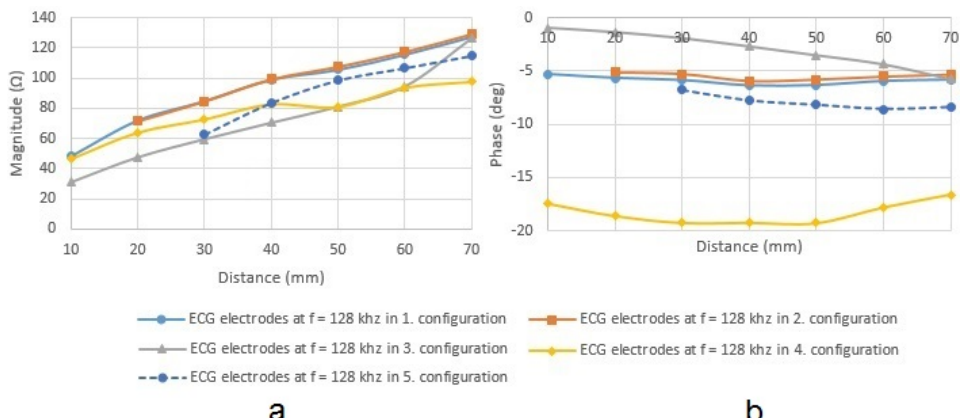


Figure 4.7 Influence of different electrode configurations in the case of increasing distance between the electrodes on magnitude (a) and phase (b) of the EBI of wrist

The instant analyze is presented in the author's 5th main publication with the following important conclusions:

- There is no significant effect of unused electrodes placed in between the measuring electrodes on the measured magnitude and phase.
- In the case of 3rd configuration the magnitude is in average about 22 Ω lower in the full range of experimented distances (until the distance of 60 mm) than in the case of 1st configuration, illustrating the different sensitivity distributions in local volume while excitation is performed remotely.
- The increase in magnitude per 10 mm in the case of electrodes on radial artery (1st configuration) is about 35 % higher than in the case of electrodes on FCU muscle (4th configuration), assumed to illustrate the difference in sensitivity distributions when the local volume is formed by relatively uniform matter—muscle.

In the case of 5th configuration, the increase per 10 mm is rather similar to 1st configuration, though, the magnitude is increased in the average of 11 Ω in the full range of experimented distances. This is showing the effect of unconventional configuration of measuring on a bit wider length of volume than excitation on measured signal of EBI but still describing the possibility of utilizing such configurations. The magnitude is increasing

on average by 13Ω per 10 mm in the case of 1st configuration and by even lower resistance in the case 4th configuration (on average about 8.5Ω per 10 mm).

But what about the phase, which alteration can be related to all the matter that lies between the relatively well conducting blood and electrode itself? In the case of 1st and 2nd configuration, the phase angle is found also to slightly increase relatively linearly in the case of increasing distance between the electrodes: about 0.16 degrees per 10 mm at the excitation frequency of 128 kHz (author's 5th main publication). This seems to indicate that the majority of the effect on measured Z of wrist is originated from the varying amount of blood in radial artery. Though, as the doubts concerning the origin of the signal are expressed in literature (Grimnes & Martinsen, 2008), one cannot claim this with full certainty until thorough experimentation has been performed.

The increase in phase angle is expected to originate merely from the increasing amount of biological matter that is worse electrical conductor and comes from the increasing distance between the electrodes that increases the volume of this matter in the measured volume.

The Z is showing the total impedance while the $\Delta Z(t)$ is indicating the magnitude of change that is caused by the changes in volumes in object. Being of the object of interest, one can argue that the $\Delta Z(t)$, together with the sensitivity (S_{card}), is an important indicator concerning the quality of the signal. The origin of the $\Delta Z(t)$ is still under debate (Patterson, 2010), though if one presumes that it is caused by the volume change of blood that occurs due to pulse wave, then this could give additional option to evaluate the suitability of variety of electrode positions for monitoring cardiac activity from wrist.

The $\Delta Z(t)$, measured by using ECG electrodes in the cases of 1st, 3rd and 5th configuration at the excitation signal amplitude of 500 mV and frequency of 128 kHz and the calculated S_{card} are available in Figure 4.8a and Figure 4.8b respectively. In the case of 4th configuration, the $\Delta Z(t)$ is not visually retrievable as arteries are not in fair closeness to contribute on current distribution and modulate the measured Z .

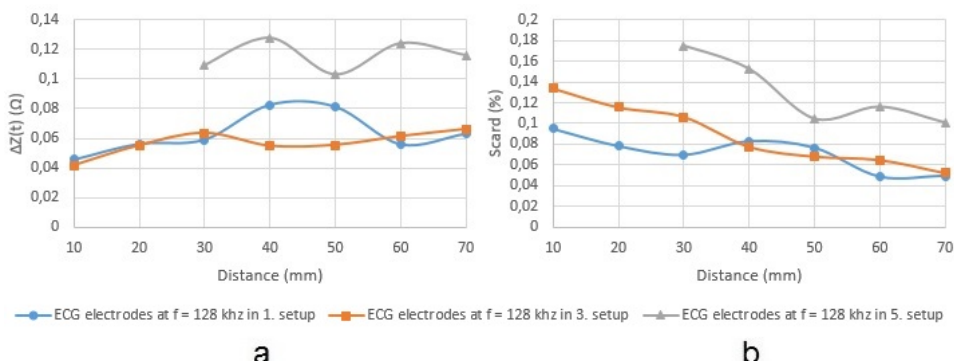


Figure 4.8 Influence of different electrode configurations in the case of increasing distance between the distally placed electrodes on wrist on the $\Delta Z(t)$ (a) and calculated S_{card} (b)

One can realize the rising trend of $\Delta Z(t)$ in the case of 1st configuration, acquiring the highest value at the distance of 40 mm. However, the $\Delta Z(t)$ is relatively small through the whole distance, confirming the hypothesis of minor influence of the distance between the measuring electrodes—this conclusion applies generally to all three configurations (Figure 4.8a). But what is interesting, the magnitude of $\Delta Z(t)$ in the cases of 1st and 3rd configuration is approximately twice worse than the same parameter 5th

configuration. This is assumed to be caused by the sophisticated sensitivity distribution in the volume of wrist, related to the placement of excitation electrodes relative to measuring electrodes, shape of the volume conductor and the placement of volumes of lower and higher conductivity (Seppä, 2014).

The sensitivity of the utilized configuration can be evaluated in order to compare the different electrode placements to provide the highest modulation in the measured signal of cardiac activity. The sensitivity is acquired likewise the S_{card} , marked similarly as in the case of other chosen types of coupling as S_{card} . The measurement results can be seen in Table 4.2, shown for 1st, 3rd and 5th experimented configurations (the same data is graphically represented in Figure 4.8b).

Table 4.2 The calculated results of the S_{card} that denote the sensitivity by using the 1st, 3rd and 5th configuration when measuring the EBI of wrist

Distance between the meas. electrodes (mm)	S_{card} in the case of 1 st conf. (%)	S_{card} in the case of 3 rd conf. (%)	S_{card} in the case of 5 th conf. (%)
10	0.095	0.134	-
20	0.078	0.116	-
30	0.070	0.106	0.175
40	0.083	0.078	0.152
50	0.077	0.068	0.105
60	0.048	0.065	0.116
70	0.049	0.052	0.101

One can realize, that the S_{card} is the highest in the case of 5th measuring configuration. In the comparison of the results of 1st and 3rd configurations, the result tends slightly to the second chosen configuration—though, being relatively in the same order. The value of S_{card} is decreasing with increasing distance, denoting the larger increase of Z than $\Delta Z(t)$ while the distance between the measuring electrodes is increasing.

As a conclusion concerning the most suitable placements and configurations of electrodes, the following main points can be listed:

- The best $\Delta Z(t)$ was gained, when placing the electrodes in four-electrode system on top of the location of radial artery close to the scaphoid bone—though, some distance towards elbow is accepted.
- The best $\Delta Z(t)$ was gained, when using the electrodes in four-electrode system on top of the location of radial artery while the positions of excitation and measuring electrodes are swapped (i.e. the excitation is done by using the inner electrodes).
- With the increasing distance between the measuring electrodes, the S_{card} slightly increases.

4.3.2 Experimental determination of the effect of circular placement of electrodes around wrist on the results of monitoring pulse wave in radial artery

In the light of all the presented experimentation setups and the gained results, the question appears: would the circular placement of electrodes around wrist propose comparable results? There are papers present, where the solution of circularly placed electrodes around wrist, by focusing onto the locations of radial and ulnar artery, is used and considerable results achieved (Liu et al., 2017). The sensitivities in local volume are

expected to distribute differently than in the case of distally placed electrodes relative to wrist. This is expected to permit dissimilar placement of electrodes that propose the best outcome concerning the $\Delta Z(t)$. As in the case of circular placement, the perimeter of wrist can be fully coved with electrodes, the sensitivity distribution can be mapped.

In order to explore sensitivity distributions in wrist, standard ECG monitoring electrodes with foam tape of part number 2228 (3M Health Care) were used. Electrodes were cut into reduced dimensions (Figure 4.9) and 14 electrodes were placed on wrist (Figure 4.10). As the circumference of wrist of volunteer was 160 mm, the distance between the centers of electrodes in the case of equal positioning of electrodes was about 11.5 mm. The electrodes were placed relative to the location of radial artery, which is positioned to lie between the electrodes F and G (Figure 4.9). The location of ulnar artery was not determined and its position in Figure 4.9 is imaginary.

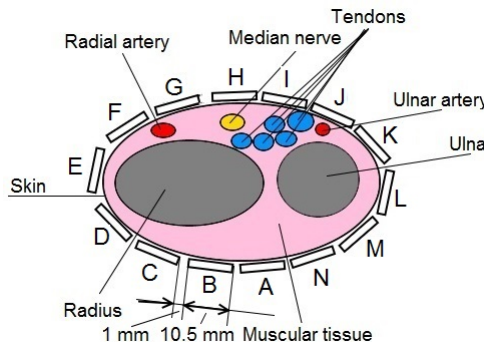


Figure 4.9 Simplified illustration of cross-section of wrist with the approximate positions and the dimensions of electrodes (author's previously unpublished illustration)

The electrodes were placed approximately onto a circular line which falls into the location of gap between the measuring electrodes in the case of distally placed electrodes at the distance on 10 mm (Figure 4.4). The location of radial artery is located between the electrodes F and G, denoted by thick red line (Figure 4.10).

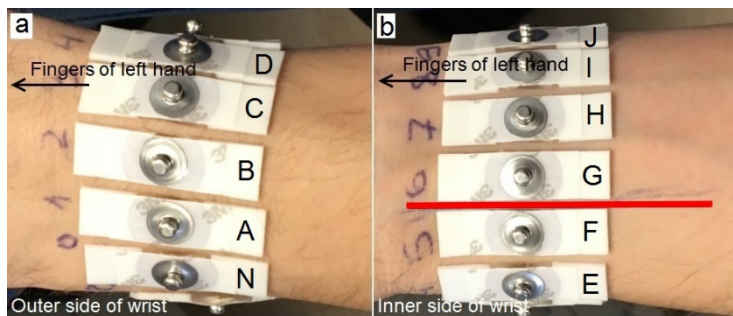


Figure 4.10 Transverse placement of electrodes on outer side (a) and inner side (b) of wrist where the bold red line denotes the location of radial artery (author's previously unpublished illustration)

The whole circumference of wrist was mapped by using the following two setups:

1. distance of 10 mm between the measuring electrodes;
2. distance of 30 mm between the measuring electrodes.

To achieve comparable outcome, the only difference between the above listed setups was the distance between the electrodes, where the central line between the measuring electrodes remain the same independently of the distance between the electrodes. The center of measured volume applies for both chosen setups (i.e. the distances between the electrodes)—the electrode placement numbers can be seen in Table 4.3.

Table 4.3 The numbers of electrode placements and the markings of corresponding electrodes that were used for excitation and measuring in the case of circular placement

Electrode placement no.	The marking of electrode in the case of 1 st setup (distance of 10 mm)		The marking of electrode in the case of 2 nd setup (distance of 30 mm)	
	Excitation electrodes	Measuring electrodes	Excitation electrodes	Measuring electrodes
1	A and D	B and C	N and E	A and D
2	B and E	C and D	A and F	B and E
3	C and F	D and E	B and G	C and F
4	D and G	E and F	C and H	D and G
5	E and H	F and G	D and I	E and H
6	F and I	G and H	E and J	F and I
7	G and J	H and I	F and K	G and J
8	H and K	I and J	G and L	H and K
9	I and L	J and K	H and M	I and L
10	J and M	K and L	I and N	J and M
11	K and N	L and M	J and A	K and N
12	L and A	M and N	K and B	L and A
13	M and B	N and A	L and C	M and B
14	N and C	A and B	M and D	N and C

The magnitude and phase were measured by using the excitation signal amplitude of 500 mV at the frequency of 128 kHz in the case of four-electrode system. The excitation was performed by the outer electrodes and signal measured by using the inner electrodes. The results can be seen as graphical representation of magnitude (Figure 4.11a) and phase (Figure 4.11b).

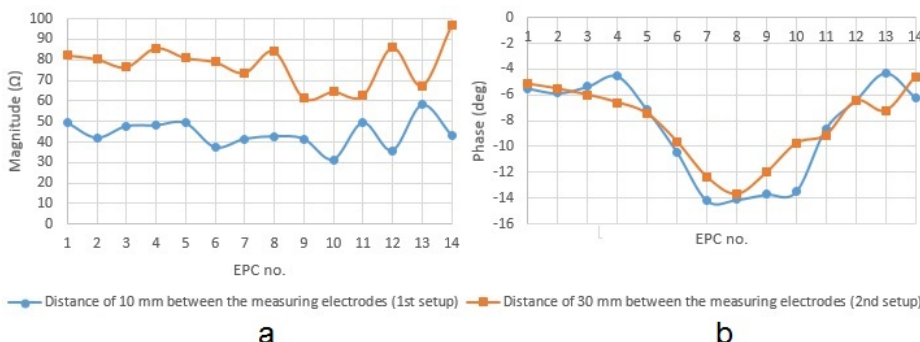


Figure 4.11 Influence of the placement and varying distance between the circularly placed electrodes on the measured magnitude (a) and phase (b) of the EBI of wrist

One can expect that the sensitivities in both setups distribute differently as in the case of four-electrode system negative and zero sensitivities apply (Seppä, 2014)—presumably affecting the value of measured Z. Figure 4.11a reveals that in the case of chosen setups, the shape of the line of Z generally follows the same trend. The value of measured magnitude in the case of 1st setup is on average 33.2 Ω lower than in the case of 2nd setup when taking into account the results concerning all electrode placements.

The lowest value of Z in the case of 1st setup is achieved at the electrode placement no. 10. In this case, the electrodes are covering the volume of muscle, ulnar artery and veins on top of ulna bone. The sensitivity distribution tends to be contributed by the muscular tissue and resulting as the lowest measured value of Z. The results in the case of 2nd setup confirm the distribution of sensitivities in local volume, proposing the lowest values of Z at electrode placements no. 9–11. The phase is comparable in both experimented setups, denoting the invariable effect of volumes of greater resistivity irrespective to the used electrode placement.

What about the $\Delta Z(t)$, which can be consider to be important indicator of the suitability of the measured signal of EBI for estimating the CAP? Also, based on the $\Delta Z(t)$, the S_{card} was calculated by using the (25). The $\Delta Z(t)$ and S_{card} for both setups can be seen in Figure 4.12a and Figure 4.12b respectively.

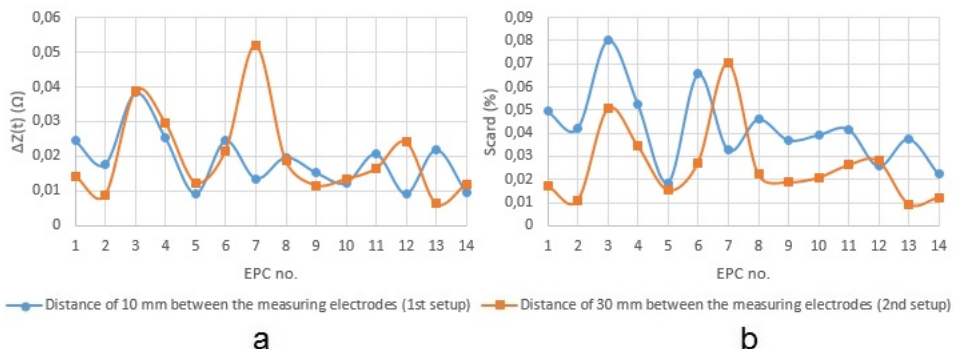


Figure 4.12 Influence of the placement and varying distance between the circularly placed electrodes on the $\Delta Z(t)$ (a) and calculated S_{card} (b)

The analyze of the $\Delta Z(t)$ reveals interesting results related to placement of electrodes in four-electrode system and the location of volumes of significantly different conductivity (like arteries and bones). The electrode placement no. 5 denotes the situation where the radial artery is located approximately in the center of the volume that lies in between the electrodes and expectedly should grant the highest interval of $\Delta Z(t)$. However, Figure 4.12a demonstrates the opposite—the $\Delta Z(t)$ in the case of electrode placement no. 5 belongs among the worst ones (the same applies to S_{card}).

The best electrode placement for measuring the $\Delta Z(t)$ and S_{card} in the case of 2nd setup is no. 3. This result is somewhat surprising, because in this EPC, the electrodes are basically located on top of radius bone, which is expected to behave as relatively non-conducting volume. Yet, when relying on the theory of development of sensitivity distributions in the case of four-electrode system (Seppä, 2014), the result can be explained. One can expect that the majority of current prefers to flow through the volume of higher conductivity which in the case of EPC no. 3 is constituted by muscular tissue. One can see (Figure 4.9), that radial artery lies close to skin surface on top of

pronator quadratus muscle, quite near to radius bone. The lead fields of current and voltage are expected to form around the radius bone and to cross each other's with the angle of more than 90° in the volume of highest conductivity—blood. Blood, in turn, is the volume where the $\Delta Z(t)$ is taking place. The results demonstrate the effect of presence of relatively non-conducting volume (in the form of bone) on the measured value of $\Delta Z(t)$ in the case of different distance between the electrodes while the lead fields are expected to be formed in similar traces.

Additionally, Figure 4.12a shows that the best $\Delta Z(t)$ is gained in the case of electrode placement no. 7 at 2nd setup. This result can be explained similarly on the base of lead field formation i.e. the effect of crossing each other's the angle of more than 90° . According to Figure 4.9, radial artery is located under the first pair of excitation-measurement electrode (exc. F and meas. G) and ulnar artery under the second pair of excitation-measurement electrode (exc. K and meas. J). One can imagine that the lead fields are expected to follow the volume of better conductivity, which is primarily constituted by arteries (and veins) and secondarily by muscular tissue and tendons. Anyhow, the fields are expected to fall on blood vessels, causing the angle of more than 90° and the major contribution of time varying volume of blood on measured Z.

However, when considering the S_{card} , the best sensitivity is achieved by using the EPC no. 3 in 1st setup. Generally the sensitivity is higher in the case of 1st setup—explained by the twice shorter distance between the measuring electrodes. As the sensitivity is characterizing the ratio of the interval, that is caused by pulse wave in measured signal of EBI, the cause is either in the increase of $\Delta Z(t)$ or in decrease of measured Z. The Figure 4.12a reveals that as the $\Delta Z(t)$ is lower than for the EPC no. 7, the reason must be in the decrease of measured Z. The vantage of the EPC no. 3 in 1st setup can be explained by the decrease in the value of measured Z while the $\Delta Z(t)$ is remaining its relative value—expectedly caused by the presence of radius bone to one excitation-measuring electrode pair and the location of second electrode pair on top of radial artery.

The worst outcome of $\Delta Z(t)$ in the case of 1st setup is appearing equally at the electrode placements no. 5 and 12. The poor outcome at the electrode placement no. 5 is somewhat surprising as the radial artery is clearly lying in the volume between the electrodes. However, this result is once again confirming the distribution of sensitivities which seems not to be contributed so much by the center of the volume between the electrodes. The electrode placement no. 12 contains the electrodes that are placed on top side of wrist, where the bones are reaching the skin surface without significant amount of volume of muscular tissue and no arteries in close vicinity. The same applies on the worst outcome of $\Delta Z(t)$ in the case of 2nd setup (electrode placement no. 13)—the electrodes are located on top side of wrist and radial artery is located behind radius bone.

When considering the numeric value of $\Delta Z(t)$, one has to admit that it on average about 0.019Ω in the case of 1st setup and about 0.02Ω in the case of 2nd setup. The corresponding values of S_{card} are on average about 0.042 % and 0.026 %. If one should propose the most suitable configurations of circularly placed electrodes relative to wrist, the following statement can be made:

- The best configuration for monitoring pulse wave in radial artery in the case of circular placement of electrodes by using the 1st setup is electrode placement no. 3 (exc. C and F, meas. D and E).
- The best configuration for monitoring pulse wave from radial artery in the case of circular placement of electrodes by using the 2nd setup and the best of all is the electrode placement no. 7 (exc. F and K, meas. G and J).

The results tend to indicate that the positioning of electrodes in a way that artery is located in center of volume between the electrodes is not proposing the best result in the sense of $\Delta Z(t)$. Instead, sensitivities tend to distribute respectively to the distribution of volumes of better conductivity and the formation of current and voltage lead fields.

The results show the slightly greater suitability (in the comparison of $\Delta Z(t)$) of distal than the circular placement of electrodes relative to wrist for monitoring pulse wave in radial artery. The highest gained value of $\Delta Z(t)$ in the case of distal placement of electrodes is about 2.5× higher than in the case of circular placement of electrodes.

4.4 Experimental Determination of the Effect of Exact Positioning of Small Area Electrodes on the Results of Monitoring Pulse Wave

The usage of standard ECG monitoring electrodes with foam tape is not an option in the case of wearable detection of cardiac activity. This is because the placement of ECG electrodes requires time, is uncomfortable and may cause skin irritation (McAdams, 2006). Moreover, in the case of standard dimensions (2228 (3M Health Care)), they have larger contact area than the diameter of radial artery of a man in average.

Through the prism of the measurements of EBI of wrist, the reduction of electrode surface area is presumed to require the vicinity of the interesting object—the radial artery. Radial artery is reaching the subcutaneous layers of skin i.e. achieving the greatest vicinity to skin surface in forearm until it is divided into smaller branches in hand and wrist. The location enables to attach small area electrodes directly on top of radial artery. The exact location of small area electrodes is presumed to have effect on the measured values of Z and $\Delta Z(t)$ due to the difference in presence of volumes of different conductivities. Also the externally applied pressure is expected to have influence on the measured values of Z and $\Delta Z(t)$. To evaluate these presumptions, the experiment by using small area electrodes in resistive coupling to wrist was set up and performed.

A custom designed rigid electrode PCB, containing circular gold plated electrodes that are located straight in-line, was used in five predetermined positions on the surface of wrist relative to radial artery (Figure 4.13). The distance between the measuring electrodes was 5 mm. Position C was determined by palpation and drawn as single line on skin. Other horizontal lines were drawn by 5 mm (positions B and D) and 10 mm (positions A and E) in both directions from position C (author's 4th main publication).

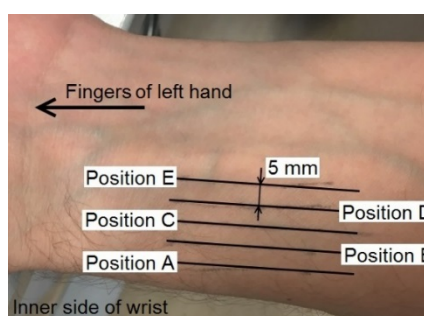


Figure 4.13 Determined location of radial artery (position C) and four drawn lines in parallel (positions A, B, D and E) on wrist (modified from the author's 4th main publication)

The results confirmed the effect of exact positioning of small area electrodes while the shift of the electrodes by 10 mm in parallel to radial artery resulted as visually not

recognizable pulse wave in measured signal of EBI (author's 4th main publication). In further illustrations and discussions, only the results of positions B–D are shown. The frequency response of Z in the cases of positions B–D can be seen in Figure 4.14.

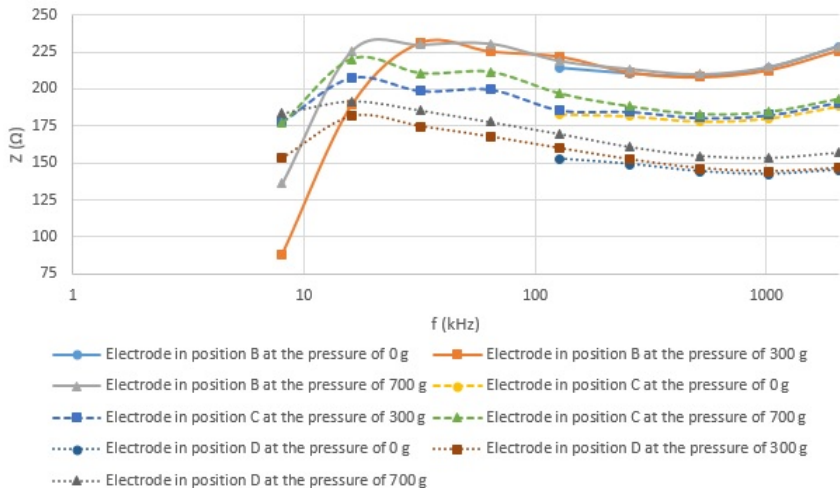


Figure 4.14 Frequency response of measured Z of wrist in the cases of different positioning of electrodes relative to radial artery while different pressure is applied

An interesting outcome can be realized from Figure 4.14, confirming the effect of conductivity differences of volumes near the small area electrodes. In the case of position B, the electrode is located nearly on top of radial bone where almost no muscle seems to be present. The conductivity of bone is about 17× worse than the same value for muscular tissue and even worse for blood (Table 4.4). Therefore, it is expected that bone is contributing more in the measured Z of wrist in this position than in other positions. Figure 4.14 confirms this expectation, showing the highest Z for the position B.

Concerning the value of Z in the positions C and D, an effect that is described to be experimentally determined also in the Paragraph 4.3.1, can be realized: the Z is generally lower when there is larger volume of conductive matter in the vicinity. In the case of position D, the electrode is lying on the location of FCR tendon, which conductivity is even slightly better than the conductivity of muscle. The radius bone in turn, is 5 mm farther away than in the case of position C and 10 mm farther away than in the case of position B. The Z is decreasing with increasing distance from radius bone which appears to contribute to the measured Z in the way of reducing the volume of matter of better conductivity and affecting the sensitivity distributions.

What about the $\Delta Z(t)$, is this also affected by the exact positioning of electrodes? The answer is yes and the result is exhaustively described in the author's 4th main publication. The difference between the results of measuring Z and $\Delta Z(t)$ by using different positions has to be emphasized. The best $\Delta Z(t)$ is gained in the case of position C i.e. the location of electrode approximately on top of radial artery. The worse $\Delta Z(t)$ is gained in the case of position B i.e. the nearest location of electrode to the radial bone. When comparing this result with the outcome of Z , one can see that the pulsating volume of blood is contributing to sensitivity distributions the most, when placing the electrode approximately on top of radial artery. Can this confirm the source of the signal: the time varying amount of blood in radial artery, caused by cardiac activity?

Another important observation that can be made in the light of Figure 4.14 is the dependency of the measured Z on externally applied pressure. One can realize the increasing influence of increasing pressure on the measured value of Z while moving farther away from radial bone. This can be explained by the increase in the volume of elastic matter (muscle, connective tissues etc.) between the radius bone and rigid electrode. If this volume is low, there is not much to compress and the difference reflects in unnoticeable change in the value of Z in the case of changing amount of external pressure. In the case of increasing distance from radius bone, the volume of elastic matter increases and the effect of changing distance on measured value of Z increases.

4.5 Development of Wrist Wearable Electrode for Optimal Detection of Pulse Wave and the Evaluation of Preliminary Results

It is clear that the property of resistively coupled electrodes to follow the contours of wrist surface with the goal of achieving the absolute contact surface between the electrode and skin is essential. However, the utilization of standard ECG electrodes is not a conceivable option in the sense of wrist wearable device because of the reasons, listed in the Section 1.4. However, the utilization of custom designed rigid electrode PCB is also outside the listed reasons just because of the rigidness and relatively small electrodes that require the exact positioning (Section 4.4).

In order to plan experiments by using electrodes that possess the property of being flexible while no contact gel is applied, a custom designed flexible electrode set (Figure 4.15b) was used. The electrode set contained four gold plated copper electrodes with fixed distances between the electrodes (Figure 4.15a), capable of being placed either distally (Figure 4.15c) or circularly (Figure 4.15d) relative to wrist.

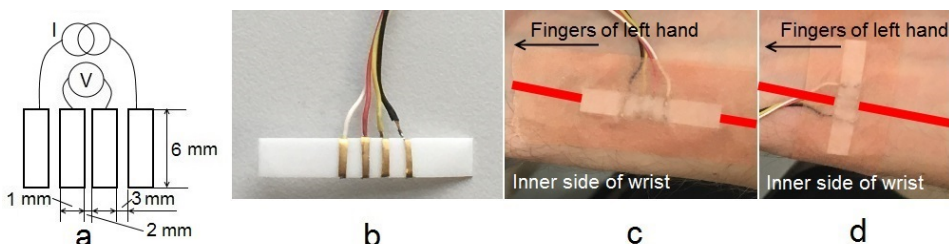


Figure 4.15 Dimensions (a), realization (b) and example of distal (c) and circular (d) placement of custom made flexible electrode relative to wrist where the thick red line denotes the approximate location of radial artery (author's previously unpublished illustration)

The experiments were performed to fulfill the following tasks:

- To evaluate the accessibility of the data of pulse wave by using single set of flexible electrodes in resistive coupling to skin surface.
- To compare the results of distal and circular placement on top of the approximate location of radial artery by using electrodes with fixed distance.

The Z was measured and $\Delta Z(t)$ found by using the excitation signal amplitude of 500 mV at the frequency range of 10 kHz–5 MHz in the case of four-electrode system. The results can be seen as graphical representation of measured Z (Figure 4.16a) and $\Delta Z(t)$ (Figure 4.16b) respectively.

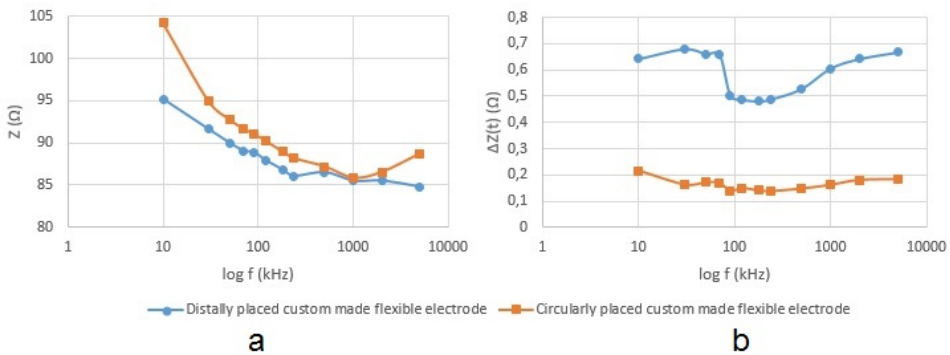


Figure 4.16 Frequency response of measured Z (a) and $\Delta Z(t)$ (b) of wrist in the cases of distal and circular placement of electrodes

The resulting Z confirms the results of using circularly placed standard ECG electrodes: the evidential rise of measured Z because of the property of biological matters of different conductivity in wrist to constitute the distally located volumes (Figure 4.16a). This is forcing the excitation signal to pass the network of impedances, constituted by crosswise located volumes of different conductivities. However, in the sense of $\Delta Z(t)$, the clear distinction between the distal and circular placement of electrodes relative to wrist can be realized. The value of $\Delta Z(t)$ through the chosen frequency range is on average about 3x larger in the case of distal placement.

The Z is decreasing with increasing excitation frequency while the $\Delta Z(t)$ is maintaining its relative value regardless of excitation frequency. The final conclusion of the Section 4.4 is confirmed, including the statement of higher suitability of distal than circular placement of electrodes relative to wrist.

Concerning the constructional issues, the need for applying slight pressure on the flexible electrode was determined and employed by using adhesive tape (Figure 4.15c and Figure 4.15d). The reason is the required skin-electrode contact to achieve resistive coupling with skin.

4.6 Theoretical Considerations of the Origin of Cardiac Activity Waveform when Measuring the EBI of Wrist

ICG has been a tool for monitoring stroke volume and cardiac output for over a half of century now but there is still an ongoing discussion concerning the source of the signal. The computer simulations tend to show the major contribution of skeletal muscle and small contribution of aorta to total Z . Moreover, the current density seem to distribute largely into the upper parts of thorax: shoulders and neck (Kauppinen et al., 1998; Patterson, 2010). This is illustrating the dependency of current distribution on number and placement of electrodes but also the effect of simultaneous parasitic couplings (Aliau-Bonet & Pallas-Areny, 2012).

Wrist, however, is of noticeably smaller volume than trunk, of round like shape and with less constituents in the form of organs and layers of biological matter, presumably simplifying the understanding of current distributions. It is agreed that the majority of current prefers to distribute in the volume of greater conductivity. In corresponding publications (Bang et al., 2009; Lee & Cho, 2015), explained and illustrated also in the Paragraph 4.1.1, such paths are expected to be formed by blood in blood vessels: arteries and veins. The variable of interest: $\Delta Z(t)$ is supposed to be caused by the

varying amount of blood in arteries. However, in the case on non-invasive measurements, the electrodes will lie on top the surface of wrist, unintentionally dictating the presence of skin, body tissues, blood vessel walls etc. between the electrode and the volume of blood. Though, it is feasible to focus the electrodes on radial artery, the distribution of sensitivities in the case of measurement of EBI by using four-electrode system is dependent on the layered structure of biological matter in each case.

Let's try to simplify the physiological structure of wrist and calculate the resistivities of prescribed volumes. Let's declare that the electrodes are of shape of rectangle (Figure 4.17) and these are placed with the gap of 1 mm on the location of radial artery for monitoring the EBI by using four-electrode system.

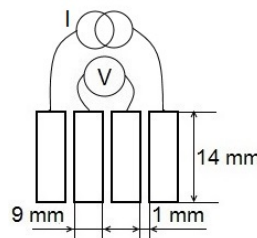


Figure 4.17 Prescribed dimensions and spacing's between electrodes in four-electrode system for estimating the EBI of local volume of wrist

The distance between the center lines of electrodes is 10 mm. As the electrodes will cover only small part of the expected amount of typical circumference of standard male's wrist, the distribution of current in local volume under the electrodes is expected. The measuring depth is claimed to increase with the increase in distance between the electrodes (Grimnes & Martinsen, 2008). Based on this, let's prescribe the presence of skin, muscle, tendons, superficial radial nerve, radius bone, radial artery and two radial veins with the volumes of arterial and venous blood (conductivities and resistivities can be seen in Table 4.4).

Table 4.4 Tissue conductivities and resistivities (determined from the conductivity values) (Andreuccetti, Fossi, & Petrucci, 1997)

Tissue type	Conductivity σ (S/m) at 100 kHz	Resistivity ρ ($\Omega \cdot m$) at 100 kHz
Skin (wet)	0.066	15.15
Muscle	0.362	2.762
Tendon	0.389	2.571
Blood	0.703	1.422
Blood vessel wall	0.319	3.135
Bone (cortical)	0.021	47.62
Nerve	0.081	12.35
Fat	0.024	41.67

If assuming that current prefers to flow through blood in blood vessels, then the presence of radial artery and radial veins is expected to have effect on the result. By referring Table 4.4, this assumption tends to be true because of the lowest resistivity of blood when compared to other compartments.

Let's set the internal diameter of radial artery $D_{radial_artery_internal}$ to be 2.7 mm (the corresponding radius r of radial artery is $r_{radial_artery_internal} = 1.35$ mm) and imagine it to be a cylinder. The area of circle $A_{radial_artery_internal}$ with $r_{radial_artery_internal} = 1.35$ mm is 5.72 mm^2 . Now, let's expect that the same value applies also to both of the radial veins and multiply $A_{radial_artery_internal}$ with three: the expected total area A_{blood} of blood vessels in local volume is then 17.2 mm^2 . The impedance of the length of homogenous conductive material can be calculated according to

$$Z = \rho \frac{L}{A} \quad (34)$$

The resulting Z_{blood} in the case of blood in radial artery and veins in local volume is 833Ω per 10 mm. When comparing the calculated result with the result of measurements in the Paragraph 4.3.1, about $60\times$ difference can be realized (author's 5th main publication). This leads to the debate concerning the actual distribution of currents in local volume of wrist, introduced in the case of ICG in the beginning of this chapter.

The measurement result seems to suggest wider distribution of currents, not just being limited to the volume of blood in arteries and veins. One is forced to widen the area of possible volumes in wrist that contribute to volume of lower resistivity, expanding the possible distribution of currents. According to Table 4.4, the resistivities of muscle and tendons differ only about $2\times$ from the resistivity of blood. It is tricky to determine the proportions of volumes of muscle and tendons in local volume under the spot electrodes but some estimations can be made. As unconventionally the highest resistivity is proposed by bone, the assumption can be made that only a minority amount of current is distributed in it.

The majority of volume between the radius bone and skin tends to be muscular tissue with the tendons. By rough estimation for the prescribed setup, the proximity of the flexor carpi radialis (FCR) tendon should be consider. It can be safely assumed that the diameter D_{tendon} of FCR tendon, which is of cylinder shape, is not more than 8 mm. At this value, the area A_{tendon} of circle of this cylinder is 50.2 mm^2 . The resulting Z_{tendon} in the case of tendon in local volume is 512Ω per 10 mm. One can realize that probably the current distribution in tendons exceeds the same value for blood vessels that are present in local volume, but the comparison with the measured Z of the length of volume of 10 mm shows the presence of a larger volume of nearby resistivity. This volume is expected to be provided by muscle which presence in local volume is hard to estimate. Though, presumably it is safe to consider the volume of muscle $50\times$ larger than the volume of radial artery in local volume.

Let's simplify the calculations by assuming the volume of muscle to be a cylinder—in this case the area A_{muscle} of circle of this cylinder is 286 mm^2 . The resulting Z_{muscle} in the case of muscle in local volume is 84Ω per 10 mm. When compared to measured value of 13Ω per 10 mm (presented in the Paragraph 4.3.1), even wider distribution of currents can be expected than the calculations show.

One can imagine the similar setup of electrodes, but placed on an area of forearm where the volume of muscles is expected to dominate—for example on the location of flexor carpi ulnaris (FCU) muscle. In this case the diameter (D_{FCU}) of a cylindrical shape of volume can minimally be estimate to be 25 mm. At this value, the area of circle A_{FCU} of this cylinder is 1963 mm^2 . The result (Z_{FCU}) in the case of muscle in local volume is 14.1Ω per 10 mm.

Now, when imaging the layered structure of volumes of different conductivities in wrist to resemble a parallel circuit, the total impedance can be calculated according to

$$Z = \frac{Z_1 Z_2}{Z_1 + Z_2} \quad (35)$$

where Z_1 is the impedance of finite length on one volume and Z_2 is the impedance of finite length on another volume. From the (35) one can deduce that the volume of lowest impedance dictates the impedance of total volume as the current prefers to follow through the medium if highest conductivity.

What has to be noted hereby is the defined prerequisite that the current is pervading the boundaries of volumes of different conductivities in wrist just like a network of resistors and capacitors of different values. However, the forming of sensitivity fields in simulation models of complex sets of volumes like human trunk, have been declared to be considerably affected by thoracic inhomogeneity's (F. Yang & Patterson, 2008). The results of simulations have shown the largest effect near the boundaries of different tissues.

The conclusion concerning wider distribution of currents in local volume can be declared, most probably originated from muscular tissue. Being of twice worse electric conductor than blood, it still possess the pathways for current to flow in the finite volume of wrist. Moreover, the tendons, being even of slightly better electric conductors than muscle propose more pathways and decreasing the resistivity of total volume even more. Also, to be exact, the effect of blood vessel wall should also be consider, though because of its relatively low contribution to total area of the volume of wrist can be consider to be very small.

4.7 Comparative Evaluation of the Results of Monitoring Pulse Wave in Radial Artery by Using Capacitive, Inductive and Resistive Coupling

The primary coupling type, used for monitoring pulse wave in radial artery in this thesis is resistive. This choice is explained by the desire to suppress motion artifacts and gain the electrical contact with the underlying tissues to provide the best possible signal of pulse wave for further processing. The volume change of blood in radial artery is relatively small and as demonstrated in the Chapters 2 and 3, varies significantly depending on the exact positioning of electrodes. In this reason, the other coupling types are expected to be of either not capable of granting access into interesting data or being of relatively unreliable.

However, as it was demonstrated in preceding sections, cardiorespiratory activity can be monitored by using all three chosen types of couplings on thoracic surface, the same hypothesis related to the possibility of monitoring pulse wave in radial artery was set up as well. The implemented flexible coils (Section 3.4.) were experimented on the surface of wrist by measuring the varying R_p of coil and post-processing the gathered signals with the goal of determining cardiac activity.

The results in the case of inductive coupling revealed the uncertainties of monitoring small volume changes of blood in local volume by using a single coil. As the goal of this chapter was to judge the possibility of determining pulse wave in radial artery by using the chosen types of coupling, the sure result by using the magnetic induction monitoring was not possible to achieve. In this reason, the decision concerning inductive coupling by

using the implemented means is: pulse wave can't be monitored with complete certainty in radial artery and no results are shown in further development of this chapter.

In order to alter the resistive electrodes to operate in capacitive coupling, the same standard ECG monitoring electrodes with foam tape were attached on a piece of cotton fabric. The idea was to follow the same approach as it was utilized in implementing the electrode shirts (Section 2.5)—to constitute the layer of insulating material between the electrode and skin surface by using the relatively badly electrically conductive cotton. The electrodes were attached in the same setup as shown in Figure 4.17 and positioned on radial artery similarly to the 1st electrode placement (defined in Table 4.1)—showing the largest $\Delta Z(t)$ at highest experimented excitation frequency (256 kHz).

The results of EBI measurements by using capacitively coupled electrodes showed the unrecognizability of pulse wave from appearing interferences at lower excitation frequencies than 5 MHz—though, pulse wave was possible to recognize at higher frequencies. For this reason, the experimentation was performed at the frequencies 5–20 MHz and range of S_{card} found. The comparative evaluation can be made on the same basis as it was done in the case of comparing the different couplings to thoracic surface—by finding the sensitivities (the (25)). The ranges of S_{card} for all coupling types, when measuring pulse wave in wrist by using the electrodes of same type, same size and same position on wrist, can be seen in Table 4.5.

Table 4.5 The results of monitoring cardiorespiratory activity on wrist by using the capacitive and resistive coupling for comparative evaluation

Coupling type	S_{card} (%)
Resistive	0.104–0.131
Capacitive	0.391–0.844

The Table 4.5 reveals the more than 6× higher sensitivity in the case of capacitive than in the case of resistive coupling. The results are comparable in the sense of electrodes and the position on the surface of wrist. The results are incomparable in the sense of the excitation signal frequency and coupling to wrist. What has to be bear in mind, is the same hypothesis that was proposed during the comparison of the three chosen types of couplings for monitoring cardiorespiratory activity on thoracic surface (Section 4.6)—up to what extent the measured $\Delta Z(t)$ is caused by varying amount of blood and up to what extend by other factors.

Moreover, related to the absence of galvanic contact between the electrode and skin surface in the case of capacitive coupling, the concurrent movement of hand has significant effect on the measured signal. The effect is increased by the loose attachment of capacitively attached electrodes—the factor of changing distance and the possible shift relative to skin surface is expected.

However, the general conclusion can be made: capacitive coupling proposes a viable alternative to resistive coupling for measuring the EBI with the goal of monitoring pulse wave in some artery in local volume. The potentiality of capacitive coupling is realized, constituting the means for being implemented as future work for creating applications for monitoring cardiac activity in the volumes of limited extent.

4.8 Chapter Summary

In this chapter I showed the vast influence of electrode positioning relative to radial artery on the detectability of cardiac activity in the form of pulse wave by utilizing resistive coupling. It has been stated in the literature (Grimnes & Martinsen, 2008), that around 85 % of problems in EBI measurement result from the electrodes. The effect of electrode skin contact surface, the sensitivity distribution which is dependent on the exact placement of sensors (Patterson, 2010), the effect parasitic couplings inside the object (Aliau-Bonet & Pallas-Areny, 2012) etc. are influencing the resulting measurement of EBI that is expected to grant access to cardiac activity.

The sensitivity distribution in local volume of wrist is predicted by the depth of modulation on the measured signal of EBI, caused by time varying pulsation of blood in radial artery. The presented results suggest the wider distribution of currents in inhomogenous volumes of living biological objects that it is expected till now: only slightly worse electric properties of muscular tissue is expected to contribute largely. The utilization of standard ECG electrodes in the experiments is justified by the desire of applying equivalent conditions for determining the most suitable placements and configurations on the surface of wrist.

The better suitability of distal placement of electrodes on top of the location of radial artery than the circular placement was determined. The deepest cardiac modulation in the measured signal of EBI when the electrodes are placed as close to scaphoid bone as possible, with the distance between the measuring electrodes of 10 mm was confirmed. The irrelevant effect of distance between the excitation electrodes on wrist, when the measuring electrodes in four-electrode system are placed on the same straight line in between was observed. The most suitable placement of electrodes in the case of circular positioning was declared—the configuration where one pair of excitation-measuring electrode pair overlaps the location of radial artery and the second one the location of ulnar artery.

The performed experimentation was planned in order to explain the effect of displacement of small area electrodes relative to the location of radial on the measured value of EBI and, throughout, to the detectability of pulse wave in wrist. The experimental evaluation demonstrated the substantial effect of positioning of small area electrodes, appearing in the unachievable data in the case of displacement. The effect of externally applied pressure in the case of resistively coupled EBI electrodes was determined as interesting subject of research as its effect was determined. As a result of the experiments, the evidence of presence of an optimal pressure point was determined, applying generally in the cases of different individuals.

Conclusions

In this thesis I engaged with the matter of developing solutions for wearable devices that utilize capacitive, inductive and resistive coupling with the purpose of monitoring cardiorespiratory activity. As a result, based on experimental measurements the following summary can be made:

- I have proved the feasibility of utilizing capacitive sensing for unnoticeable detection of processes of breathing and heart beating.
- I have verified the potentiality of using magnetic induction monitoring for following cardiorespiratory activity by single coil as alternative to EBI measurements.
- I have evaluated the option of detecting cardiac activity in radial artery by using resistive coupling to wrist in order to gain exclusive access to cardiac activity and proposed the post suitable means for fulfilling the set task.

More specifically, in the case of capacitive coupling I have done the following.

- To prove the applying of this assumption in the case of large area electrodes, I have developed experimental methodology and implemented wearable experimental EBI measurement devices in the form of electrode shirts (author's 1st main and 2nd-3rd other publication).
- I have determined experimentally the most suitable placements and configurations of large area capacitively coupled electrodes on surface of human trunk, proposing the best outcome concerning cardiorespiratory activity (author's 1st main publication).
- I have demonstrated the phenomenon of lesser influence of body movements on non-contact measurement of EBI in the case of monitoring cardiorespiratory activity at certain electrode placements and configurations (author's 1st main and 2nd other publication).
- I have shown the possibility of monitoring cardiorespiratory activity in the case where large area conductive fabric textile electrodes in capacitive coupling to trunk are used (author's 3rd main publication).
- I have demonstrated the feasibility of detecting respiratory activity waveform from measured signal of EBI in the case of concurrent rhythmical movements of human body.
- I have shown the fact that some EPC's are less influenced by concurrent movements, which may be considered as input for developing an approach of cancelling the effect of motion artifact

My solution to monitoring of cardiorespiratory activity differs from previous similar research by the utilization of large area electrodes in capacitive coupling.

In the case of inductive coupling I have done the following.

- I have confirmed the variations in cardiorespiratory waveform, depending on the position of a single coil on thoracic surface.
- I have developed a technique of preparing flexible coils for following the curvilinear surface of thorax by using off-the-shelf materials.
- I have experimentally proved that the differences in distribution of current densities, induced by O and Fo8 shaped coils have major effect on the

monitored cardiorespiratory waveform in the case of inductive coupling to thoracic surface.

- I have demonstrated the utilization of coils as capacitive electrodes for measuring the EBI by utilizing two-electrode system.

In the case of resistive coupling I have done the following.

- I have experimentally verified the different effect of distally and circularly placed electrodes on wrist on monitoring pulse wave in wrist.
- I have proposed the most suitable electrode placements and configurations on the wrist for monitoring pulse wave.
- I have shown the destructive effect of displacement of small area electrodes relative to the location of radial artery on the measurability of pulse wave.
- I have shown the presence of an optimal pressure point of an externally applied pressure on the electrodes for monitoring pulse wave in radial artery.
- I have demonstrated the effect of anatomical differences of individuals, appearing in varying thicknesses of layers of biological tissues and other matter of distinct electrical conductivity has been evaluated by me and suggestions proposed concerning the most suitable placements of electrodes.

The future work in the topic is expected to include the following research areas.

- The recognition of the mechanisms and classification of body movements that cause the motion artifact related disturbance in the measured signal of EBI in the case of using large area capacitive electrodes for monitoring cardiorespiratory activity. The outcome is expected to relate the body movements to specific patterns in the measured waveform and thereby, forming an attribute to suppress the motion artifacts.
- Cancelling of the effect of concurrent movements of the monitoring of cardiorespiratory activity by utilizing the data from the proposed concurrently implemented single coil magnetic induction monitoring by using flexible coils that are prepared according to developed technique. The degree of bending the coils is expected to correlate with the motion-related changes in EBI waveform.
- Extensive experimentation in the case of large number of volunteers to gather large amount of data concerning the effect individual differences of humans on the measured pulse wave in radial artery. The data is expected to propose valuable input of the design on a wrist wearable monitoring device.

List of Figures

Figure 0.1 Illustration of the principles of coupling types on which the focus of current thesis is turned to: resistive (a), capacitive (b) and inductive (c)	11
Figure 1.1 The impedance vector with its real and imaginary parts	26
Figure 1.2 Serial RC circuit (a) and its phasor diagram (b)	27
Figure 1.3 Serial 2R-1C circuit (a) and its phasor diagram (b)	27
Figure 1.4 Drawing of a single cell and its expected equivalent circuit	28
Figure 1.5 Equivalent circuit for single cell: simplified model (a), Fricke-Morse model (b) and Cole model (c)	28
Figure 1.6 Current paths in tissue in the cases of low and high frequency	29
Figure 1.7 Vector diagram of relative complex dielectric permittivity	31
Figure 1.8 Cross section of skin anatomy (picture provided by the National Institute of general Medical Sciences, source: https://images.nigms.nih.gov/Pages/Home.aspx)	33
Figure 1.9 Equivalent circuit of skin-electrode contact interface	33
Figure 1.10 Cardiovascular (a) and pulmonary (b) systems of human (picture provided by OpenStax, Anatomy & Physiology. OpenStax CNX. May 18, 2016, source: http://cnx.org/contents/14fb4ad7-39a1-4eee-ab6e-3ef2482e3e22@8.25.)....	34
Figure 1.11 Idealized dispersion regions of the biological matter (modified from (Herman P. Schwan, 1988)).....	35
Figure 1.12 Impedance measurement of cylinder like body with four-electrode system....	38
Figure 1.13 Example signals of ECG, ICG and PW together with illustrations of defined time intervals (redrawing from https://medis.company/cms/index.php?page=icg-impedance-cardiography).....	39
Figure 1.14 Systolic pressure waveforms from central to peripheral arteries (modified from (Brandão et al., 2017)).....	40
Figure 1.15 Example signal of IP in the case of spot electrodes according to Figure 1.16c (authors' previously unpublished illustration)	40
Figure 1.16 An effective placement of electrodes for monitoring IP (a) and the traditional placements of electrodes for monitoring ICG by using the band (b) and spot (c) electrodes	42
Figure 1.17 Electrical model of electrode-electrolyte interface—formation of electric double layer	46
Figure 1.18 Common impedance measurement systems: two- (a) and four-electrode (b).	47
Figure 1.19 EBI measurement setup scenario together with sources of error (author's previously unpublished illustration)	48
Figure 1.20 Construction techniques of textiles: woven fabric (a) and knitted fabric (b)	49
Figure 2.1 Positions of electrodes in the ES1 (modified from the author's 2 nd other publication) (Margus Metshein & Parve, 2015)	59
Figure 2.2 Positions of electrodes in the ES2 (modified from the author's 3 rd main publication)	59
Figure 2.3 Positions of electrodes in the ES3 (modified from the author's 3 rd main publication)	60
Figure 2.4 Block diagram of the proposed idea of EBI measurement device (modified from the author's 2 nd other publication) (Margus Metshein & Parve, 2015)	61

Figure 2.5 Attachment of the implemented prototype of EBI measurement device on ES1 (author's previously unpublished illustration)	61
Figure 2.6 Gathered waveforms of the impedance of the body of volunteer according to the EPC EFGHIJKL / OP (ES1) that are measured by using the commercial EBI measurement device in capacitive coupling	62
Figure 2.7 Gathered waveforms of the impedance of the body of volunteer according to the EPC NPRMOQ / AEIDHL (ES1) that are measured by using the commercial EBI measurement device in capacitive coupling	63
Figure 2.8 Gathered waveforms of the impedance of the body of volunteer according to the EPC K / J (ES2) that are measured by using the commercial EBI measurement device in capacitive coupling	63
Figure 2.9 Gathered waveforms of the impedance of the body of volunteer according to the EPC E / D (ES2) that are measured by using the commercial EBI measurement device in capacitive coupling	64
Figure 2.10 Gathered waveforms of the impedance of the body of volunteer according to the EPC ABCDIJ / EFGHKLMN (ES3) that are measured by using the commercial EBI measuring device in capacitive coupling.....	64
Figure 2.11 Gathered waveform of the impedance of the body of volunteer according to the EPC ABCDIJ / EFGHKLMN (ES3) at $f_{exc} = 20$ MHz that is measured by using the implemented EBI measurement device in capacitive coupling (modified from the author's 3 rd main publication).....	65
Figure 2.12 Spectrum of the cardiorespiratory signal in the case of capacitive coupling to thorax of volunteer according to the EPC E / D (ES2) at $f_{exc} = 20$ MHz (author's previously unpublished illustration)	66
Figure 2.13 Gathered waveform of impedance of the body of volunteer who is imitating swimming of crawl while breathing freely according to the EPC ABCDIJ / EFGHKLMN (ES3) at $f_{exc} = 20$ MHz (author's previously unpublished illustration).....	67
Figure 2.14 Spectrum of the signal of the impedance of the body of volunteer who is imitating swimming of crawl while breathing freely according to the EPC ABCDIJ / EFGHKLMN (ES3) at $f_{exc} = 20$ MHz (author's previously unpublished illustration).....	67
Figure 2.15 Influence of the choice of EPC on the measured S_{resp} (parameter no. 1) and S_{card} (parameter no. 2).....	69
Figure 2.16 Influence of the choice of EPC on the measured $S_{resp:move}$ (parameter no. 3) and $S_{card:move}$ (parameter no. 4)	69
Figure 2.17 The best EPC's of electrodes for monitoring respiratory activity by using capacitive coupling in the case of the 1 st and 3 rd parameter (author's previously unpublished illustration)	70
Figure 2.18 The best EPC's of electrodes for monitoring respiratory activity by using capacitive coupling in the case of the 2 nd and 4 th parameter (author's previously unpublished illustration)	70
Figure 2.19 Frequency response of ΔZ_{resp} (a) and calculated S_{resp} (b) when monitoring respiratory activity by using the commercial EBI measurement device	74
Figure 2.20 Frequency response of ΔZ_{card} (a) and calculated S_{card} (b)when monitoring cardiac activity by using the commercial EBI measurement device	77
Figure 2.21 Frequency response of measured Z in the cases of using coils no. 4 and 7 as capacitively coupled EBI measuring electrodes in positions no. 1 and 7.....	79

Figure 2.22 Frequency responses of ΔZ_{resp} (a) and ΔZ_{card} (b) in the cases of using coils no. 4 and 7 as capacitively coupled EBI measuring electrodes in positions no. 1 and 7	80
Figure 2.23 Frequency response of the S_{resp} (a) and the S_{card} (b) in the cases of using coils no. 4 and 7 as capacitively coupled EBI measuring electrodes in positions no. 1 and 7	80
Figure 2.24 Measured signal of Z by using the coil no. 4 (O) as capacitively coupled EBI measuring electrode in positions no. 1 and 7	81
Figure 2.25 Measured signal of Z by using the coil no. 7 (Fo8) as capacitively coupled EBI measuring electrode in positions no. 1 and 7	81
Figure 3.1 Principle of magnetic eddy current monitoring of biological events by using single coil: the emergence of magnetic fields (a) and the equivalent circuit (b) (author's previously unpublished illustration)	84
Figure 3.2 The chosen positions on thoracic surface for monitoring cardiorespiratory activity in the experiments of using single coil inductive coupling (modified from the author's 2 nd main publication)	90
Figure 3.3 Influence of the choice of coil position on thoracic surface on the S_{resp} and S_{card} (author's previously unpublished illustration)	90
Figure 3.4 Influence of the choice of coil position on thoracic surface on the S_{move} (author's previously unpublished illustration)	91
Figure 3.5 Pattern for understanding the dimensions of the designed coils (author's previously unpublished illustration)	93
Figure 3.6 Examples of the prepared flexible O (b and d) and Fo8 coils (a and c) (author's previously unpublished illustration)	94
Figure 4.1 Illustration of four-electrode system for monitoring pulse wave in radial artery by measuring the $\Delta Z(t)$ (modified from the author's 4 th main publication)	105
Figure 4.2 Illustration of pulse wave in the case of measured Z of wrist with the reference signal of PPG (author's previously unpublished illustration)	106
Figure 4.3 The two principal approaches of placing the electrodes relative to wrist: distal (a) and circular (b) (the bold red line denotes the location of radial artery)	109
Figure 4.4 Distally placed electrodes on the wrist of left hand where the bold red line denotes the location of radial artery (author's previously unpublished illustration)	110
Figure 4.5 Influence of the increasing distance of electrodes in fixed four-electrode system from scaphoid bone towards elbow by the steps of 10 mm on magnitude (a) and phase (b) of the EBI of wrist	111
Figure 4.6 Influence of increasing distance between electrodes in fixed four-electrode system from scaphoid bone towards elbow by the steps of 10 mm on $\Delta Z(t)$..	112
Figure 4.7 Influence of different electrode configurations in the case of increasing distance between the electrodes on magnitude (a) and phase (b) of the EBI of wrist	113
Figure 4.8 Influence of different electrode configurations in the case of increasing distance between the distally placed electrodes on wrist on the $\Delta Z(t)$ (a) and calculated S_{card} (b)	114

Figure 4.9 Simplified illustration of cross-section of wrist with the approximate positions and the dimensions of electrodes (author's previously unpublished illustration).....	116
Figure 4.10 Transverse placement of electrodes on outer side (a) and inner side (b) of wrist where the bold red line denotes the location of radial artery (author's previously unpublished illustration)	116
Figure 4.11 Influence of the placement and varying distance between the circularly placed electrodes on the measured magnitude (a) and phase (b) of the EBI of wrist	117
Figure 4.12 Influence of the placement and varying distance between the circularly placed electrodes on the $\Delta Z(t)$ (a) and calculated S_{card} (b).....	118
Figure 4.13 Determined location of radial artery (position C) and four drawn lines in parallel (positions A, B, D and E) on wrist (modified from the author's 4 th main publication)	120
Figure 4.14 Frequency response of measured Z of wrist in the cases of different positioning of electrodes relative to radial artery while different pressure is applied	121
Figure 4.15 Dimensions (a), realization (b) and example of distal (c) and circular (d) placement of custom made flexible electrode relative to wrist where the thick red line denotes the approximate location of radial artery (author's previously unpublished illustration)	122
Figure 4.16 Frequency response of measured Z (a) and $\Delta Z(t)$ (b) of wrist in the cases of distal and circular placement of electrodes.....	123
Figure 4.17 Prescribed dimensions and spacing's between electrodes in four-electrode system for estimating the EBI of local volume of wrist.....	124

List of Tables

Table 0.1 Contribution matrix of this PhD work	14
Table 1.1 Half-cell potentials for chosen materials and reactions (Neuman, 2000).....	45
Table 2.1 The chosen EPC's in the case of using the ES1 (modified from the author's 1 st main publication)	68
Table 2.3 Results of the S_{resp} by using the commercial EBI measurement device	72
Table 2.4 x of the results of the S_{resp} by using the implemented and commercial EBI measurement devices at all chosen excitation frequencies	73
Table 2.5 x of the results of the S_{resp} by using the implemented and commercial EBI measurement devices at the chosen excitation frequencies in the cases of all chosen EPC's.....	73
Table 2.6 x of the ΔZ_{resp} by using the commercial EBI measurement device at the chosen excitation frequencies in the cases of all chosen EPC's.....	74
Table 2.7 x of the ΔZ_{resp} by using the commercial EBI measurement device in the case of single volunteer at all chosen excitation frequencies	75
Table 2.8 Results of the S_{card} by using the commercial EBI measurement device	76
Table 2.9 x of the results of the S_{card} by using the commercial EBI measurement device in the cases of all chosen EPC's at all experimented excitation frequencies	76
Table 2.10 x of the S_{card} by using the commercial EBI measurement device at the chosen excitation frequencies in the cases of all experimented EPC's	76
Table 2.11 x of the ΔZ_{card} by using the commercial EBI measurement device at the chosen excitation frequencies in the cases of all experimented EPC's	78
Table 2.12 x of the ΔZ_{card} by using the commercial EBI measurement device at all chosen excitation frequencies.....	78
Table 3.1 The shapes, diameters and the number of windings of the prepared flexible coils together with the results of measured inductance (author's previously unpublished results).....	93
Table 3.2 Results of the measurements of R_p of O and Fo8 coils in inductive coupling to predetermined positions on thorax by using the LDC1101EVM (author's previously unpublished results)	95
Table 3.3 x of the R_p of different configurations of O coils in inductive coupling to thorax of volunteer in predetermined positions by using the LDC1101EVM (author's previously unpublished results)	96
Table 3.4 x of the R_p of different configurations of Fo8 coils in inductive coupling to thorax of volunteer in predetermined positions by using the LDC1101EVM (author's previously unpublished results)	96
Table 3.5 x of the R_p of O and Fo8 coils in inductive coupling to thorax of volunteer in all predetermined positions by using the LDC1101EVM (author's previously unpublished results).....	97
Table 3.6 The results of monitoring cardiorespiratory activity on thoracic surface by using the inductive, capacitive and resistive coupling for comparative evaluation....	99
Table 4.1 The numbers of electrode placements and the markings of corresponding distally placed electrodes on wrist that were used for excitation and measuring	111

Table 4.2 The calculated results of the S_{card} that denote the sensitivity by using the 1 st , 3 rd and 5 th configuration when measuring the EBI of wrist.....	115
Table 4.3 The numbers of electrode placements and the markings of corresponding electrodes that were used for excitation and measuring in the case of circular placement.....	117
Table 4.4 Tissue conductivities and resistivities (determined from the conductivity values) (Andreuccetti, Fossi, & Petrucci, 1997).....	124
Table 4.5 The results of monitoring cardiorespiratory activity on wrist by using the capacitive and resistive coupling for comparative evaluation	127

References

- Åberg, P. (2004, November 5). *Skin Cancer as Seen by Electrical Impedance*. Karolinska Institutet, Stockholm, Sweden. Retrieved from <http://openarchive.ki.se/xmlui/handle/10616/40085>
- Ahmed, S. P., Kadir, M. A., Quaderi, G. D. A., Rahman, R., & Rabbani, K. S. e. (2017). Improved Understanding of the Sensitivity of Linear Tetrapolar Impedance Measurement (TPIM) and 8-Electrode Focused Impedance Method (FIM) in a Volume Conductor. *Bangladesh Journal of Medical Physics*, 8(1), 22–31. <https://doi.org/10.3329/bjmp.v8i1.33931>
- Al-Hatib, F. (1998). Patient-instrument Connection Errors in Bioelectrical Impedance Measurement. *Physiological Measurement*, 19(2), 285. <https://doi.org/10.1088/0967-3334/19/2/015>
- Aliau-Bonet, C., & Pallas-Areny, R. (2012). On the Effect of Body Capacitance to Ground in Tetrapolar Bioimpedance Measurements. *IEEE Transactions on Biomedical Engineering*, 59(12), 3405–3411. <https://doi.org/10.1109/TBME.2012.2216880>
- Alizadeh-Taheri, B., Smith, R. L., & Knight, R. T. (1995). An Active, Microfabricated, Scalp Electrode-array For EEG Recording. In *The 8th International Conference on Solid-State Sensors and Actuators, 1995 and Eurosensors IX.. Transducers '95* (Vol. 1, pp. 67–70). <https://doi.org/10.1109/SENSOR.1995.717088>
- Allen, J. (2007). Photoplethysmography and its Application in Clinical Physiological Measurement. *Physiological Measurement*, 28(3), R1. <https://doi.org/10.1088/0967-3334/28/3/R01>
- Anand, G., Lowe, A., & Al-Jumaily, A. M. (2016). Simulation of Impedance Measurements at Human Forearm within 1 kHz to 2 MHz. *Journal of Electrical Bioimpedance*, 7(1), 20–27. <https://doi.org/10.5617/jeb.2657>
- Andreuccetti, D., Fossi, R., & Petrucci, C. (1997). An Internet Resource for the Calculation of the Dielectric Properties of Body Tissues in the Frequency Range 10 Hz - 100 GHz.
- Arcelus, A., Sardar, M., & Mihailidis, A. (2013). Design of a Capacitive ECG Sensor for Unobtrusive Heart Rate Measurements. In *2013 IEEE International Instrumentation and Measurement Technology Conference (I2MTC)* (pp. 407–410). <https://doi.org/10.1109/I2MTC.2013.6555449>
- Augousti, A. T., Maletras, F.-X., & Mason, J. (2005). Improved Fibre Optic Respiratory Monitoring Using a Figure-of-Eight Coil. *Physiological Measurement*, 26(5), 585. <https://doi.org/10.1088/0967-3334/26/5/001>
- Bang, S., Lee, C., Park, J., Cho, M. C., Yoon, Y. G., & Cho, S. (2009). A Pulse Transit Time Measurement Method Based on Electrocardiography and Bioimpedance. In *2009 IEEE Biomedical Circuits and Systems Conference* (pp. 153–156). <https://doi.org/10.1109/BIOCAS.2009.5372060>
- Beckmann, L., Riesen, D. van, & Leonhardt, S. (2007). Optimal Electrode Placement and Frequency Range Selection for the Detection of Lung Water Using Bioimpedance Spectroscopy. In *2007 29th Annual International Conference of the IEEE Engineering in Medicine and Biology Society* (pp. 2685–2688). <https://doi.org/10.1109/IEMBS.2007.4352882>

- Bera, T. K. (2014). Bioelectrical Impedance Methods for Noninvasive Health Monitoring: A Review. *Journal of Medical Engineering*, 2014, 1–28. <https://doi.org/10.1155/2014/381251>
- Bogómez-Franco, P., Nescolarde, L., Bragós, R., Rosell-Ferrer, J., & Yandiola, I. (2009). Measurement Errors in Multifrequency Bioelectrical Impedance Analyzers With and Without Impedance Electrode Mismatch. *Physiological Measurement*, 30(7), 573. <https://doi.org/10.1088/0967-3334/30/7/004>
- Brandão, A. A., Amodeo, C., Alcântara, C., Barbosa, E., Nobre, F., Pinto, F., ... Oigman, W. (2017). I Luso-Brazilian Positioning on Central Arterial Pressure. *Arquivos Brasileiros de Cardiologia*, 108(2), 100–108. <https://doi.org/10.5935/abc.20170011>
- Braun, D., Schmolngruber, M., & Steinhauser, O. (2017). Towards a Complete Characterization of the δ -dispersion in Dielectric Spectroscopy of Protein–water Systems. *Physical Chemistry Chemical Physics*, 19(39), 26980–26985. <https://doi.org/10.1039/C7CP05216B>
- Brown, B. H., Barber, D. C., Morice, A. H., & Leathard, A. D. (1994). Cardiac and Respiratory Related Electrical Impedance Changes in the Human Thorax. *IEEE Transactions on Biomedical Engineering*, 41(8), 729–734. <https://doi.org/10.1109/10.310088>
- Brown, B. H., Wilson, A. J., & Bertemes-Filho, P. (2000). Bipolar and Tetrapolar Transfer Impedance Measurements from Volume Conductor. *Electronics Letters*, 36(25), 2060–2062. <https://doi.org/10.1049/el:20001439>
- Cañadas, G. E., Dell'Aquila, C. R., & Laciar, E. (2016). Development of Portable Device to Measure Respiratory Activity Based on Impedance Pneumography. In *II Latin American Conference on Bioimpedance* (pp. 60–63). Springer, Singapore. https://doi.org/10.1007/978-981-287-928-8_16
- Care, A. A. for R. (2003). Capnography/Capnometry during Mechanical Ventilation. *Respiratory Care*, 48(5), 534–539.
- Casanella, R., Casas, O., & Pallàs-Areny, R. (2005). Differential Synchronous Demodulator for Modulating Sensors and Impedance Measurements. *Measurement Science and Technology*, 16(8), 1637. <https://doi.org/10.1088/0957-0233/16/8/014>
- Charlton, P. H., Bonnici, T., Tarassenko, L., Alastruey, J., Clifton, D. A., Richard Beale, & Watkinson, P. J. (2017). Extraction of Respiratory Signals from the Electrocardiogram and Photoplethysmogram: Technical and Physiological Determinants. *Physiological Measurement*, 38(5), 669. <https://doi.org/10.1088/1361-6579/aa670e>
- Chi, Y. M., & Cauwenberghs, G. (2010). Wireless Non-contact EEG/ECG Electrodes for Body Sensor Networks. In *2010 International Conference on Body Sensor Networks* (pp. 297–301). <https://doi.org/10.1109/BSN.2010.52>
- Chi, Y. M., Jung, T. P., & Cauwenberghs, G. (2010). Dry-Contact and Noncontact Biopotential Electrodes: Methodological Review. *IEEE Reviews in Biomedical Engineering*, 3, 106–119. <https://doi.org/10.1109/RBME.2010.2084078>
- Cho, M. C., Kim, J. Y., & Cho, S. (2009). A Bio-impedance Measurement System for Portable Monitoring of Heart Rate and Pulse Wave Velocity Using Small Body Area. In *2009 IEEE International Symposium on Circuits and Systems* (pp. 3106–3109). <https://doi.org/10.1109/ISCAS.2009.5118460>

- Cohen, L. G., Roth, B. J., Nilsson, J., Dang, N., Panizza, M., Bandinelli, S., ... Hallett, M. (1990). Effects of Coil Design on Delivery of Focal Magnetic Stimulation. Technical Considerations. *Electroencephalography and Clinical Neurophysiology*, 75(4), 350–357.
- Cole, K. S., & Cole, R. H. (1941). Dispersion and Absorption in Dielectrics I. Alternating Current Characteristics. *The Journal of Chemical Physics*, 9(4), 341–351.
- Cordes, A., Heimann, K., & Leonhardt, S. (2012). Magnetic Induction Measurements with a Six Channel Coil Array for Vital Parameter Monitoring. In *2012 Annual International Conference of the IEEE Engineering in Medicine and Biology Society* (pp. 602–604). <https://doi.org/10.1109/EMBC.2012.6346003>
- Cunico, F. J., Marquez, J. C., Hilke, H., Skrifvars, M., & Seoane, F. (2013). Studying the Performance of Conductive Polymer Films as Textile Electrodes for Electrical Bioimpedance Measurements. *Journal of Physics: Conference Series*, 434(1), 012027. <https://doi.org/10.1088/1742-6596/434/1/012027>
- Curran, J. (2008). The Yellow Emperor's Classic of Internal Medicine. *BMJ : British Medical Journal*, 336(7647), 777. <https://doi.org/10.1136/bmj.39527.472303.4E>
- de Almeida Whiteman Catarino, A. P., de Jesus Dias, M., Teixeira Carvalho, H. M., & Moreira Ferreira Rocha, A. M. (2013, December 11). EP2671506 A1. Retrieved from <http://www.google.com/patents/EP2671506A1>
- Debye, P. (1929). Polar Molecules. *Journal of Chemical Technology and Biotechnology*, 48(43), 1036–1037.
- Eilebrecht, B., Willkomm, J., Pohl, A., Wartzek, T., & Leonhardt, S. (2013). Impedance Measurement System for Determination of Capacitive Electrode Coupling. *IEEE Transactions on Biomedical Circuits and Systems*, 7(5), 682–689. <https://doi.org/10.1109/TBCAS.2013.2237905>
- Farrington, B. (1981). *Greek Science*. Nottingham: Dufour Editions.
- Foster, K. R., & Schwan, H. P. (1989). Dielectric Properties of Tissues and Biological Materials: a Critical Review. *Critical Reviews in Biomedical Engineering*, 17(1), 25–104.
- Gabriel, C., Gabriel, S., & Corthout, E. (1996). The Dielectric Properties of Biological Tissues: I. Literature Survey. *Physics in Medicine & Biology*, 41(11), 2231. <https://doi.org/10.1088/0031-9155/41/11/001>
- Gandevia, B. (1970). The Breath of Life: an Essay on the Earliest History of Respiration: Part I. *Australian Journal of Physiotherapy*, 16(1), 05–11. [https://doi.org/10.1016/S0004-9514\(14\)61085-0](https://doi.org/10.1016/S0004-9514(14)61085-0)
- Gargiulo, G., Bifulco, P., Calvo, R. A., Cesarelli, M., Jin, C., & Schaik, A. van. (2008). Mobile Biomedical Sensing with Dry Electrodes. In *2008 International Conference on Intelligent Sensors, Sensor Networks and Information Processing* (pp. 261–266). <https://doi.org/10.1109/ISSNIP.2008.4761997>
- Gargiulo, G. D., Cohen, G., McEwan, A. L., Oh, T. I., Mohamed, A., Tapson, J., ... Wabnitz, A. (2012). Active Electrode Design Suitable for Simultaneous EIT and EEG. *Electronics Letters*, 48(25), 1583–1584. <https://doi.org/10.1049/el.2012.3212>
- Gaw, R. L. (2010). *The Effect of Red Blood Cell Orientation on the Electrical Impedance of Pulsatile Blood with Implications for Impedance Cardiography* (Thesis). Queensland University of Technology, Queensland, US. Retrieved from <https://eprints.qut.edu.au/39448/>

- Geddes, L. A., Voelz, M. H., Babbs, C. F., Bourland, J. D., & Tacker, W. A. (1981). Pulse Transit Time as an Indicator of Arterial Blood Pressure. *Psychophysiology*, 18(1), 71–74. <https://doi.org/10.1111/j.1469-8986.1981.tb01545.x>
- Geselowitz, D. B. (1971). An Application of Electrocardiographic Lead Theory to Impedance Plethysmography. *IEEE Transactions on Biomedical Engineering*, BME-18(1), 38–41. <https://doi.org/10.1109/TBME.1971.4502787>
- Ghasemzadeh, N., & Zafari, A. M. (2011). A Brief Journey into the History of the Arterial Pulse. *Cardiology Research and Practice*, 2011. <https://doi.org/10.4061/2011/164832>
- Gi, S. O., Lee, Y. J., Koo, H. R., Khang, S., Kim, K.-N., Kang, S.-J., ... Lee, J.-W. (2015). Application of a Textile-based Inductive Sensor for the Vital Sign Monitoring. *Journal of Electrical Engineering and Technology*, 10(1), 364–371. <https://doi.org/10.5370/JEET.2015.10.1.364>
- Gorgels, A. P. M. (2007). Electrocardiography. In *Cardiovascular Medicine* (pp. 43–77). Springer, London. https://doi.org/10.1007/978-1-84628-715-2_3
- Gracia, J., Seppä, V. P., Viik, J., & Hyttinen, J. (2012). Multilead Measurement System for the Time-Domain Analysis of Bioimpedance Magnitude. *IEEE Transactions on Biomedical Engineering*, 59(8), 2273–2280. <https://doi.org/10.1109/TBME.2012.2202318>
- Grenvik, A., Ballou, S., McGinley, E., Millen, J. E., Cooley, W. L., & Safar, P. (1972). Impedance Pneumography: Comparison between Chest Impedance Changes and Respiratory Volumes in 11 Healthy Volunteers. *Chest*, 62(4), 439–443. <https://doi.org/10.1378/chest.62.4.439>
- Grimnes, S., & Martinsen, Ø. G. (2007). Sources of Error in Tetrapolar Impedance Measurements on Biomaterials and Other Ionic Conductors. *Journal of Physics D: Applied Physics*, 40(1), 9. <https://doi.org/10.1088/0022-3727/40/1/S02>
- Grimnes, S., & Martinsen, Ø. G. (2008). *Bioimpedance and Bioelectricity Basics - 2nd Edition*.
- Grlica, J., Martinović, T., & Džapo, H. (2015). Capacitive Sensor for Respiration Monitoring. In *2015 IEEE Sensors Applications Symposium (SAS)* (pp. 1–6). <https://doi.org/10.1109/SAS.2015.7133567>
- Gruetzmann, A., Hansen, S., & Müller, J. (2007). Novel Dry Electrodes for ECG Monitoring. *Physiological Measurement*, 28(11), 1375. <https://doi.org/10.1088/0967-3334/28/11/005>
- Guardo, R., Trudelle, S., Adler, A., Boulay, C., & Savard, P. (1995). Contactless Recording of Cardiac Related Thoracic Conductivity Changes. In *Proceedings of 17th International Conference of the Engineering in Medicine and Biology Society* (Vol. 2, pp. 1581–1582 vol.2). <https://doi.org/10.1109/IEMBS.1995.579839>
- Gursoy, D., & Scharfetter, H. (2010). Magnetic Induction Pneumography: a Planar Coil System for Continuous Monitoring of Lung Function via Contactless Measurements. *Journal of Electrical Bioimpedance*, 1(1), 56–62. <https://doi.org/10.5617/jeb.136>
- Hahn, J.-O., Reisner, A. T., & Asada, H. H. (2010, January 21). *US20100016736 A1*. Retrieved from <http://www.google.com/patents/US20100016736>

- Hallett, M. (2007). Transcranial Magnetic Stimulation: A Primer. *Neuron*, 55(2), 187–199. <https://doi.org/10.1016/j.neuron.2007.06.026>
- Hamdani, S. T. A., & Fernando, A. (2015). The Application of a Piezo-Resistive Cardiorespiratory Sensor System in an Automobile Safety Belt. *Sensors (Basel, Switzerland)*, 15(4), 7742–7753. <https://doi.org/10.3390/s150407742>
- Hanic, M., Sládek, L., Horínek, F., Jagelka, M., Donoval, M., Daříček, M., & Donoval, D. (2014). BIO-monitoring System with Conductive Textile Electrodes Integrated into T-shirt. In *2014 24th International Conference Radioelektronika* (pp. 1–4). <https://doi.org/10.1109/Radiolek.2014.6828472>
- Herisson, J. (1834). Measurement of the Pulse. The Sphygmometer.: ‘ An Instrument which Makes Every Action of the Arteries Apparent to the Eye.’ *The Lancet*, 23(578), 22–27. [https://doi.org/10.1016/S0140-6736\(02\)96308-7](https://doi.org/10.1016/S0140-6736(02)96308-7)
- Hernandez, J., McDuff, D., & Picard, R. W. (2015). Biowatch: Estimation of Heart and Breathing Rates from Wrist Motions. In *2015 9th International Conference on Pervasive Computing Technologies for Healthcare (PervasiveHealth)* (pp. 169–176). <https://doi.org/10.4108/icst.pervasivehealth.2015.259064>
- Hoog Antink, C., Schulz, F., Leonhardt, S., & Walter, M. (2017). Motion Artifact Quantification and Sensor Fusion for Unobtrusive Health Monitoring. *Sensors (Basel, Switzerland)*, 18(1). <https://doi.org/10.3390/s18010038>
- Hu, D., Cheng, T. K., Xie, K., & Lam, R. H. W. (2015). Microengineered Conductive Elastomeric Electrodes for Long-Term Electrophysiological Measurements with Consistent Impedance under Stretch. *Sensors*, 15(10), 26906–26920. <https://doi.org/10.3390/s151026906>
- Huang, J.-J., Huang, Y.-M., & See, A. R. (2017). Studying Peripheral Vascular Pulse Wave Velocity Using Bio-impedance Plethysmography and Regression Analysis. *ECTI Transactions on Computer and Information Technology (ECTI-CIT)*, 11(1), 63–70.
- Hung, P. D., Bonnet, S., Guillemaud, R., Castelli, E., & Yen, P. T. N. (2008). Estimation of Respiratory Waveform Using an Accelerometer. In *2008 5th IEEE International Symposium on Biomedical Imaging: From Nano to Macro* (pp. 1493–1496). <https://doi.org/10.1109/ISBI.2008.4541291>
- Ikarashi, A., Nogawa, M., Yamakoshi, T., Tanaka, S., & Yamakoshi, K. (2006). An Optimal Spot-electrodes Array for Electrical Impedance Cardiography through Determination of Impedance Mapping of a Regional Area along the Medial Line on the Thorax. In *2006 International Conference of the IEEE Engineering in Medicine and Biology Society* (pp. 3202–3205). <https://doi.org/10.1109/IEMBS.2006.260748>
- Islam, N., Rabbani, K. S., & Wilson, A. (2010). The Sensitivity of Focused Electrical Impedance Measurements. *Physiological Measurement*, 31(8), S97. <https://doi.org/10.1088/0967-3334/31/8/S08>
- Isop, C. (2017). *Pöörivoolu mähisega vere pulsatsiooni mõõtmise simulatsioon inimese pindmistes kudedes*. Tallinn University of Technology, Tallinn.
- Jawbone. (2018). UP3 by Jawbone | A Smarter Activity Tracker For A Fitter You. Retrieved 19 February 2018, from <https://jawbone.com/fitness-tracker/up3>
- Jivet, I. (2014). Wrist Pulse Monitoring by Electrical Impedance Using a 3D Model of the Arm. In *2014 11th International Symposium on Electronics and Telecommunications (ISETC)* (pp. 1–4). <https://doi.org/10.1109/ISETC.2014.7010760>

- Kang, T. H., Merritt, C. R., Grant, E., Pourdeyhimi, B., & Nagle, H. T. (2008). Nonwoven Fabric Active Electrodes for Biopotential Measurement During Normal Daily Activity. *IEEE Transactions on Biomedical Engineering*, 55(1), 188–195. <https://doi.org/10.1109/TBME.2007.910678>
- Kang, T.-H. (2006). *Textile-embedded Sensors for Wearable Physiological Monitoring Systems*. North Carolina State University. Retrieved from <https://repository.lib.ncsu.edu/handle/1840.16/5143>
- Kao, T. Y. J., Chen, A. Y. K., Yan, Y., Shen, T. M., & Lin, J. (2012). A Flip-chip-packaged and Fully Integrated 60 GHz CMOS Micro-radar Sensor for Heartbeat and Mechanical Vibration Detections. In *2012 IEEE Radio Frequency Integrated Circuits Symposium* (pp. 443–446). <https://doi.org/10.1109/RFIC.2012.6242318>
- Karki, S., Kaariainen, M., & Lekkala, J. (2007). Measurement of Heart Sounds with EMFi Transducer. In *2007 29th Annual International Conference of the IEEE Engineering in Medicine and Biology Society* (pp. 1683–1686). <https://doi.org/10.1109/IEMBS.2007.4352632>
- Kauppinen, P. K., Hyttinen, J. A., & Malmivuo, J. A. (1998). Sensitivity Distributions of Impedance Cardiography Using Band and Spot Electrodes Analyzed by a Three-Dimensional Computer Model. *Annals of Biomedical Engineering*, 26(4), 694–702. <https://doi.org/10.1114/1.44>
- Kazani, I., Hertleer, C., De Mey, G., Schwarz, A., Guxho, G., & Van Langenhove, L. (2012). Electrical Conductive Textiles Obtained by Screen Printing. *FIBRES & TEXTILES IN EASTERN EUROPE*, 20(1), 57–63.
- Klomjai, W., Katz, R., & Lackmy-Vallée, A. (2015). Basic Principles of Transcranial Magnetic Stimulation (TMS) and Repetitive TMS (rTMS). *Annals of Physical and Rehabilitation Medicine*, 58(4), 208–213. <https://doi.org/10.1016/j.rehab.2015.05.005>
- Kolev, N., & Zimpfer, M. (1995). Left Ventricular Ejection Time and End-Systolic Pressure Revisited. *Anesthesia & Analgesia*, 81(4), 889.
- Koo, H. R., Lee, Y.-J., Gi, S., Khang, S., Lee, J. H., Lee, J.-H., ... Lee, J.-W. (2014). The Effect of Textile-Based Inductive Coil Sensor Positions for Heart Rate Monitoring. *Journal of Medical Systems*, 38(2). <https://doi.org/10.1007/s10916-013-0002-0>
- Krehel, M., Schmid, M., Rossi, R. M., Boesel, L. F., Bona, G.-L., & Scherer, L. J. (2014). An Optical Fibre-Based Sensor for Respiratory Monitoring. *Sensors*, 14(7), 13088–13101. <https://doi.org/10.3390/s140713088>
- Krivošei, A. (2009). *Model Based Method for Adaptive Decomposition of the Thoracic Bio-impedance Variations into Cardiac and Respiratory Components*. Tallinn University of Technology, Tallinn. Retrieved from <https://digi.lib.ttu.ee/i/?447>
- Krivošei, A., Lamp, J., Min, M., Uuetoa, T., Uuetoa, H., & Annus, P. (2013). Non-invasive Method for the Aortic Blood Pressure Waveform Estimation Using the Measured Radial EBI. *Journal of Physics: Conference Series*, 434(1), 012048. <https://doi.org/10.1088/1742-6596/434/1/012048>
- Krotov, A. (2017). *Elektrilise impedantsi mõõtmise simulatsioon 3D inimese käe mudelil*. Tallinn University of Technology, Tallinn.
- Kuang, W., & Nelson, S. O. (1998). Low-frequency Dielectric Properties of Biological Tissues: a Review with Some New Insights. *Transactions of the ASAE (USA)*. Retrieved from <http://agris.fao.org/agris-search/search.do?recordID=US1997080386>

- Kubicek, W. G., Karnegis, J. N., Patterson, R. P., Witsoe, D. A., & Mattson, R. H. (1966). Development and Evaluation of an Impedance Cardiac Output System. *Aerospace Medicine*, 37(12), 1208–1212.
- Kundu, S. K., Kumagai, S., & Sasaki, M. (2013). A Wearable Capacitive Sensor for Monitoring Human Respiratory Rate. *Japanese Journal of Applied Physics*, 52(4S), 04CL05. <https://doi.org/10.7567/JJAP.52.04CL05>
- Kwok, M. C., & Pepper, M. G. (1991). Noninvasive Detection of Ventricular Wall Motion by Electromagnetic Coupling. *Medical and Biological Engineering and Computing*, 29(2), 136–140. <https://doi.org/10.1007/BF02447098>
- Lad, V. D. (2006). *Secrets of the Pulse: The Ancient Art of Ayurvedic Pulse Diagnosis*. (M. S. Peet, G. Crowther, & B. Cook, Eds.) (2 edition). Albuquerque, N.M: The Ayurvedic Press.
- Lee, W., & Cho, S. (2015). Integrated All Electrical Pulse Wave Velocity and Respiration Sensors Using Bio-Impedance. *IEEE Journal of Solid-State Circuits*, 50(3), 776–785. <https://doi.org/10.1109/JSSC.2014.2380781>
- Lehr, J. (1972). A Vector Derivation Useful in Impedance Plethysmographic Field Calculations. *IEEE Transactions on Biomedical Engineering*, BME-19(2), 156–157. <https://doi.org/10.1109/TBME.1972.324058>
- Lewandowska, M., Wtorek, J., & Mierzejewski, L. (2010). Analysis of Sensitivity Distribution in Human Chest During Multichannel Bioimpedance Measurements. In *2010 2nd International Conference on Information Technology*, (2010 ICIT) (pp. 267–270).
- Li, H., Chen, X., Cao, L., Zhang, C., Tang, C., Li, E., ... Liang, H. (2017). Textile-based ECG Acquisition System with Capacitively Coupled Electrodes. *Transactions of the Institute of Measurement and Control*, 39(2), 141–148. <https://doi.org/10.1177/0142331215600254>
- Li, J. Q., Lia, R., Chen, Z. Z., Deng, G. Q., Wang, H., Mavromoustakis, C., ... Ming, Z. (2018). Design of a Continuous Blood Pressure Measurement System based on Pulse Wave and ECG Signals. *IEEE Journal of Translational Engineering in Health and Medicine*, 6. <https://doi.org/10.1109/JTEHM.2017.2788885>
- Liu, S.-H., Cheng, D.-C., & Su, C.-H. (2017). A Cuffless Blood Pressure Measurement Based on the Impedance Plethysmography Technique. *Sensors (Basel, Switzerland)*, 17(5). <https://doi.org/10.3390/s17051176>
- Lu, M., & Ueno, S. (2015). Deep Transcranial Magnetic Stimulation Using Figure-of-Eight and Halo Coils. *IEEE Transactions on Magnetics*, 51(11), 1–4. <https://doi.org/10.1109/TMAG.2015.2436977>
- Luo, S., Afonso, V. X., Webster, J. G., & Tompkins, W. J. (1992). The Electrode System in Impedance-based Ventilation Measurement. *IEEE Transactions on Biomedical Engineering*, 39(11), 1130–1141. <https://doi.org/10.1109/10.168692>
- Luprano, J., Carvalho, P. de, Eilebrecht, B., Kortelainen, J., Muehlsteff, J., Sipila, A., ... Ulbrich, M. (2013). HeartCycle: Advanced Sensors for Telehealth Applications. In *2013 35th Annual International Conference of the IEEE Engineering in Medicine and Biology Society (EMBC)* (pp. 6984–6987). <https://doi.org/10.1109/EMBC.2013.6611165>

- Luprano, J., Sola, J., Dasen, S., Koller, J. M., & Chetelat, O. (2006). Combination of Body Sensor Networks and on-body Signal Processing Algorithms: the Practical Case of MyHeart Project. In *International Workshop on Wearable and Implantable Body Sensor Networks (BSN'06)* (pp. 4 pp. – 79). <https://doi.org/10.1109/BSN.2006.15>
- Mandal, S., Turicchia, L., & Sarapeshkar, R. (2010). A Low-Power, Battery-Free Tag for Body Sensor Networks. *IEEE Pervasive Computing*, 9(1), 71–77. <https://doi.org/10.1109/MPRV.2010.1>
- Martinsen, Ø. G., Grimnes, S., & Nilsen, S. H. (2008). Water Sorption and Electrical Properties of a Human Nail. *Skin Research and Technology*, 14(2), 142–146. <https://doi.org/10.1111/j.1600-0846.2007.00267.x>
- Mayer, M., Brunner, P., Merwa, R., & Scharfetter, H. (2005). Monitoring of Lung Edema Using Focused Impedance Spectroscopy: a Feasibility Study. *Physiological Measurement*, 26(3), 185. <https://doi.org/10.1088/0967-3334/26/3/004>
- McAdams, E. (2006). Bioelectrodes. In J. G. Webster (Ed.), *Encyclopedia of Medical Devices and Instrumentation*. Hoboken, NJ, USA: John Wiley & Sons, Inc. <https://doi.org/10.1002/0471732877.emd013>
- Merritt, C. R., Nagle, H. T., & Grant, E. (2009). Fabric-Based Active Electrode Design and Fabrication for Health Monitoring Clothing. *IEEE Transactions on Information Technology in Biomedicine*, 13(2), 274–280. <https://doi.org/10.1109/TITB.2009.2012408>
- Metshein, M. (2014). Alternatives of Measurement of Electrical Bioimpedance of the Body with the Aim to Determine the Cardiac and Respiratory Activity. In *2014 14th Biennial Baltic Electronic Conference (BEC)* (pp. 197–200). <https://doi.org/10.1109/BEC.2014.7320590>
- Metshein, M., & Gordon, R. (2016). On the Possibility of Detecting the Electrical Bioimpedance of Human Body by Using Non-contact Electrodes in Capacitive Connection. In *2016 15th Biennial Baltic Electronics Conference (BEC)* (pp. 171–174). <https://doi.org/10.1109/BEC.2016.7743756>
- Metshein, Margus, & Parve, T. (2015). Electrical Bioimpedance Based Monitoring of Cardiac and Respiratory Activity: Positioning of Capacitive Electrodes for Wearable Human Monitoring Device. *International Journal of Bioelectromagnetism*, 17(2), 64–74.
- Min, M., Annus, P., Köiv, H., Krivošei, A., Uuetoa, T., & Lamp, J. (2017). Bioimpedance Sensing - a Viable Alternative for Tonometry in Non-invasive Assessment of Central Aortic Pressure. In *2017 IEEE International Symposium on Medical Measurements and Applications (MeMeA)* (pp. 373–378). <https://doi.org/10.1109/MeMeA.2017.7985905>
- Min, M., Ojarand, J., Märtens, O., Paavle, T., Land, R., Annus, P., ... Parve, T. (2012). Binary Signals in Impedance Spectroscopy. In *2012 Annual International Conference of the IEEE Engineering in Medicine and Biology Society* (pp. 134–137). <https://doi.org/10.1109/EMBC.2012.6345889>
- Min, M., Parve, T., Annus, P., & Paavle, T. (2006). A Method of Synchronous Sampling in Multifrequency Bioimpedance Measurements. In *2006 IEEE Instrumentation and Measurement Technology Conference Proceedings* (pp. 1699–1703). <https://doi.org/10.1109/IMTC.2006.328200>

- Młyńczak, M. C., Niewiadomski, W., Żyliński, M., & Cybulski, G. P. (2014). Ambulatory Impedance Pneumography Device for Quantitative Monitoring of Volumetric Parameters in Respiratory and Cardiac Applications. In *Computing in Cardiology 2014* (pp. 965–968).
- Moderhak, M., Madej, M., Wtorek, J., & Truyen, B. (2011). Pulse Pressure Velocity Measurement - A Wearable Sensor. In *2011 Federated Conference on Computer Science and Information Systems (FedCSIS)* (pp. 411–416).
- Mooney, J. W., Ghasemi-Roudsari, S., Banham, E. R., Symonds, C., Pawłowski, N., & Varcoe, B. T. H. (2016). A Portable Diagnostic Device for Cardiac Magnetic Field Mapping. *Biomed. Phys. Eng. Express*, 3. Retrieved from <http://arxiv.org/abs/1609.05771>
- Muehlsteff, J., Dellimore, K., Aarts, V., Derkx, R., Peiker, C., & Meyer, C. (2015). Pulse Detection with a Single Accelerometer Placed at the Carotid Artery: Performance in a Real-life Diagnostic Test During Acute Hypotension. In *2015 37th Annual International Conference of the IEEE Engineering in Medicine and Biology Society (EMBC)* (pp. 434–437). <https://doi.org/10.1109/EMBC.2015.7318392>
- Mughal, Y. M., Annus, P., Min, M., & Gordon, R. (2014). An Overview of the Impedance Models of the Thorax and the Origin of the Impedance Cardiography Signal for Modelling of the Impedance Signals. In *2014 IEEE Conference on Biomedical Engineering and Sciences (IECBES)* (pp. 526–531). <https://doi.org/10.1109/IECBES.2014.7047557>
- Muhlsteff, J., & Such, O. (2004). Dry Electrodes for Monitoring of Vital Signs in Functional Textiles. In *The 26th Annual International Conference of the IEEE Engineering in Medicine and Biology Society* (Vol. 1, pp. 2212–2215). <https://doi.org/10.1109/IEMBS.2004.1403645>
- Mundt, C. W., Montgomery, K. N., Udo, U. E., Barker, V. N., Thonier, G. C., Tellier, A. M., ... Kovacs, G. T. A. (2005). A Multiparameter Wearable Physiologic Monitoring System for Space and Terrestrial Applications. *IEEE Transactions on Information Technology in Biomedicine*, 9(3), 382–391. <https://doi.org/10.1109/TITB.2005.854509>
- Nelson, M. R., Stepanek, J., Cevette, M., Covalciuc, M., Hurst, R. T., & Tajik, A. J. (2010). Noninvasive Measurement of Central Vascular Pressures With Arterial Tonometry: Clinical Revival of the Pulse Pressure Waveform? *Mayo Clinic Proceedings*, 85(5), 460–472. <https://doi.org/10.4065/mcp.2009.0336>
- Neuman, M. R. (2000). Biopotential Electrodes. In J. D. Bronzino (Ed.), *The Biomedical Engineering Handbook, Second Edition. 2 Volume Set.* Retrieved from http://www.fis.uc.pt/data/20062007/apontamentos/apnt_134_5.pdf
- Ng, C. L., & Reaz, M. B. I. (2017). Characterization of Textile-Insulated Capacitive Biosensors. *Sensors*, 17(3), 574. <https://doi.org/10.3390/s17030574>
- Nyboer, J., Kreider, M. M., & Hannapel, L. (1950). Electrical Impedance Plethysmography: A Physical and Physiologic Approach to Peripheral Vascular Study. *Circulation*, 2(6), 811–821. <https://doi.org/10.1161/01.CIR.2.6.811>
- Ojarand, J., Pille, S., Min, M., Land, R., & Oleitšuk, J. (2015). Magnetic Induction Sensor for the Respiration Monitoring. In *The 10th International Conference on Bioelectromagnetism*. Tallinn. Retrieved from <http://www.isbem.org/conf/2015/proc/27.pdf>

- Oum, J. H., Lee, S. E., Kim, D. W., & Hong, S. (2008). Non-contact Heartbeat and Respiration Detector Using Capacitive Sensor with Colpitts Oscillator. *Electronics Letters*, 44(2), 87–88. <https://doi.org/10.1049/el:20082336>
- Pallas-Areny, R., & Webster, J. G. (1993). AC Instrumentation Amplifier for Bioimpedance Measurements. *IEEE Transactions on Biomedical Engineering*, 40(8), 830–833. <https://doi.org/10.1109/10.238470>
- Paradiso, R., Loriga, G., Taccini, N., Gemignani, A., & Ghelarducci, B. (2005). WEALTHY - A Wearable Healthcare System: New Frontier on E-textile. *Journal of Telecommunications and Information Technology*, 4, 105–113.
- Patterson, R. P. (1989). Fundamentals of Impedance Cardiography. *IEEE Engineering in Medicine and Biology Magazine*, 8(1), 35–38. <https://doi.org/10.1109/51.32403>
- Patterson, R. P. (2010). Impedance Cardiography: What is the Source of the Signal? *Journal of Physics: Conference Series*, 224(1), 012118. <https://doi.org/10.1088/1742-6596/224/1/012118>
- Payne, R. A., Symeonides, C. N., Webb, D. J., & Maxwell, S. R. J. (2006). Pulse Transit Time Measured from the ECG: An Unreliable Marker of Beat-to-beat Blood Pressure. *Journal of Applied Physiology*, 100(1), 136–141. <https://doi.org/10.1152/japplphysiol.00657.2005>
- Pethig, R., & Kell, D. B. (1987). The Passive Electrical Properties of Biological Systems: Their Significance in Physiology, Biophysics and Biotechnology. *Physics in Medicine & Biology*, 32(8), 933. <https://doi.org/10.1088/0031-9155/32/8/001>
- Pettersen, F. J., Ferdous, H., Kalvøy, H., Martinsen, Ø. G., & Høgetveit, J. O. (2014). Comparison of Four Different FIM Configurations—A Simulation Study. *Physiological Measurement*, 35(6), 1067. <https://doi.org/10.1088/0967-3334/35/6/1067>
- Pfützner, H., & Futschik, K. (2000). Electric Field Plethysmography for Monitoring of Cardiac and Respiratory Activity. Presented at the XVI IMEKO World Congress.
- Poh, M.-Z., McDuff, D. J., & Picard, R. W. (2010). Non-contact, automated cardiac pulse measurements using video imaging and blind source separation. *Optics Express*, 18(10), 10762–10774. <https://doi.org/10.1364/OE.18.010762>
- Raaijmakers, E., Faes, T. J. C., Goovaerts, H. G., Meijer, J. H., Vries, P. M. J. M. de, & Heethaar, R. M. (1998). Thoracic Geometry and its Relation to Electrical Current Distribution: Consequences for Electrode Placement in Electrical Impedance Cardiography. *Medical and Biological Engineering and Computing*, 36(5), 592–597. <https://doi.org/10.1007/BF02524429>
- Rabbani, K. S., Sarker, M., Akond, M. H. R., & Akter, T. (1999). Focused Impedance Measurement (FIM): A New Technique with Improved Zone Localization. *Annals of the New York Academy of Sciences*, 873(1), 408–420. <https://doi.org/10.1111/j.1749-6632.1999.tb09490.x>
- Rattfält, L. (2013). *Smartware Electrodes for ECG Measurements: Design, Evaluation and Signal Processing*. Linköping University Electronic Press. <https://doi.org/10.3384/diss.diva-100134>

- Ruiz, J. C. M. (2013). *Sensor-Based Garments that Enable the Use of Bioimpedance Technology : Towards Personalized Healthcare Monitoring*. Retrieved from <http://www.diva-portal.org/smash/record.jsf?pid=diva2:877035>
- Sahakian, A. V., Tompkins, W. J., & Webster, J. G. (1985). Electrode Motion Artifacts in Electrical Impedance Pneumography. *IEEE Transactions on Biomedical Engineering, BME-32*(6), 448–451. <https://doi.org/10.1109/TBME.1985.325453>
- Scalise, L. (2012). *Non Contact Heart Monitoring*. INTECH Open Access Publisher, 2012. Retrieved from <http://www.intechopen.com/books/advances-in-electrocardiograms-methods-and-analysis/non-contact-heart-monitoring>
- Schwan, H. P. (1957). Electrical Properties of Tissue and Cell Suspensions. In J. H. Lawrence & C. A. Tobias (Eds.), *Advances in Biological and Medical Physics* (Vol. 5, pp. 147–209). Elsevier. <https://doi.org/10.1016/B978-1-4832-3111-2.50008-0>
- Schwan, H. P. (1988). Biological Effects of Non-ionizing Radiations: Cellular Properties and Interactions. *Annals of Biomedical Engineering, 16*(3), 245–263. <https://doi.org/10.1007/BF02368002>
- Schwan, H. P. (1999). The Practical Success of Impedance Techniques from an Historical Perspective. *Annals of the New York Academy of Sciences, 873*(1), 1–12. <https://doi.org/10.1111/j.1749-6632.1999.tb09443.x>
- Searle, A., & Kirkup, L. (2000). A Direct Comparison of Wet, Dry and Insulating Bioelectric Recording Electrodes. *Physiological Measurement, 21*(2), 271–283.
- Seppä. (2014). *Development and Clinical Application of Impedance Pneumography Technique*. Tampere University of Technology, Tampere.
- Seppä, V. P., Viik, J., & Hyttinen, J. (2010). Assessment of Pulmonary Flow Using Impedance Pneumography. *IEEE Transactions on Biomedical Engineering, 57*(9), 2277–2285. <https://doi.org/10.1109/TBME.2010.2051668>
- Sherwood, A., Allen, M. T., Fahrenberg, J., Kelsey, R. M., Lovallo, W. R., & van Doornen, L. J. P. (1990). Methodological Guidelines for Impedance Cardiography. *Psychophysiology, 27*(1), 1–23. <https://doi.org/10.1111/j.1469-8986.1990.tb02171.x>
- Shuvo, O. I., & Islam, M. N. (2016). Sensitivity Analysis of the Tetrapolar Electrical Impedance Measurement Systems Using COMSOL Multiphysics for the non-uniform and Inhomogeneous Medium. *Dhaka University Journal of Science, 64*(1), 7–13.
- Sigman, E., Kolin, A., Katz, L. N., & Jochim, K. (1937). Effect of motion on the electrical conductivity of the blood. *American Journal of Physiology-Legacy Content, 118*(4), 708–719. <https://doi.org/10.1152/ajplegacy.1937.118.4.708>
- Steffen, M., Aleksandrowicz, A., & Leonhardt, S. (2007). Mobile Noncontact Monitoring of Heart and Lung Activity. *IEEE Transactions on Biomedical Circuits and Systems, 1*(4), 250–257. <https://doi.org/10.1109/TBCAS.2008.915633>
- Stern, O. (1924). Zur theorie der elektrolytischen doppelschicht. *Zeitschrift Für Elektrochemie Und Angewandte Physikalische Chemie, 30*(21-22), 508–516. <https://doi.org/10.1002/bbpc.192400182>
- Stoppa, M., & Chiolero, A. (2014). Wearable Electronics and Smart Textiles: A Critical Review. *Sensors (Basel, Switzerland), 14*(7), 11957–11992. <https://doi.org/10.3390/s140711957>

- Storck, K., Karlsson, M., Ask, P., & Loyd, D. (1996). Heat Transfer Evaluation of the Nasal Thermistor Technique. *IEEE Transactions on Biomedical Engineering*, 43(12), 1187–1191. <https://doi.org/10.1109/10.544342>
- Sullivan, T. J., Deiss, S. R., & Cauwenberghs, G. (2007). A Low-Noise, Non-Contact EEG/ECG Sensor. In *2007 IEEE Biomedical Circuits and Systems Conference* (pp. 154–157). <https://doi.org/10.1109/BIOCAS.2007.446332>
- Tan, K. S., Saatchi, R., Elphick, H., & Burke, D. (2010). Real-time vision based respiration monitoring system. In *2010 7th International Symposium on Communication Systems, Networks Digital Signal Processing (CSNDSP 2010)* (pp. 770–774).
- Tarjan, P. P., & McFee, R. (1968). Electrodeless Measurements of the Effective Resistivity of the Human Torso and Head by Magnetic Induction. *IEEE Transactions on Biomedical Engineering*, BME-15(4), 266–278. <https://doi.org/10.1109/TBME.1968.4502577>
- Teichmann, D., Foussier, J., Jia, J., Leonhardt, S., & Walter, M. (2013). Noncontact Monitoring of Cardiorespiratory Activity by Electromagnetic Coupling. *IEEE Transactions on Biomedical Engineering*, 60(8), 2142–2152. <https://doi.org/10.1109/TBME.2013.2248732>
- Teichmann, D., Matteis, D. D., Bartelt, T., Walter, M., & Leonhardt, S. (2015). A Bendable and Wearable Cardiorespiratory Monitoring Device Fusing Two Noncontact Sensor Principles. *IEEE Journal of Biomedical and Health Informatics*, 19(3), 784–793. <https://doi.org/10.1109/JBHI.2015.2417760>
- Teichmann, Daniel, Kuhn, A., Leonhardt, S., & Walter, M. (2014). The MAIN Shirt: A Textile-Integrated Magnetic Induction Sensor Array. *Sensors (Basel, Switzerland)*, 14(1), 1039–1056. <https://doi.org/10.3390/s140101039>
- Thakor, N. V., & Zhu, Y. S. (1991). Applications of Adaptive Filtering to ECG Analysis: Noise Cancellation and Arrhythmia Detection. *IEEE Transactions on Biomedical Engineering*, 38(8), 785–794. <https://doi.org/10.1109/10.83591>
- Thoms, L.-J., Colicchia, G., & Girwidz, R. (2017). Phonocardiography with a Smartphone. *Physics Education*, 52(2), 023004. <https://doi.org/10.1088/1361-6552/aa51ec>
- Tong, D. A., Bartels, K. A., & Honeyager, K. S. (2002). Adaptive Reduction of Motion Artifact in the Electrocardiogram. In *Proceedings of the Second Joint 24th Annual Conference and the Annual Fall Meeting of the Biomedical Engineering Society] [Engineering in Medicine and Biology* (Vol. 2, pp. 1403–1404 vol.2). <https://doi.org/10.1109/IEMBS.2002.1106451>
- Ueno, A., Akabane, Y., Kato, T., Hoshino, H., Kataoka, S., & Ishiyama, Y. (2007). Capacitive Sensing of Electrocardiographic Potential Through Cloth From the Dorsal Surface of the Body in a Supine Position: A Preliminary Study. *IEEE Transactions on Biomedical Engineering*, 54(4), 759–766. <https://doi.org/10.1109/TBME.2006.889201>
- Ueno, S., Tashiro, T., & Harada, K. (1988). Localized Stimulation of Neural Tissues in the Brain by Means of a Paired Configuration of Time-varying Magnetic Fields. *Journal of Applied Physics*, 64(10), 5862–5864. <https://doi.org/10.1063/1.342181>
- Vas, R. (1967). Electronic Device for Physiological Kinetic Measurements and Detection of Extraneous Bodies. *IEEE Transactions on Biomedical Engineering*, BME-14(1), 2–6. <https://doi.org/10.1109/TBME.1967.4502453>

- Vedru, J. (1994). Electrical Impedance Methods for the Measurement of Stroke Volume in Man: State of Art. In *Acta et commentationes Universitatis Tartuensis* (pp. 110–129).
- Vedru, J., & Solntseva, O. (2007). Variation of Magnetic Induction Plethysmogram on Human Thoracic Surface. In *13th International Conference on Electrical Bioimpedance and the 8th Conference on Electrical Impedance Tomography* (pp. 743–746). Springer, Berlin, Heidelberg. https://doi.org/10.1007/978-3-540-73841-1_192
- Vuorela, T., Seppä, V. P., Vanhala, J., & Hyttinen, J. (2010). Design and Implementation of a Portable Long-Term Physiological Signal Recorder. *IEEE Transactions on Information Technology in Biomedicine*, 14(3), 718–725. <https://doi.org/10.1109/TITB.2010.2042606>
- Wang, H., Yen, C., Liang, J., Wang, Q., Liu, G., & Song, R. (2014). A Robust Electrode Configuration for Bioimpedance Measurement of Respiration. *Journal of Healthcare Engineering*, 5(3), 313–328. <https://doi.org/10.1260/2040-2295.5.3.313>
- Wang, L. F., Liu, J. Q., Peng, H. L., Yang, B., Zhu, H. Y., & Yang, C. S. (2013). MEMS-based Flexible Capacitive Electrode for ECG Measurement. *Electronics Letters*, 49(12), 739–740. <https://doi.org/10.1049/el.2012.4064>
- Wang, Y., Haynor, D. R., & Kim, Y. (2001). A Finite-element Study of the Effects of Electrode Position on the Measured Impedance Change in Impedance Cardiography. *IEEE Transactions on Biomedical Engineering*, 48(12), 1390–1401. <https://doi.org/10.1109/10.966598>
- Wartzek, T., Weyer, S., & Leonhardt, S. (2011). A Differential Capacitive Electrical Field Sensor Array for Contactless Measurement of Respiratory Rate. *Physiological Measurement*, 32(10), 1575. <https://doi.org/10.1088/0967-3334/32/10/006>
- Weyer, S. N., Weber, H., Kleeberg, C., Leonhardt, S., & Wartzek, T. (2015). Development of a Real-time, Semi-capacitive Impedance Phlebography Device. *Journal of Electrical Bioimpedance*, 6(1), 2. <https://doi.org/10.5617/jeb.953>
- Wiesner, S., & Yaniv, Z. (2007). Monitoring Patient Respiration using a Single Optical Camera. In *2007 29th Annual International Conference of the IEEE Engineering in Medicine and Biology Society* (pp. 2740–2743). <https://doi.org/10.1109/IEMBS.2007.4352895>
- Xu, D., Ryan, K. L., Rickards, C. A., Zhang, G., Convertino, V. A., & Mukkamala, R. (2010). Robust Pulse Wave Velocity Estimation by Application of System Identification to Proximal and Distal Arterial Waveforms. In *2010 Annual International Conference of the IEEE Engineering in Medicine and Biology* (pp. 3559–3562). <https://doi.org/10.1109/IEMBS.2010.5627718>
- Xu, J., Gao, X., Lee, A., Yamada, S., Yavari, E., Lubecke, V., & Boric-Lubecke, O. (2016). Wrist-worn Heartbeat Monitoring System Based on Bio-impedance Analysis. In *2016 38th Annual International Conference of the IEEE Engineering in Medicine and Biology Society (EMBC)* (pp. 6294–6297). <https://doi.org/10.1109/EMBC.2016.7592167>
- Yang, D., Xu, B., Qiao, H., & Wang, X. (2017). Cardiopulmonary Signal Detection Based on Magnetic Induction. *Journal of Sensors*, 2017. <https://doi.org/10.1155/2017/1752560>

- Yang, F., & Patterson, R. P. (2008). A Simulation Study on the Effect of Thoracic Conductivity Inhomogeneities on Sensitivity Distributions. *Annals of Biomedical Engineering*, 36(5), 762–768. <https://doi.org/10.1007/s10439-008-9469-0>
- Yang, J., Chen, B., Zhou, J., & Lv, Z. (2015). A Low-Power and Portable Biomedical Device for Respiratory Monitoring with a Stable Power Source. *Sensors (Basel, Switzerland)*, 15(8), 19618–19632. <https://doi.org/10.3390/s150819618>
- Zhao, F., Li, M., & Tsien, J. Z. (2015). Technology Platforms for Remote Monitoring of Vital Signs in the New Era of Telemedicine. *Expert Review of Medical Devices*, 12(4), 411–429. <https://doi.org/10.1586/17434440.2015.1050957>
- Zito, D., Pepe, D., Neri, B., Zito, F., De Rossi, D., & Lanatà, A. (2008). Feasibility Study and Design of a Wearable System-on-a-Chip Pulse Radar for Contactless Cardiopulmonary Monitoring. *International Journal of Telemedicine and Applications*, 2008. <https://doi.org/10.1155/2008/328597>
- Zuckerwar, A. J., Pretlow, R. A., Stoughton, J. W., & Baker, D. A. (1993). Development of a Piezopolymer Pressure Sensor for a Portable Fetal Heart Rate Monitor. *IEEE Transactions on Biomedical Engineering*, 40(9), 963–969. <https://doi.org/10.1109/10.245618>

Acknowledgements

This work greatly relies on the support and advice from my colleagues and teachers from Thomas Johann Seebeck Department of Electronics at Tallinn University of Technology. The support of Dr. Marek Rist and Eero Haldre in creating the means in hardware for on-time measurement experiments, the support of Dr. Raul Land in preparing the software and supporting the practical experimental work; the support of Dr. Jaan Ojarand for providing the environment for performing the experiments by using inductive coupling and sharing his thorough knowledges. I have got inspiration from the high-flown ideas of Dr. Rauno Gordon and from the educational discussions with Dr. Olev Märtens. This thesis would not have been realized without your cordiality.

I thank my supervisor Dr. Paul Annus for his immense storehouse of ideas and suggestions, widening my “scientific” frames of the way of looking at things. The spot on recommendations and the ability of relating current research problems to philosophic and historical background of Dr. Annus influenced greatly my direction of synthesizing the data. Many thanks go to my co. supervisor Prof. Mart Min, whose fields of research have influenced my scientific activities and who's confident and supporting mentoring based on his tremendous experience made it possible to compile this thesis. I thank my co. supervisor Prof. Alvo Aabloo and his team at University of Tartu for giving valuable advice concerning the topicality and main directions of my research with providing the possibility for experiencing the intersections of other scientific disciplines. I thank Prof. Toomas Rang for providing me the opportunity of working in academic position, resulting as the most fruitful period of my PhD studies and for applying mild pressure on me for finishing the thesis on time. My utmost thanks go to Dr. Toomas Parve, who motivated me to start my studies towards the PhD, providing his support and help in setting my sprawling focus on relevant subjects. Dr. Parve's merit of always being there if one needs mentoring or simple advice on formatting an presentation slide or a research paper is something that we tend to miss more and more in today's world of rush.

I thank my parents for raising me in the spirit of constantly aspiring for new knowledges while approving my choices by providing their permanent and kind support. I thank my partner Piret and my daughter Tuuli for providing the home that is filled with love and caring, waiting for me after long days and nights of research.

This work has been supported financially by the following entities in alphabetical order.

- Estonian Ministry of Education and Research
- Estonian Research Council grant IUT1911
- European Social Fund through ICT Doctoral School at Tallinn University of Technology
- European Union European Regional Development Fund through Estonian Centre of Excellence in ICT Research “EXCITE” and through DoRa program
- Information Technology Foundation for Education (HITSA) through Study IT in Estonia Scholarship for PhD students of Information and Communication Technology of Tallinn University of Technology
- Zurich Instruments AG through Student Travel Grant 2017 program

Lühikokkuvõte

Kehal kantavad vahendid kardiorespiratoorse aktiivsuse jälgimiseks

Käesoleva töö eesmärk on uue teadmise loomine inimese kardiorespiratoorse aktiivsuse jälgimiseks läbi kehal kantavate seadmete arenduse. Kardiorespiratoorne signaal sisaldab kasulikku infot inimese tervisliku seisundi kohta: südame löögi- ja hingamise sagedus, südame ja veresoonkonna üldine seisund, vedeliku kogunemine ja hulk kopsus jne. Nimetatud kardiorespiratoorse signaali salvestamiseks arendatud mahtuvuslikul, induktiivsel, ja takistuslikul sidestusel, lahenduste kirjeldus moodustabki käesoleva töö põhiosa.

Motivatsioon käesoleva töö teostamiseks on tulnud vajadusest igapäevaelu mittesegavate ja kehal kantavate lahenduste järele, mille abil jälgida mahumuutusi organismis. Lisaks vajadusele monitoorida krooniliste haigete seisundit, on nutiseadmete lai levik loonud pinnase personaalmeditsiini rakenduste igapäevaellu jõudmiseks läbi keha seisundi pideva ja pikajalise jälgimise. Inimese kehaline aktiivsus on ka suurima probleemi põhjustajaks antud valdkonnas – sensorite paigutus on äärmiselt tundlik keha liigutuste suhtes, tekidades probleemi millele ei ole leitud head lahendust. Lahendus võib peituda sensorite asetuse ja konfiguratsiooni optimeerimises kehapinna suhtes.

Mahtuvuslikku, induktiivset ja takistuslikku sidestust kasutatavate sensorite tööpõhimõte on kirjeldatav samadel alustel: objektile rakendatakse teatud elektriline ergutussignaal ja tekkiv vastussignaal mõõdetakse samuti elektrilisel kujul. Objekti spetsiifiline tundlikkuste jaotus, osaliselt põhjustatud kehas toimuvate mahumuutuste poolt mõjutab voolu liikumist ja omakorda ka mõõdetud vastussignaali. Kõige haavatavam osa mõõteahelast on sensori ja keha vaheline sidestus, milles toimuvate mitte kardiorespiratoorse päritoluga muutuste põhjustatud häired on tüüpilised põhjused mõõdetud kasuliku signaali koheseks häirumiseks. Seega tegeleb käesolev töö järgnevaga: sensorite konfiguratsioonid kardiorespiratoorse aktiivsusess monitoorimiseks; sensorite paigutuse mõju salvestatavale signaalile, arvestades hingamis- ja vereringelundite paiknemist; mõõtmisega samaaegsete liigutuste mõju mõõdetavale signaalile.

Saavutatud tulemused lubavad väita elektroodide paigutuse ja konfiguratsiooni valiku olulisust et salvestada parim võimalik kardiorespiratoorse aktiivsuse infot sisaldav signaal. Väljakutud vahendid suurepinnaliste, rindkerega mahtuvuslikus sidestuses olevate elektroodide kasutamiseks elektrilise impedansi mõõtmiseks, eesmärgiga määrama kardiorespiratoorse aktiivsust, loob tehnikas küllaltki uudse lahenduse.

Sama võib väita ka induktiivse sidestuse jaoks arendatud painduvate kaheksakujuliste poolide kohta, mis on traditsiooniliselt kasutusel transkraniaalses magneetilises stimulatsioonis – võimaldades suunata tekkivat magnetvälja soovitavasse suunda. Paigutades nimetatud pooli eelmääratud hingamis- ja vereringelundi paiknemise kohale, on reaalne saavutada parim võimalik ligipääs huvipakkuvale muutusele.

Teades, et pulseeriv veri kannab informatsiooni südametegevuse kohta üle kogu keha on käesoleva töö viimases osa tähelepanu seadud randmele paigutatavate sensorite arendamisele. Olulise tulemusena on välja pakutud optimaalne surve tugevus, mida rakendada elektrilise impedantsi mõõtmise elektroodidele pulsilaine määramise ajal. Nimelt, leiti, et alates mingist kindlast surve tugevusest, pulsilaine põhjustatud impedantsi muutus ei kasva enam märkimisväärselt, olles saavutanud piisava taseme.

Abstract

Wearable solutions for monitoring cardiorespiratory activity

The principle objective of this thesis is to propose the knowledge of the means for providing the best possible signal that contains the information of cardiorespiratory activity. Cardiorespiratory signal carries useful data of the condition and status of the subject: heart rate, respiratory rate, the condition of cardiovascular system, the presence of lung water etc. In order to gain access to cardiorespiratory activity, the goal of implementing the components of wearable experimental systems, based on capacitive, inductive and resistive coupling, was established and fulfilled.

The work is motivated by the need for wearable and unnoticeable solutions for monitoring the defined volumetric changes in an organism. The trend of continuously following the physiological parameters, either in everyday life for personal body condition monitoring, or as a medical observation of patients in the risk groups of some aggravated illness, is demanding the means for implementing the assigned tasks. Although the effect of motions is moderately researched, the techniques based on electrical methods for monitoring cardiorespiratory activity in remote are strongly affected, proposing an obstacle in the development of sensors. Currently, there is a lack of knowledge for the positioning of electrical sensors relative to body in order to monitor cardiorespiratory activity.

The principle of capacitive, inductive and resistive coupling is conceptually the same: by using some sort of electrical stimulation, the object is excited and the response in the form of an electrical signal is measured. The sensitivities and the relevant current distribution, affected by the volumetric changes, is expected to influence the measured response. The most vulnerable part is the interface between the sensors and the object i.e. coupling, which is capable of causing interferences that corrupt the interesting signal. This thesis deals with the following: the schemes of sensors for providing the signal of cardiorespiratory activity, the effect of positioning sensors on the surface of the body on relative organs, the effect of concurrent movements and the variations relative to cardiorespiratory activity.

The achieved results show the significance of the exact positioning and the need for aware choice of configurations and placements of electrodes. The solution of utilization of large area electrodes in capacitive connection for mapping the thoracic surface in order to measure the EBI for monitoring cardiorespiratory activity, constitutes a relatively new field and the results give grasp to the future of contactless monitoring.

The effect of two essentially different shapes of inductively coupled coils on the measured signal was experimentally determined, from which the Fo8 coil proposes a novel approach in focused field.

The most suitable positions and configurations of electrodes have been experimentally determined and proposed, showing the vantage of distal arrangement relative to radial artery in front of circular. The optimal pressure point for externally applied pressure on rigid electrodes, located on radial artery, was determined since

which the modulation in the measured signal of EBI is not increasing significantly any more. As the resistive solution presumes the galvanic contact, the externally applied pressure contributes to further improve the quality of measured signal of pulse wave, designating a relevant outcome.

Appendix

Publication 1

Metshein, Margus (2015). A device for measuring the electrical bioimpedance with variety of electrode placements for monitoring the breathing and heart rate. [Proceedings of the 26th Irish Signals and Systems Conference (ISSC2015), 24 – 26 June, 2015, Carlow, Ireland]: IEEE, 1-4.

A Device for Measuring the Electrical Bioimpedance With Variety of Electrode Placements for Monitoring the Breathing and Heart Rate

Margus Metshein

Th. J. Seebeck Dept. of Electronics
Tallinn University of Technology
Tallinn, Estonia
mmetshein@elin.ttu.ee

Abstract—In this paper the determination of the positions of surface plate electrodes on human trunk for measuring the breathing and heart rate by using the electrical bioimpedance is presented. The designed and implemented measurement device – electrode shirt – is described. The novelty of current work is incorporated into the solution of placing the large surface plate electrodes into the garment. Focus is set on the capacitive connection to the object, revealing the problems of the influence of motions and displacement of the electrodes to the result. The best configurations for heart rate are showing the portion of change of the real part of total body impedance up to 5 percent. The result concerning the breathing rate is showing promising results, reaching up to 90 percent of real part of total body impedance. The best determined electrode placement configurations are showing the possibility of detecting the breathing and heart rate by using single electrode placement.

Keywords—*bioimpedance; breathing measurements; capacitive sensors; pulse measurements.*

I. INTRODUCTION

The interest in wearable devices for monitoring the vital signs of human is receiving increasing attention in today's world of personal healthcare. The keywords hereby are the continuous tracking of heart rate for monitoring elderly, the concurrent supervision of the condition of the organism of athletes during the performance, the biometric applications for following the health of combat soldiers etc.

Electrical bioimpedance (EBI) proposes a possibility for monitoring the vital processes of human. The idea behind the usage of EBI includes the excitation of human body with a small electrical current or voltage and measuring the response [1]. As the vital processes of human body are variable in essence, the periodical changes in organs can be followed by measuring the EBI [2].

Breathing is causing the impedance of trunk to change during the in- and exhalation, caused mainly by the lungs. The same effect appears in the case of heart rate: pulsating blood, being highly more conductive than the surrounding tissues, causes the diameter of blood vessels to change and the EBI to vary significantly during the heart cycle.

For detecting the cardiac and respiratory activity, different technologies have been developed: the usage of fibre optic sensors and fibres, integrated into garment [3]; the tracking of changes in magnetic field with magneto-impedance sensor [4] etc. The usage of EBI has also served promising results: in an experimental wearable device for monitoring breathing with small contact electrodes on the chest [5]; in the usage of textile electrodes in the composition of a prototype of a wearable system, attached directly onto the skin [6] etc.

The usage of single electrode placement configuration (EPC) for monitoring breathing and heart rate by using the EBI has also been reported: monitoring of the vital signs by placing the electrodes on the trapezius muscles and on the first rib [7]; measuring the EBI of the body by applying current on the left hand and foot and measuring the response on the right hand and foot [8] etc. Nevertheless, there is no ready-made wearable measurement device described, capable of detecting the breathing and heart rate of human by measuring the EBI through capacitive connection.

A measurement device was prepared and a number of experiments were carried out to study the impact of capacitive connection to the non-invasive monitoring of breathing and heart rate of human, the selection of EPC's and the possibility of reducing the influence of motions. Analyse of the gathered data was performed to compare the different EPC's and to determine the best ones. All the described operations are directed to the design of wearable device for capacitive measurements of EBI.

II. DEVICES AND PROPERTIES

As a measuring device in experiments, HF2IS impedance spectroscope of Zurich Instruments with HF2TA trans-impedance amplifier was used. The specification of these devices defines the frequency range up to 50 MHz using either two- or four-electrode measurements [9].

Single types of electrodes were used in experiments: large wet plate surface electrodes of type 22 4773 Electrosurgical Grounding Plates by Niko Medical Products. The contact surface of the electrode was of dimensions 80 mm x 170 mm, made of aluminium foil and covered with contact gel.

III. METHODS

A custom made measurement device – electrode shirt (ES) – was prepared. The device included the idea of covering the surface of trunk with surface plate electrodes to determine the best EPC's for following the breathing and heart rate.

The electrodes were attached onto the outer surface of a cotton shirt by using the sticky properties of contact gel. All the electrodes on the shirt were indexed so that the different EPC's were set to be changed and documented easily.

Total of 18 large wet plate surface electrodes were used to cover the whole back, sides and the shoulders of a human with the goal of determining the best EPC's for granting the access to the lungs and large blood vessels (Fig. 1). The reason for this choice reflects the main course of the current paper – to design a wearable measurement device in the form of garment.

Fifteen different EPC's were experimented (Table 1). In the cases where there were more electrode positions used for one operation (measuring or exciting), electrodes were connected together with wires to achieve the required EPC's.

By imaging the trunk of human being a cylinder, the experimented EPC's can be divided into four approaches:

- A. excitation and measuring on the edges of stem;
- B. excitation and measuring on the sides of stem;
- C. excitation on the edges and measuring on the sides of stem;
- D. excitation on the sides and measuring on the edges of stem.

All the measurements were done by using four-electrode method at the frequency of 10 MHz and excitation voltage with the amplitude of 500 mV. The reason for high frequency was the desire of reducing the influence of the cap between electrodes and the skin. To increase the capacitive element, another cotton shirt was placed under the ES – the thickness of the two shirts together was about 1 mm.

In the experiments, only a single individual was employed. The reason lies in the objective of current paper – the determination of areas for the large plate electrodes on the trunk of human. As the locations of the parts of respiratory and

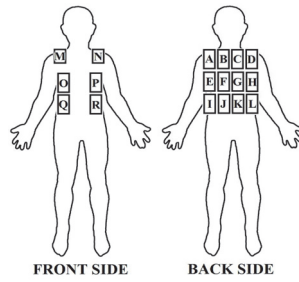


Fig. 1. Position of the electrodes on the electrode shirt.

circulatory systems in human body are, with small differences, the same, this is acceptable.

IV. MEASUREMENT RESULTS

A cycle of measurement experiments were carried out by using different EPC's. As the outcome of the measurements, the real part (ReZ) of total impedance (modulus $|Z|$) was used as an instantaneous value without calculations. This was chosen because of the property of biological objects to have mostly active character [10].

The assumption for the measurements was: the pulsation of the blood flow in the blood vessels and the change of the volume of air in the lungs during breathing are causing a portion of measured ReZ to change.

To evaluate the EPC's, two parameters were retain:

1. the ratio of change of ReZ , caused by the respiratory and cardiac activity of total ReZ ;
2. the ratio of change of ReZ , caused by the respiratory and cardiac activity of the interval of ReZ , caused by motions.

The results of the measurements can be seen in Table I. The table shows the results of breathing and heart rate separately: the ratio of change of ReZ , caused by breathing and pulse of total ReZ ; the ratio of change of ReZ , caused by breathing and pulse to interval of ReZ , caused by motions.

TABLE I. THE RESULTS OF THE MEASUREMENTS WITH THE ELECTRODE SHIRT

EPC. Nr.	ЕРС	Ratio of breathing from total ReZ (%)	Ratio of breathing from interval of ReZ of motions (%)	Ratio of pulse from total ReZ (%)	Ratio of pulse from interval of ReZ of motions (%)
1	Exc. MN and IJKL, meas. ABCD and EFGH	44 - 83	34 - 71	0,3 - 0,7	0,4 - 0,7
2	Exc. AEIN and DHLM, meas. BFJ and CGK	54 - 90	34 - 50	0,6 - 1,0	0,1 - 0,2
3	Exc. MN and OP, meas. ABCD and EFGH	66 - 90	80 - 90	1,6 - 5,3	1 - 4
4	Exc. O and P, meas. ABEFIJN and CDGHKLM	33 - 62	56 - 87	0,5 - 2,0	0,9 - 1,3
5	Exc. NP and MO, meas. ABEFIJ and CDGHKL	21 - 62	77 - 83	0,7 - 3,0	1,5 - 8,3
6	Exc. AB and KL, meas. CD and IJ	40 - 60	34 - 48	0,4 - 0,8	0,6 - 1,0
7	Exc. NA and MD, meas. B and C	32 - 42	7 - 10	0,4 - 0,8	0 - 0,1
8	Exc. NPR and MOQ, meas. EFJJ and GHKL	64 - 90	44 - 90	1,4 - 3,6	0,7 - 1,8
9	Exc. EFJJ and GHKL, meas. O and P	80 - 90	43 - 70	1,5 - 3,6	0,4 - 0,9
10	Exc. NPR and MOQ, meas. ABEFIJ and CDGHKL	21 - 27	21 - 30	0,5 - 1,2	0,6 - 1,4
11	Exc. NPR and MOQ, meas. FJ and GK	38 - 90	44 - 90	0,2 - 0,7	0,4 - 0,7
12	Exc. PR and OQ, meas. ABCD and IJKL	74 - 90	24 - 30	1,2 - 2,2	0,2 - 0,3
13	Exc. MN and OPQR, meas. ABCD and IJKL	28 - 90	80 - 90	1,2 - 2,3	2,0 - 8,3
14	Exc. MN and OPQR, meas. EFGH and IJKL	47 - 90	50 - 90	1,3 - 2,2	0,9 - 1,0
15	Exc. BFJ and CGK, meas. NPR and MOQ	73 - 90	51 - 59	0,7 - 0,8	0,2 - 0,3

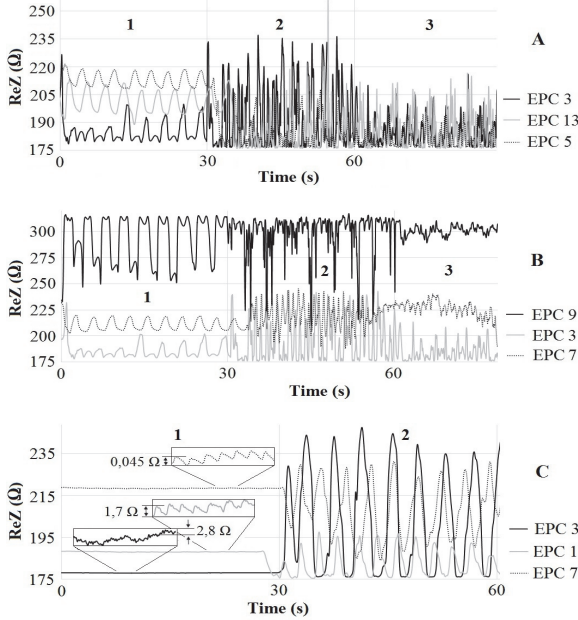


Fig. 2. Comparison of the best and worst results of breathing (parts A and B) and heart rate (part C).

In current paper, the results are presented in percentages, separately for respiratory and cardiac activity, showing the outcomes of repeated measurements for each EPC. The reason is the high dependability of the measurement results to motions and the variation in wide range. The accuracy of the measurements depends merely of the HF2IS impedance spectrooscope, staying in the order of 0.1% [9].

During the experiments, the illustrative charts were generated (Fig. 2 – 3). The object was dressed into the ES and asked to fulfil certain movements. The movements were planned to show the affectability of the measured signal to motions of human body – the result differs for breathing and heart rate in a large scale. The effects of breathing, heart rate and motions are extracted visually by following the real-time activities of the object. The study of the influence of motions to the measured signal can be done in the light of Table I and Fig. 2 (parts A and B), where the best and worst results of measuring experiments are visually recognizable.

Concerning pulse, the visual comparison of the numerical results in the form of the graph is more complicated. The reason is the low magnitude of the change of ReZ of pulse in both cases: parameters 1 and 2. The fact that the influence of the change of ReZ, caused by motions, is burying the signal of pulse completely, can be seen in part C of Fig. 2.

When comparing the results in Table I for finding the EPC's that suit the best for the measurements of breathing and heart rate together, the choice could be EPC 3. This EPC shows the best results concerning the parameter 1 of pulse and the parameter 2 of breathing. Concerning the other combinations, the results are within the top four (Fig. 3).

Part A. Comparison of the three best results (EPC's 3, 13 and 5 accordingly) of the measurements of the ratio of change of ReZ, caused by breathing to the interval of ReZ of motions in the cases of deep breathing (1), squatting with deep breathing (2) and splurging the hands with holding the breath (3).

Part B. Comparison of the best result of the ratio of change of ReZ, caused by breathing of total ReZ (EPC 9) and the best result of the ratio of change of ReZ, caused by breathing to the interval of ReZ of motions (EPC 3) to the worst result of the measurements of breathing (EPC 7) in the cases of deep breathing (1), squatting with deep breathing (2) and splurging the hands with holding the breath (3).

Part C. Comparison of the best result of the ratio of change of ReZ, caused by pulse of total ReZ (EPC 3) and the ratio of change of ReZ, caused by pulse to the interval of ReZ, caused by motions (EPC 13) to the worst result (EPC 7) of the measurements of pulse in the cases of standing still while holding the breath (1) and squatting while holding the breath (2).

V. DISCUSSION

The comparison of the parameters 1 and 2 of breathing and heart rate can be done on the ground of measurement results. The possibility to categorize the experimented EPC's according to the availability and proportions of measured signals of breathing and heart rate is expected.

A. Measurement of Breathing

The best result concerning the parameter 1 was achieved when exciting on the back and measuring on the axillae (EPC 9). The best result for the parameter 2 was gained when exciting on the chest and measuring on the upper back (EPC 3). The measuring electrodes on the axillae in EPC 9 were four times smaller than in EPC 3. It was observed that axillae are less affected by motion artefact (MA) – the reasons could be the absence of large muscles and the property of garments to stay nearby the surface of the skin of axillae.

By omitting the EPC's that include the positions in the area of axillae, the alternative results may appear. The second best result concerning the parameter 1 is achieved with the EPC of exciting on the lower chest and measuring on the scruff and lower back (EPC 12). There is large similarity with EPC 3 – the number and the area of the electrodes are the same.

In the case of worst results, breathing forms about half of total ReZ, but only about tenth of the interval of ReZ of motions. Part B in Fig. 2 confirms the numerical results – in the case of EPC 7, breathing cannot be recognized. It can be deduced that the larger the area of measuring electrodes, the more it tolerates the MA. The reason could be the presence of

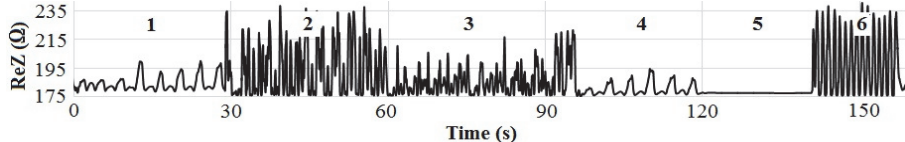


Fig. 3. Graph of deep breathing (1), squatting with deep breathing (2), splurging the hands with holding the breath (3), deep breathing (4), pulse with holding the breath (5) and holding the breath during the imitation of swimming (6) in the case of EPC 3.

some area of measuring electrodes that is always in close proximity to the skin, improving the electrical connection.

B. Measurement of Heart Rate

The magnitude of pulse and the affection of motions are not visually comparable in the same scale (Fig. 2 part C) - the comparison can be made according to the numerical results. The best result concerning the parameter 1 was achieved by using EPC 3 that showed also the best result concerning the parameter 2 of breathing. The best result for parameter 2 was gained by exciting on the chest and measuring on the upper and lower back (EPC 13). This is similar to EPC's 3 and 12 - large volume of the trunk is located in between the electrodes.

Concerning the worst result of measurement of heart rate – EPC 7 – it excites on the shoulders and measures on the scruff. This includes the idea of finding the access to the blood vessels that flow into hands. The reasons for the low magnitude of ReZ , caused by pulse may be the unsuitability of large plate electrodes for rounded body parts like shoulders and the property of scruff to afford deficient access to pulsating blood.

C. Combined Measurement of Breathing and Heart Rate

The difference between the EPC's for detecting breathing and heart rate appear when comparing the approaches by using an imaginary cylinder. The dominating approach for pulse, concerning the both described parameters, seems to be B, forming 3 from 4 best results. This means the longitudinal placement of the trunk between the electrodes.

Regarding breathing, no dominating approach can be emphasized. However, the trend is more towards the approach A than it was in the measurements of pulse. According to this, conclusion can be made: for breathing, the transverse location of the trunk between the electrodes proposes better access to the data. Moreover, while the preferable EPC's for measuring breathing and pulse are different, the usage of single EPC for following both processes is possible.

The large influence of MA can be stated, when referring to Fig. 3, concluded already in [10]. “During the longer experiments, the results deteriorate also because of the displacement of the shirt, movement of the wires etc. Breathing can be imitated by splurging the hands” [10].

VI. CONCLUSIONS

The measurements of EBI of the trunk of human through the capacitive connection showed the possibility of monitoring the breathing and heart rate. The best determined EPC's match the locations of the heart, lungs and large blood vessels. The influence of MA is dominating, especially in the case of

monitoring the heart rate because of its lower magnitude.

The novelty of current paper appears in the usage of large wet plate surface electrodes in the capacitive connection to the human body for detecting the best placements for monitoring the cardiac and respiratory activity. The results show the difference in the suitable EPC's while still proposing a possibility for monitoring the both processes.

The next step will be the implementation of the ES by concentrating the electrodes onto the areas of trunk, where the best results were achieved. This will also include the experiments of reducing and enlarging the areas of electrode contact surfaces and guarded ring electrodes. As a future work, the development of electronic circuits for fulfilling the excitation and measurement tasks will proceed. The longer perspective includes the installation of the electronic circuits and electrodes into the clothing.

ACKNOWLEDGMENT

This research was supported by European Union through the European Regional Development Fund in frames of the research centre CEBE and competence centre ELIKO.

REFERENCES

- [1] S. Grimnes, Ø.G. Martinsen, “Bioimpedance & Bioelectricity basics,” London, Great Britain: Academic, 2008.
- [2] T. K. Bera, “Bioelectrical impedance methods for noninvasive health monitoring: A review,” *J. of Med. Eng.*, vol 2014, 2014, pp. 1-28.
- [3] Z. Chen, D. Lau, J.T. Teo, S.H. Ng, X.Yang, P.L. Kei, “Simultaneous measurement of breathing rate and heart rate using a microbend multimode fiber optic sensor,” *J. Biomed. Opt.* 19 (5):57001, 2014.
- [4] S. Corodeanu, H. Chiriac, L. Radulescu, N. Lupu, “Magneto-impedance sensor for quasi-noncontact monitoring of breathing, pulse rate and activity status,” *J. Appl. Phys.* 115, 17A301, 2014.
- [5] T. Vuorela, V.-P. Seppä, J. Vanhalta, and J. Hyttinen, “Design and implementation of a portable long-term physiological signal recorder,” *IEEE Trans. on Inf. Tech. in Biomed.*, vol. 14, no. 3, May 2010, pp. 718-725.
- [6] F. Seoane, I. Mohino-Herranz, J. Ferreira, L. Alvarez, RR Buendia et al. “Wearable biomedical measurement systems for assessment of mental stress of combatants in real time,” *Sensors 2014*, 14, 2014, pp. 7120-7141.
- [7] J. Wtorek, A. Bujnowski, M. Lewandowska, J. Rumiński, M. Kaczmarek, “Simultaneous monitoring of heart performance and respiration activity,” In: *Proc. of 3rd Conf. on Human System Interactions (HIS)*, 2010, pp. 661-665.
- [8] B.H. Brown, D.C. Barber, A.H. Morice, A.D. Leathard, “Cardiac and respiratory related electrical impedance changes in the human thorax,” *IEEE Trans. on Biomed. Eng.* vol. 41, iss. 8, 1994, pp. 729-734.
- [9] HF2 User Manual, Zurich Instruments, 2014. Available at: <http://www.zhinst.com/manuals/hf2>.
- [10] M. Metschein, “Alternatives of measurement of electrical bioimpedance of the body with the aim to determine the cardiac and respiratory activity.” In *Proc. of 14th Biennial Baltic Electronics Conference (BEC2014)*, Tallinn, Estonia, Oct, 2014, pp. 197-200.

Publication 2

Metshein, Margus; Annus, Paul; Land, Raul; Krivošei, Andrei; Ojarand, Jaan; Aabloo, Alvo; Min, Mart (2017). Variation of cardiac and respiratory waveform on human thorax in the case of inductive coupling. [IFMBE Proceedings Vol. 65 - Joint Conference of European Medical and Biological Engineering Conference (EMBEC'17) and Nordic-Baltic Conference on Biomedical Engineering and Medical Physics (NBC'17), 11 – 15 June, 2017, Tampere, Finland]: Springer Nature, 671-674.

Variation of Cardiac and Respiratory Waveform on Human Thorax in the Case of Inductive Coupling

M. Metshein¹, P. Annus¹, R. Land¹, A. Krivošei¹, J. Ojarand¹, A. Aabloo² and M. Min¹

¹Thomas Johann Seebeck Department of Electronics, Tallinn University of Technology, Tallinn, Estonia

²Institute of Technology, University of Tartu, Tartu, Estonia

Abstract— The usage of magnetic induction monitoring on human thorax for detecting the cardiorespiratory activity is shown in this paper. The utilized device for measuring the changes in equivalent parallel resonant impedance of a single coil, caused by the breathing and heart beating, is represented. The waveforms of cardiac and respiratory activity together with the waveforms of reference monitoring of ECG and breathing are depicted. The measurements were done in twelve positions on the surface of the thorax of a single volunteer by using predetermined protocol. The respiratory activity was found to be available in all of the chosen positions. The cardiac activity was found to be recognizable in the positions on both sides and front side of the thorax. The influence of the concurrent movements was verified. The positions, suitable for monitoring the both processes of breathing and heart rate, are proposed.

Keywords— Cardiac monitoring, magnetic induction sensor, respiratory monitoring, telemonitoring.

I. INTRODUCTION

The cardiac and respiratory processes are most often used in personal health monitors to evaluate the health condition of human. The reasons are the easiness of interpretation and the potential of calculating other interesting parameters from the gathered data – energy consumption, burnt calories etc.

Historically, there have been number of methods for monitoring the cardiac and respiratory activity of human but not many of these are capable of gaining access into both of these processes. One of such method is electrical bioimpedance, where the gained result contains the peaks of pulse, carried by the respiratory waveform.

For following the cardiac and respiratory processes in human body, magnetic eddy current induction measurements can be used. The approach of using a single coil exempts from precise calibration of more than one coil in a geometric alignment [1] and allows plain estimation of the induced magnetic field.

The experiments of monitoring the variation of equivalent parallel resonance impedance (R_p) of a LC resonator, caused by cardiorespiratory activity in human body, are described in current paper. In the setup of an AC resonator, a single coil, operating in predetermined resonant frequency, was used at twelve predetermined positions on thorax.

The question of positioning of the sensor on the thorax appears when planning the monitoring of cardiorespiratory activity. In the case of impedance pneumo- and cardiography, several results, reflecting the different shape of the gathered waveform and varying ohmic value of the result, measured at different locations of the thorax, has been reported [2]-[3].

In the case of using the magnetic eddy current induction measurements, Vedru and Solntseva have done the detection of waveforms of cardiac activity at various positions on the front side thoracic surface by using a single-turn coil. The results show the change of the shape of the waveform depending on the location of the coil [4]. Teichmann et al. have also done the experiments with inductive and capacitive sensors on the backside of the thorax and the differences in the sense of the position of the sensor can be emphasized [5].

The presented study is planned to output the comparable data of simultaneous measurements of cardiorespiratory activity by using magnetic induction measurements in synchronous setup of the measurements of ECG and in- and exhalation. The expected favor of the analyze of the gathered data is the selection of the positions on the thorax that suit the best for monitoring the cardiorespiratory activity.

II. DEVICES AND PROPERTIES

Three devices were used in the measuring experiments: the primary measurement device in the form of magnetic induction sensor and the reference signal measurement devices in the forms of ECG monitor and spirometer.

A. Single Coil Magnetic Induction Sensor

The cardiorespiratory activity was monitored by using the telemonitoring system of single coil magnetic induction sensor, described in [1]. The sensor module of this device is based on chip LDC1000, manufactured by Texas Instruments (TI), allowing the measurement of the impedance and the resonant frequency of a LC resonator. The device can be configured and is capable of gathering the measured waveforms by using corresponding LabView program.

A single coil was used in the experiments (eight windings and the diameter of 75 mm) – denoting the coil no. 6 that is

shown in [1]. The coil is placed into rigid plastic form and its backside is shielded with a flexible ferrite sheet. The resonant frequency of the coil in chosen setup was 4.2144 MHz.

B. Devices for Reference Measurements of Cardiorespiratory Activity

The ECG was measured by using a custom-made measurement device that allows the 3-wire measurements. The ECG solid gel electrodes of type 849760 Clinical S45C of diameter of 45 mm were used in the experiments.

A spirometer was utilized for detecting the respiration [6]. This device is compiled by using a validated digital turbine flow meter (LDS Hospital) and custom prepared active electronics device to measure the number of turns of the turbine in seconds. The device has two outputs that carry the digital signal, showing the presence of in- and exhalation – depending on the direction of the airflow and the speed of air.

The HF2IS impedance spectroscope of Zurich Instruments was used for recording the analog signal output of ECG measuring device and digital signal outputs of spirometer by utilizing its auxiliary analog and digital signal inputs [7].

III. METHODS AND MEASUREMENT SETUP

The change of R_p of the coil, caused by the breathing and heart beating, was measured in twelve positions on the thorax of a volunteer. The spacing between the positions (denoting the center of the coil) was about 80 mm. The central positions on the front and backside of the thorax (positions no. 4 and 10 respectively) were designated according to xiphisternum and backbone. The positions lie at the horizontal line, which is approximately 10 mm below xiphisternal joint.

Table I The changes of the R_p in chosen positions

Position no.	Change of R_p caused by breathing (%)	Change of R_p caused by heart beating (%)	Change of R_p caused by movements (%)
1	1,05	0,104	3,76
2	4,32	0,104	8,74
3	3,67	0,078	9,18
4	1,12	0,176	5,45
5	2,81	0,248	6,55
6	0,34	0,038	4,65
7	1,02	0,083	2,88
8	1,18	not recognized	4,09
9	2,41	not recognized	6,18
10	4,55	not recognized	8,43
11	2,77	not recognized	7,53
12	0,74	not recognized	3,93



Fig. 1 The placement of the telemonitoring device on the thorax of a volunteer with spirometer and ECG monitor (not seen on the photo)

A cotton shirt with thickness of 0.5 mm was prepared for the experiments, containing the markings of positions and the horizontal line visually available (Fig. 1). The coil was placed at the desired position on the thorax of a volunteer by fixing it with a belt and was shifted along the horizontal line according to the chosen order of positions. The error of positioning of the center of the coil can be estimated to remain in the range of 10 mm in horizontal and vertical axis.

Only the results of a single volunteer (healthy male, 33 years old, height of 183 cm and weight of 70 kg) are presented in current paper because of the goal of gathering and analyzing the initial results. The ECG electrodes were attached according to the Eindhoven's lead III.

The measurement results were gathered from all twelve positions by using the following protocol:

1. Normal breathing in standing position for 10 sec.
2. Holding the breath in standing position for 10 sec.
3. Walking imitation while breathing freely for 10 sec.

IV. MEASUREMENT RESULTS

The changes of the measured waveform of R_p , caused by breathing, heart beating and concurrent movements of the body can be seen in Table 1. The results are shown in percentages, calculated from the median value of R_p in the entirety of each measured data set.

The visual representation of the results can be seen in Fig. 2, where two sets of waveforms are available in time scale in four columns (A – D). Columns A and D show the results of the implemented protocol in the cases of measurements by using the induction sensor and spirometer. Columns B and C show the magnitude of the change of R_p , caused by cardiac activity in correlation with the concurrent ECG in the case of holding the breath.

The reference signal waveforms are shown in the graphs with gray color and the waveforms of the variation of R_p with black color. The graphs have the same fixed scale in y-axis in both sets of waveforms. The waveforms of ECG and

breathing (spirometer) are normalized in y-axis to the changes of R_p , represented by relative changes of volume.

The ECG signal is filtered digitally by using Savitsky-Golay filter to remove the power line interference. The high frequency noise, accompanied with the measured R_p is reduced by using second-order Bessel type of band-pass filter in the frequency band of 10 mHz – 10 Hz. The signals at the output of spirometer are processed to convert the data into the cycles of breathing in time scale.

v. DISCUSSION

The changes of R_p of the coil, caused by the in- and exhalation are available in all of the chosen positions.

Teichmann et al [5] report the same conclusion concerning the availability of breathing.

The best result concerning the respiratory activity is achieved in position no. 10 (backside of the thorax), constituting about 0.6Ω of interval of change of R_p , caused by breathing. The lowest change of R_p of breathing is gained in position no. 6; but also in 1 and 7 (sides of the thorax); and 8 and 12 (outermost positions on back side of the thorax).

The described outcome is expected, as the coil that is placed on the front or backside of the thorax, creates the magnetic field that is affected by both of the lungs. At the outermost positions, some portions of lungs are not at the outreach, having less influence on the magnetic field.

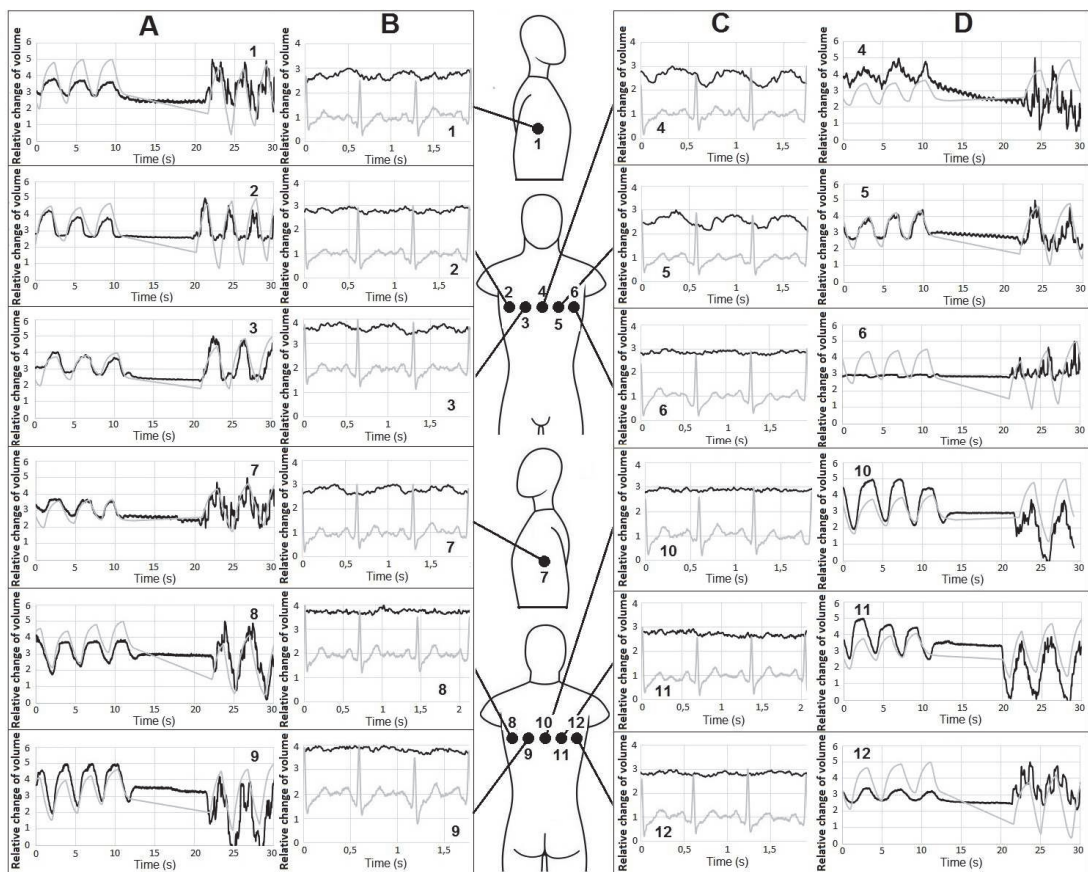


Fig. 2 The results of monitoring the cardiorespiratory activity of a single volunteer by measuring the change of equivalent parallel resonance impedance (relative change of volume) of a coil simultaneously with ECG and air flowing during the in- and exhalation (shown as normalized waveform) in time scale.

The amplitude of change of R_p , caused by the concurrent movements shows the lowest value when monitored on the sides of the thorax (positions no. 1 and 7). Visually the most interfered results are detected in positions no. 4 and 6.

The best outcome concerning the cardiac activity is gained in the positions no. 4 and 5 – close to the location of heart. The best change of R_p is 0.035 Ω (interval of change of R_p , caused by pulsating blood). The same location is reported to be optimal for monitoring the cardiac activity by using the magnetic induction sensor also in [8].

In the positions on the backside of the thorax, the expected waveform of heart beating was not recognized. The heart beating can be recognized in all of the other positions, being of varying shape and amplitude in the cases of measured waveform of R_p . This can be explained by the variability of cardiac-synchronous energy absorption in the body that is caused by the changing shape, volume and liquid content of organs in thorax [4].

The relatively good availability of breathing in position no. 6 and the worse change of R_p in position no. 2 in the outermost positions on front side of the thorax can be related to the properties of the used magnetic induction monitoring device. The applied resonant frequency is lower than in similar studies [4]-[5] – this can be increased by using new generation of LDC chips of TI. The current setup of the coil in rigid plastic form is more intended for the placement on planar surfaces, than on uneven surface of thorax. The diameter of the coil and the number of windings have influence to the direction and the shape of the induced magnetic field. This may propose a possibility to focus the magnetic field directly to the lungs and heart.

The estimation of the position from which the respiratory and cardiac activity are available together can be done in the basis of the ratio of change of R_p in normalized graphs, caused by both of these processes. The best one can be considered to be position no. 3.

VI. CONCLUSIONS

The cardiorespiratory activity was monitored on human thorax by measuring the change of R_p of a single coil. Twelve positions on the front and backside of the thorax were experimented and the variations concerning the shape, amplitude and the affection of the concurrent movements of the detected waveform were found.

The respiratory activity was found to be available in all of the positions. In the case of movements, in some positions on the central and left front side of the thorax, the gathered waveform of respiration is interfered. The cardiac activity is clearly available in the positions near to the location of the heart and not available on the backside of the thorax.

The setup of the magnetic induction monitoring device needs reconsidering in the sense of resonant frequency, the physical setup of the coil and its enclosure. The latter implies the development of specialized solution for coils, following the shape of the thorax. Several volunteers should be used in the experiments to have diversification in the results.

ACKNOWLEDGMENT

This research was supported by Estonian Research Council grant IUT1911 and the European Regional Development Fund in frames of the Estonian Centre of Research Excellence EXCITE. The work was partly financed also through the European Research Area project H2020-WIDESPREAD-2014-2-668995-Cognitive Electronics.

CONFLICT OF INTEREST

The authors declare that they have no conflict of interest.

REFERENCES

1. Ojarand J, Pille S, Min M (2015) Magnetic induction sensor for the respiration monitoring. Proc. of 10th Int. Conf. on Bioelectromagnetism (icBEM), Tallinn, Estonia, 2015, pp. 1-4
2. Seppä V-P, Viik J, Hyttinen J (2010) Assessment of pulmonary flow using impedance pneumography. IEEE Trans. Biomed. Eng., Sep.;57(9):2277-85. DOI: 10.1109/TBME.2010.2051668
3. Metshein M (2015) A device for measuring the electrical bioimpedance with variety of electrode placements for monitoring the breathing and heart rate, Proc of 26th Irish Signals and Systems Conference (ISSC), Carlow, Ireland, 2015, pp. 1-4
4. Vedru J, Solntseva O (2007) Variation of magnetic induction plethysmogram on human thoracic surface. 13th Int. Conf. on Electrical Bioimpedance & 8th Conf. on Electrical Impedance Tomography, Graz, Austria, 2007, pp 743-746
5. Teichmann D, Foussier J, Jia J et al. (2013) Noncontact monitoring of cardiorespiratory activity by electromagnetic coupling. IEEE Trans. Biomed. Eng., 2013 Aug;60(8):2142-52. DOI: 10.1109/TBME.2013.2248732
6. Samiepour A (2013) Thoracic bioimpedance measurement, Master Thesis, Tallinn University of Technology, 2013
7. HF2 User Manual – LabOne Edition, Zurich Instruments, 2016. Available at: <http://www.zhinst.com/manuals/hf2>
8. Teichmann D, Kuhn A, Leonhardt S et al. (2014) The MAIN shirt: a textile integrated magnetic induction sensor array, Sensors 2014 14(1), 1039-1056; DOI:10.3390/s140101039

Information of the corresponding author:

Author: Margus Metshein
 Institute: Tallinn University of Technology
 Street: Ehitajate tee 5
 City: Tallinn
 Country: Estonia
 Email: margus.metshein@tuu.ee

Publication 3

Metshein, Margus; Parve, Toomas; Annus, Paul; Rist, Marek; Min, Mart (2017). Realization and evaluation of the device for measuring the impedance of human body for detecting the respiratory and heart rate. [Elektronika ir Elektrotehnika 23 (3)]: 36-43.

Realization and Evaluation of the Device for Measuring the Impedance of Human Body for Detecting the Respiratory and Heart Rate

Margus Metshein¹, Toomas Parve¹, Paul Annus¹, Marek Rist¹, Mart Min¹

¹*Th. J. Seebeck Department of Electronics, Tallinn University of Technology,
Ehitajate tee 5, 19086 Tallinn, Estonia
margus.metshein@ttu.ee*

Abstract—The idea of a device for measuring the impedance of human body with the target of monitoring the respiratory and heart rate is proposed in this paper. Hardware realization of the proposed idea is described with the illustration of the custom designed printed circuit board. Preparation of electrode shirts with various electrode placement configurations is introduced. Series of experimental measurements in the cases of dynamic bioimpedance reference and single human subject are described and results shown to evaluate the custom made device. The excitation frequencies in the range of 2 MHz–20 MHz are utilized in the cases of large foil and textile electrodes to focus on the use of the capacitive connection to the object – constituting the novelty of the current paper. The results are analysed concerning the dependency of the visual availability of the interesting signal of breathing and heart rate of the material and the placement of the electrodes. Availability of breathing is found to be evident in all of the experimented cases. The heart rate is found to be challenging because of the presence of high frequency noise.

Index Terms—Capacitive electrode; electrical bioimpedance; synchronous detection; textile electrode.

I. INTRODUCTION

The monitoring of the vital signs has gained great interest in recent years – mainly because of the increasing availability of commercial smart monitoring devices and the wide spread usage of smartphones. The interest in personal health has grown through the self-awareness of the healthy lifestyle and the change of the daily movement habits in developed countries.

Several approaches are available for accessing to the respiratory rate (RR) and heart rate (HR): piezo-resistive belt [1], different optical methods [2], inductive sensors [3] etc. A possibility of measuring the electrical bioimpedance (EBI) for tracking the changes of impedance of human body, caused by RR and HR, proposes an alternative.

There are number of papers, describing the ideas and realizations of wearable measurement devices, developed for monitoring the vital signs of human by using the EBI

[4]–[6]. The approach of measuring the EBI by using the capacitive connection for monitoring the vital signs, is a product of recent years. The reasons are the concurrent problems of capacitive measurements, related to the affection of body movements in the form of motion artifact.

The motion artifact affects the results of the measurements of EBI, where the changes of impedance of the organism, caused by RR and HR, are relatively small. Currently, the influence of the motion artifact have not been considered and the measurements done in the cases where the object was sitting on the chair without moving.

The choice of the shape and the frequency of the excitation signal offers a point of decision in the case of the EBI measurements. Typically, the frequencies, proposed in different papers, stay below 1 MHz [7] and sine wave is used. The square wave signal of frequencies in the range of 2 MHz–20 MHz are utilized in the current work despite the concurrent higher harmonics.

An impedance measurement device for detecting the RR and HR is presented in this paper. The basic idea and the realization of the device by using the custom designed printed circuit board is proposed. The results of the experimental measurements by using the prototype of the device in the cases of various large and small electrodes and electrode placements are shown and analysed.

II. DEVICES AND PROPERTIES

Number of laboratory devices were utilized in the experiments to implement the simulation models and support the experiments. For designing the printed circuit board (PCB) the Easily Applicable Graphical Layout Editor (EAGLE) of version 7.4.0 was used.

For powering the custom made measurement device, the Triple Output DC Power Supply of type E3631A, manufactured by Agilent Technologies, was used. Oscilloscope Infiniium DSO8104A, offering bandwidth of 1 GHz and sampling rate of 4 GSa/s, manufactured by Agilent Technologies, was utilized.

For the imitation of the changing impedance of human body, caused by RR and HR, the dynamic bioimpedance reference (DBR), designed at Tallinn University of Technology [8] was used.

The reference ECG was measured by custom-made

Manuscript received 11 November, 2016; accepted 2 February, 2017.

This research was supported by Estonian Research Council grant IUT1911 and the European Regional Development Fund in frames of the Estonian Centre of Research Excellence EXCITE. The work was partly financed also through the European Research Area project H2020-WIDESPREAD-2014-2-668995-Cognitive Electronics.

measurement device in the case of using standard ECG solid gel electrodes according to the Einthoven's lead III. A custom made spirometer with validated digital turbine flow meter was used for detecting the respiration.

As a reference device for measuring the impedance and its corresponding voltage level changes, HF2IS impedance spectroscope of Zurich Instruments with HF2TA transimpedance amplifier was used. The specification of these devices defines the frequency range up to 50 MHz using either two- or four-electrode measurements [9]. Simultaneously, HF2IS was used to record the signals at the outputs of ECG measuring device and spirometer by using its auxiliary analog and digital signal inputs.

The gathering of the reference waveforms of HR and RR and processing of signals for gaining the spectrum was done by using corresponding Labview program.

III. OVERVIEW OF THE CUSTOM MADE MEASUREMENT DEVICE FOR DETECTING THE RR AND HR

A. The Basic Idea and the Structure of the Device

The idea of the device is to measure the impedance of the object by applying a certain signal, and measuring of the real part ($\text{Re}Z$) of the total impedance by using two-electrode configuration [10]. In current paper, the calculation of the real part ($\text{Re}Z$) of the total impedance is not discussed as the proposal is given only for the analog portion of the circuit.

The device consists of 7 blocks (Fig. 1): excitation signal generator (1); inverting amplifier (2); synchronous detector (3); active signal filter (4); DC blocking high-pass filter (5); final stage amplifier (6); low-pass filter (7).

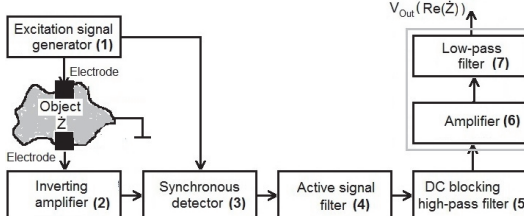


Fig. 1. Block diagram of the custom made measurement device.

The device was powered from bipolar power supply of ± 3 V. At the output of the excitation signal generator, the square wave signal with adjustable frequency in the range of 0.5 MHz–33 MHz, was available.

The gain of the inverting amplifier was set to 10 and the gain of the amplifier at the final stage was set to 220. The ratio of change of the voltage at the output of the fifth stage of the block diagram of the device stays in the order of 1 mV. The reason of the choice of the gain of the final stage amplifier is the desire of making the signals of RR and HR visible at the output of the device by using an oscilloscope.

The active signal filter is formed by using an AC op-amp integrator with DC gain control with the corner frequency of 15.92 kHz. This is used to smooth the waveform.

The high-pass filter was of 1st order with the cut-off frequency of 1.05 Hz and the low-pass filter was of 2nd order with the cut-off frequency of 1.94 Hz. The reason for the

choice of the bandwidth is the wish to recognize the HR and reduce the amplitude of RR, although RR is still available.

The output of the device is low frequency voltage, induced by the in- and exhalation and the changing amount of blood in the object [10].

B. The Hardware Realization of the Device

In comparison to the first prototype of the impedance measurement device, described in [10], several changes were implemented. As an excitation signal generator, a special resistor set oscillator of type LTC1799CS5#PBF, manufactured by Linear Technology, was used instead of logic gates. The frequency of the excitation signal was adjustable by changing the value of the frequency setting resistor.

A dual op-amp of type LT1813CS8#PBF, manufactured by Linear Technology, was used for amplification instead of two discrete op-amps. LT1813CS8#PBF offers the bandwidth of 100 MHz and slew rate of 750 V/ μ s.

The device was realized by using custom designed PCB with surface-mount technology electronic components. The material of the PCB was FR-4 with the dimensions of 50 mm \times 80 mm and the thickness of 1.6 mm. The PCB was designed as 2-sided board, where the whole bottom side was drawn as ground plane. The ground plane was drawn in two polygons, connected together with a line of width 0.41 mm – the reason is the intention to separate the ground of analog switch. The width of the signal lines on the PCB were set to 0.41 mm and for power lines to 0.61 mm.

The layout of the designed PCB and the placement of the blocks can be seen in Fig. 2(a). The realized device can be seen in Fig. 2(b). E1 and E2 mark the connections for the wires of the electrodes.

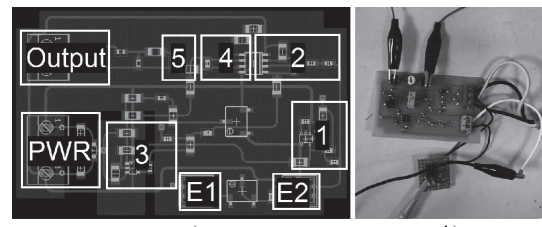


Fig. 2. Layout of the designed PCB for the prepared measurement device.

The blocks of final stage amplifier and low pass filter (surrounded by grey line in Fig. 1) have not been added to the designed PCB because of the need for later implementations. These blocks were realized by using a small piece of prototyping PCB, connected to the device with short wires. Op-amp TLV2782IP of Texas Instruments was used, offering the bandwidth of 8 MHz with slew rate of 4.8 V/ μ s.

IV. METHODS AND MEASUREMENT SETUP

Measurement experiments were carried out to evaluate the capability of the implemented measurement device to follow the RR and HR in the cases of DBR and single volunteer (author of the current paper).

A. Measurement Setup in the Experiments by Using the DBR

The DBR was used in the experiments – this device permits to adjust the parameters of the imitated impedance of human trunk separately, caused by both: the RR and HR [8]. For the measurements, the capacitive properties of the imitated RR and HR were disabled. The changes in the peak-to-peak amplitudes of the resistances, caused by the RR and HR were set to 99.9Ω and 20Ω accordingly with the minimum value of 0Ω . The frequencies of the RR and HR at the output of DBR have been set close to the same parameters of the human subject.

The electrode wires of the custom made measurement device were connected to the output of the DBR and the measurements done by using the direct electrical contact.

B. Measurement Setup in the Experiments on Human by Using the Electrodes in Direct Connection

Small monitoring electrodes with foam tape of type 2228 by 3M Health Care were used in the experiments. The electrodes were attached directly onto the skin in the predetermined positions (Fig. 3).

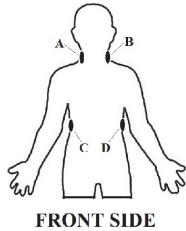


Fig. 3. Positions of the electrodes in the case of direct contact measurements.

The positions were chosen to cover the trunk vertically so that the lungs and heart with the large blood vessels stay between the electrodes. The placement of the electrodes was inspired by [11], where, though, eight electrodes were used in four-electrode configuration.

C. Measurement Setup in the Experiments on Human by Using the Various Electrodes in Capacitive Connection

Three custom made electrode shirts with various electrode dimensions, materials and placements, were used in the experiments. Concerning all the shirts, the electrodes were used in noncontact setup, attached onto the outer surface of the shirt.

Electrode shirt no. 1 (ES1) included the large wet plate surface electrodes of original size that were positioned to cover the whole back, sides and shoulders of human (Fig. 4) [10], [12]. The placement was expected to grant access to the periodical changes that take place in lungs and heart.

Electrode shirt no. 2 (ES2) included the wet plate surface electrodes that were positioned onto the shoulders and upper arms (Fig. 5). The placement was expected to give access to the pulsating blood in subclavian arteries and veins.

The dimensions of the electrodes J and K were cut to $60 \text{ mm} \times 80 \text{ mm}$ and the dimensions of the electrodes D and E were cut to $80 \text{ mm} \times 120 \text{ mm}$. The electrodes were attached onto the outer surface of the cotton shirt by using

the original foam tape of the electrodes.

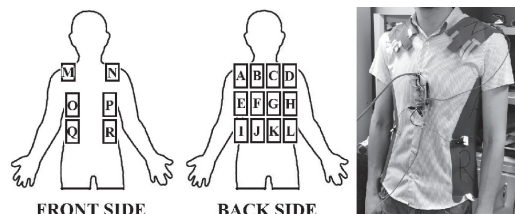


Fig. 4. Positions of the electrodes in the case of ES1 [5].

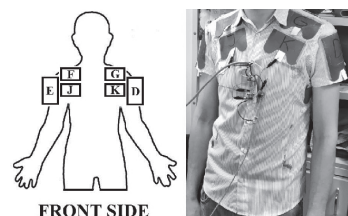


Fig. 5. Positions of the electrodes in the case of ES2.

In the case of ES1 and ES2, the electrodes were connected together with wires to achieve the desired electrode placement configurations (EPC).

The electrodes, used in ES1 and ES2, were of type 22 4773 Electrosurgical Grounding Plates by Niko Medical Products with the contact surfaces of dimensions of $80 \text{ mm} \times 170 \text{ mm}$.

Electrode shirt no. 3 (ES3) included the conductive metallized nylon fabric (rip-stop) textile electrodes of part number 1500101130, manufactured by Statex Productions & Vertriebs GmbH, with dimensions of $80 \text{ mm} \times 150 \text{ mm}$. The chosen placement was directed to the use of two-electrode configuration (Fig. 6).

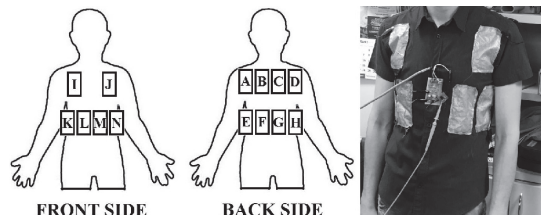


Fig. 6. Positions of the electrodes in the case of ES3.

The textile electrodes were connected by using the conductive thread of type Electro-Fashion Conductive Thread, manufactured by Kitronik, to constitute the desired EPC.

During the measurement experiments on human subject by using ES1–ES3, an additional cotton shirt with the thickness of 0.5 mm was placed under the electrode shirt. The human subject was sitting on chair with straight back without moving.

V. MEASUREMENT RESULTS

All the measurements were done in the frequency range of 2 MHz–20 MHz. The choice of the value of the lower level of the frequency is explained by the disappearance of the

useful signal into the noise below 2 MHz. Moreover, the choice of the higher frequency range is related to the intention to use the device in noncontact measurement setup to the object and to cope with capacitive measurements. The chosen frequencies for the presentation in the figures are: 2 MHz, 5 MHz, 10 MHz and 20 MHz.

In the cases of ES1-ES3, the reference waveforms of ECG and respiration were simultaneously gathered.

A. Results of the Measurements by Using the DBR

The results for evaluating the custom made measurement device and comparing the results in the case of human subject with the measurements that were done by using the DBR can be seen in Fig. 7.

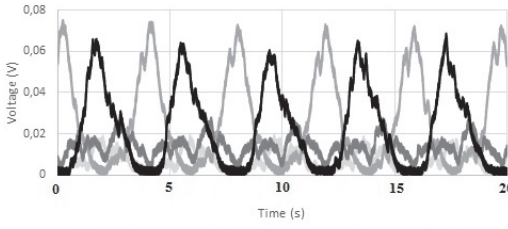


Fig. 7. Results of the measurements by using the custom made measurement device in the case of DBR.

It can be seen that the HR appears most clearly in the case of 5 MHz but is available also at 20 MHz. The RR is distinct at all of the chosen frequencies, showing the highest amplitudes at 5 MHz.

B. Results of the Measurements on Human by Using the Electrodes in Direct Connection

The measurements in the case of using the electrodes in direct contact to human body were carried out with the purpose of achieving the data for comparison with the results of capacitive measurements. The used EPC was: AB and CD (Fig. 3). The results can be seen in Fig. 8.

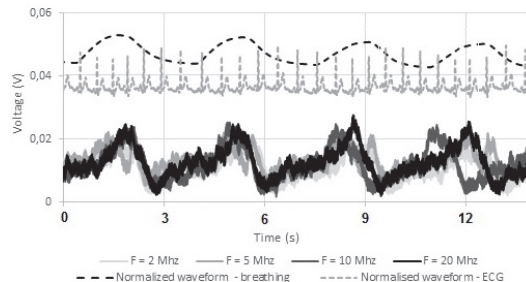


Fig. 8. Results of the measurements by using the custom made device in the case of using the electrodes in direct connection to human body.

The HR is lost into the high frequency noise, though, the RR is visible. The amplitude of RR shows similar value at all of the chosen excitation frequencies.

C. Results of the Measurements by Using the Electrodes in Capacitive Connection in the Case of ES1

With the intention of comparing the results of the measurements by using the custom made measurement device in different setups, the measurements were carried

out by using two EPC's.

In the case of ES1, the following EPC's were used:

- EF1JGKHL and OP;
- NRPMQO and AEIDHL.

The first EPC sets the trunk vertically and second EPC horizontally between the electrodes (Fig. 4). The results can be seen in Fig. 9 and Fig. 10.

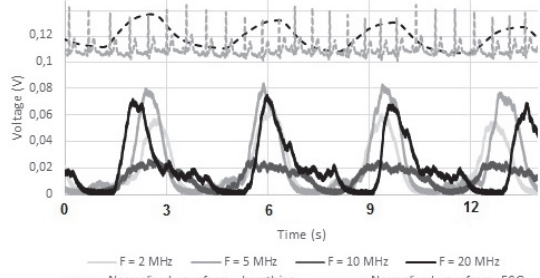


Fig. 9. Results of the measurements by using the custom made device in the case of EPC EF1JGKHL and OP of ES1.

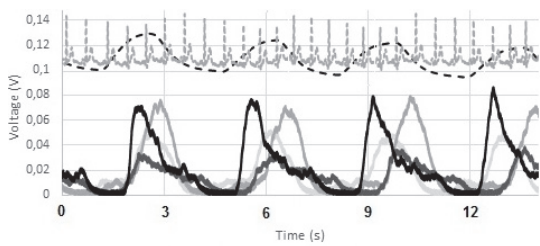


Fig. 10. Results of the measurements by using the custom made measurement device in the case of EPC NRPMQO and AEIDHL of ES1.

Concerning both figures (Fig. 9–Fig. 10), the HR can be assumed to be seen visually in the cases of two higher excitation frequencies, carried by the signal of RR. The RR is distinct at all of the chosen frequencies and in the cases of both experimented EPC's in the case of ES1.

D. Results of the Measurements by Using the Electrodes in Capacitive Connection in the Case of ES2

In the case of ES2, the following EPC's were used:

- K and J;
- E and D.

EPC's of ES2 were orientated to find the access to HR. The result can see in Fig. 11 and Fig. 12.

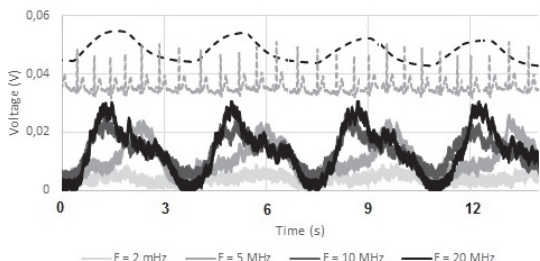


Fig. 11. Results of the measurements by using the custom made measurement device in the case of EPC K and J of ES2.

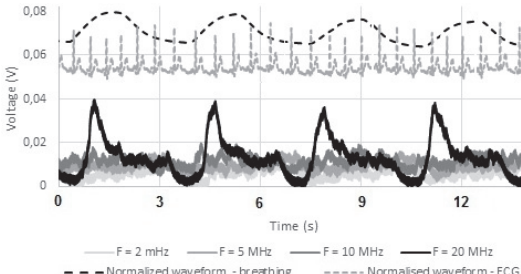


Fig. 12. Results of the measurements by using the custom made device in the case of EPC E and D of ES2.

It can be seen that the level of amplitude of RR increases with the increasing excitation frequency. The HR can't be visually fully recognized with certainty in any of the experimented EPC's in the case of ES2 because of the concurrent noise.

E. Results of the Measurements by Using the Electrodes in Capacitive Connection in the Case of ES3

Concerning ES3, the textile electrodes were connected to cover the trunk of human vertically. The only experimented EPC for ES3 was: ABCDIJ and EFGHKLMN. The results can be seen in Fig. 13.

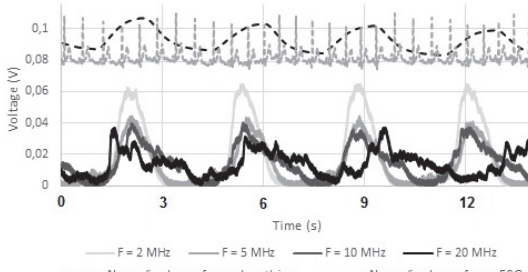


Fig. 13. Results of the measurements by using the custom made measurement device in the case of ES3.

In the case of Fig. 13, the amplitude of RR is the highest for the lowest chosen excitation frequency and the lowest for the highest chosen excitation frequency. The HR is visually most clearly available at the frequency of 20 MHz.

VI. DISCUSSION

The frequency of the excitation signal has influence on the amplitude of RR in all the results. The excitation current finds a way through the mediums with lower impedance and at some point it may even not pervade the human body but travel through the skin surface. This means that the change of the voltage at the output of the device does not reflect the change of the impedance, caused by RR and HR, but the change of the cap between the capacitive electrodes and the skin surface. Anyhow, in the sense of the access to the RR and HR, the requirement is the recognizable waveform at the output of the device, ready for the further analysis.

The amplitudes of the RR in the cases of contact electrodes and ES2 are showing the similar values. This reflects the impact of the size of the area of the electrodes. In the case of contact electrodes, the total area of contact

surfaces is roughly 12.56 cm^2 and in the case of K and J (ES2) – 96 cm^2 . The total area of the electrodes EFJGKHL and OP in the case of ES1 is 1360 cm^2 .

For comparing the results of the measurements by using different EPC's and shirts at the same excitation frequency, the following graphs were created (Fig. 14–Fig. 17).

As the EPC's of ES2 were orientated to find the access to HR and the results of amplitudes of RR were two times lower than in the cases of ES1 and ES3, these results are not shown in the following graphs.

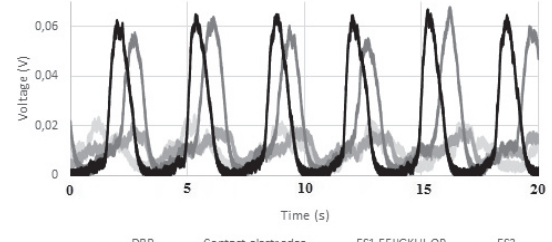


Fig. 14. Comparison of the results of the measurements by different electrodes and EPC's at the excitation frequency of 2 MHz.

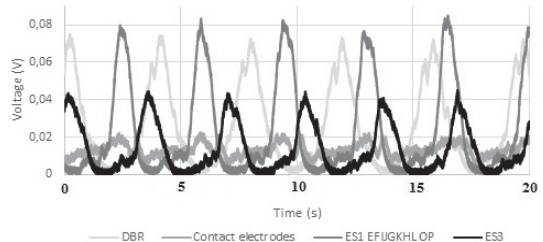


Fig. 15. Comparison of the results of the measurements by different electrodes and EPC's at the excitation frequency of 5 MHz.

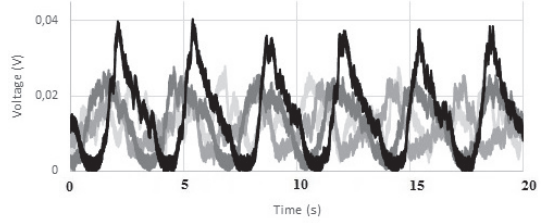


Fig. 16. Comparison of the results of the measurements by different electrodes and EPC's at the excitation frequency of 10 MHz.

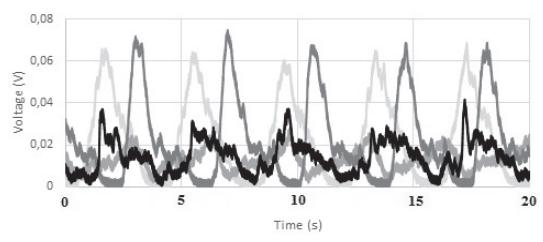


Fig. 17. Comparison of the results of the measurements by different electrodes and EPC's at the excitation frequency of 20 MHz.

The peak values of the amplitudes of the measured signals at chosen frequencies, caused by RR, can be seen in Table I.

TABLE I. PEAK VALUES OF THE AMPLITUDES OF THE SIGNALS, CAUSED BY RR, SHOWN IN FIG. 14—FIG. 17.

Item	Amplitude of RR in the case of F = 2 MHz (mV)	Amplitude of RR in the case of F = 5 MHz (mV)	Amplitude of RR in the case of F = 10 MHz (mV)	Amplitude of RR in the case of F = 20 MHz (mV)
DBR	24.7	72.8	27.1	67.9
Contact electrodes	20.4	22	24.4	23.3
ES1 EFIJGKHL LOP	64.9	84.2	27.8	74.5
ES3	65.3	44.2	40.1	40.8

The RR is showing the highest amplitude in the case of ES1 at the frequency of 5 MHz – reaching up to 80 mV. The best result in the case of ES3 is achieved at the frequency of 2 MHz, achieving the amplitude of more than 60 mV. This is illustrating the effectiveness of larger surface area of the electrodes.

In the case of 10 MHz, the amplitude of the signal of RR in the case of chosen EPC of ES1 is two times lower than in other frequencies. This can be explained by the influence of the parasitic capacitances and inductances, caused for example by the length of the wires [13].

Concerning HR, the best results have been achieved by using ES3 in the case of 20 MHz (Fig. 18) – the amplitude of the change reaches about 10 mV. The typical parameters of HR and RR are 60–100 heart beats per minute and 12–18 breaths per minute respectively. This makes about 5 heart beats per one breathing cycle (depending on different factors). This ratio can be seen also in Fig. 18.

The waveform that can be seen Fig. 18, is measured at the output of custom made impedance measurement device is filtered by using a Bessel bandpass filter in the frequency band of 10 mHz–2 Hz. The result is shown together with synchronously gathered ECG. The result and the reference waveform of ECG are normalised in y-axis.

The results of the measurements by using the custom made device contain the high frequency noise, blurring the graphs. The low pass filtering should be done as close to the oscilloscope input as possible to diminish the noise.

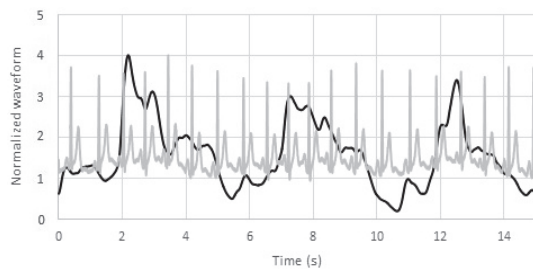


Fig. 18. Result of the measurement by using the custom made measurement device in the case of ES3 at the frequency of 20 MHz and the reference ECG in normalized scale (y-axis).

The spectrum of the signal, presented in Fig. 18, can be seen in Fig. 19, where the distribution of the energy in frequency axis is available. The fundamental frequency of respiration is clearly available. Nevertheless, due to the high

frequency noise, HR is not surely identifiable. It can be expected that in the case of longer measurement data sets (current sets are of the length of 5 breathing cycles) the result concerning HR would give visible result.

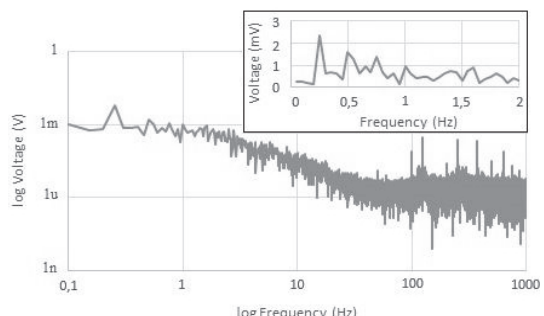


Fig. 19. Spectrum of the signal, measured by custom made impedance measurement device in the case of ES3 at the excitation frequency of 20 MHz (the smaller graph in the frame shows the same spectrum in narrower linear scale).

For comparison with the results of a commercial impedance measurement device, reference measurement was done by using HF2IS impedance spectroscope. The results in the case of ES3 at the excitation frequency of 20 MHz can be seen in Fig. 20. In the graph, only the trends of the normalized signals are presented while the ratios of the signal remain the same. The DC offsets are shifted during the signal processing for better visual representation.

In the case of HF2IS impedance spectroscope, the RR is available at all of the excitation frequencies. The amplitudes of the signals are of similar value with slightly better result in the case of ES3 – the change may come from the displacement of the electrode shirt during the measurement.

HR is visually available in the case of using the DBR and apparent also in the case of ES1. In fact, concerning Fig. 19, the HR is available in all of the cases if the signal is magnified, carried by the RR – discussed already in [12].

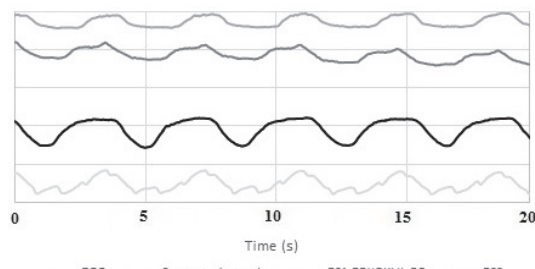


Fig. 20. Trends of the normalized signals, measured by HF2IS impedance spectroscope in the case of ES3 at the excitation frequency of 20 MHz.

The change of the amplitude of measured signal, caused by the movements of the subject's body during the measurement experiments, is distracting the result for visual interpretation. Nevertheless, in the case of periodical movements like imitating swimming or lifting the shoulders, the RR can still be recognized. Concerning the motion artifact, the help of the elaborate design in the form of tight clothing and special algorithms should be developed.

VII. CONCLUSIONS

The prototype of an impedance measurement device has been implemented and number of electrode shirts prepared to evaluate the properties and the behaviour of the device. The measurements on human subject have been done using the direct contact and capacitive electrodes of different types in various EPC's to assess the availability of RR and HR. The influence of motion artifact is not considered, though, the occasional study of hand movements during the experiments showed the vast effect.

The results of the measurements showed the visible availability of RR in all of the experiment setups at all of the chosen excitation frequencies. HR is visually available, typically in the cases of highest chosen excitation frequency: 20 MHz. HR is interfered by the high frequency noise.

The results are promising, exhibiting the usability of the proposed idea and realization of the measurement device.

The future work includes the redesign of the blocks 6–7 to suit for incorporation into an outer case. The usage of sine wave as excitation signal and the switching onto battery power will be researched. The plans include also the development of next generation of electrode shirt according to the previously published [13] and the current results, with the attention to the influence and reduction of the motion artifacts. The final outcome is presumed to be constituted as a wearable device for monitoring the RR and HR.

REFERENCES

- [1] L. Guo, L. Berglin, U. Wiklund, H. Mattila, "Design of a garment-based sensing system for breathing monitoring", in *Textile Research J.*, vol. 83, no. 5, pp. 499–509, 2012. [Online]. Available: <http://journals.sagepub.com/doi/pdf/10.1177/0040517512444336>
- [2] P. Sanchez, C. R. Zamarreno, M. Hernaez, I. R. Matias, F. J. Arregui, "Exhaled breath optical fiber sensor based on LMRs for respiration monitoring", in *IEEE Sensors*, 2014. [Online]. Available: <https://doi.org/10.1109/ICSENS.2014.6985209>
- [3] A. Richer, A. Adler, "Eddy current based flexible sensor for contactless measurement of breathing", in *Proc. IEEE IMTC 2005 Instr. Meas.*, Ottawa, Canada, 2005 pp. 257–260. [Online]. Available: <https://doi.org/10.1109/IMTC.2005.1604112>
- [4] T. Vuorela, J. Vanhala, V.-P. Seppa, J. Hyttinen, "Two portable long term measurement devices for ECG and bioimpedance", in *Proc. 2nd IEEE Int. ICST Conf. on Pervasive Computing Technologies for Healthcare*, Tampere, Finland, 2008, pp. 159–162. [Online]. Available: <https://doi.org/10.1109/PCTHEALTH.2008.4571061>
- [5] J. Wtorek, A. Bujnowski, M. Lewandowska, J. Ruminski, M. Kaczmarek, "Simultaneous monitoring of heart performance and respiration activity", in *Proc. 3rd Conf. on Human System Interactions (HIS)*, 2010, pp. 661–665. [Online]. Available: <https://doi.org/10.1109/HSL.2010.5514499>
- [6] S. Hong, J. Lee, H.-J. Yoo, "Wearable lung-health monitoring system with electrical impedance tomography", in *Proc. Annual Int. Conf. 37th IEEE Eng. Med. Bio. Soc. (EMBC)*, 2015, pp. 1707–1710. [Online]. Available: <https://doi.org/10.1109/EMBC.2015.7318706>
- [7] S. Grimnes, O. G. Martinsen, *Bioimpedance & Bioelectricity Basics*. London, Great Britain: Academic, 2008. p. 201.
- [8] M. Rist, M. Min, "Dynamic reference for evaluation of bioimpedance spectroscopy devices", in *Proc. IEEE 16th Biennial Baltic Electronics Conf. (BEC 2016)*, Tallinn, Estonia, 2016, pp. 107–110. [Online]. Available: <https://doi.org/10.1109/BEC.2016.7743740>
- [9] HF2 User Manual – LabOne Edition, Zurich Instruments, 2016. [Online] Available: <http://www.zhinst.com/manuals/hf2>
- [10] M. Metshein, T. Parve, "Electrical bioimpedance based monitoring of cardiac and respiratory activity: positioning of capacitive electrodes for wearable human monitoring device", in *Int. J. of Bioelectromagnetism*, vol. 17, no. 2, pp. 64–74, 2015. [Online]. Available: http://www.ijbem.org/volume17/number2/ijbem_vol17_no2_pp64-74.pdf
- [11] D. P. Bernstein, "A new stroke volume equation for thoracic electrical bioimpedance: theory and rationale", in *Crit. Care Med.*, vol. 14, pp. 904–909, 1986. [Online]. Available: <https://doi.org/10.1097/00003246-198610000-00017>
- [12] M. Metshein, "A device for measuring the electrical bioimpedance with variety of electrode placements for monitoring the breathing and heart rate", in *Proc. IEEE 26th Irish Signals and Systems Conf. (ISSC)*, Carlow, Ireland, 2015, pp. 1–4. [Online]. Available: <https://doi.org/10.1109/ISSC.2015.7163748>
- [13] M. Metshein, R. Gordon, "On the possibility of detecting the electrical bioimpedance of human body by using non-contact electrodes in capacitive connection", in *Proc. IEEE 16th Biennial Baltic Electronics Conf. (BEC 2016)*, Tallinn, Estonia, 2016, pp. 171–174. [Online]. Available: <https://doi.org/10.1109/BEC.2016.7743756>

Publication 4

Metshein, Margus; Annus, Paul; Land, Raul; Min, Mart; Aabloo, Alvo (2018). Availability and variations of cardiac activity in the case of measuring the bioimpedance of wrist. [Proceedings of the 2018 IEEE International Instrumentation & Measurement Technology Conference (I2MTC2018), 14 – 17 May, 2018, Houston, USA]: IEEE, 147-151.

Availability and Variations of Cardiac Activity in the Case of Measuring the Bioimpedance of Wrist

Margus Metshein, Paul Annus, Raul Land, Mart Min

Th. J. Seebeck Dept. of Electronics
Tallinn University of Technology
Tallinn, Estonia
margus.metshein@ttu.ee

Alvo Aabloo

Institute of Technology
University of Tartu
Tartu, Estonia

Abstract—The utilization of technique for monitoring pulse wave from wrist by using the electrical bioimpedance has been implemented in this paper. A four electrode printed circuit board was used to evaluate the influence of positioning of the electrodes, pressure on the electrodes and individual differences of several volunteers on the availability of pulse wave from wrist. The influence of positioning of the electrode relative to radial artery was verified experimentally, allowing 5 mm shift in both transverse directions. The increasing pressure on the electrode was found to give rise to the time varying change of impedance, caused by pulse wave. This result was confirmed in the case of measurements on several volunteers, proposing the convergence in time varying change of impedance above the pressure of 400 g.

Keywords—electrical bioimpedance; frequency response; pulse wave; radial artery

I. INTRODUCTION

Cardiovascular diseases are the primary causes of death, having lethal effect on average of 31 % in the cases of all global deaths [1]. The need for noninvasive and time effective solutions for monitoring the cardiovascular parameters like pulse rate, pulse wave velocity, blood pressure etc. is evident.

The basic method for detecting the condition of vascular system is the palpation by sensing the pulse. This is typically done by placing the tips of two or three fingers on the location of artery. In Traditional Chinese Medicine, the purpose of pulse diagnosis is to determine the evaluation, causes, position and cure for disease. Two types of pulse are recognized: floating pulse and sinking pulse. First one denotes the pulse that can be felt with very slight pressure and which disappears when the pressure is increased. Second one denotes the pulse that can be best determined with increased pressure [2].

However, in practice, the availability of pulse is related to the differences of individuals. Radial artery of a slim individual may be more easily accessible than radial artery of an individual whose subcutaneous layer of tissue (because of layer of body fat) is thicker and the palpation is more difficult [3].

A method for determining the pulse rate (and other cardiovascular parameters), is the electrical bioimpedance (EBI). The principle of EBI measurements for detecting the time varying change of impedance ($\Delta Z(t)$) of wrist to determine the pulse wave can be seen in Fig. 1A.

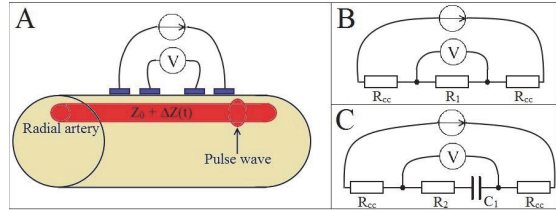


Fig. 1. Tetrapolar setup for monitoring the pulse wave in radial artery by measuring the time varying impedance on wrist (A) and equivalent circuits for verifying the measurement setup (B-C).

The impedance (Z) of wrist can be considered to consist of the basal impedance (Z_0) i.e. the invariable impedance of the local volume of wrist and ($\Delta Z(t)$), caused by pulse wave:

$$Z = Z_0 + \Delta Z(t). \quad (1)$$

Wrist is excited by alternative current and voltage across it is measured (or vice versa). When a pulse wave arrives, the volume of artery increases and the value of impedance decreases because of the conductive properties of blood. The variations in the value of impedance generate the amplitude modulation on top of the carrier i.e. excitation signal and the pulse wave can be detected [4].

The assumption for the presented setup is that positioning of the electrodes directly onto radial artery results in larger value of $\Delta Z(t)$ and thereby in better availability of cardiac activity in the form of pulse wave. The similar characterization of forearm is reported in literature but with electrodes of larger area and larger gap between the measuring electrodes [5]. In the case of small area electrodes, the positioning relative to radial artery is assumed to become vital while in the case of the band-shaped electrodes the probability of falling in the vicinity of radial artery is higher. Though, the current distribution is assumed to decrease in the case of larger electrodes, decreasing the sensitivity and, thereby also the detected $\Delta Z(t)$.

Secondly, it was observed that in the case of increasing pressure on the electrode on radial artery, the value of Z tends to decrease. This can initially be related to the decrease of the impedance of skin, ensuing from the compression of skin. Therefore, the second hypothesis was set up: the decreasing

value of Z in the case of increasing pressure on the radial artery results in larger $\Delta Z(t)$.

The influence of pressure has been reported in literature to be experimented in several approaches of monitoring the pulse wave. One of the techniques for detecting pulse is to use piezoresistive sensors, which electric resistance will change because of the pressure. By placing the sensor on the surface of skin on top of the location of radial artery, the pulse can be determined [3]. The effect of pressure on the electrode-skin interface has been studied in [6], where the conclusion has been made: until the pressure of approximately 900 g, the electrode-skin impedance decreases; while in the case pressure of approximately 2270 g, the impedance may start to increase. The effect of motion artifact has been extensively studied in [7] and induced as partly resulting from varying pressure.

The similar experiments on wrist have been described in literature to be implemented by using the pre-gelled ECG monitoring electrodes [6] or by examining the effect of pressure on electrode-skin impedance in the case of relatively large textile electrodes [8].

The current work has been done in the frames of the project of developing a technique for estimating the central aortic pressure (CAP) of blood by measuring the $\Delta Z(t)$ of radial artery close to the scaphoid bone. The results of such measurements have shown good correlation with the results of invasive measurements of CAP [9]. The most susceptible parts of the implementation of this technique are the electrodes – raising the questions of positioning and pressure.

There are two expected outcomes of this research that are assumed to give valuable input to the development of a wearable device for estimating the CAP from wrist. Firstly, to determine the relevance of the exact positioning of the EBI measuring electrodes relative to radial artery. Secondly, to determine the influence of increasing pressure on the electrodes during the measurement of $\Delta Z(t)$.

II. DEVICES AND PROPERTIES

The primary devices, used in the experiments were HF2IS impedance spectrometer and the accompanying HF2TA transimpedance amplifier. These devices are specified to propose the frequency range up to 50 MHz and the possibility of utilizing both: two- and four electrode measurements [10].

For carrying out the measurements of $\Delta Z(t)$, caused by pulse wave, a custom designed electrode printed circuit board (PCB) with circular gold plated electrodes was used (Fig. 2).

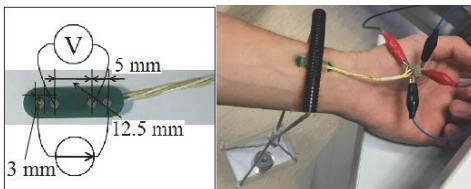


Fig. 2. The electrode PCB together with its specified dimensions and the setup for monitoring pulse wave with the goal of determining the influence of increasing weight.

As the means of applying pressure on the electrode, the weights of classical shape were utilized. In the experiments with weights, a custom made device with pendent platform for weights was used (Fig. 2). The weight of the device itself was 20 g and together with the weight of the electrode of 3 g (Fig. 2), the summed weight of these is by default constantly added to the value of weights.

III. METHODS AND MEASUREMENT SETUP

Altogether two measurement experiments were carried out for monitoring pulse wave. The experiments were done on wrists of volunteers during which the volunteer was sitting comfortably on the chair with the hand lying on the armrest in the height of about the last rib in the case of horizontally bended arm.

Firstly, the question of the influence of positioning of electrodes on wrist related to the measured value of $\Delta Z(t)$ in the case of increasing pressure on the electrode PCB, was research. The location of radial artery was determined and pulse found in the case of single volunteer by palpation. A line was drawn on the surface of skin onto the determined location of radial artery (position C in Fig. 3). Then the distances of 5 mm and 10 mm in both directions from radial artery were measured and four additional horizontal lines drawn.

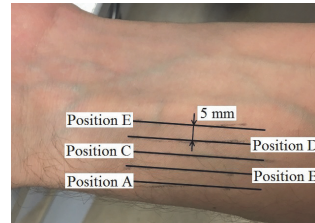


Fig. 3. The determined location of radial artery (position C) and four additional parallel lines for the experiments of investigating the influence of positioning of the electrodes on the availability of pulse wave.

The electrode PCB was attached onto wrist with its central line approximately on top of the chosen position, attached with sticky tape and the arm of the custom made device with pendent platform for weights resting on top of it (Fig. 2). In described setup, the platform was hanging freely on attached cords, maintaining its relatively horizontal position. The weights of 0 and 700 g were used in three measurement experiment series.

Secondly, the influence of increasing pressure on the electrode PCB and thereby, on radial artery, was research relative to the change of $\Delta Z(t)$. Moreover, the influence of the physiological differences of individuals on monitoring of pulse wave from wrist was evaluated. The weights in the range of 0...700 g were used with the step of 100 g – related to the feedback from the first volunteer concerning the discomfort in the case of greater weights.

In the beginning of each measurement experiment, the chosen maximum pressure was applied on the electrode by putting the necessary quantity of weights on the platform. The EBI measurement was performed concurrently at

predetermined frequencies and waveforms gathered. Then, the required number of weights was removed from the platform to obtain the next chosen amount of pressure on the electrode and the EBI measurement was performed. The procedure was continued until the measurement at the pressure of the weight of 0 g.

IV. RESULTS OF MEASUREMENTS

The Z of wrist was measured by using tetrapolar electrode configuration with the excitation voltage amplitude of 100 mV and at the frequencies in the range of 8...2048 kHz. This range was chosen to include the frequencies that are typically used in direct contact EBI measurement of biological material. Likewise, the same excitation frequency of 125 kHz is applied in wireless multichannel impedance cardiograph, utilized during selective coronary angiography for estimating the CAP in East-Tallinn Central Hospital, Estonia [9]. The reason for the lowest frequency of the range is the unrecognizability of pulse wave from measured signal of EBI below 8 kHz. The inclusion of higher frequencies (until few MHz) is explained by the desire to investigate the influence of electrode-skin contact interface, which, in the dry conditions of stratum corneum, may appear to include a layer of dielectric.

The gathered waveforms were filtered in LabView by using Savitzky-Golay filter at side points of 100. $\Delta Z(t)$ was determined visually during the post processing by finding the maximum and minimum values of the EBI from gathered waveform, caused by pulse wave. For comparability considerations, the proportion of $\Delta Z(t)$ from the peak value of Z was found and presented in percentages in the figures hereinafter according to:

$$Ratio_{Z_{from\Delta Z}} = (\Delta Z(t) \times 100) / Z. \quad (2)$$

The reason for showing $\Delta Z(t)$ in percentages in the following figures lies in the desire of presenting the results of measurements in the cases of all volunteers in comparable scale. Specifically, in addition to the expected influence of applied pressure, the measured Z of wrist is expected to be dependent on individual properties of different volunteers: dryness or wetness of skin, the volume of blood that is flowing through the radial artery during pulse wave etc. When calculating the $\Delta Z(t)$ to appear as portion of Z in percentages, the results can be compared related to the degree of availability of pulse wave.

To verify the measurement setup, an experiment was done by using firstly a single resistor of value 100Ω (R_1 in Fig. 1B) and secondly a series connection of resistor of value $1 k\Omega$ and capacitor of value $22 nF$ (R_2 and C_1 in Fig. 1C) to represent the Z of wrist. The $10 k\Omega$ resistors were chosen to represent the resistances of current carrying electrodes (R_{cc} in Fig. 1B and 1C). The gathered waveforms in both cases can be seen in Fig. 4, shown together with the results of the calculated values of Z in the cases of proposed verification circuits.

The Z was calculated according to:

$$Z = \sqrt{R^2 + \frac{1}{(2\pi f C)^2}}, \quad (3)$$

where R is resistance, C is the capacitance in series connection and f is frequency. The resistances of current carrying electrodes were not considered during the calculation as in ideal approach these are not applying. The increase in Z that starts from 256 kHz in the case of experimental measurement is explained by the effective parasitic elements that reveal at higher excitation frequencies because of the finite length of connecting leads, input capacitance of measurement device etc. The calculation confirms the agreement with the results of experimental measurement which, in turn, confirm the validity of the measurement setup.

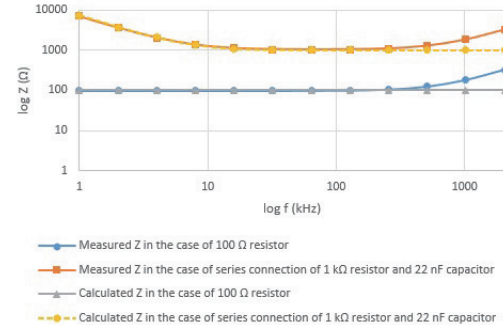


Fig. 4. Frequency response of the measured and calculated Z in the cases of two equivalent circuits (Fig. 1B and 1C) for verifying the measurement setup.

A. The Results of the Measurements in the Case of Different Positioning of the Electrodes with Respect to Radial Artery

It was determined during the experiments that the pulse wave is not visually available in current setup in the cases of two outermost positions (A and E in Fig. 3). In the case of position A, the electrode PCB tends to lie on top of radius and in the case of position E, the electrode PCB is resting on top of median nerve and tendons to fingers. The results are comparable for positions B...D – shown in Fig. 5 for pressures of weights 0 and 700 g.

The quantitative evaluation can be done on the basis of Table I, where $\Delta Z(t)$ in Ohm's is shown for pressure of 700 g. In the table, the mean value of three measurement series together with standard deviation (σ) is shown.

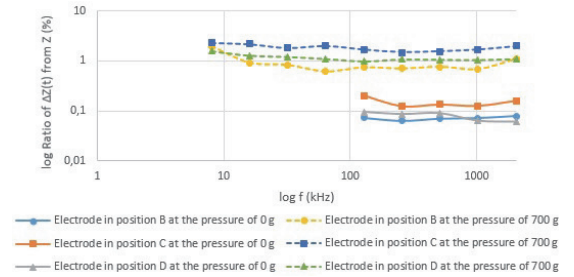


Fig. 5. Ratio of $\Delta Z(t)$ from Z in the cases of measurements from different positions on wrist while no pressure and pressure of the weight of 700 g is applied on the electrode PCB.

TABLE I. RESULTS IN THE CASES OF DIFFERENT POSITIONS OF ELECTRODES ON WRIST WHILE THE PRESSURE OF WEIGHT 700 G IS APPLIED

f (kHz)	Mean value of $\Delta Z(t)$ at the pressure of 700 g in position B $\pm \sigma$ (Ω)	Mean value of $\Delta Z(t)$ at the pressure of 700 g for position C $\pm \sigma$ (Ω)	Mean value of $\Delta Z(t)$ at the pressure of 700 g for position D $\pm \sigma$ (Ω)
8	2.384 ± 0.276	3.911 ± 0.239	3.008 ± 0.071
16	1.884 ± 0.138	4.637 ± 0.480	2.571 ± 0.118
32	1.696 ± 0.184	3.738 ± 0.379	2.251 ± 0.152
64	1.341 ± 0.096	4.098 ± 0.447	1.983 ± 0.119
128	1.394 ± 0.170	3.282 ± 0.263	1.665 ± 0.094
256	1.473 ± 0.057	2.503 ± 0.308	1.789 ± 0.081
512	1.573 ± 0.021	2.587 ± 0.294	1.736 ± 0.121
1024	1.436 ± 0.068	2.708 ± 0.319	1.577 ± 0.262
2048	2.234 ± 0.229	3.438 ± 0.476	1.842 ± 0.167

B. The Results of the Measurements in the Case of Increasing Pressure on the Electrodes

Four volunteers were participating the experiment of studying the influence of individual differences on the measured pulse wave in the case of increasing pressure. 1st volunteer was male of age 34, weight of 70 kg and height of 183 cm. 2nd volunteer was female of age 27, weight of 61 kg and height of 171 cm. 3rd volunteer was male of age 55, weight of 105 kg and height of 192 cm. 4th volunteer was male of age 30, weight of 65 kg and height of 176 cm. The physiological parameters of volunteers are gathered into Table II. Body mass index (BMI) is calculated according to:

$$BMI = \text{weight}/\text{height}^2. \quad (4)$$

TABLE II. PHYSIOLOGICAL PARAMETERS OF THE VOLUNTEERS

Volunteer	Sex	Calculated BMI	Circumference of wrist (mm)	Hairiness of forearm
1 st	Male	20.90	155	slight
2 nd	Female	20.86	160	no hair
3 rd	Male	28.43	195	slight
4 th	Male	20.98	160	slight

The graphical representation of the ratio of $\Delta Z(t)$ from Z in the cases of all volunteers can be seen in Fig. 6 – 9.

V. DISCUSSION

The relevance of positioning of the electrode reveals in the unavailability of the pulse wave in the cases of two extreme positions (A and E). It is claimed that the measuring depth decreases with the decrease in the distance between two electrodes [11]. As the electrodes are of small diameter, they do not give rise to sufficient current density to reach the pulse wave when placed on radial bone or tendons to fingers.

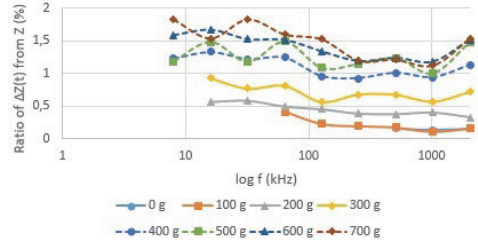


Fig. 6. Ratio of $\Delta Z(t)$ from Z in the case of measurements on wrist of 1st volunteer while different weights are applied on the electrode PCB.

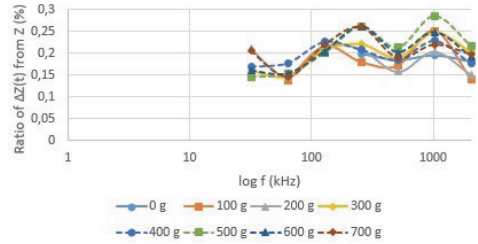


Fig. 7. Ratio of $\Delta Z(t)$ from Z in the case of measurements on wrist of 2nd volunteer while different weights are applied on the electrode PCB.

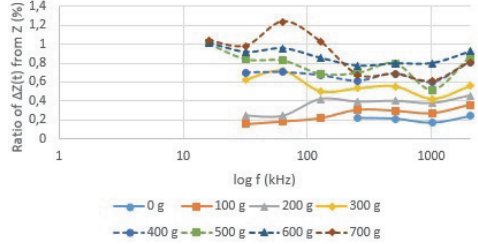


Fig. 8. Ratio of $\Delta Z(t)$ from Z in the case of measurements on wrist of 3rd volunteer while different weights are applied on the electrode PCB.

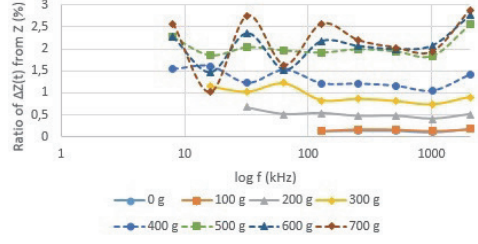


Fig. 9. Ratio of $\Delta Z(t)$ from Z in the case of measurements on wrist of 4th volunteer while different weights are applied on the electrode PCB.

The pulse wave is most clearly available, when electrodes are placed on top of radial artery, not depending on the pressure on the electrode (Fig. 5). The shift of 5 mm in either transverse directions does not influence the visual availability. Though, the $\Delta Z(t)$ for positions C and D in comparison with position B differ at times more than double (Table I).

Position D i.e. the direction to the tendons, proposes slightly better result than position B, explained by the presence of radius that influences the current distribution.

The above can also be related to the feature of tetrapolar setup, where the sensitivity field is expected to form areas of zero and negative sensitivity. Zero sensitivity appears when the fields are perpendicular or only a single field is present. Negative sensitivity appears when the fields are overlapping less than 90°, revealing in the decrease of the value of total impedance, caused by increase of the impedivity [11-12].

The influence of the applied pressure on the electrode PCB can be realized in the amount of $\Delta Z(t)$. The tenfold difference in the value of $\Delta Z(t)$ in the cases of pressure of 0 and 700 g is evident in Fig. 5. The results are generally following the trend line that is slightly falling with increasing excitation frequency, though the start of the rise of $\Delta Z(t)$ at the highest excitation frequency (2048 kHz) is distinct, reported also in [6].

The results of the measurements on wrists of volunteers reveal the influence of the physiological differences. The waveforms in the cases of the 1st, 3rd and 4th volunteer trace generally the similar route (Fig. 6, 8-9). Though, the physiological parameters of the 3rd volunteer differ greatly. The value of $\Delta Z(t)$ increases with the pressure of increasing weights. The generalization can be made that in the cases of lower weights than 500 g, $\Delta Z(t)$ is increasing with recognizable differences. In the cases of weights above 400 g, the differences in $\Delta Z(t)$ are decreasing and are, in some cases, even overlapping, proposing the closeness of maximum effect of the pressure on electrode-skin impedance.

In the case of the 2nd volunteer, $\Delta Z(t)$ is in overall of lower value and the differences in the cases of different pressures are of smaller order (Fig. 7). This is assumed to demonstrate the elasticity and thickness of skin and its subcutaneous layers that differ from the similar properties of the other volunteers. The absence of body hair on wrist does not have influence on the availability of pulse wave in the case of measuring $\Delta Z(t)$.

The assumption is that the modifications in the shape, dimensions and the material of the electrodes can possess different result concerning the availability of pulse wave. Also, the alternative locations of exciting and measuring electrodes relative to radial artery are assumed to influence the results.

VI. CONCLUSIONS AND FUTURE WORK

The experiments of measuring the EBI of wrist were implemented to evaluate the influence of positioning of the electrodes, pressure on the electrodes and individual differences of volunteers on the availability of pulse wave.

The relevance of the presented research appears in examination of different positions of small area circular electrodes that are placed on skin longitudinally to radial artery. It is reported that some amount of shift (5 mm) of the electrode in transverse direction relative to radial artery is acceptable for visualization of pulse wave.

The utilization of small area circular electrodes that are placed on radial artery in the case of determining the influence

of varying pressure is proposing a fresh approach. Together with the analyze of the varying value of $\Delta Z(t)$ in the cases of several volunteers, the results emphasize the impact of individual differences. The increasing pressure on the electrodes is considered to increase the value of $\Delta Z(t)$ noticeably, applying generally likewise in the cases of all experimented volunteers. Though, in the case of heavier weights (> 400 g), the differences of $\Delta Z(t)$ are decreasing and converging.

The experimentation is ongoing to determine the influence of different electrode materials and dimensions on the measurement of EBI for monitoring the pulse wave – also in the case of larger number of volunteers. The future tasks to implement are the proposal of a solution for electrode interface for monitoring the pulse wave from wrist by the means of EBI.

ACKNOWLEDGMENT

This research was supported by Estonian Research Council grant IUT1911 and the European Regional Development Fund in frames of the Estonian Center of Research Excellence EXCITE. The work was partly financed also through the European Research Area project H2020-WIDESPREAD-2014-2-668995-Cognitive Electronics.

REFERENCES

- [1] "Global Hearts Initiative Infographic (Flyer)." [Online]. Available: http://www.who.int/cardiovascular_diseases/global-hearts/HEARTS_Infographic_rev1.pdf?ua=1.
- [2] H. Kim, J. Y. Kim, Y.-J. Park, Y.-B. Park, "Development of pulse diagnostic devices in Korea," *J. Integrative Medicine Research*, vol. 2, iss. 1, pp. 7–17, March 2013.
- [3] S.K. Yoo, K.Y. Shin, T.B. Lee, S.O. Jin, "New pulse wave measurement method using different hold-down wrist pressures according to individual patient characteristics," *SpringerPlus* 2:406, Aug. 2013.
- [4] W. Lee and S. Cho, "Integrated all electrical pulse wave velocity and respiration sensors using bio-impedance," *IEEE J. Solid-State Circuits*, vol. 50, iss. 3, pp. 776–785, Jan. 2015.
- [5] M-C. Cho, J-Y. Kim, SH. Cho, "A bio-impedance measurement system for portable monitoring of heart rate and pulse wave velocity using small body area," *IEEE Int. Symp. on Circuits Syst.*, pp. 3106-9, May 2009.
- [6] A. Albulbul, A.D.C. Chan, "Electrode-skin impedance changes due to an externally applied force," *IEEE Int. Symp. on Med. Meas. and Appl. (MeMeA)*, pp. 1-4, May 2012.
- [7] A. Cömert, M. Honkala, J. Hyttinen, "Effect of pressure and padding on motion artifact of textile electrodes," *Biomed. Eng. Online* 12: 26, Apr. 2013.
- [8] C.C. Oliveira, J.M. da Silva, I.G. Trindade, F. Martins, "Characterization of the electrode-skin impedance of textile electrodes," *IEEE Conf. on Design of Circuits and Integr. Circuits (DCIS)*, pp. 1-6, Nov. 2014.
- [9] M. Min, P. Anrus, H. Kõiv, A. Krivošei, T. Uuetoa, J. Lamp, "Bioimpedance sensing – a viable alternative for tonometry in non-invasive assessment of central aortic pressure," *IEEE Int. Symp. on Med. Meas. and Appl. (MeMeA)*, pp. 373-8, May 2017.
- [10] "HF2 User Manual – ziControl Edition," Zurich Instruments, 2017.
- [11] S. Grimes and Ø. G. Martinsen, *Bioimpedance & Bioelectricity Basics* (Book style), London, Great Britain Academy, 2008, p. 190.
- [12] B.H. Brown, A.J. Wilson, P. Bertemes-Filho, "Bipolar and tetrapolar transfer impedance measurements from volume conductor," *Electronic Letters*, vol. 36, iss. 25, pp. 2060-2, Dec. 2000.

Publication 5

Metshein, Margus; Kõiv, Hip; Annus, Paul; Min, Mart (2018). Electrode optimization for bioimpedance based central aortic blood pressure estimation. [IFMBE Proceedings Vol. 68/2 – World Congress on Medical Physics & Biomedical Engineering (IUPESM2018), 3 – 8 June, 2018, Prague, Czech Republic]: Springer Nature.

Electrode Optimization for Bioimpedance Based Central Aortic Blood Pressure Estimation

Margus Metshein¹, Hip Kõiv¹, Paul Annus¹ and Mart Min¹

¹ Thomas Johann Seebeck Department of Electronics, School of Information Technologies,
Tallinn University of Technology, Ehitajate tee 5, 19086 Tallinn, Estonia
paul.annus@ttu.ee

Abstract. Evidence suggests that assessment of the central aortic pressure (CAP) of blood is vital for accurate detection of cardiovascular events and for making treatment decisions. Direct CAP measurement is possible and is used in clinical environment, however it is both costly and carries increased risk, therefore it is not suitable for preliminary screening and monitoring. Indirect noninvasive assessment of CAP has been around for several years. Applanation tonometry which is largely based on the research by O'Rourke et al., is method of choice and sometimes even described as gold standard for the noninvasive assessment of the central pressures, the pulse wave velocity and the heart rate variability. Pressure sensor is typically placed on the radial artery, and central aortic pressure is estimated by generalized mathematical transformation of the recorded waveform. While widely used the method has serious drawback – strong dependence on operator skills. The electrical bioimpedance (EBI) has emerged as viable alternative in search for the measurement methods with better repeatability. Its applicability has been confirmed in several studies involving simultaneous invasive CAP measurement, and comparative measurements with AtCor Medical SphygmoCor device. Further refinement of the method is considered in proposed paper. Electrical attachment of the bioimpedance measurement unit to the body is investigated and discussed.

Keywords: Bioimpedance, Electrodes, Pressure, Current distribution.

1 Introduction

Measurement system must be connected to the tissue under investigation with electrodes. Yet it turns out to be the most vulnerable part of the system. Around 85% of the problems in EBI measurement can be associated with the electrodes [1]. First of all sensitivity distribution depends on the number and placement of the electrodes [2], [3]. There are also simultaneous parasitic couplings distorting the current distribution inside the object [4]. Current investigation tackles the problem of coupling uncertainties in case of the bioimpedance based CAP estimation [5]. Different flexible electrode materials are compared, and impact of the contact pressure is investigated in case of tetrapolar electrode configuration. The tetrapolar impedance measurement should minimize the impact of the electrode impedances to the EBI measurement, even if it cannot be

fully eliminated [6]. Minimal or optimal pressure on the electrodes is desirable in order to avoid deformation of the artery under them, and to ensure true noninvasiveness of the measurement. Both the invariable part of the EBI of the local volume (Z_0) and the information carrying time varying part of the impedance ($\Delta Z(t)$) caused by the blood pulsation will be investigated:

$$Z = Z_0 + \Delta Z(t) \quad (1)$$

Frequency dependence of the measured bioimpedance should also be investigated, as well as the impact of the electrode materials on different parameters. The HF2IS impedance spectrometer [7] together with the HF2TA transimpedance amplifier was used as measurement instrument of choice in all of the experiments.

2 Effect of the increasing distance between the electrodes on the measured impedance of the wrist

It is proposed in the literature that blood is mainly resistive in kHz region of frequencies. The measured change in the impedance, because of the varying amounts of the blood, can be however complex, due to the actual current distribution. There is also tissue that lies between the electrode and the blood vessel and an unknown sensitivity distribution. Experiments were performed to evaluate the effect of the increasing distance between the electrodes, by using the electrocardiogram (ECG) electrodes. Standard ECG monitoring electrodes with foam tape (type 2228 - 3M) were cut narrower (width of 9 mm) and attached in line on radial artery with the gap of 1 mm between the electrodes (center distance: 10 mm) (Fig. 1a).

The following four setups were used to measure the magnitude and the phase in the tetrapolar electrode configuration with the excitation signal amplitude of 500 mV and at the frequency of 128 kHz:

- Distance between the electrodes was increased in 10 mm steps by lifting the pair of exciting and measuring electrodes by one step (1).
- Distance between the electrodes was increased in 10 mm steps by lifting the pair of exciting and measuring electrodes by one step and removing the unused electrodes from in between the measuring electrodes (2).
- Distance between the electrodes was increased in 10 mm steps by lifting one measuring electrode by one step while the exciting electrodes were permanently set to outermost positions (3).
- Placing the electrodes in setup (1) on top of the ulnar bone region (4).

Graphical representation of the measured magnitude and phase can be seen on Fig. 2. Concerning the phase in the case of setups (1)-(2), the result is maintaining its horizontal trend, which was expected if the underlying tissues do not change much. The setup (3) shows the effect of the increasing phase shift for the increasing distance, which needs explanation. In the case of setup (4), the phase shift is bigger, indicating different tissues under the electrodes, which is true due to different location.

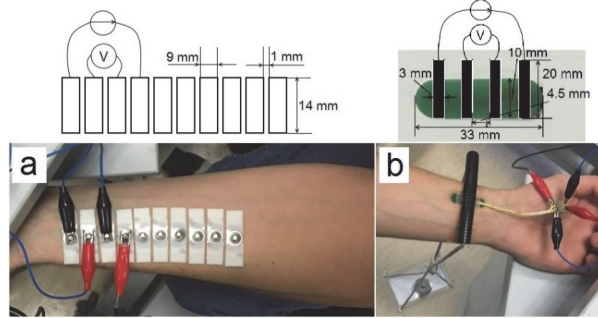


Fig. 1. Electrodes and setup for EBI measurement on the wrist in tetrapolar configuration: a) in the case of the increasing distance between the electrodes and b) for comparison between different conductive electrode fabrics under the pressure.

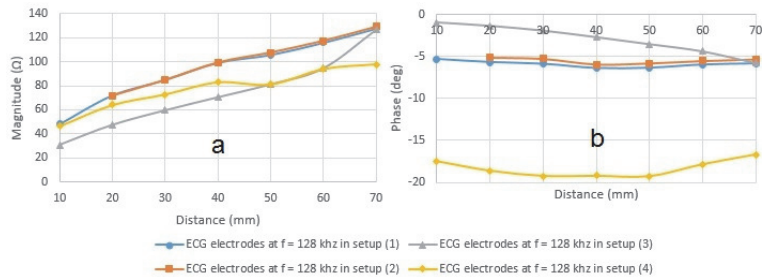


Fig. 2. Influence of the increasing distance between the measuring electrodes in the cases of different setups on: a) the magnitude and b) the phase of the EBI on the wrist.

The magnitude in all of the setups is increasing quite linearly – approximately by 13Ω per 10 mm in the case of setup (1) and by shorter steps in the case of setup (4) – about 8.5Ω per 10 mm. One can realize that the presence of unused electrodes on the volume of the wrist in between the measuring electrodes does not influence the result. In the case of setup (3), the effect of excitation by distant electrodes is present, appearing in approximately 22Ω lower magnitudes than in case of the setups (1)-(2).

Quite often it is assumed that [8], [9] electric current prefers to flow through blood in vessels because of the low resistivity, typically $1.5 \Omega\text{m}$. In reality also the presence of the skin, muscles, radial bone, radial artery and two radial veins should be considered. Calculation of the impedance of just the blood vessels in the local volume per 10 mm gives 830Ω instead of the measured value of 13.3Ω . Inner diameters of the radial artery and veins were taken to be 2.7 mm, and volumes of the blood were summed. This leads to speculations about the actual distribution of the current in the

local volume of the wrist. Sizable impact of the muscles is expected because of their longitudinal resistivity of $2.4 \Omega\text{m}$. If the area of the hypothetical cylindrical volume of the muscle is taken to be ten times larger than the summed area of the radial artery and the two veins, then the calculated impedance is 140Ω per 10 mm, still an order of magnitude larger than the measured value. Presence of other layers of lower resistivity like tendons and vessel walls should be taken into account as well, and complex current distribution picture will emerge. Further research is due here.

3 Influence of the usage of different electrode materials for monitoring pulse wave by measuring the impedance of wrist

From one side it seems plausible that the change in the electrode pressure will have some impact also on the EBI value. Question however is how big that impact is, and does it significantly depend on the electrode material. On the other side it seems beneficial to acquire also some information regarding the applied pressure during the measurement, which could enable to control it in more deterministic manner. Therefore specific pressure sensitive fabric was included in the list of potential candidates for the EBI electrodes. The goal therefore was investigation of the influence of the different electrode materials on the value of the measured Z_0 and on the magnitude of the $\Delta Z(t)$ under different pressures. Three different materials were chosen for evaluation as electrodes.

1. Nickel/cuprum (Ni/Cu) polyethylene terephthalate polyurethane conductive foam of part number Sui-78-20 (Seiren Co., Ltd.) with surface resistivity of $0.07 \Omega/\text{m}^2$.
2. Ni/Cu polyester taffeta conductive fabric of part number 3035-535 (Laird Technologies) with surface resistivity of $0.07 \Omega/\text{m}^2$.
3. EonTex pressure sensing fabric of part number COM-14111 (SparkFun Electronics) with surface resistivity of $2 \text{k}\Omega/\text{m}^2$ at non-pressured state.

All of the electrodes were cut into equivalently sized pieces and attached onto a rigid printed circuit board (PCB) (Fig. 1B) for the experiments. The crocodile clips were attached to the ends of the fabric, and external pressure was applied on other side of the PCB. Single comfortably sitting volunteer was participating in the experiment. The hand was lying on the armrest at the height of about the lower rib. The weights used to apply the controlled pressure onto the radial artery where in the range of 0...700 g, with the step of 100 g. EBI of the wrist was measured by using tetrapolar electrode configuration with the excitation signal amplitude of 500 mV and at the frequency of 128 kHz. The graphical representation of the resulting EBI values can be seen in Fig. 3.

Out of three candidates the pressure sensitive textile has the worst highly nonlinear result. 2nd material however performs rather well showing slight nearly linear increase in magnitude. Graphical representation of the dependence of the magnitude of $\Delta Z(t)$ for all three fabrics can be seen in Fig. 4. The rising trend of $\Delta Z(t)$ is visible for all chosen materials when the external pressure on the radial artery is increasing.

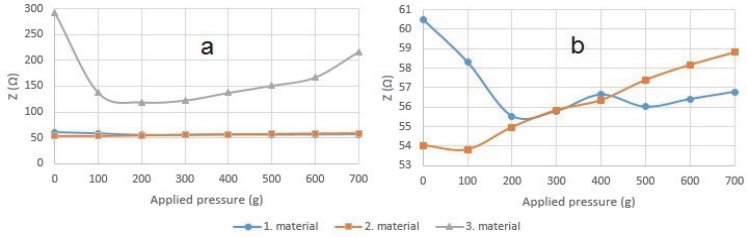


Fig. 3. Influence of the increasing external pressure on the magnitude of the EBI on the wrist for three different electrode materials: a) all three materials, b) zoomed in picture of the two best options.

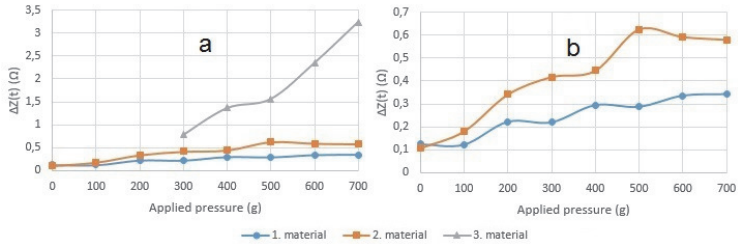


Fig. 4. Influence of the increasing external pressure on the value of $\Delta Z(t)$ for three different materials: a) all three materials, b) zoomed in picture of the two best options.

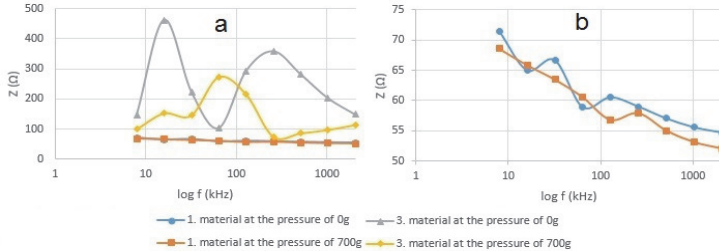


Fig. 5. Influence of the frequency of the excitation signal on the magnitude of: a) all results, b) zoomed in picture of the two best options.

Last but not least the frequency dependence of the acquired EBI was investigated. The graphical representation of the magnitude of the EBI for 1st and 3rd electrode material can be seen in Fig. 5. As the 1st and 2nd material tend to behave quite similarly, only the first one is presented in the following figure. Also, only the results at two pressures are shown: 0 g and 700 g. Clearly 3rd material exhibits strange nonlinear properties under different pressure and frequency combinations.

4 Conclusions

In some works it is assumed that the current density is greater in the path of least impedance i.e. in the blood in the artery under the electrodes, than in the surrounding tissue. In other works it is regarded as a largely unsolved basic problem: “To what extent does an externally applied electric current follow blood vessels?” [1]. Cause for the time variance of the impedance is also still debatable [1]. Is it blood volume change or orientation of the erythrocytes, or something else? Measurement results seem to suggest that the current is distributed more widely and in more complex manner than expected, as the roughly calculated impedance of the blood vessels in the local volume is about 830Ω per 10 mm, instead of the measured value of 13.3Ω .

Attempt to get multimodal readings from the same textile electrodes, both the EBI and the pressure, has failed with tested material, which is behaving very poorly for the EBI assessment. Nevertheless the idea is appealing, and further investigation will follow with different pressure sensitive materials. It is probably safe to conclude that there is optimal pressure point (roughly 300 g of applied weight), where the artery is not deformed too much, and the EBI readings are good. Placement and configuration of the electrodes plays an essential role as well, and should be investigated further.

The results should be considered preliminary, experiments were conducted only on a single person, and conclusions debatable, but hopefully provoking some thoughts. The authors declare that they have no conflict of interest.

Acknowledgements

The research was supported by Estonian Research Council (Grant IUT1911) and European Regional Development Fund in frames of Estonian ICT Center EXCITE. Partly also by the EU project H2020-2014-2-668995-Cognitive Electronics.

References

1. Grimnes, S.: Bioimpedance and bioelectricity basics. Elsevier, Boston, MA (2014).
2. Grimnes, S., Martinsen, Ø.G.: Sources of error in tetrapolar impedance measurements on biomaterials and other ionic conductors. *J. Phys. Appl. Phys.* 40, pp. 9–14 (2007).
3. Patterson, R.P.: Impedance cardiography: What is the source of the signal? *J. Phys. Conf. Ser.* 224, 012118 (2010).
4. Aliau-Bonet, C., Pallas-Areny, R.: On the Effect of Body Capacitance to Ground in Tetrapolar Bioimpedance Measurements. *IEEE Trans. Biomed. Eng.* 59, pp. 3405–3411 (2012).
5. Min, M., Annus, P., Koiv, H., Krivosei, A., Uuetoa, T., Lamp, J.: Bioimpedance sensing - a viable alternative for tonometry in non-invasive assessment of central aortic pressure. In: Proc. 12th IEEE Int. Symp on Med. Meas. and Appl. (MeMeA), pp. 373–378 (2017).
6. Cömert, A., Hyttinen, J.: Impedance spectroscopy of changes in skin-electrode impedance induced by motion. *Biomed. Eng. OnLine.* 13, 149 (2014).
7. HF2 User Manual ziControl, <https://www.zhinst.com/>, (2017).

8. Bang, S., Lee, C., Park, J., Cho, M.-C., Yoo, Y.-G., Cho, S.H.: A pulse transit time measurement method based on electrocardiography and bioimpedance. In: Proc. of Biomed. Circuits Syst. Conf. (BioCAS), pp. 153-156. IEEE, Beijing, China (2009).
9. Lee, W., Cho, S.H.: Integrated all electrical pulse wave velocity and respiration sensors using bio-impedance. IEEE J. Solid-State Circuits 50(3), 776-785 (2015).

Curriculum Vitae

Personal data

Name:	Margus Metshein
Date of birth:	04.09.1983
Place of birth:	Kuressaare, Estonia
Citizenship:	Estonia

Contact data

E-mail:	margus.metshein@gmail.com
---------	---------------------------

Education

2012 – 2018	Tallinn University of Technology	PhD, Electronics and Telecommunication
2007 – 2010	Tallinn University of Technology	MSc, Electronics and Bionics
2002 – 2006	Tallinn University of Technology	BSc, Electronics and Bionics
1999 – 2002	Kuressaare Gümnaasium	High-school education

Language competence

Estonian	Native
English	Fluent
German	Basic
Finnish	Basic

Professional employment

2016 – ...	Tallinn University of Technology, Thomas Johann Seebeck Department of Electronics, Research Laboratory for Cognitronics	Early Stage Researcher
2014 – ...	Fineltec Baltic OÜ	New Product Introduction Manager
2006 – 2013	Incap Electronics Estonia	Component Engineer

Elulookirjeldus

Isikuandmed

Nimi:	Margus Metshein
Sünniaeg:	04.09.1983
Sünnikoht:	Kuressaare, Estonia
Kodakondsus:	Eesti

Kontaktandmed

E-post:	margus.metshein@gmail.com
---------	---------------------------

Hariduskäik

2012 – 2018	Tallinna Tehnikaülikool	PhD, Elektroonika ja telekommunikatsioon
2007 – 2010	Tallinna Tehnikaülikool	MSc, Elektroonika ja bioonika
2002 – 2006	Tallinna Tehnikaülikool	BSc, Elektroonika ja bioonika
1999 – 2002	Kuressaare Gümnaasium	Keskharidus

Keelteoskus

Eesti keel	Emakeel
Inglise keel	Kõrgtase
Saksa keel	Algtaase
Soome keel	Algtaase

Teenistuskäik

2016 – ...	Tallinna Tehnikaülikool, Thomas Johann Seebeki elektroonikainstituut	Doktorant-nooremteadur
2014 – ...	Fineltec Baltic OÜ	Uute toodete juurutamise juht
2006 – 2013	Incap Electronics Estonia	Komponendiinsener

